MOLECULAR APPROACH WITH FOURIER TRANSFORM INFRARED SPECTROSCOPY TO DIFFERENT PATHOLOGICAL SYSTEMS (DIABETES MELLITUS AND ARTERIOVENOUS MALFORMATION) WITH VARIOUS TREATMENTS

A THESIS SUBMITTED TO
THE GRADUATE SCHOOL OF NATURAL AND APPLIED SCIENCES
OF
THE MIDDLE EAST TECHNICAL UNIVERSITY

BY

NESLİHAN TOYRAN AL-OTAİBİ

IN PARTIAL FULFILLMENT OF THE REQUIREMENTS FOR THE DEGREE OF
DOCTOR OF PHILOSOPHY
IN
THE DEPARTMENT OF BIOLOGY

AUGUST 2003

Approval of the Graduate School of Natural and Applied Sciences

_____
Prof. Dr. Canan Özgen
Director

I certify that this thesis satisfies all the requirements as a thesis for the degree of Doctor of Philosophy.

_____
Prof. Dr. Mesude İşcan
Head of the Department

This is to certify that we have read this thesis and that in our opinion it is fully adequate, in scope and quality, as a thesis for the degree of Doctor of Philosophy.

_____
Prof. Dr. Feride Severcan
Supervisor

Examining committee members

Prof. Dr. Feride Severcan _____

Prof. Dr. Mesude İşcan _____

Prof. Dr. Meral Yücel _____

Prof. Dr. Necla Öztürk _____

Prof. Dr. Sevgi Bayarı _____

ABSTRACT

MOLECULAR APPROACH WITH FOURIER TRANSFORM INFRARED SPECTROSCOPY TO DIFFERENT PATHOLOGICAL SYSTEMS (DIABETES MELLITUS AND ARTERIOVENOUS MALFORMATION) WITH VARIOUS TREATMENTS

Toyran Al-Otaibi, Neslihan

Ph.D., Department of Biology

Supervisor: Prof. Dr. Feride Severcan

August 2003, 183 pages

In the first part of this study, the effect of diabetes mellitus on apex, left ventricle muscle, right ventricle muscle, and the small vessels on the left ventricle muscle of the rat heart; and the effect of selenium (Se) treatment on these regions of the diabetic heart are investigated at molecular level by Fourier Transform Infrared (FTIR) Microspectrosopy. In the second part of the study, the effect of hypoperfusion and/or radiosurgery on rat brain homogenates have been studies by FTIR spectroscopy.

The results reveal that diabetes causes lipid peroxidation (mainly for the vessels), an increase in lipid content, an increase in the order of lipids, alteration of

protein profile, increases in glycogen and glycolipid contents. The findings regarding all parts of the rat heart reveal that, diabetes exerts more significant effects on the vessels than the muscles of the ventricles and the apex. Injection of diabetic rats with 5 μmole/kg/day Se i.p. for 4 weeks is found to restore some of the changes caused by diabetes, such as the increase in the content of glycogen in all parts of rat heart. However, with the dose and treatment time of Se mentioned above, some of the alterations caused by diabetes were not completely restored despite the changes observed towards control values.

In the second part of the thesis, FTIR results suggest that hypoperfusion causes significant effects on the structure and content of lipids and proteins on rat brain homogenates. An increase in the content of lipids, a decrease in the content of proteins, an increase in lipid to protein ratio, and an increase in the order of lipids are observed. The proteins are affected in terms of both content and secondary structure in favor of β sheets and random coils. After a single high dose of X-ray to the healthy rat brain, a number of spectral changes occur revealing slight increase in the lipid synthesis, significant decrease in protein content, and slight decrease in protein-to-lipid ratio. The results show that radiation causes similar but more significant changes on hypoperfused brain samples. In addition to this, the application of radiation increases the order of lipids, the stiffness in the deep interior of the bilayer in the hypoperfused brains, but not in the non-hypoperfused ones. These findings suggest that chronically hypoperfused brain might be more vulnerable to the effects of radiation than the control ones, at least for the parameters mentioned above. The findings of this study also revealed that the secondary structure of the proteins are altered in the irradiated brain samples in a way that the content of α-helical structures decreases significantly and random coil increases dramatically, which suggest denaturation of the proteins.

Key words: Diabetes mellitus, Heart, Selenium, Brain, Hypoperfusion, Radiosurgery, FTIR, Microscopy

ÖZ

FOURİER TRANSFORM İNFRARED SPEKTROSKOPİ YÖNTEMİ İLE DEĞİŞİK PATOLOJİK SİSTEMLERİN (DİYABETES MELLİTUS VE ARTERİOVENOZ MALFORMASYON) VE ÇEŞİTLİ TEDAVİ YÖNTEMLERİNİN MOLEKÜLER DÜZEYDE İNCELENMESİ

Toyran Al-Otaibi, Neslihan

Doktora, Biyoloji Bölümü

Tez Yöneticisi: Prof. Dr. Feride Severcan

Ağustos 2003, 183 sayfa

Bu çalışmanın ilk bölümünde, diyabetes mellitus hastalığının kalbin apeks, sol ventrikül kası, sağ ventrikül kası ve sol ventrikül kasında bulunan küçük damarlar üzerine olan etkisi; ve selenyum (Se) uygulamasının diyabetik kalbin bu bölgeleri üzerine olan etkisi Fourier Transform Infrared (FTIR) Mikrospektroskopi tekniği ile moleküler düzeyde araştırılmıştır. Çalışmanın ikinci bölümünde, hipoperfüzyonun ve/veya radyocerrahinin sıçan beyin homojenatları üzerine olan etkisi FTIR spektroskopi tekniği kullanılarak incelenmiştir.

Elde edilen sonuçlar ile, diyabet hastalığının lipit peroksidasyona (özellikle damarlarda), lipit miktarında bir artışa, lipitlerin düzenliliğinde bir artışa, protein profilinde değişikliğe, glikojen ye glikolipit miktarlarında artışa neden olduğu

gösterilmiştir. Sıçan kalbinin incelenen tüm bölgelerinden elde edilen sonuçlar, diyabetin damarlarda, ventrikül ve apeks kaslarına göre daha önemli derecede etkili olduğunu ortaya çıkarmıştır. Diyabetik sıçanlara 4 hafta boyunca 5 μmol/kg/gün Se enjekte edilmesi sonucunda kalbin incelenen tüm bölgelerinde diyabetin neden olduğu bazı etkilerin, glikojen miktarının artması gibi, ortadan kalktığı görülmüştür. Yukarıda bahsedilen doz ve sürede Se tedavisinin diyabetin neden olduğu bazı etkileri kontrol değerlerine yaklaştırdığı, fakat tamamen ortadan kaldırmadığı gözlemlenmiştir.

Tezin ikinci bölümünden elde edilen FTIR sonuçları, hipoperfüzyonun sıçan beyin homojenatlarındaki lipit ve protein miktarlarını önemli derecede etkilediğini göstermiştir. Lipit miktarında artış, protein miktarında azalış, lipit-protein oranında artış, lipitlerin düzenli yapısında artış olduğu gözlemlenmiştir. Proteinlerin hem miktarı hem de ikincil yapıları, β plakalı tabakalı yapı ve tesadüfi kıvrımlar artacak şekilde etkilenmiştir. Sıçan beyinlerine tek doz X ışını gönderildiğinde spektral değişikliklerin incelenmesi ile lipit sentezinde az miktarda artış, protein miktarında önemli derecede azalış, protein-lipit oranında hafif bir azalış olduğu anlaşılmıştır. Elde edilen sonuçlar, radyasyonun hipoperfüze beyin örneklerine uygulanması ile benzer fakat daha önemli değişikliklerin ortaya çıktığını göstermiştir. Ayrıca, radyasyonun hipoperfüze beyne uygulanması sonucu lipitlerin düzenliliğinin ve sistemin iç derinliklerinin dinamiğinin azaldığı, hipoperfüze olmamış beyin örneklerine uygulanması sonucunda ise azalmadığı görülmüştür. Bu bulgulardan elde edilen sonuç, kronik olarak hipoperfüze edilmiş beynin kontrol beyinlere göre, en azından yukarıda bahsedilen parametreler açısından, radyasyondan daha kolay etkilendiğidir. Bu çalışmadan elde edilen bulguların ortaya koyduğu diğer bir sonuç da, proteinlerin ikincil yapısının radyasyon uygulaması sonucu etkilenerek α-heliks miktarının önemli derecede azalması ve tesadüfi kıvrımların artması, dolayısı ile denatüre olmasıdır.

Anahtar kelimeler: Diyabetes mellitus, Kalp, Selenyum, Beyin, Hipoperfüzyon, Radyocerrahi, FTIR, Mikroskopi

To My Mother, Meryem Toyran

ACKNOWLEDGEMENTS

I am grateful to my supervisor Prof. Dr. Feride Severcan for her advice, encouragement and supervision throughout my work.

I would like to thank to Prof. Dr. Naumann (Robert Koch Institute, Berlin-Germany) for his valuable suggestions and support in his lab during my stay in Germany. I would like to extend my thanks to Angelika, Maren, Fabian, Cecillia and Peter for their assistance and friendship in the lab during my work in Berlin.

Many thanks to Prof. Dr. Belma Turan (Ankara University, Faculty of Medicine, Department of Biophysics) for preparing the rat heart samples that I used in my experiments and for her valuable suggestions and comments during the progress of my studies.

I would like to extend my thanks to Prof. Dr. Faruk Zorlu (Hacettepe University, Faculty of Medicine, Department of Radiation Oncology) and Assoc. Prof. Dr. Kamil Öğe (Hacettepe University, Faculty of Medicine, Department of Neurosurgery) for preparing the rat brain samples for my studies.

Special thanks to my husband, Hani, for his endless patience, support and understanding without which I would never be able to complete this work.

Many thanks to my family for their endless care, understanding and encouragement throughout my studies.

Finally I wish to extend my thanks to my friends and my lab-mates for their support and friendship.

TABLE OF CONTENTS

LIST OF TABLES

TABLE

LIST OF FIGURES

FIGURE

CHAPTER I

INTRODUCTION

In the present study, some commonly seen pathological systems and their possible treatment methods will be investigated. We have chosen to study diabetes mellitus as the first pathological condition, and arteriovenous malformation (AVM) as the second pathological condition. The possible treatment effect of selenium (Se) on diabetic heart; and the effect of radiosurgery on AVM of the brain will be examined at molecular level by Fourier Transform Infrared (FTIR) spectroscopy.

1.1 Part I: Effect of Diabetes Mellitus on Rat Heart and the Effect of Selenium Treatment on Diabetic Rat Heart

1.1.1 Diabetes Mellitus

Insulin, a peptide hormone, is secreted by the β cells in response to a rise in blood glucose levels. Insulin is necessary to promote the entry of glucose into tissues. The lack of critical concentrations of circulating insulin or the ability of insulin to function properly leads to the onset of diabetes mellitus (Stapleton, 2000).

The most common forms of diabetes are type I, insulin dependent diabetes mellitus (IDDM) and type II, non-insulin dependent diabetes mellitus (NIDDM). IDDM usually begins before the age of 40, often in childhood and adolescence. The clinical picture is usually more severe in patients with IDDM than in patients with NIDDM. Type I is caused by autoimmune destruction of the pancreatic insulin-producing β cells. Type I diabetics therefore have little to no circulating insulin levels. The disease is usually managed with injections of insulin (Stapleton, 2000).

NIDDM usually begins in middle life or after. Symptoms begin more gradually than IDDM, and the diagnosis is frequently made when an asymptomatic person is found to have elevated plasma glucose on routine laboratory experimentation. In NIDDM, the β cells are producing some insulin, but the insulin is too little or is not physiologically effective. Many of this type of patients are treatable with diet and exercises alone (Öztürk *et al*., 1996).

1.1.1.1 Experimental Models of Diabetes Mellitus

There are many advantages in studying diabetes mellitus in animals. Almost every diabetic complication can be detected in experimental models of diabetes to investigate their mechanisms. Models of experimental diabetes permit the study of the involvement of environmental factors, such as diet, exercise, drugs, toxins, and infection agents. In addition, they exhibit many features of clinical diabetes. However none of the models is exactly equivalent to clinical diabetes. The following methodologies have been applied for experimental diabetes: Surgical diabetes, spontaneous diabetes, viral diabetes and chemical diabetes (Öztürk *et al*., 1996).

1.1.1.2 STZ-Induced Diabetes Mellitus

STZ is the most commonly used chemical agent to induce Type I diabetes mellitus in experimental animals. STZ is an antibiotic extracted from Streptomyces achromogenes. This antibiotic causes a sustained insulin deficiency and elevation of serum glucose levels by selectively destroying pancreatic β cells (Junod *et al*., 1969). Rats treated with STZ display many of the features seen in human subjects with uncontrolled diabetes mellitus, including hyperglycaemia, polydipsia, polyuria, and weight loss (Tomlinson *et al*., 1992). The diabetogenic effects of STZ were found to be dose dependent, ranging from mild diabetes following a dose 35 mg kg^{-1} to a severe ketotic state, leading to death within 2 to 3 days after a dose of 100 mg kg^{-1}.

1.1.1.3 Complications of Diabetes Mellitus

Diabetes mellitus is not a single disease but a cluster of disorders (Stapleton, 2000). This disease is associated with an extensive list of complications involving nearly every tissue in the body, including brain (like neuropathy) (Barbano *et al*.,

2003), cardiovascular system (like atherosclerosis, macro and microangiopathies) (Factor *et al*., 1980b; Kakkar *et al*., 1996), eyes (like cataract, blindness) (Prasad *et al*., 2001; Trautner *et al*., 2003), kidneys (like renal failure) (Iyoda *et al*., 2003) and liver (like hepatomegaly) (Herrman *et al*., 1999). Non enzymatic free radical mediated oxidation of biological molecules, membranes and tissues is associated with diabetes mellitus. There has recently been interest in the hypothesis that oxidative stress may contribute to the development of complications in diabetes mellitus. Under normal physiological conditions, there is a balance between free radical production and antioxidant defense systems. Increased oxidative stress may arise either as a result of increased free radical production or reduced activity of antioxidant defenses, and in patients with diabetes there is evidence for both of these phenomena (Young *et al*., 1995). In 1998, Sano *et al*. measured *in vivo* the oxidative stress by electron spin resonance spectroscopy in rats with STZ-induced diabetes (Sano *et al*., 1998). In diabetes mellitus, oxidative stress seems to be mainly due to increased production of plasma free radical concentrations and a sharp reduction of antioxidant defenses. Among the causes of enhanced free radical production, hyperglycemia seems to play a major role. Hyperglycaemia is a widely known cause of enhanced plasma free radical concentration. It is generally accepted that high glucose levels for many years are a primary cause of most long-term complications and are caused by the hyperglycaemia-accelarated formation of non-enzymatic glycated products. Non-enzymatic glycation, however, has been recently demonstrated to be linked to glucose auto-oxidative process (Ceriello, 1999). As a result of auto-oxidative reactions reduced oxygen products are formed, which are super oxide anion (O_2^-), hydroxyl radical (OH^-) and hydrogen peroxide (H_2O_2). All can damage proteins through cross linking and fragmentation; and lipids through lipid oxidation (Paolisso *et al*., 1999). At the same time, glycated proteins have been shown to be a source of free radicals. These findings raised the hypothesis of a link between oxidative stress and the development of diabetic complications (Ceriello, 1999). The generation of reactive oxygen species and free radicals has been shown to be increased in patients with diabetes mellitus (Sano *et al*., 1998). There is considerable evidence that oxidative damage is increased in diabetes, though the mechanisms are not clear (West, 2000). Auto-oxidation of glucose results in the

generation of reactive ketoaldehydes and subsequent formation of advanced glycosylation end-products (AGEs). Protein glycation results from the formation of a covalent binding between the aldehydic glucose function and the free amino groups of proteins. In the presence of transition metals (such as cupper, iron), glycated proteins can give an electron to the molecular oxygen, leading to oxygenated free radicals. This property has been shown for the first time by Gillery *et al* (1988) and has been further confirmed by others (Sakurai and Tsuchiya, 1988), even in the absence of transition metal ions (Mossine *et al*., 1999; Ortwerth *et al*., 1998). When the protein half-life is longer than ten weeks, glycated proteins undergo irreversible modifications leading to AGEs (Brownlee *et al*., 1988; Trivin *et al*., 1999). As glycated proteins, AGEs are also able to produce oxygenated free radicals via complex biochemical mechanisms (Mullarkey *et al*., 1990). Wautier *et al*. demonstrated that AGEs on the surface of diabetic erythrocytes bind to the vessel wall via a specific receptor, inducing an oxidative stress in the endothelium (Wautier *et al*., 1994).

1.1.2 Free Radicals

1.1.2.1 Free Radicals in Biological Systems

A free radical can be defined as "any species capable of independent existence that contains one or more unpaired electrons" occupying an atomic orbital by itself. This situation is energetically unstable, often making such species highly reactive and short-lived. Stability is achieved by the removal of electrons from (i.e. oxidation of) surrounding molecules to produce an electron pair. However, the remainder of the attacked molecule then possesses an unpaired electron and has therefore become a free radical (figure 1).

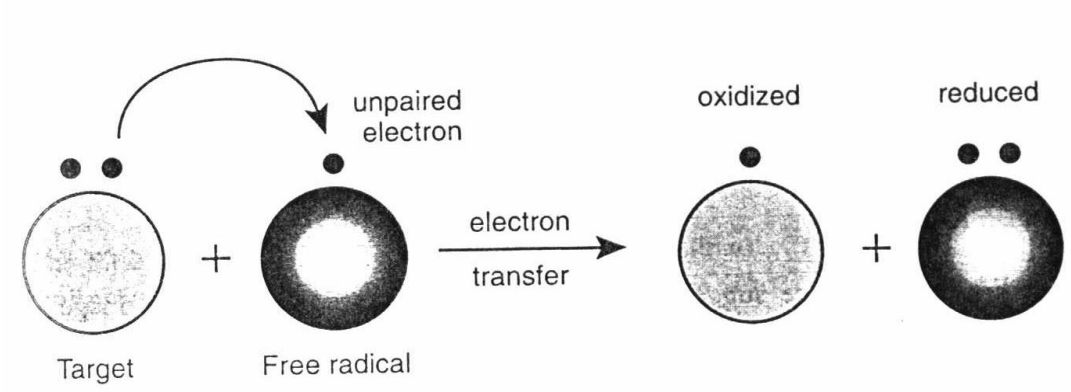

Figure 1. The initiation and propagation steps of lipid peroxidation.

Subsequent events depend on the reactivity of the target radical. If the reactivity of the target radical is high, further target molecules will be attacked and lead to propagation of a free radical chain reaction. In this way, the presence of a single radical may initiate a sequence of electron transfer reactions. In the case of antioxidant targets, the resultant radical has low reactivity and the chain is broken (Maxwell and Lip, 1997a).

Most of the radicals in human biology are derived from oxygen. The reduction of oxygen in the mitochondrial electron transport is necessary to generate energy. However, the reduction is not 100 % efficient and some partially reduced oxygen may leak from the system in the form of superoxide radical ($O_2^{\cdot -}$). Superoxide radicals may form hydrogen peroxide (H_2O_2) either spontaneously or, more rapidly, catalyzed by superoxide dismutase. Neither species is a particularly powerful oxidant but both may interact with transition metal ions, such as Fe^{2+} and Cu to generate the highly reactive hydroxyl radical ($OH^{\cdot}$). The latter is probably responsible for much of the biological damage *in vivo*. Other sources of free radicals include the reperfusion of previously hypoxic tissues, autoxidation of molecules such as glucose, presence of transition metal ions and exogenous sources such as cigarette smoke (Maxwell and Lip, 1997a).

1.1.2.2 The Possible Consequences of Free Radical-Mediated Tissue Damage

All biological macromolecules, such as lipids, proteins, nucleic acids and carbohydrates are nonradical possible targets of free radicals. Reaction of a radical

with a nonradical produces a free radical chain reaction with the formation of new radicals, which in turn can react with further macromolecules. Important examples are lipid peroxidation and protein damage (Stadtman and Oliver, 1991). Lipid peroxidation is perhaps the most extensively studied consequence of free radical attack and is of potential importance in diabetic vascular damage. For these reasons, lipid peroxidation will be described in detail (figure 2). Reactive free radicals, e.g. the hydroxyl radical, have the capacity to abstract a hydrogen atom (H) from a methylene group (-CH_2-) of fatty acids, leaving behind an unpaired electron on the carbon (-CH-). Polyunsaturated fatty acids are particularly prone to free radical attack because the presence of a double bond weakens the carbon-hydrogen bond at the adjacent carbon atom. The remaining carbon-centered radical undergoes molecular rearrangement resulting in a conjugated diene. Conjugated dienes can combine with oxygen forming a peroxyl radical. This is itself able to abstract a further hydrogen atom and begin a chain reaction that continues either until the substrate is consumed or the reaction is terminated by a chain-breaking antioxidant, such as vitamin E.

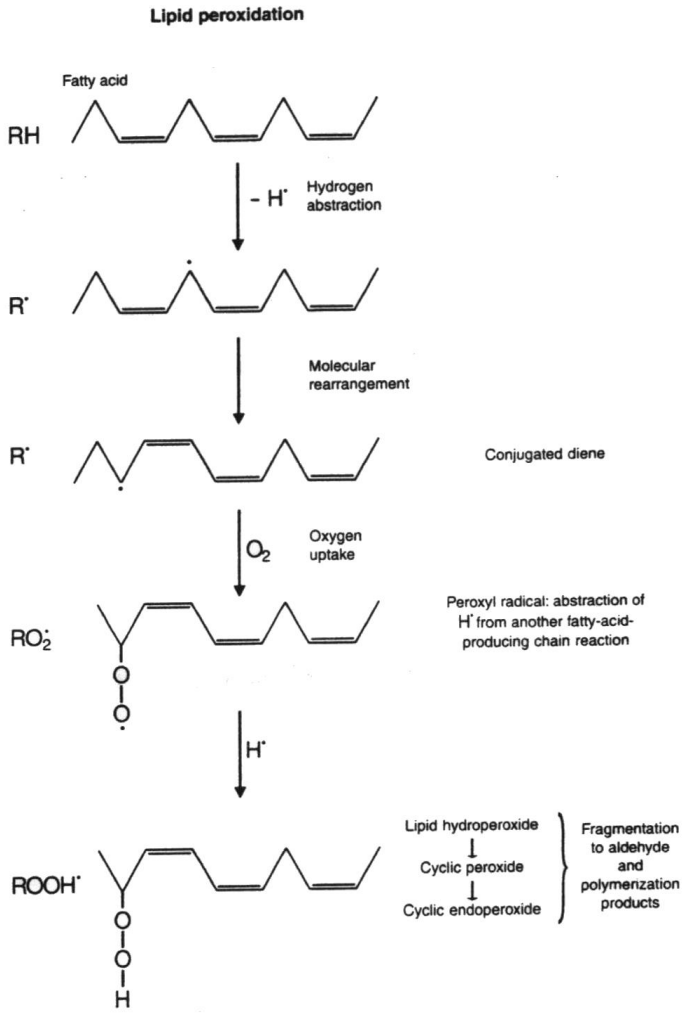

Figure 2. Lipid peroxidation as an example of free radical-mediated tissue damage

The resulting lipid peroxides are reasonably stable compounds, but their decomposition can be catalyzed by transition metals. It is of interest that disrupted tissue is more susceptible to lipid peroxidation. Lipid peroxidation can have profound effects on cellular function. Extensive peroxidation in cell membranes will result in changes in fluidity, increased permeability, a decrease in membrane potential, and eventually membrane rupture (Maccarrone *et al*., 1995; Shertzer *et al*., 1992).

1.1.2.3 Summary of the Biological Influence of the Oxidative Free Radicals

- Free radicals alter structure, composition, and function of the biological cell membranes which are made up of phospholipids (Frol'kis *et al*., 1983).

- Free radicals damage cell membranes by altering permeability and fluidity (Gressier *et al*., 1993).
- Free radicals damage enzymes and proteins which in turn result in cell denaturation. (Ferrari *et al*., 1991).
- Oxidative products bind with nucleic acids and alter their structure and functions (Kamimura *et al*., 1992).
- Free radicals play a vital role in lipid peroxidation.
- Myocardial damage is an important example of adverse chemical manifestation of free radicals (Ahlskog *et al*., 1996).
- Oxidative reactive products have an important role in alteration of smooth aging process (Zarling *et al*., 1993).
- Free radicals play crucial role in the pathogenesis of Parkinson disease (Ahlskog *et al*., 1996), Alzheimer disease (Zarling *et al*., 1993), and other neurodegenerative diseases (Loeffler *et al*., 1995).

1.1.3 Oxidative Stress and Diabetes Mellitus

Oxidative stress occurs when there is an imbalance between free radical production and antioxidant capacity. This could be due to increased free radical formation in the body and/or loss of normal antioxidant defenses (Halliwell, 1994).

An increased accumulation of protein and lipid oxidative products has been noted in the tissues of diabetic subjects (Altomare *et al*., 1992; Altomare *et al*., 1995). This is related to impaired antioxidant capacity of both serum and cells of diabetic patients (Lyons *et al*., 1994; Maxwell *et al*., 1997b). This imbalance is thought to be involved in the genesis of diabetic complications (Baynes, 1991), and originates from impairment of the pentose phosphate pathway, which is due to the deficiency of insulin. This metabolic impairment results in a decreased availability of reduced substrates, such as reduced NADPH (nicotinamide adenine dinucleotide phosphate), and consequently of GSH, because of the decreased glutathione reductase activity, which utilizes NADPH (Cheng and Gonzalez, 1986). The consequence is an increased susceptibility to oxidation of proteins and membrane lipids. One study reported that the plasma lipid peroxides were significantly higher in diabetic patients than healthy controls. In the same study, the level of lipid peroxides in poorly controlled diabetes was higher compared to good control (Penckofer *et al*., 2002). The following things were not reported in the study: type of diabetes,

management (insulin, oral agents, or diet), and analysis by gender. Finally, Nourooz-Zadeh *et al*. examined healthy volunteers and persons with type 2 diabetes mellitus (1997), and reported that the level of lipid peroxides was significantly elevated in those with diabetes. In the same study, the level of lipid peroxides was examined among the diabetics with and without complications of disease, and no significant difference was observed between the two groups. They concluded that oxidative stress may occur in the early stages of diabetes and may in fact contribute to the development of vascular complications associated with this chronic disease.

Oxidative stress is increased in diabetes because of multiple factors (figure 3). Dominant among these factors is glucose autoxidation. Other factors include cellular oxidation/reduction imbalances and reduction in antioxidant defenses (including decreased cellular antioxidant levels and a reduction in the activity of enzymes that dispose of free radicals). Another important factor is the interaction of advanced glycation end products (AGEs) with specific cellular receptors called AGEs receptors (RAGE). Binding of AGEs to their receptors can lead to modification in cell signaling and further production of free radicals (Penckofer *et al*., 2002).

Free radicals, elevated under hyperglycaemic conditions in diabetes influence key factors involved in the development and evolution of cardiovascular disease (CVD) (figure 4). This process can lead to acceleration and amplification of vascular pathology. In addition, pathological changes that occur in the vasculature can stimulate further free radical production resulting in a damaging positive feedback system. Key factors involved in the development and evolution of CVD are 1-abnormalities in plasma lipids, 2- endothelial cell dysfunction, 3- increased vascular reactivity (primarily due to endothelial cell dysfunction, 4- platelet activation and stimulation of the coagulation cascade, and 5-activation of inflammatory processes. These factors are interactive and amplified in persons with diabetes by mechanisms related to the derangement of carbohydrate and lipid metabolism.

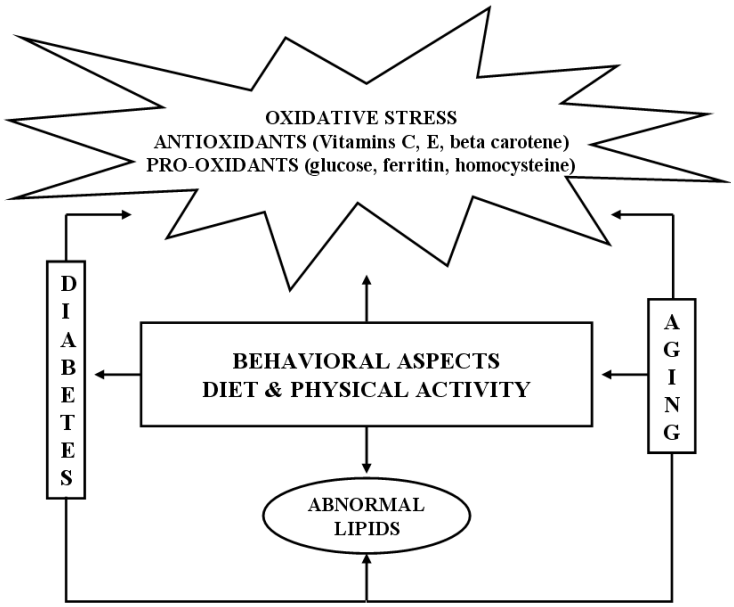

Figure 3. Factors affecting potential for oxidative stress

One of the consequences of these metabolic alterations is increased oxidative stress. In this regard, evidence has clearly linked increased oxidative stress to the acceleration of the development and evolution of CVD (Penckofer *et al*., 2002).

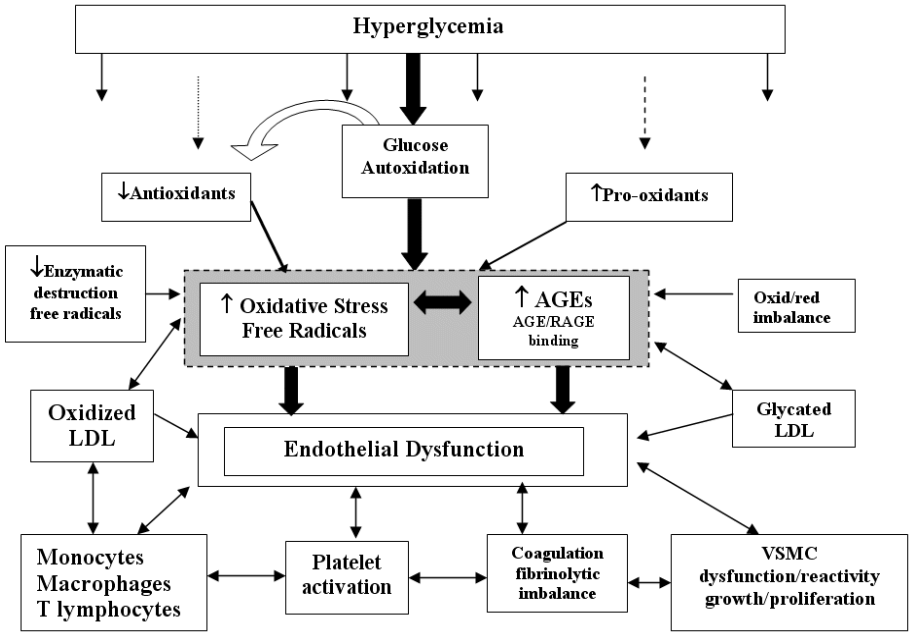

Figure 4. Theoretical association between oxidative stress and cardiovascular disease in diabetes

1.1.3.1 Greater Pro-oxidants and Oxidative Stress in Type 2 Diabetes Mellitus

There are a number of pro-oxidants, particularly glucose, ferritin and homocysteine that may play an important role in increasing oxidative stress (figure 3). The metabolism of these factors may be altered in diabetes. The metabolism of glucose in diabetes mellitus is explained like the following: As stated previously, glucose contributes to the production of reactive oxygen species (ROS) by a biochemical pathway called glucose autoxidation, thereby producing free radicals. Free radicals initiate a cascade of events leading to the generation of lipid peroxides and subsequent damage to membrane proteins.

1.1.4 Antioxidants

An antioxidant can be considered as a molecule that, when present at low concentrations compared with those of an oxidizable substrate, significantly inhibits oxidation of that substrate (Maxwell and Lip, 1997a).

The biologic reduction of molecular oxygen is accompanied by the production of potentially toxic reactive free radical intermediates (Asayama *et al*., 1986). Humans, along with other aerobic organisms, have evolved a variety of mechanisms to protect themselves from the potentially deleterious effects of reactive oxygen species (ROS). These mechanisms include: 1- enzymes, such as catalase, glutathione peroxidase and superoxide dismutases, and repair enzymes such as DNA glycosylases, 2- proteins such as transferrin that can bind metals which stimulate the production of free radicals, and 3-antioxidant vitamins, such as vitamin C and E that act as free radical scavengers (Halliwell, 1994).

In the last few years, there has been a growing interest in the role played by oxidative reactions in human disease. A number of cell functions appear to be up regulated by the release of oxygen free radicals, such as DNA expression and mitochondrial energy production. Several experimental and human pathological conditions have been closely related to an over-production of free radicals or to an impairment of the oxidative/antioxidative balance, which seems to be involved in the

cell differentiation process, activation of specific metabolic pathways, and liver regeneration (Vendemiale *et al*., 1999).

It is important to know whether antioxidant vitamins are protective against the negative effect of oxidative stress observed in diabetics (Paolisso *et al*., 1999). Antioxidant nutrients have received new attention from scientists in many disciplines because of their potential to prevent or delay the development of some chronic diseases.

The biological benefits of antioxidants can be listed like the following (Pandya, 2001):

1. Inhibit vascular cell dysfunction,
2. Diminish cytotoxic effects of oxidized LDL,
3. Inhibit cell mediated LDL oxidation,
4. Inhibit peroxidation of polyunsaturated fatty acids,
5. Inhibit cellular production of reactive oxygen species,
6. Inhibit proliferation of vascular smooth muscle,
7. Inhibit vascular cell necrosis and lesion progression,
8. Provide protection against different types of programmed cell death,
9. Enhance protective immune response.

1.1.4.1 Antioxidants and Diabetes Mellitus

Impaired generation of naturally occuring antioxidants in diabetes can also be expected to result in increased oxidative cell damage (Giugliano *et al*., 1995). Some studies have recently demonstrated that antioxidants, such as vitamin C and E, may reduce in vitro and *in vivo* protein glycation. At the same time some antioxidants act as scavengers of the free radicals produced by non-enzymatic glycation in vitro. Such studies may lead to therapeutic approaches for limiting the damage from glycation and oxidation reactions and for complementing existing therapy for treatment of the complications of diabetes. Diabetes mellitus has been related to alteration in the homeostasis of certain elements such as selenium.

Antioxidants have been found to have potential value in the treatment of diabetes-induced heart disease. Ascorbic supplementation improves myocardial performance in diabetic rats (Dai and McNeill, 1995), and α-tocopherol supplementation inhibits diabetes-induced myocytosis, and prevents autonomic neuropathy in hearts of diabetic rats (Rosen *et al*., 1995). Antioxidants normalize diabetes-induced abnormalities in ATPases, PKC and oxidative stress in other tissues such as retina (Kowluru *et al*., 1999). Since cardiac tissue develops these similar biochemical abnormalities in diabetes, antioxidant might have beneficial actions also on cardiac tissue metabolism. Recent clinical and epidemiological studies suggest that antioxidant treatment might reduce the risk of diabetes-induced cardiac disease (Rosen *et al*., 1998).

1.1.4.2 Antioxidant Defense Against Free Radical Attack

Major antioxidant defense mechanisms can be conveniently considered as cellular, membrane and extracellular mechanisms (Betteridge, 2000). Cellular antioxidant defenses include the dismutase, peroxidase, and catalase enzymes. In addition, the potential for intracellular free radical production is greatly diminished by the ability of mitochondrial cytochrome oxidase to function catalytically in the electron transport chain without releasing reactive oxygen species (Chance *et al*., 1979). Superoxide dismutase (containing cupper and zinc) in cytosol and mitochondria (containing manganese) catalyze the dismutation of superoxide to hydrogen peroxide and oxygen:

$$2O^{\cdot}{}_2^{-} + 2H^+ \rightarrow H_2O_2 + O_2$$

The product of this reaction, hydrogen peroxide, is a weak oxidant and is relatively stable. However, unlike superoxide, hydrogen peroxide can rapidly diffuse across cell membranes, and in the presence of transition metal ions it can be converted to hydroxyl radicals:

$$Fe^{2+} + H_2O_2 \rightarrow Fe^{3+} + {}^{\cdot}OH + OH^{-}$$

Two enzyme systems can break down hydrogen peroxide. Glutathione peroxidases present in cytosol and mitochondria have major role in removing hydrogen peroxide generated by superoxide dismutase with the oxidation of glutathione (GSH):

$$2GSH + H_2O_2 \rightarrow GSSG + 2H_2O$$

Catalases that are present in peroxisomes in many tissues remove hydrogen peroxide when present at high concentrations:

$$2H_2O_2 \rightarrow O_2+2H_2O$$

Antioxidants such as vitamin E, β-carotene, and coenzyme Q are present within cell membranes.

Major extracellular antioxidant defences include the metal binding proteins. The free metals, such as iron and cupper, can promote free radical damage, accelerating lipid peroxidation and catalysing hydroxyl radical formation. The body is protected against these potentially adverse affects by binding proteins such as transferring which ensure that these metals are maintained in a nonreactive state.

1.1.5 Diabetes Mellitus and Cardiovascular Diseases

Cardiovascular disease is the leading cause of death among patients with diabetes mellitus (Panzram, 1987). It is a major health problem throughout the world where approximately 2-3% of individuals are affected (Levander and Burk, 1994). With the development of effective treatment for the infectious, metabolic and renal complications of diabetes mellitus, cardiovascular disease now looms as the most dreaded complication, striking earlier and with greater severity than in the general population. Good management reduces the frequency of complications (Levander and Burk, 1994). Thus the study of the cardiovascular diseases in diabetic patients is of great clinical importance and its prevention, or treatment has become an urgent health care issue in recent years.

The diabetes induced cardiovascular diseases can be examined separately as "diabetes mellitus and its effect on heart" and "diabetes mellitus and its effect on vascular system".

1.1.5.1 Diabetes Mellitus and Heart

Heart disease is one of the leading causes of death among diabetics (Battell *et al*., 1998). Clinical studies utilizing a number of non-invasive techniques have revealed preclinical dysfunctions of the myocardium among a large portion of the diabetic population (Ahmed *et al*., 1975; Rubler *et al*., 1978; Shapiro *et al*., 1981; Sykes *et al*., 1977). Diabetic cardiomyopathy, a kind of heart muscle disease, presents a contractile dysfunction in individuals with no evidence of macrovascular disease and leading to cardiac pump failure. Cardiomyopathy occurs due to altered hormonal and biochemical milieu resulting from the lack of insulin (McNeill, 1996; Parinandi *et al*., 1990). Diabetes-induced cardiomyopathy is now a recognized clinical entity and, in addition, can be induced in experimental animal models of diabetes such as STZ treated rat.

Table 1. Metabolic derangements in diabetic cardiomyopathy.

Metabolic derangements in diabetic cardiomyopathy
Enhanced fatty acid usage leading to reduced ATP synthesis
Carnitin deficiency
Decreased calcium storage and release by the sarcoplasmic reticulum
Decreased myocardial magnesium
Non enzymatic glycosylation of proteins
Abnormalities of the polyol pathway
Alteration in cell membranes and enzyme activity
Reduced K+ currents
Altered myosin isoenzyme distribution and decreased myosin adenosine triphosphate activity

Diabetes mellitus produce cardiomyopathy and myocardial dysfunction that accelerate cardiovascular morbidity and mortality (Kannel *et al*., 1974). Several clinical and experimental studies have indicated that diabetes mellitus is associated with cardiomyopathy independent of atherosclerotic coronary artery disease (Factor

et al., 1981; Hamby *et al*., 1974; Kannel *et al*., 1974; Regan *et al*., 1977; Sohar *et al*., 1970). Various metabolic derangements can contribute to the development of diabetic cardiomyopathy (table 1).

The diabetic myocardium uses ketones, which leads to reduced ATP synthesis (Kainulinen *et al*., 1994; Taegtmeyer and Passmore, 1985). Glatz *et al*. (1994) found higher levels cytoplasmic fatty acid-binding protein in diabetic rats than in respective age-matched controls. This protein may be involved in the enhanced fatty acid usage by the diabetic heart. Decreased calcium binding and uptake by the sarcoplasmic reticulum has been described in diabetic hearts (Lee *et al*., 1992; Yu *et al*., 1994). A decrease in cardiac sarcoplasmic reticulum calcium pump activity was observed in STZ-induced diabetes. The defect in calcium pump activities is not related to changes at the transcriptional or translational levels in the diabetic heart because no reduction was observed in the relative level of the messenger RNA expression of the calcium pump proteins. These abnormalities are corrected by controlling hyperglycaemia with insulin (Zarain-Herzberg *et al*., 1994).

Diabetic cardiomyopathy is characterized by cardiomegaly, ventricular dysfunction, and congestive heart failure (Ahmed *et al*., 1975; Hamby *et al*., 1974; Regan *et al*., 1977; Rubler *et al*., 1978).

Chronic congestive heart failure is a common and serious complication of diabetes mellitus (Kannel *et al*., 1974). Congestive heart failure is twice as common in diabetic men, and five times more common in diabetic women than in age-matched cohorts (Kannel *et al*., 1974). Although congestive heart failure is usually ascribed to the effects of obstructive extramural coronary artery disease (Wohaieb and Godin, 1987), myocardial dysfunction was recently reported to be associated with diabetes mellitus in the absence of extensive coronary artery atherosclerosis (Regan *et al*., 1977). The exact mechanism is still unknown, however several findings have been proposed including microvascular disease, metabolic disorders, and interstitial fibrosis.

It was found in a previous study that, structural changes in patients with diabetes are associated with impaired ventricular performance (Grossman and Messerli, 1996). Over 8 and 16 weeks of diabetes, the left ventricular myocardium of the diabetic rats sustained damage that was progressively more serious with the duration of the diabetic state. In rats after 8 week of diabetes, the myocardium contained large numbers of lipid droplets and glycogen granules around mitochondria which showed patchy swelling, and slight loss of miyofilaments (Hsiao *et al*., 1987).

Most clinical studies of the diabetic heart in failure have the marked diminution of ventricular function (Factor *et al*., 1980a), which is characterized by impairment of left ventricular relaxation and systolic performance (Litwin *et al*., 1990). Kagumi *et al*., studied with the rats treated with STZ to induce diabetes mellitus. Hemodynamic and echocardiographic measurements showed thickening of the wall and an increase in the internal dimension of the left ventricle in diabetes mellitus rats at 8th week. These changes were further developed in diabetes mellitus rats after 12 weeks. Immunohistochemical estimation showed an increase in type IV collagen in diabetes mellitus hearts.

Fein *et al*., (1980) demonstrated prolongation of isometric papillary muscle relaxation in normotensive rats with streptozotocin-induced diabetes. Shapiro (1982) detected abnormal diastolic function by echocardiography in patients with diabetes mellitus who were free from heart disease. The extent of diastolic dysfunction was significantly correlated with the extent of microvascular complications. Systolic impairment in diabetic rat heart model is mainly due to an intrinsic abnormality of the cardiac myocytes (Okayama *et al*., 1994; Yu *et al*., 1994).

As mentioned in the previous paragraphs, there are many studies showing that diabetes mellitus seriously effects the left ventricle. However, the number of studies investigating the effect of diabetes on the right ventricle is rather limited. In one of them (Factor *et al*., 1996) there was evidence, comparable to the observations in men, that the right ventricle was affected by pathological alterations (van Hoeven and Factor, 1990). The right ventricle in these animals was even more damaged then

the left (Fein *et al*., 1989). In another study, it was found that, in the hypertensive diabetic rat, the degree of right ventricular necrosis and fibrosis paralleled that in the left ventricle, but was unexpectedly several times greater in magnitude (Fein *et al*., 1989).

Diabetes-induced alterations in myocardial function include altered intracellular signaling mechanisms (Ingebretsen *et al*., 1981), impaired Ca2+ homeostasis (Gotzsche, 1983a; Gotzsche, 1983b), electrophysiological changes (Shimoni *et al*., 1994), and various metabolic alterations (Horackova and Murphy, 1988; Lopaschuk *et al*., 1992). Malhotra *et al*. have shown that STZ- treated rats show a significant decrease in cardiac contractile protein ATPase activity (1981). Ca2+-ATPase and actin-activated ATPase activities were both depressed in diabetic rat hearts. Furthermore, cardiac relaxation is prolonged in experimental diabetes mellitus (Tomlinson *et al*., 1992), a phenomenon that may be explained by impaired Ca2+ uptake from the sarcoplasmic reticulum in diabetic cardiomyocytes (Penpargkul *et al*., 1981).

Multiple biochemical sequelae of hyperglycemia have been postulated to contribute the heart disease initiated by diabetes (Kowluru *et al*., 2000). Diabetes has been shown to impair (Na-K)-ATPase and calcium ATPase activities of the myocardium (Lopaschuk *et al*., 1983; Ng *et al*., 1993; Zarain-Herzberg *et al*., 1994). And alterations in the activities of these enzymes, possibly by altering ion concentrations in myocytes, have been implicated in the development of cardiomyopathy (Afzal *et al*., 1989; Lopaschuk *et al*., 1983; Ng *et al*., 1993; Schaffer, 1991). Likewise, diabetes increases activity of protein kinase C (PKC) in cardiomyocytes (Inoguchi *et al*., 1992; Lee *et al*., 1989; Shiba *et al*., 1993), which can result in ventricular hypertrophy and impaired contractility. In diabetes elevated levels of free radicals in heart muscle have been reported to be involved in the regulation of activities of both ATPases and PKC (Morris and Sulakhe, 1997; Santini *et al*., 1996; Stauble *et al*., 1994).

It was shown in a previous study that, alterations in cardiac extra cellular matrix (ECM) may be responsible for changing heart function in various disease

conditions based on its adverse influence on myocardial wall stiffness (cardiac compliance) (Liu *et al*., 1999). Abnormal accumulation of ECM has been associated with hypertrophied myocardium, appearing as reactive interstitial and perivascular fibrosis or as replacement fibrosis for necrosed muscle. Alteration of cardiac collagen concentration may contribute to the pathogenesis of heart failure in the cardiomyopathic hamster. From a clinical perspective, cardiac fibrosis associated with reduced compliance has important functional implications, including disturbances in diastolic cardiac filling with attendant loss of normal cardiac output. Thus, any tool that may facilitate the rapid and simple detection of collagen proteins will contribute significantly to the armament of the clinician when diagnosing the onset of heart failure.

Although the routine use of insulin therapy over the past 60 years has dramatically improved the prognosis of this disease, the mortality due to heart disease remains significantly elevated, accounting for more than half of all deaths in diabetic individuals (Thompson, 1988).

1.1.5.2 Diabetes Mellitus and Vascular System

Free radical mediated oxidative stress has been implicated in the pathogenesis of the vessels. Among all cardiovascular causes, coronary artery disease is the leading cause of death among patients with diabetes mellitus. Women with diabetes are at twice the risk of developing coronary artery disease than nondiabetic women (Kannel and McGee, 1979). Diabetes mellitus represents a typical chronic degenerative disease associated with an early onset of atherosclerotic alterations. The high incidence of arteriosclerosis in diabetics has been associated with increased intracellular oxidative stress: an increased accumulation of protein and lipid oxidative products has been noted in the tissues of diabetic subjects. This is related to die impaired antioxidant capacity of both serum and cells of diabetic patients (Vendemiale *et al*., 1999). Thus, antioxidant might be expected to be useful in preventing atherosclerosis (Paolisso *et al*., 1999).

IDDM often leads to coronary atherosclerosis related to hypertriglyceridemia and altered lipoprotein profiles, resulting in vascular insuffiency, ischemia and a markedly increased risk of myocardial infraction (Parinandi *et al*., 1990).

Small-vessel coronary artery disease frequently occurs in diabetic patients (Factor *et al*., 1980b). However, the role of small-vessel disease in the pathophysiology of cardiomyopathy remains unclear. Hamby *et al*., (1974) suggested based on necropsy findings that, changes in the small vessels of the myocardium are responsible for diabetic cardiomyopathy. Fein and Sonnenblick (1985) suggested that diabetic patients have an increased sensitivity to catecholamines, which may cause myocardial ischemia by focal small coronary artery vasoconstriction.

A variety of pathological lesions of the small, intramural arterioles, capillaries, and venules have been described in the diabetic heart. Ultrastructural studies have demonstrated a significant increase in the thickening of the basement membranes of small blood vessels in the diabetic heart (Silver *et al*., 1977). The relative contributions of these lesions to the pathogenesis of the diabetic heart disease are unknown. Small vessel disease is a clinicopathologic syndrome in which myointimal thickening of small coronary vessels (50 to 1000 microns in diameter) leads to a decrease in the diameter of the vascular lumen with consequent microcirculatory compromise.

The defense system in the vessels against oxidative attack is altered by diabetes (Halushka *et al*., 1977; Karpen *et al*., 1982; Valentovic and Lubawy, 1983). However, little is known about the influence of diabetes on the activity of the antioxidant system in blood vessels.

Glucose hypothesis proposes that hyperglycaemia mediates many of the deleterious effects of the disease (Pennathur *et al*., 2001). This hypothesis has gained strong support from recent clinical trials demonstrating that intensive glucose-lowering therapy dramatically reduces the incidence of microvascular disease (DCCT_Research_Group, 1993; Nathan, 1998; UKPDS_Group, 1998). Possible links between glucose and vascular disease include mitochondrial dysfunction

(Nishikawa *et al*., 2000) and production of AGE products (Brownlee, 1995; Bucala and Cerami, 1992). Indeed, glucose promotes protein glycation and AGE product formation in vitro. AGE products accumulate in the tissues of diabetic humans and animals. They also are formed by oxidative reactions in vitro, leading to the proposal that diabetes increases oxidative stress (Baynes and Thorpe, 1999; Brownlee, 1995; Brownlee *et al*., 1988; Bucala and Cerami, 1992; Bucala *et al*., 1993; Sell *et al*., 1992; Sell and Monnier, 1989; Wells-Knecht *et al*., 1995a; Wells-Knecht *et al*., 1995b; Wolff and Dean, 1987; Wolff *et al*., 1991). The findings of these studies support the hypothesis that, glucose-induced oxidative stress contributes to the vascular dysfunction and accelerated atherosclerosis of diabetes.

1.1.6 Selenium and Diabetes Mellitus

Selenium is a trace element whose essentiality in mammals was discovered in 1957. During recent years, interest concerning selenium has increased considerably due to the combined behavior it can have in humans, either as a toxic or an essential element depending on its levels in the environment and food. Thus, when daily dietary intakes of Se exceed the capacity of the human body to eliminate it, some type of intoxication can appear. In 1980, the Food and Nutrition Board of the United States Research Council established the recommended dietary allowances (RDA) for his element as 70 and 55 μg Se/day for a healthy adult man and woman, respectively (Navarro-Alarcon and Lopez-Martinez, 2000). In food, the highest Se content is found in fish products (Hershey *et al*., 1988).

Many studies have been performed in different countries and communities throughout the world, as indicated in table 2, which summarizes the recent literature on Se intake for healthy adults. The Se intakes range from <10 μg/day in Se-deficient areas to approximately 5000 μg/day in those where there exists an endemic selenosis (Robberecht and Deelstra, 1994).

No direct signs for the essential needs of Se in human nutrition were found until 1979, when a research group from China discovered relationships between the low concentration of Se in the geographical area of Keshan in China and a pathology called “Keshan disease”, which was an endemic congestive cardiomyopathy with

myocardial insufficiency. Inadequate dietary selenium can contribute to heart disease, arthritis, hypothyroidism, cataracts, and perhaps even Alzheimer's.

Table 2. Daily dietary intake of Se in human beings from several countries.

Country (Region)	**Mean ± Standard Deviation (µg)**	**Range (µg)**
Belgium	-	28.4-61.1
Netherlands	-	55.9±12.5
USA (Beltsville)	71	-
Spain (Galicia)	95	-
Greece	100±6	68-727
Nepal	23±26	-
Turkey	52±34	-
France	42	-
Finland	42.5	-
Japan	97±22	45-135
Sweden	40±4	-
Germany (Western)	-	38-48
Italy	90	60-90
Netherlands	55.9±12.5	-
Denmark	57	-
Portugal (Pinhel)	37	7-67
USA	-	60-160
New (Guinea)	20	-
Lithuania	100	-
Norway	80	-
Burundi	-	16.9-82.4
Mexico northern	-	60.6-72.9
Croatia	27.3	-

The benefits of adequate levels of selenium in the diet can be attributed in part to its functional role in the antioxidant enzymes, glutathione peroxidases (Selenium is an activating component of the enzyme glutathione peroxidase, which has been shown to protect cells from free radical damage) and its role in controlling the effects of thyroid hormone on fat metabolism (Navarro-Alarcon and Lopez-Martinez, 2000).

Selenium has a large number of biological functions in the human organism (Navarro-Alarcon and Lopez-Martinez, 2000). The most important and known action is its antioxidant effect because it forms selenocysteine, part of the active center of the glutathione peroxidase enzyme (GSH-Px) (Levander and Burk, 1994). On the other hand, in the cell GSH-Px plays an important function, because the reduced form of this enzyme reduces the hydrogen peroxide and lipidic hydroperoxides (Asayama *et al*., 1986). Other molecules, such as the vitamin E and superoxide dismutase enzyme also collaborate in this protection against cellular oxygenated by-products (Levander and Burk, 1994; NavarroAlarcon *et al*., 1998).

In recent years, the scientific concern of Se has increased as a result of the descriptive and prospective studies performed in several countries USA, Germany, Norway, China, Spain, etc. since it seems that low Se levels could be another factor in the origin of some human diseases as cancer, cardiovascular sclerosis, cirrhosis, diabetes, etc. In general, tissues with a high vulnerability to the oxidative stress are those with a high metabolic activity such as liver, heart, diaphragm and striate muscle (Navarro-Alarcon and Lopez-Martinez, 2000).

A review of the literature shows that there is controversy among the different clinical studies performed on the serum Se levels in diabetic patients. Some researchers found a significant decrease in patients with different types of diabetes mellitus (Navarro-Alarcon *et al*., 1999; Twardowska-Saucha *et al*., 1994). Others observed that serum selenium levels were similar in patients and controls (Armstrong *et al*., 1996; Holecek *et al*., 1995; Wang *et al*., 1995). Nevertheless, other investigators even found a statistically significant increase in Se concentrations in diabetic patients to those determined in the control group (Cser *et al*., 1993; Gebre-Medhin *et al*., 1984), which was interpreted as a possible protective mechanism of the vascular system against the aggressiveness of pro-oxidant agents and free radicals (Cser *et al*., 1993; Gebre-Medhin *et al*., 1984). Taking into consideration these contradictory results and the limited number of literature in this field, future research is needed in order to have a better knowledge of the Se metabolism in diabetic

subjects, which could help us to decide the convenience of Se supplementation in these patients.

Nyyssonen *et al*. (1994) established that Se and other antioxidants have a protective effect against oxidation, shown as a higher resistance against the oxidation of serum LDL- and VLDL-cholesterol, in a double-blind clinical trial.

The selenium supplementation as selenate (Becker *et al*., 1996) or selenomethionineqtocopherol acetate (Douillet *et al*., 1996) decreased plasma glucose levels in diabetic rats. This finding has also been observed in diabetic human beings (Wang *et al*., 1995). The Se induces a sustained improvement of glucose homeostasis in diabetic individuals by an insulin-like action (Becker *et al*., 1996; Berg *et al*., 1995). Taking into consideration all these, a Se supplementation with this element cannot be discarded because this element facilitates a better homeostatic regulation of the blood glucose levels and a significant increase in the activity of the GSH-Px enzyme. In 1990, Ezaki reported that sodium selenate has insulin-like effects in vitro in fat cells in that it caused the translocation of glucose transporters to the plasma membrane, and resulted in tyrosine kinase phosphorylation (1990). In this study, Ezaki found that selenate stimulates glucose transport activity in a dose-dependent manner in isolated rat adipocytes. Like insulin, the observed increase in glucose transport activity by selenate was due to translocation of glucose transporters (GLUT-1 and GLUT-2) to the membrane surface. This insulin-like effect of selenate on glucose uptake and metabolism was also more recently studied in rat soleus muscle (Zhong *et al*., 1990). McNeill *et al*., expanded on Ezaki's original observations and showed that selenium also acted as an insulin-mimetic *in vivo* (1991). Insulin mimetic effects of selenite have been reported in diabetic mice in which the selenite treatment was commenced prior to induction of diabetes (Ghosh *et al*., 1994).

Several studies have shown selenate to mimic insulin in regard to glycolysis, gluconeogenesis, fatty acid synthesis, and the pentose phosphate pathway. The increase in the ability of these pathways to shuttle glucose through, maybe due in part to, the increased expression of key enzymes in these pathways. Increased

expression of these important metabolic enzymes is controlled through the insulin signal transduction pathway which selenium does activate (Stapleton, 2000).

Because of these reasons, in recent years, the enthusiasm has surfaced for using insulin-mimetic agents to not only help better define the mechanisms of insulin action but also to investigate the action and possible implications of these agents in the design of future treatments of diabetics (Stapleton, 2000). In 1998, Battel *et al*. found that sodium selenate corrects glucose tolerance and heart function in STZ diabetic rats (1998). In another study, it was reported that oral selenate improves glucose homeostasis and partially corrects liver enzymes in diabetic rats (Becker *et al*., 1996). In a recent study, therapeutic effects of some antioxidants, including Se and lipoic acid, on ocular disorders have been investigated and improved visual acuity has been reported (Head, 2001). Another study about this topic reported the protective role of intra-peritoneally administered Se on the levels of lipid peroxidation in the lens of STZ-induced diabetic rats. The results from this study indicate that selenium can protect the lens against oxidative damage (Naziroğlu *et al*., 1999). In 1998, Douillet *et al*. investigated the effect of selenium supplements on tissue lipids, peroxides and fatty acid distribution in experimental diabetes. The results showed that, Se supplementation in experimental diabetes could play a role in controlling oxidative status and altered lipid metabolism in liver, thereby maintaining favorable fatty acid distribution in the major tissues affected by diabetic complications (Douillet *et al*., 1998; Turan *et al*., 2000). In another study, the effect of nutritional antioxidants, like selenium, on red cell membrane fluidity and blood viscosity in insulin dependent diabetes mellitus was investigated. It was found that reduced selenium concentrations in red blood cells contribute to impaired haemorheology in insulin dependent diabetes mellitus patients (Osterode *et al*., 1996). The protective effect of selenium on kidney of diabetic rats has been investigated by Douillet *et al.* It was found that the beneficial effect of selenium was associated with the protection of kidneys in the diabetic rats which found expression in a significant correction of renal hyper-filtration and in a diminution of the number and severity of glomerulus lesions (Douillet *et al*., 1996). Protective role of intraperitoneally administered vitamin E and selenium on the antioxidant defense

mechanism in diabetic rats have been studied by Naziroğlu and Çay (2001). The results indicated that intraperitoneally administered vitamin E and Se have significant protective effects on the blood, liver and muscle against oxidative damage of diabetes. A novel effect of selenium on STZ-induced diabetic mice was detected in 1994. In this study, the effect of oral administration of sodium selenite on glucose homoeostasis was studied in male Swiss albino mice 6 weeks after they were made diabetic with STZ. Diabetes caused hyperglycaemia (2.5-fold), a marked decrease (4.5-fold) in liver glycogen, a 4-fold increase in the glucose-6-phosphatase activity and significant decrease in plasma insulin levels and protein kinase activity. Although selenium administration in control animals showed no significant effect on various parameters measured, selenite treatment of diabetic mice restored these parameters to near control values. Thus the results showed insulin-like *in vivo* action of selenium in diabetic mice (Douillet *et al*., 1998). It was found by Doillet and co-workers that, in heart and aorta, diabetes produced some changes in lipid content and fatty acid distribution, especially an increase in the heart triglycerides which was also corrected by the Se supplement.

Biologically, mammals have a limited reservoir of selenate and thus need a regular supply through diet and water (Bedwal *et al*., 1993; Daniels, 1996). Recently, selenate supplementation has been popularized by its availability either as a nutritional additive or in combination with antioxidant vitamins. If proven successful as an antidiabetic agent, selenate would be an attractive therapy since it is already available for individual use as oral supplement (Stapleton, 2000).

1.1.6.1 Selenium Bioavailability

Selenium is a micronutrient which causes deficiency or toxicity at quite close concentrations. Therefore it is of importance to know its abundance or deficiency in food (Jaffe, 1992). It is not sufficient to measure the total content, but it is also important to know the bioavailability or amount absorbed and used by the organism. Therefore the Se bioavailability depends not only on its absorption by the intestine but also on its conversion to a biologically active form (Navarro-Alarcon and Lopez-Martinez, 2000).

The technique of evaluation of bioavailable Se is based upon the fact that its absorption and conversion into biologically active forms is different for the several chemical forms of Se (Levander, 1983). The *in vivo* evaluation is the unique and safer technique to evaluate the Se bioavailability. Nevertheless, these procedures are very expensive and difficult; therefore the in vitro methods constitute a good alternative for the study of Se bioavailability, taking the precaution to select the appropriate conditions (Johnson, 1989). On the other hand, there are no perfect animal models in order to study and interpret the micronutrient bioavailability in humans. Taking all this into consideration, to determine the Se bioavailability it is necessary to coordinate the use of *in vitro* and *in vivo* methods using cell, animal and human models (Greger, 1992; Levander and Burk, 1994)

In *in vivo* studies, one effective manner to estimate the bioavailability is by the determination of the GSH-Px activity (Favier, 1993) in blood platelets, which have demonstrated as previously indicated for blood samples, that organic forms enhance the activity of this enzyme compared with selenate or selenite, which can be correlated with the fact that different Se forms follow distinct metabolic pathways in the organism (Thomson *et al*., 1982). In relation to this, Burk (1986) observed the existence of several Se pathways in the human organism depending on its source. The selenomethionine can be stored in a protein pool when the methionine is limited or catabolized with the release of Se which passes to another pool. On the other hand, the selenocysteine is not stored but it is directly catabolized and the resulting Se goes into a pool to be used later. Selenocysteine can also be incorporated into selenoproteins (Levander and Burk, 1994). The inorganic forms selenite and selenate go directly into the pool, from which independent of its origin, all the Se is used in the synthesis of selenoproteins as the GSH-Px and the excess is excreted. If the selenomethionine should be necessary for the cells it would suffer a physiological proteolysis and a delayed release (Favier, 1993). However, when the excretion capacity is overcome, some toxic forms of Se appear in the tissues. Consequently, GSH-Px levels are mainly regulated by the levels of selenocysteine or inorganic forms of Se (Burk, 1986; Ekholm *et al*., 1991; Hassan *et al*., 1990; Lane *et al*., 1991).

Selenium bioavailability has a high enough variability, principally due to the different chemical forms and factors previously indicated that exist in foods. In most vegetables, the Se present is highly available 85-100%, while in seafood it ranges from 20 to 50%, being usually less than 25%, despite the usually highest Se content in seafood. Meat products have a bioavailability for Se of approximately 15 % (Navarro Alarcon *et al*., 1998). Finally, dairy products have the lowest bioavailability ranging from <2 % in ewe milk to 7 % in cow and goat milk (Shen *et al*., 1993).

1.1.6.2 Selenium Absorption and Excretion

In view of selenium's multiple metabolic pathways, it is important to recognize that all forms of Se are not equal. Selenium supplements come in two basic varieties-inorganic salts like selenate (SeO4--) and selenite (SeO3--), and organic compounds like selenomethionine (SeMet).

There are clear differences between selenate and selenite as well, the most important of which is that selenite is much more toxic than selenate both *in vivo* and in vitro (Biswas *et al*., 2000; Biswas *et al*., 1999). In addition, for relatively low doses of Se fed to humans, the absorption of selenate was observed to be greater and the urinary excretion faster than that of selenite, although retention was about the same (Van Dael *et al*., 2001).

Table 3. The absorption of Se.

Absorption (Percent of Se intake absorbed)
Rat: > 90%
Human: 44 -70%
Swine: 72-75%
Dairy Cows: 2848%
Sheep: 40%

Table 4. The excretion of Se.

Excretion
Urine is primary route in monogastric animals
Feces is primary route in ruminants
Amount of Se excreted in bile is small (~2%)
When large quantities of Se are ingested, some is lost in breath as dimethyl selenide

The increased absorption and excretion of selenate may contribute to its lower toxicity compared to selenite. In the presence of stomach acid, selenite is converted

to selenious acid and is further converted to inactive, elemental selenium if vitamin C is taken at the same time (Ganther and Kraus, 1989). In addition, nutritionally important minerals such as copper are capable of forming complexes with selenide, a metabolite of selenite; the resulting mineral complexes can tie up Se and its mineral partner in a form in which both remain metabolically unavailable (Tatum *et al*., 2000). The absorption and the excretion of Se is summarized in table 3 and table 4, respectively.

1.1.7 Heart

1.1.7.1 Basic Anatomy of the Heart

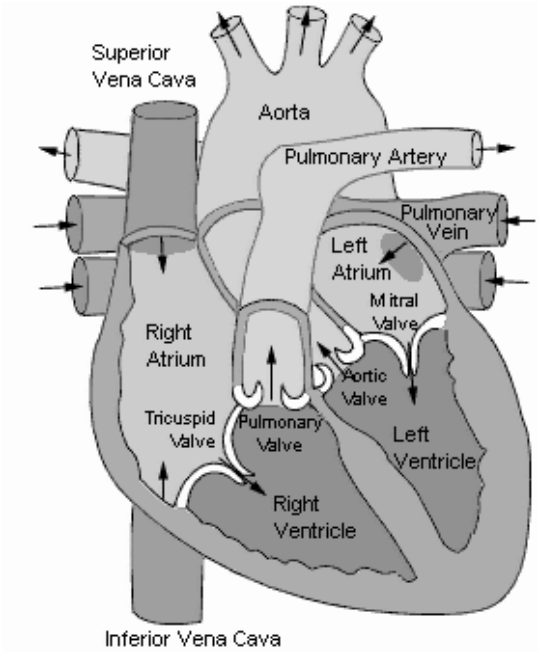

Figure 5. Anatomy of the heart.

The simple anatomy of the mammalian heart is shown in figure 5. The mammalian heart has for chambers. The upper chambers are called the left and right atria, and the lower chambers are called the left and right ventricles. A wall of the muscle called the "septum" separates the left and right atria and the left and right ventricles. The left ventricle is the largest and strongest chamber in the heart. The left ventricle's chamber walls have enough force to push blood through the aortic valve and into the body.

1.1.7.2 Tissues of the Heart

Heart is composed of three distinct layers (figure 6). The outermost layer is the pericardium, which is a serous membrane made up of mesothelium and a layer of loose connective tissue. The middle layer is the myocardium, or muscular wall of the heart. It contains cardiac muscle tissue, other related connective tissues, blood vessels, and nerves.

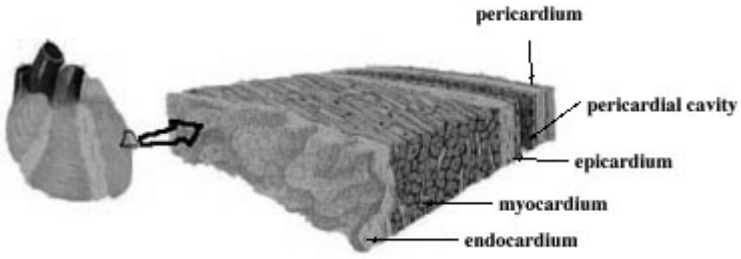

Figure 6. Tissues of the heart.

The cardiac muscle is arranged in concentric layers, which wrap around the atria and spiral around the ventricles. The innermost layer, the epicardium, is composed of squamous epithelium and covers the entire inner surface of the heart including the valves. It continues into the endothelium of the attached blood vessels.

1.2 Part II: Effect of Stereotactic Radiosurgery en Hypoperfused Rat Brain Tissue Homogenates

1.2.1 AVM and Hypoperfusion

AVMs are masses of abnormal blood vessels, which grow in the brain. These are congenital vascular malformations that bypass the blood from the arterial side to the venous side mimicking an arteriovenous fistula. Because of this bypass, blood in the arterial side drains to the venous side and this drainage causes a hypoperfusion (a condition of inadequate tissue perfusion and oxygenation resulting in abnormal tissue metabolism at molecular level.) on the surrounding brain tissue which is called as the steal phenomenon. This phenomenon is caused by the diversion of the blood flow from high resistance tissue capillaries to low resistance AVM nidus. AVM can occur in any area of the brain, and may be either small or large. These lesions are surrounded by a very discrete layer of hypoperfused brain tissue.

AVMs come to clinical attention mainly in young adults, typically before the age of 40. It was reported in a previous study that about 53 % of patients with AVMs present with a hemorrhage (Hofmeister *et al*., 2000). In addition to this, chronic cerebral hypoperfusion is also shown to cause learning and memory impairments (Wang *et al*., 2000).

In the case of hypoperfusion, there is a reduction of both O_2 and glucose supplies (Kawaguchi *et al*., 2002). Since brain cells are unusually sensitive to oxygen lack (Siesjo, 1988) and glucose is the only substrate used by the brain, it is very crucial to investigate the effect of hypoperfusion on brain samples.

1.2.2 Radiation

An entire spectrum of electromagnetic radiations is present in our environment in the form of radio waves, infrared, visible, ultraviolet, x-rays, and gamma rays. The electromagnetic radiations with shorter wavelengths, x-rays and gamma rays, produce both ionization and excitation in the media through which they travel. The biological effects of this radiation apparently result largely from the ionization which is produced (Casarett, 1968).

1.2.2.1 Ionizing Radiation

Ionization normally means the removal of an electron from an atom or a molecule (Mozumder, 1999). Ionizing radiation is a high energy radiation which has the ability to remove electrons from atoms creating ions. The most common kinds of ionizing radiation are X-rays, gamma rays, α and β particles and neutrons. X-rays and gamma rays are electromagnetic radiations with wavelengths in the range 10-11 to 10-7 cm. Those radiations which originate from atomic nuclei are termed gamma rays; those which originate from the inner shells of the electrons are termed X-rays. In all aspects other than the origin, these two radiations are identical (Casarett, 1968).

1.2.2.2 Dose Units

The energy absorbed causes chemical changes. Therefore, dose usually means absorbed dose, defined as the amount of energy absorbed per unit mass of the irradiated material (Mozumder, 1999).

In the measurement of radiation, mainly three units are used:

1) Roentgen (R)

Roentgen is a unit of exposure of X- or gamma radiation based on the ionization that these radiations produce in air. An exposure of one roentgen results in 2.584x10-4 coulomb per kilogram of air. It relates to the quantity of ionization which is called exposure produced by X- or gamma radiation in air and defined as the charge of 2.58x 10-4 coulomb per kg of air (Casarett, 1968)

2) Radiation Absorbed Dose (Rad)

The basic unit of measurement of radiation is called a rad or CentiGray (Cameron and Skofronick, 1978). The rad is a unit of absorbed dose. This relates to the amount of energy absorbed per gram of material, and is used for any type of radiation and any material. One rad is defined as the absorption of 100 ergs per gram of material. Instead of rad, the international unit, Gray is used for absorbed dose; it is defined as being equal to 100 rads.

3) Roentgen Equivalent Man (Rem)

The rem is a unit used to derive a quantity called equivalent dose. This relates the absorbed dose in human tissue to the effective biological damage of the radiation. To determine equivalent dose (rem), you multiply absorbed dose (rad) by a quality factor (Q) that is unique to the type of incident radiation (Casarett, 1968).

1.2.2.4 X-rays

X-rays are the most common sources of radiation exposure for the general public, because they are so commonly used in dentistry and medicine. Since X-rays move at the speed of light, they penetrate and accordingly travel through material easily.

The machine source of ionizing radiation is the X-ray generator. An X-ray is a wave-form of energy similar to light. Unlike accelerated electrons, X-rays have great power to penetrate some materials. The shorter wavelength radiation with its

higher penetrating power is said to be hard, whereas the radiation of lower penetrating power is soft. Also X-rays are produced when the electrons from the accelerator are stopped by a metal target.

The primary effect produced by X-rays in atoms is in every case excitation or ionization. Another fundamental effect is the formation of secondary X-radiation (X-ray scattering). The two types of X-ray spectrum are due to two kinds of origin of radiation, namely Bremsstrahlung and characteristic radiation. Bremsstrahlung gives the continuous spectrum, whereas the other type, the characteristic radiation, is responsible for the line spectrum. The Bremsstrahlung is produced by electrons colliding with the atoms and subsequently being stopped by the atomic force field (or more precisely by the atomic nucleus rather than the whole atom). The characteristic radiation, on the other hand, is produced by the atoms of the anode, and is characteristic of the anodic target material. The greater part of the energy of the emitted radiation, and consequently its power is due to the Bremsstrahlung.

The optical spectrum provides information about the changes in the state of the outer electrons, also called “optical electrons”, and thus about processes occurring in the outer energy levels, the characteristic X-ray spectra shed light on the processes within the inner electron shells. Optical spectra are generated by exciting the outer electrons from the state with principal quantum number n=4 into some higher unoccupied state (possibly in the continuum), after which the electron returns in one or more steps to the level of the principal quantum number n=4. X-radiation, however, is generated if some of the electrons of the inner shells are excited to higher levels or into the continuum and the electrons in higher energy state return to the holes generated by the excitation in these shells. In order for X-radiation to be produced, the creation of free sites or holes in the inner shells is necessary. The differences between the inner energy levels are much larger than those in the optical range, and hence the energy of X-ray photons is much larger than the energy of optical photons.

Excitation can be created by any charged particle (e.g. on alpha particle) striking some target with sufficiently high energy. Excitation of ionization is always accompanied by the release of characteristic X-radiation (Tarjãan and Berkes, 1987).

Transitions also exist in which both the initial and final states belong to continuous energy range (the continuum). In this case free electrons pass over from one state into another. Two possibilities exist: the free electron returns from a higher to a lower state, or conversely the transition is from a lower to a higher energy state. In the first case, the electron becomes decelerated in the atomic or ionic force field, while in the second it is accelerated. The first case maybe accompanied by the emission of radiation, whereas in the second case radiation maybe absorbed. Since both the initial and the final states now lie in the continuous energy range. From the practical viewpoint, especially emission spectra induced by the deceleration of high-velocity electrons in the force field of an atom or ion are important. The decelerated electrons lose various amounts of energy. The energy maybe lost step by step in small doses, or it maybe lost in a single act. The various energy loses result in the emission of photons of various energies.

1.2.2.5 Biological Effects of Ionizing Radiation

The two terms are important in order to express the radiation-induced damage on molecules quantitatively. These are, namely, G value and D37 dose.

G value is the number of molecules (damaged or formed) changed per 100eV of absorbed energy. That is;

G = Number of molecules changed/100eV of energy absorbed

D_{37} dose is the dose, which damages 63 % of the molecules (leaving 37 % of the molecules undamaged) (Altman *et al*., 1970).

The ions and excited molecules resulting from radiation action produces free radicals, which are highly reactive species because of their distinguishing feature, an unpaired electron or lone electron in the outermost shell.

1.2.2.5.1 Mechanisms of Damage

Injury to living tissue results from the transfer of energy to atoms and molecules in the cellular structure. Ionizing radiation causes atoms and molecules to become ionized or excited. These excitations and ionizations can:

1. Produce free radicals.
2. Break chemical bonds.
3. Produce new chemical bonds and cross-linkage between macromolecules.
4. Damage molecules that regulate vital cell processes (e.g. DNA, RNA, proteins).

The cell can repair certain levels of cell damage. At low doses, such as that received every day from background radiation, cellular damage is rapidly repaired. At higher levels, cell death results. At extremely high doses, cells cannot be replaced quickly enough, and tissues fail to function.

1.2.2.5.2 Tissue Sensitivity

In general, the radiation sensitivity of a tissue is:

- proportional to the rate of proliferation of its cells
- inversely proportional to the degree of cell differentiation.

For example, in table 5, tissues and organs are listed from most radiosensitive to least radiosensitive.

Table 5. List of tissues and organs from most radiosensitive to least radiosensitive

Most Sensitive	**Tissues and Organs**
	Blood-forming organs
	Reproductive organs
	Skin
	Bone and teeth
	Muscle
Least Sensitive	Nervous system

1.2.3 Radiosurgery and AVM

Different management strategies exist for AVMs of the brain. Radiosurgery is one of the accepted treatment modalities of AVM therapy. During the past two decades, stereotactic radiosurgery has been widely used for the treatment of cerebral AVM (Kurita *et al*., 2000). Several authors described successful radiosurgical results of AVMs located in the critical areas of the brain (Lawton *et al*., 1995; Lunsford *et al*., 1991; Sasaki *et al*., 1998; Steiner *et al*., 1992; Yamamoto *et al*., 1995). AVM obliteration and attendant low morbidity rates indicate that radiosurgery is a reasonable alternative to operative resection, especially for small AVMs and those that carry unacceptably high surgical risk (Hadjipanayis *et al*., 2001). Single fraction radiosurgery is effective treatment for AVMs provided the whole region to be treated with adequate biologically effective doses in order to achieve complete angiographic obliteration (Wigg, 1999). In this technique, single multi-port high dose, precisely collimated ionizing radiation is aimed to precisely defined target in sub millimetric errors. As the ionizing radiation is given in single high dose, the target definition must be very precise because it damages the target tissue independent of its biological nature. As a result, side effects may occur in brain tissue. With radiation therapy, the risk of radiation-induced injury of the healthy tissue depends largely on the cumulative dose, the volume irradiated, and the dose rate (Rubin *et al*., 1992).

Stereotactic radiosurgery is a specific type of an external radiotherapy technique in which multiple highly collimated radiation beams stereotactically aimed at a limited volume of tissue to deliver a single high dose of radiation. Stereotactic radiosurgery was pioneered by Lars Leksell (Solberg *et al*.., 1998). This technique offers the potential advantage of complete AVM obliteration within three years in 80 to 95 % of small AVMs (Flickinger *et al*., 1996; Lunsford *et al*., 1991). Biologically, the goal of radiosurgery is always the same despite the indication: precise damage limited to tissue within the target volume. Stereotactic radiosurgery, technique is widely used to treat benign lesions, such as arterivenous malformations, meningiomas, acoustic neurinomas and pituitary adenomas, and for malign lesions treated with external beam radiation previously. The aim of the stereotactic radiosurgery is to protect the surrounding brain tissue from the adverse effects of

ionizing radiation as much as possible. This is achieved by optimal targeting and precisely calculated doses.

Normal adult brain parenchyma in humans seems to be more radioresistant than the corresponding volume of AVM. The reasons for the higher radiosensitivity of an AVM's nidus compared with normal brain tissue are poorly defined. It is believed that the primary effect of radiation therapy on the nidus of an AVM is the induction of a microscopic scar process that eventually extends, resulting in vascular shrinkage (Pellettieri and Blomquist, 1999).

1.2.3.1 Radiosurgery and Hypoperfusion

The effects of ionizing radiation is unknown on the chronically hypoperfused brain. Both the oxidative stress and ionizing radiation are cytotoxic. DNA is damaged by the ionizing radiation via a direct and an indirect effect caused by the free oxygen radicals, which are also produced in acute ischemia. The indirect effect is more responsible for the DNA damage. In the indirect effect, free oxygen and hydroxyl radicals are produced due to the ionization of water in the cell, which are toxic molecules for the cell.

1.2.4 FTIR Spectroscopy and Tissue Studies

FTIR spectroscopy is a valuable technique due to its high sensitivity in detecting changes in the functional groups belonging to tissue components, such as lipids, proteins and nucleic acids. Traditionally, interpretation of infrared spectra of complex samples such as tissues follows the classical "group frequency" approach, in which absorption bands are assigned to specific vibrational modes of particular functional groups based on comparison with model systems. Using the group frequency approach to spectral analysis, the absorptions can be assigned to vibrational modes of chromophores within proteins, lipids, carbohydrates and nucleic acids. In the present study, the same approach was employed. The shift in the peak positions, bandwidths and the intensity of the bands all give valuable structural and functional information, which may have diagnostic value (Ci *et al*., 1999; Lui *et al*., 1996; Severcan *et al*., 2000; Yano *et al*., 1996). FTIR spectroscopy technique has

been previously applied to rat brain to investigate the effect of estradiol and tamoxifen on rat brain membranes (Dicko *et al*., 1999). It has been established that FTIR spectroscopy has an increasingly important role in the field of pathology. Disease-induced changes can easily be detected with this technique. FTIR spectroscopy has been used in characterization of tissues from cancer, Alzheimer's disease, arthritis and multiple sclerosis (Gentner *et al*., 1998).

1.2.4.1 Spectroscopy

Spectroscopy is the study of interaction of electromagnetic waves with matter. Electromagnetic wave consists of mutually perpendicular electric and magnetic fields, which oscillate sinusoidally as they propagate through space (figure 7). When such a wave interacts with matter, it can be scattered (i.e. its direction of propagation changes), absorbed (i.e., its energy is transferred to the molecule) or emitted (i.e., energy is released by the molecule) (Campbell and Dwek, 1984).

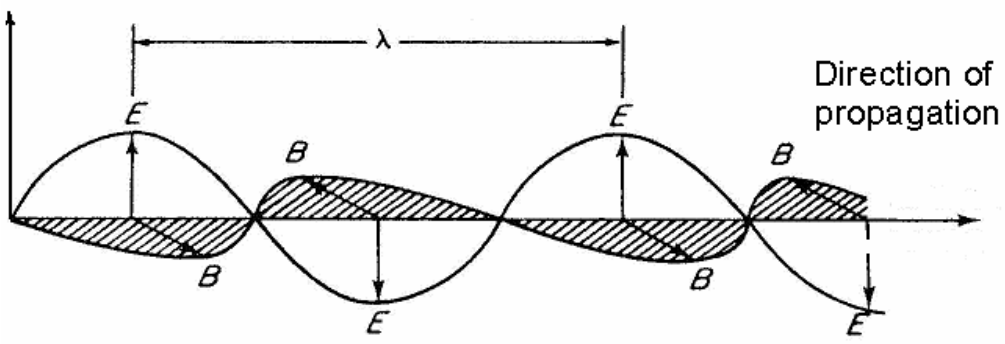

Figure 7. Electromagnetic wave

The velocity of the electromagnetic wave c (≈3.108 m/s) is the product of the wavelength λ (the distance between adjacent peak) and the frequency ν (the number of cycles per second).

$$c = \lambda \times \nu$$

During the 19th century scientists made the hypothesis that light some time behaves as if its energy were concentrated in discrete bundles called photons (light

quanta). Therefore, the energy of the photon (which is equal to the energy of electromagnetic wave) is:

$$E = h \times \nu = \frac{h \times c}{\lambda}$$

where h is the Planck constant (h=6,262x10-34 Js) and ν is frequency.

1.2.4.1.1 Infrared Spectroscopy

Infrared spectroscopy, which is used in wide variety of scientific fields, is one of the most important absorbance techniques available. It is a non-destructive tool, which gives information about the structure of material by investigating interaction between electrical component of the infrared radiation and matter. The IR region of the spectrum extends from the visible region until it overlaps the microwave, or very short radar, range at wavelengths of some millimeters (figure 8) (Naumann, 2000).

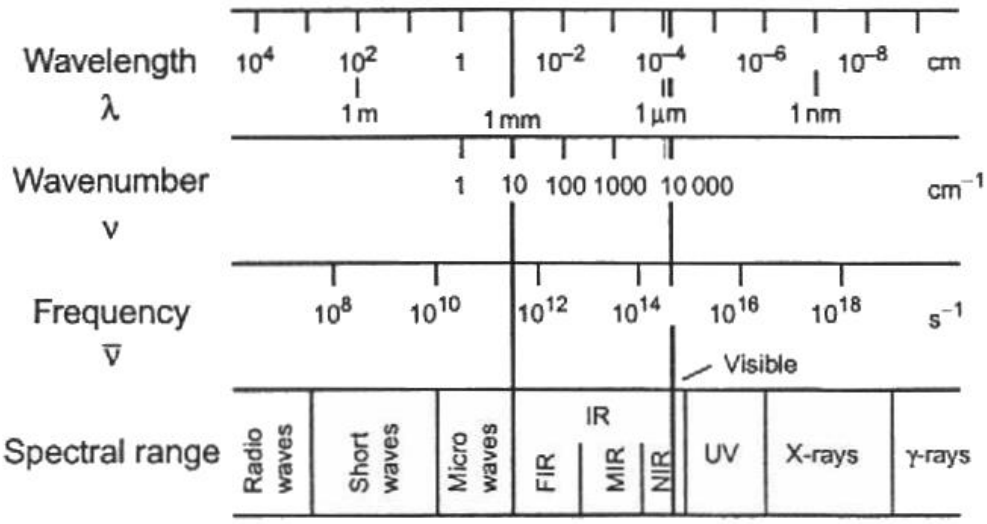

Figure 8. The electromagnetic spectrum

An Infrared spectrum is obtained by passing radiation through a sample and determining what fraction of the incident radiation is absorbed at certain energy. The energy at which any peak in an absorption spectrum appears corresponds to the frequency of a vibration of a part of a sample molecule. Infrared spectrum is graph of wavenumber vs. absorbance (or transmittance) as a measure of band intensity, where

wavenumber is number of waves in a length of one centimeter and the unit used is cm^{-1}. Wavenumber has an important advantage of being linear with energy. It is given by the following relationship (Freifelder, 1982):

$$\bar{\nu} = \frac{1}{\lambda} = \frac{\nu}{c}$$

An IR spectrum of a sample is obtained by scanning the intensity of IR radiation before and after passage of the IR beam through the sample. The IR spectrum is displayed by plotting the quantity T=I/Io as a function of wavenumber, where T is the transmittance, I the intensity of the Io beam after and I before passing through the sample. In most cases the absorbance A is used (A = -logT), since the absorbance at a given wavelength is directly proportional to the concentration of a sample according to the Beer's Law which is given below:

$$A = \log_{10}\left(\frac{I_o}{I}\right) = \varepsilon dc$$

where A is the absorbance, Io is the intensity of the incident light, I is the transmitted intensity, ε is the extinction coefficient which reflects the transition probability, c is the concentration of the sample, and d is the thickness through which radiation is traveling. Despite the fact that infrared spectrum is represented by the plot of absorbance as a function of wavenumber. The extinction coefficient (ε) is rarely used as a parameter of infrared spectra. Rather, the position and the width of the maximum of the absorption band (expressed in cm^{-1}) are the main experimental parameters of the infrared spectra (George *et al*., 1987).

The IR spectra of most materials consist of a large number of absorption bands. These bands originate from the interaction (energy exchange) between discrete light quanta and mechanical motions (vibrational and rotational modes) of the molecules which are excited by the absorption of IR radiation. Since the constituents of a typical biological sample are present in a condensed phase (solids, liquids or solutions), only vibrational modes are observed. Consequently, IR spectra of biological specimens are only vibrational spectra (Colthup *et al*., 1975).

1.2.4.1.2 Physical Basis of Infrared Spectroscopy

A molecule is not static. It is constantly in motion relative to its center of mass. The atoms in a molecule can undergo different kinds of motion, including vibrations and rotation about a bond. We are actually interested in vibrational motion whose frequency value happens to be in the same frequency range with that of infrared radiation. Stretching and contracting during molecular vibration is similar to the behavior of a spring (i.e. simple harmonic oscillator). For linear diatomic molecules consisting of "a" and "b" atoms, there is one mode of vibration-stretching of the bond and the vibration frequency is equal to:

$$\nu_{vibration} = \frac{1}{2\pi}\sqrt{\frac{k}{\mu}}$$

where k is the constant and μ is the reduced mass of molecule, which is represented by the following equation:

$$\frac{1}{\mu} = \frac{1}{m_a} + \frac{1}{m_b}$$

The equation of vibrational frequency can be modified to give the Wavenumber values.

$$\bar{v} = \frac{1}{2\pi c}\sqrt{\frac{k}{\mu}}$$

A molecular potential curve for an ideal diatomic molecule which oscillates around equilibrium bond length R0 is like on figure 9.

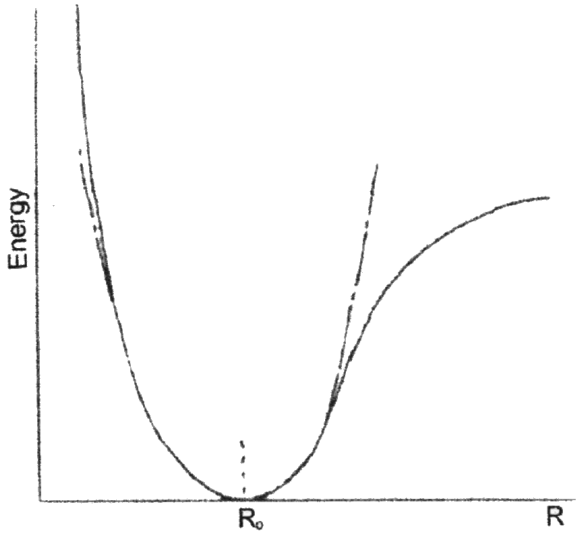

Figure 9. A molecular potential curve for an ideal diatomic molecule which oscillate around equilibrium bond length R0.

For a molecule which has n atoms, there exists 3n degrees of freedom (because of x, y, z coordinates for each atoms). For co-linear molecules, because of two possible rotational degrees, there are 3n-5 degrees of freedom of vibration (Marion and Thornton, 1988).

Different descriptive names are often given to vibrational modes. Vibrations can be subdivided into two classes, depending on whether the bond length or angle is changing: 1) Stretching (symmetric and asymmetric), 2) Bending (scissoring, rocking, wagging and twisting

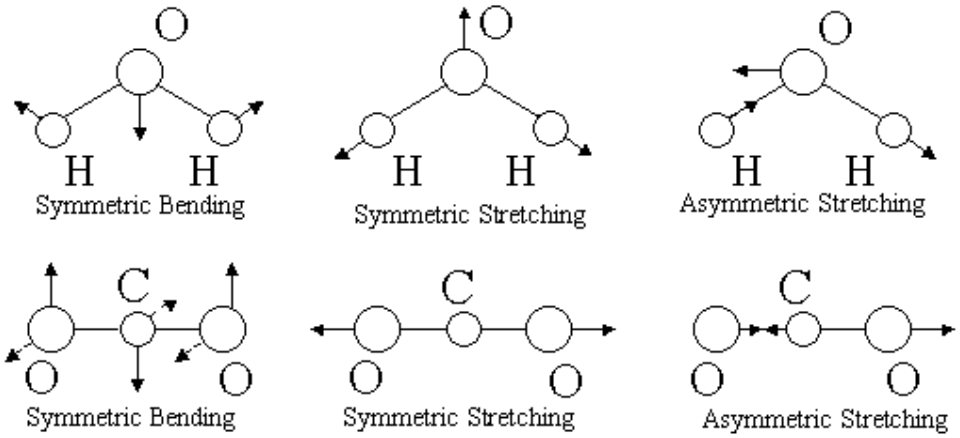

Figure 10. Normal modes of vibration of H_2O molecules and CO_2 molecule.

Real molecules do not obey the laws of simple harmonic oscillator. Motion of molecules can be represented by superposition or combination of all these fundamental modes of vibration. Therefore, the potential energy curve for real molecules is clearly more complex than that on the figure. The Morse curve on figure 11 shows the real graph of complex molecules.

In order to understand the curve, an important concept arising from wave mechanics should be remembered: energy states are quantized and only certain values of energy are allowed. The horizontal lines on the Morse curve represent allowed vibrational energies. These energy values represent the characteristics of the molecule. At higher energy values, the spacing between lines decreases. So, this shows that the oscillation done is harmonic.

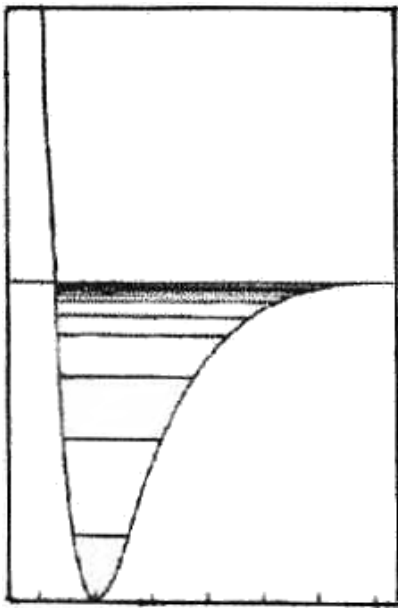

Figure 11. The Morse potential energy curve of a molecule. The horizontal lines represent the allowed vibrational energy (Campbell and Dwek., 1984).

1.2.4.1.3 Infrared Active Vibrations

For a vibration to give rise to absorption of infrared radiation, there are two criteria:

- A molecule should have a frequency of vibration similar to electromagnetic wave.

- Change of dipole moment should take place.

1.2.4.1.4 Resolution Enhancement of Infrared Spectra of Biological Systems

An IR spectrum is comprised of a number of overlapping bands. It is possible to separate out much of the underlying band structure from such a spectrum, leading to narrower bands. This does not increase the instrumental resolution, but it increases the degree to which individual component bands can be visualized. Therefore, this operation is often referred to as resolution enhancement of an IR spectrum.

An experimentally measured IR spectrum consists of the true spectrum perturbed by instrumental distortion. This distortion is of two kinds: i) irregular intensity fluctuations which comprise the random noise and ii) systematic instrumental errors which we can consider collectively as being induced by an "instrument function" (Mantsch *et al*., 1986).

1.2.4.1.4.1 Fourier Deconvolution

Fourier deconvolution is a widely used approach to extract information on protein secondary structure from infrared spectra. This procedure decreases the widths of infrared bands, allowing for increased separation and thus better identification (visualization) of the overlapping component bands present under the composite band contour. Increased separation of the overlapping bands can also be achieved by calculating the nth derivative of the absorption spectrum. A distinct advantage of the Fourier deconvolution method is that it introduces less distortion to the spectra. In particular, it does not affect the integrated intensities (areas) of the individual component bands (Surewicz *et al*., 1993).

1.2.4.1.4.2 Curve Fitting Analysis

The general tendency in the curve fitting analysis has been to assign in a unique way the individual bands resolved in the Amide I region to well-defined types of secondary structure. This procedure involves curve fitting of deconvolved Amide I band as a linear combination of individual component bands by iterative adjustment of heights, widths and position of these bands. The resulting fractional areas of the

bands assigned to different types of secondary structure have been assumed to represent percentages of these structures in a given protein. This procedure provides highly accurate estimates of protein secondary structure (Byler and Susi, 1986).

To perform curve fluting analysis, the following information should be obtainable:

1. An accurate determination of the number of peaks,
2. Knowledge of the true peak shapes, such as Gaussian and Lorentzian,
3. An approximate estimate of the peak parameters, such as height and width.

1.2.4.1.4 Fourier Transform Infrared Spectroscopy

FTIR method is based on the interference of radiation between two beams to yield an interferogram. The interferogram is a signal produced as a function of the change of path length between two beams. For rapid-scanning interferometers liquid nitrogen cooled mercury cadmium telluride (MCT) detectors are used. For slower scanning types of interferometer, pyroelectric detectors (e.g. a deuterated triglycine sulfate (DTGS) detector element) can be used. The interferometer can be thought of a means of encoding the initial frequencies into a special form which the detector can observe. The most important feature of the interferogram is that every individual data point of this signal contains information over the entire IR region. In essence, the detector is always observing all frequencies at the same time. The Fourier Transformation is simply a mathematical means of sorting out the individual frequencies for the final representation of an IR spectrum (Griffiths and De Haseth, 1986).

The radiation emerging from the source is passed to the sample through an interferometer before reaching a detector. Upon amplification of the signal in which high frequency contributions have been eliminated by a filter, the data is converted to a digital form by an analog-to-digital converter and then transferred to a computer for Fourier transformation to be carried out (figure 12) (Stuart and Ando, 1996).

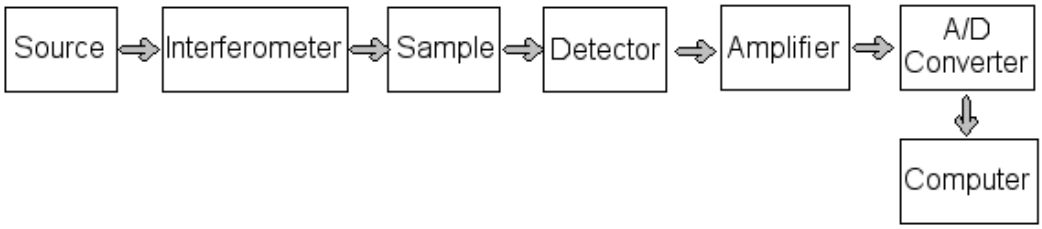

Figure 12. FTIR instrumentation.

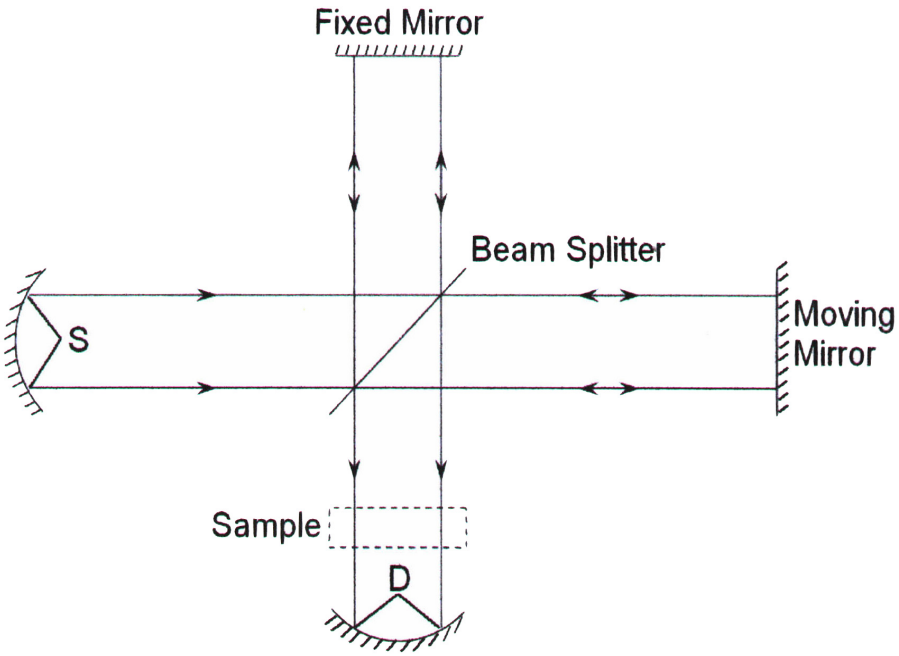

Figure 13. Michelson type interferometer (George *et al*., 1987).

The most common used interferometer is Michelson interferometer (figure 13). It consists of two perpendicular plane mirrors one of which can travel in a direction perpendicular to the plane. A semi-reflecting film called the beam-splitter bisects the planes of these two mirrors. When a collimated beam of monochromatic radiation of wavelength λ pass through an ideal beam-splitter 50 % of the incident radiation will be reflected to one of the mirrors, and the other 50 % will be transferred to the other mirror. The two beams are reflected from these mirrors returning to the beam splitter where they recombine and interfere. 50 % of beam reflected from the fixed mirror is transmitted through the beam-splitter and the other

50 % is reflected back in the direction of the source. The beam, which emerges from the interferometer at 90 degrees to the input beam, is called transmitted beam and this is the beam, which is detected in FTIR spectrometry (Stuart and Ando, 1996).

The cells used for FTIR acquisition are made up of NaCl, KBr, CaF_2 or LiF, which are virtually transparent to infrared, unlike glass which has very high absorbance in the conventional infrared range. Studies of biological samples are usually done in water, so for these samples, water insoluble cells, like CaF_2, LiF, and ZnSe must be used (Freifelder, 1982).

To minimize water vapor perturbations in the sample compartment, it is necessary to purge the instrument with dry Nitrogen or dry air (Wu and Lentz, 1991). Besides, to minimize the effect of molecules (H_2O and CO_2) in the air, it is necessary to renew background spectrum before doing any operation with FTIR spectroscopy.

1.2.4.1.5 Advantage of IR Spectroscopy

Any kind of material can be measured and that is not limited to the physical state of the sample. Samples maybe solutions, viscous liquids, suspensions, inhomogeneous solids or powders (Colthup *et al*., 1975).

There are no principle restrictions to recording IR spectra of a given sample under very different physiochemical conditions with respect to temperature, pressure, state of dispersion, pH and so on. This is of advantage for biomedical analyses, since it is imperative to test biological specimens under conditions that leave the sample's structure "as they are", preferentially hydrated, unperturbed and nondisintegrated (Naumann, 2000).

FTIR method is a rapid and sensitive technique with sampling techniques that are easy to use.

Since a computer is already used to obtain the Fourier transform, it is easy to perform many scans to improve the signal-to-noise ratio (noise adds up as the square root of the number of scans, whereas signal adds linearly).

Digital subtraction (that is, point-by-point subtraction of the separate spectra by a computer) can also be used to produce good difference spectra. This method has great advantages in obtaining infrared spectra in aqueous solutions (Campbell and Dwek, 1984).

A non-perturbing technique, since it can be applied to biological membrane preparations in a straightforward manner, which does not involve introduction of exogenous probes or potentially harmful preparative procedures. This eliminates problems that occur with other techniques involving extrapolation of results from the probe containing to the native system.

Frequency and bandwidth values now can be determined routinely with uncertainties of better than +0.05 cm^{-1}.

1.2.4.1.6 FTIR Microspectroscopy

The combination of a microscope with an infrared spectrometer results in a powerful instrument, called FTIR microscopy (figure 14) that allows for the detection of chemical species from a specific spatial region. Combining spatial specificity with information on its chemical constitution, a chemical species map may be constructed for the whole spatial area. This typically involves collecting the IR spectrum of the sample at a point, moving the sample to another location and collecting the spectrum at the second point and so on. In this manner, the whole area is mapped point-by-point.

Fourier transform infrared microspectroscopy is a powerful technique that can be used to collect infrared spectra from microscopic regions of tissue sections. The infrared spectra are evaluated to chemically characterize the absorbing molecules. This technique can be applied to normal or diseased tissues. In this latter case, FTIR microspectroscopy can reveal chemical changes that are associated with discrete regions of lesion sites, which can provide insights into the chemical mechanisms of disease processes (LeVine *et al*., 1999).

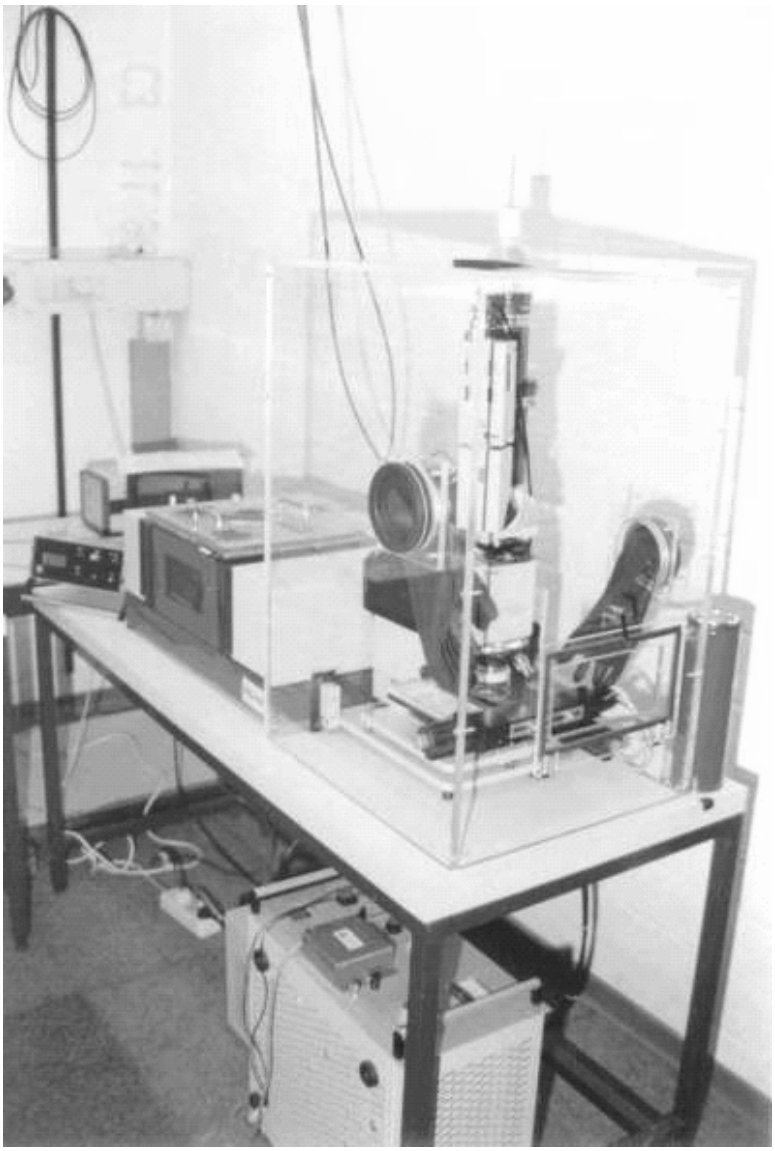

Figure 14. IR Microscope connected to a IFS48 FT-IR Spectrometer (Bruker).

The value of infrared microscopy is two fold. Firstly, it allows the analysis of very small samples of the order of 12 μm2 containing minute quantities of material. The practical advantage of this sensitivity is that it allows the analysis of trace deposits of biological materials in situ, without extraction. Secondly, infrared microscopes equipped with computer controlled stages allow the distribution of materials within tissue sections to be mapped with a high spatial resolution. This approach, termed functional group mapping, can provide a valuable aid for understanding spectral data as the distribution of a number of chromophores within tissues can be analyzed. It may be expected that functional groups arising form the

same molecule will show a similar distribution within a tissue, and therefore a comparison of the distribution of assigned and unassigned absorptions can be used to aid assignments (Jackson *et al*., 1998).

1.2.5 Aim of the Study

Among the diverse number of pathologies, we have chosen to study diabetes mellitus. Diabetes mellitus, having a prevalence of 16 million according to 1997 estimates, and an incidence of about 1700 new diagnosis everyday, certainly deserves a detailed study to explain the underlying mechanism of it.

Long-standing diabetes has been documented to cause structural and functional cardiac impairment and to lead to ischemic heart disease, cardiomyopathy, and congestive heart failure (Grossman and Messerli, 1996).

There is a great deal of study about the effect of diabetes on many types of organs (like heart, liver, eyes, kidney, brain, vascular system) and the therapeutic effects of various antioxidants (like selenium, lipoic acid, vitamin C, vitamin E) on diabetic individuals. Although the therapeutic effects of these antioxidants on diabetic organs are shown experimentally in many studies, the molecular mechanism behind these effects has not been demonstrated yet.

In the recent years, there has been a growing interest in the role played by oxidative reactions in human diseases, and diabetes mellitus is one of them. It has been shown that, protein and lipid oxidative products accumulate in diabetes (as it is mentioned in the introduction part). The findings show that, oxidative stress contribute to the development of complications in diabetes mellitus. Increased oxidative stress may arise either as a result of increased free radical production or reduced activity of antioxidant defenses and there is evidence for both of this phenomena in patients with diabetes (Young *et al*., 1995). Indeed, although there is considerable evidence for increased oxidative stress in diabetes, this is not supported by some studies (Dyer *et al*., 1993; Wells-Knecht *et al*., 1997). For instance, the level of advanced glycation end-products carboxymethyl lysine and pentosidine present on collagen in diabetes could be explained by mechanisms other than oxidative stress

(Dyer *et al*., 1993). Furthermore, oxidized amino acids, methionine sulfoxide, and ortho-tyrosine in skin collagen were not increased in diabetes (Wells-Knecht *et al*., 1997). However, these observations certainly do not exclude more localized tissue-specific oxidative stress.

Many antioxidants, like Se, have been proposed to be a potentially therapeutic agent in the treatment or prevention of different pathologies that may be related to an imbalance of the oxido-reductive cellular status, as it is die case in diabetes. There are many studies performed on diabetic samples showing the beneficial effects of Se on glucose homeostasis as mentioned previously in detail in the introduction part. However, it is possible to come across with some studies in the literature which does not support this effect of Se. For example, in 1998, Battel *et al*. reported that there was not a complete normalization of the glucose levels in Se treated diabetic individuals (1998). Ultrastructural studies of the diabetic myocardium have been undertaken by Regan *et al*. (1981), Koltai *et al*. (1984), Bakth *et al*. (1986) and Haider *et al*. (1981) in the monkey; Reinila and Akerblom (1984) and Jackson *et al*. (1985) in rats; Bhimji *et al*. (1986) in the rabbit; and Giacomelli and Wiener (1979) and Saito *et al*. (1984) in the mouse. Results of these studies are often conflicting, however, ranging from no change in the cardiocyte (Regan *et al*., 1981) to massive myocytolysis and the appearance of contraction bands (Jackson *et al*., 1985). Valid interpretation is made even more difficult by factors, such as differences in the severity or duration of diabetes, possible toxic effects of the diabetogen used and the lack of appropriate age-matched controls.

It is possible to find many studies which investigated the effect of diabetes on different regions of the heart, like the ventricles, as mentioned previously. These are studies showing that the left ventricle is seriously affected by the diabetes, whereas some other studies demonstrate that the right ventricle is more severely affected by this disease. In most of the previous studies, the right ventricle was not evaluated, partly because only the left ventricle was subject to the primary hemodynamic overload. And another reason is that, the pathologic processes were expected to primarily involve the left ventricle. Study of mechanisms of biventricular pathology

should provide insight into the pathogenesis of ventricular damage and subsequent heart failure. Taking into consideration these contradictory results and the sparse literature in this field, in our study, both right and left ventricles were examined to more carefully evaluate the functional significance of observed changes in cardiac structure.

The aim of this study is to investigate the effect of diabetes mellitus on various regions of the heart such as apex myocardium, left ventricle muscle, right ventricle muscle and the small vessels on the left ventricle muscle; and the effect of Se-treatment on these regions of the diabetic heart at molecular level by FTIR Microspectrosopy.

Infrared spectroscopy is becoming an increasingly powerful tool for the study of the composition and structure of cellular components within tissues (Takahashi *et al*., 1991). In other words, the infrared spectra of tissues provide information that reflects the biochemistry of the tissue (Jackson *et al*., 1999). In this study, the experiments are performed by FTIR microscopy. The infrared spectra are evaluated to chemically characterize the absorbing molecules. This technique can be applied to diseased tissues to reveal chemical changes that are associated with discrete regions of lesion sites, which can provide insights into the chemical mechanisms of disease processes (LeVine *et al*., 1999).

Hopefully, with improved techniques such as FTIR microscopy, further insight into the role of diabetes mellitus on different region of the rat heart and the possible treatment effect of Se will be obtained.

In the second part of the thesis, firstly, the effect of chronic hypoperfusion on rat brain tissue homogenates, then the effect of stereotactic radiosurgery on hypoperfused rat brain tissue homogenates have been investigated.

In the case of hypoperfusion, there is a reduction of both oxygen and glucose supplies (Kawaguchi *et al*., 2002). Since brain cells are unusually sensitive to oxygen lack (Siesjo, 1988) and glucose is the only substrate used by the brain, it is very crucial to investigate the effect of hypoperfusion on brain. Despite the presence of

some studies regarding this subject (de Wilde *et al*., 2002; Kawaguchi *et al*., 2002; Shi *et al*., 2000; Takagi *et al*., 2000; Wang *et al*., 2000), the precise mechanism of the effect of hypoperfusion on brain tissue still remains to be elucidated at molecular level. The aim of this part of the study is to have a more detailed picture about this effect at molecular level by using FTIR spectroscopy.

The effects of ionizing radiation is unknown on the chronically hypoperfused tissue around the AVMs of the brain. The presence of oxygen enhances the free radical production and results in increased damage (Betteridge, 2000). It was stated in a previous study that the considerable blood steal in the brain that surrounds a large AVM creates the protective hypoxia needed by the normal tissue (Pellettieri and Blomquist, 1999) It is known that the effect of radiation decreases in hypoxic tumors due to the decreased oxygen in the medium (Denny, 2000). Chronic hypoperfusion of surrounding brain due to stealing, which occurs in the case of hypoperfusion, is underestimated because it is a common sense that hypoxic areas are more resistant to radiation effects (Fyles *et al*., 1998; Wouters *et al*., 2002). On the other hand, in brain tissue ischemia or after the events causing hypoperfusion, it is shown that the amount of free radicals increases (Hossmann, 1999; Mishra and Delivoria-Papadopoulos, 1999). Both the oxidative stress and ionizing radiation are known to be cytotoxic. To the best of our knowledge, there is no detailed study showing the effect of ionizing radiation on different constituents (such as lipids and proteins) of the chemically hypoperfused brain tissues. The aim of this part of the study is to find out these effects by using FTIR spectroscopy.

CHAPTER 2

MATERIALS AND METHODS

2.1 Part I

2.1.1 Reagents

Reagents used for the preparation of experimental animals:

- Streptozotocin (STZ), pentobarbital and Selenium (Se) were purchased from Sigma.

Reagents used for Hematoxylin & Eosin (H&E) staining:

- Reagent alcohol — HPLC was purchased from Fisher,
- Eosin Y, disodium salt was purchased from Sigma,
- Harris Hematoxylin Stain, acidified was purchased from Lerner Laboratories,
- Permount was purchased from Fisher,
- Xylene was purchased from Fisher.

2.1.2 Preparation of Experimental Animals

Weanling Wistar rats (Ankara University, Faculty of Medicine, Animal Care Facility) of either sex were selected randomly and housed in stainless-steel, wire bottomed cages, initially at a density of three per cage and as they grew, were then caged individually. They were maintained at an ambient air temperature of 22±1°C and a 12-h light/dark cycle. All procedures used in the experiments were approved by the ethics committee of Ankara University, Faculty of Medicine. The rats were categorized into 3 main groups: *1*: Control, *2*: Diabetic, *3*: Se-treated diabetic.

Formation of control group

The Wistar rats were chosen randomly and the blood glucose levels were measured. Then the rats were injected with 0.1 M citrate buffer (pH 4.5) intraperitonally (i.p.) as a single dose and fed without any restriction. At the fifth week following the injections, the glucose levels were measured with Medi-Sense Card Sensor. The animals were sacrificed under anesthesia (pentobarbital, 30 mg/kg). The hearts of the rats were removed and stored at –80°C for experimental analysis.

Formation of STZ-induced diabetic group

STZ was dissolved in 0.1 M citrate buffer (pH 4.5) and injected i.p. as a single dose at a concentration of 50 mg/kg. One week after injection, blood glucose levels were measured with MediSense card sensor and the rats with a blood glucose level of higher than 2 times of control value were accepted as diabetic. Any STZ-treated rats having blood glucose level less than 2 times of the control value was excluded from further study. Within the one month after injection, rats were fed without any restriction and their blood glucose levels were measured just before they get sacrificed. The animals were sacrificed under anesthesia (pentobarbital, 30 mg/kg) by opening their chest. The hearts of the rats were removed and stored at –80°C for experimental analysis.

Formation of Se treated diabetic group

To induce diabetes, the rats were injected with STZ (dissolved in 0,1 M citrate buffer) i.p. as a single dose at a concentration of 50 mg/kg, as it was previously described. One week after STZ injection, blood glucose levels were measured as before and the diabetic animals are injected with 5 μmole/kg/day sodium selenite i.p. everyday for four weeks. At the end of the fifth week blood glucose levels were measured and the animals were sacrificed under anesthesia by opening their chest (pentobarbital, 30 mg/kg). The hearts of the rats were removed and stored at –80˚C for experimental analysis.

2.1.3 IR Mapping Experiments and Data Collection

Two adjacent cross-sections of 9 μm were taken from apex and ventricles from all groups by using cryotome and were thaw-mounted on IR-transparent CaF_2 windows. A small amount of optimum cutting tool was applied to tissue samples to allow the sample to be attached to the cryotome. The first sections taken from all samples were used for FTIR microspectroscopy measurements. Till the FTIR measurements, the samples were kept in dry environment (in a dessicator filled with nitrogen gas) at room temperature. The second serial sections were used for Hematoxylin&Eosin (H&E) staining to see the histologically defined tissue regions with their different composition. IR mapping was performed on rat heart samples from a region in the apex, right ventricle and left ventricle myocardial muscle including a vessel.

An IR microscope coupled to an IFS28B FT-IR spectrometer (both Bruker, Germany) was used to map the tissue sections. The microscope was equipped with a computer-controlled x/y stage which permitted spectral mapping of the tissue in defined steps within a rectangular area. A grid of pixel coordinates within the tissue section was defined and IR spectra were collected from each of the points in the grid. Spectra were taken in both the x and y directions in steps of 80 μm (using an aperture diameter of 100 μm) for the apex, 56 μm (using an aperture diameter of 70 μm) for the left ventricle myocardium, for the small vessel in the left myocardium and the right ventricle myocardium. In this way, IR data completely covering the chosen tissue area could be obtained. IR spectra were collected in absorption from 4000-850 cm^{-1} with a spectral resolution of 6 cm^{-1} using an Hg-Cd-Te detector. The number of coded Interferogram per spectrum was set to 64 scans for apex, and 256 scans for the right and left ventricle myocardium and the small vessel. The microscope, which was hermetically, sealed using a specially designed box, and the spectrometer was purged with dry air to reduce spectral contributions from water vapor and CO_2.

2.1.4 IR Data Evaluation

Analysis of spectral data was carried out using the OPUS 3.0 data collection software package (Bruker, Germany). Quality tests, first derivatives, vector-

normalizations, cluster analysis, spectra averaging and chemical maps were done by using a software called “Cytospec”.

The quality test was performed exclusively on the data block of original absorbance spectra. The test results were stored in the data block of preprocessed spectra. When the quality test of a given spectrum is negative, the respective file in the preprocessed data block was removed. In this way, spectra tested for poor quality were excluded from all consecutive evaluations, such as cluster analysis. The criteria for the quality test can be listed like the following:

Test for water vapor: Sharp water vapor absorption bands can be found in the Mid-IR spectral region between 1800 and 1450 cm^{-1}. It is recommended to check the IR spectra in a region where the samples normally do not exhibit absorption bands. In tissues spectroscopy, the region above 1750 cm^{-1} may be of particular interest.

Test for samples thickness: The integrated absorbance defined in large spectral region can be used as a measure to assess the sample thickness to avoid inaccuracies due to too thin samples (low absorbance: low spectral signal/noise) or due to too high absorbance (non-linear detector response). In this way it was possible to exclude data which fail this quality test. 950-1750 cm^{-1} spectral region was used for obtaining the integral. Lower limit-upper threshold was chosen as 30-300 (arbitrary unit/cm) for the integral. A spectrum has failed the sample thickness test if an integration value is determined which is higher or lower than then the defined thresholds.

Test for tissue freezing medium: A typical spectrum of tissue freezing medium was used to recognize the signals arising from the tissue freezing medium.

Cluster analysis was performed on first derivative spectra using wavenumber ranges 950-1480 cm^{-1} and 2800-3050 cm^{-1}. The original absorption spectra and their averages belonging to different clusters were saved in a format readable by the $OPUS^{NT}$.

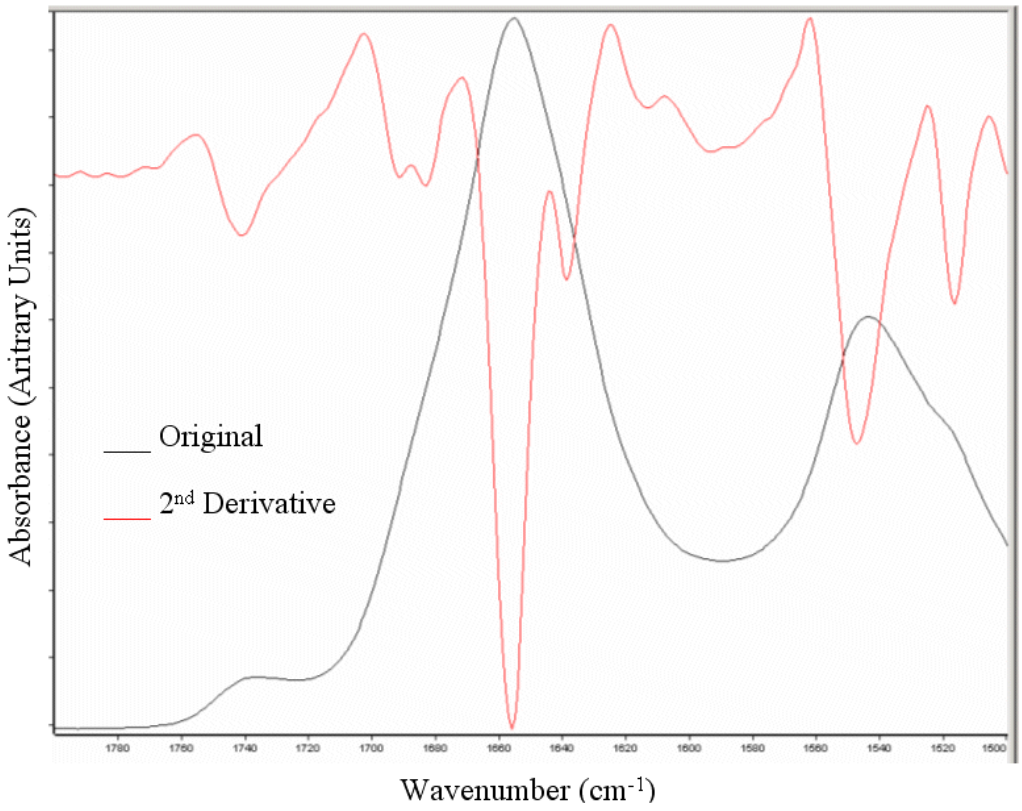

Figure 15. FTIR original absorbance and 2nd derivative spectra of rat heart in 1800-1500 cm^{-1} region.

Because most IR bands are broad and composed of overlapping components, it is necessary to preprocess the original spectra by applying a band narrowing algorithm that separates the individual bands. For this reason, direct comparisons of spectral characteristics were done on second derivatives of average spectra of the discussed spectral classes. The second derivative of the original spectra offers a direct way to identify the peak frequencies of characteristic components and thus permits much more detailed qualitative and, eventually, quantitative studies (Susi and Byler, 1983). An example of an original absorption spectrum and its second derivative spectrum in 1800-1500 cm^{-1} region is given in figure 15. The peak intensity of the second derivative is proportional to the original peak intensity and inversely proportional to the square of the halfwidth (Susi and Byler., 1983).

2.1.4.1 Cluster Analysis

Cluster analysis is a type of pattern recognition technique which attempts to find intrinsic group structures within the data set without the need of any class assignments or partitioning of the data into a training test data set.

Cluster analysis aims to classify objects, i.e. the description of the structure and property interrelationships intrinsic to a given set of objects each defined by a multiplicity of properties. The various classification algorithms use different distance measures to calculate similarity between the objects (e.g. correlation coefficients). Starting from the calculated distance matrix, an attempt is made to partition the objects into groups, classes or clusters, such that all objects belonging to the same cluster are as similar as possible and all objects belonging to different clusters are as different as possible, which means that intra-class variance should be as small as possible, while the interclass variance is a maximum.

Clustering procedures work according to the following principles:

1. In the beginning, there are n objects that have to be classified,
2. Then the two objects lying closest have to be found and are collected in one cluster,
3. The distances between this new cluster and all other objects are calculated,
4. In a next step, a search is made for the next nearest objects or clusters which are collected in one cluster.
5. This procedure is repeated until all objects are collected in one single cluster (Naumann, 2000).

2.1.5 Staining Protocols for Cryosections

2.1.5.1 Hematoxylin & Eosin Staining

The protocol is applied in the routine staining of cationic and anionic tissue components in tissue sections. This is the standard reference stain used in the study of tissue pathology from its long use.

Solutions used in the experiments

- Eosin Y, 1 % aqueous: 1 gram Eosin Y dye + 100 ml deionized water

- Harris Hematoxylin, acidified
- Alcohol 50 %: Reagent alcohol ~50 ml + Deionized water ~50 ml
- Alcohol 70 %: Reagent alcohol ~70 ml + Deionized water ~30 ml
- Alcohol 80 %: Reagent alcohol ~80 ml + Deionized water ~20 ml
- Alcohol 95 %: Reagent alcohol ~95 ml + Deionized water ~ 5 ml

Staining Procedure:

1. Slides with the section were placed in a staining rack,
2. The sections were immersed in the filtered Harris Hematoxylin for 1 minute,
3. The rack was removed to a beaker with tap water,
4. Tap water was exchanged until the water is clear,
5. Sections were immersed in Eosin stain for 1.5 minutes,
6. The rack was removed to a beaker with tap water,
7. Tap water was exchanged until the water is clear,
8. The slides were dehydrated in ascending alcohol solutions (50 %, 70 %, 80 %, 95% x 2, 100 % x 2) in a jar,
9. The slides were cleared with xylene (3 - 4 x) in a jar,
10. Coverslip was mounted onto a labeled glass slide with an organic mounting medium (Thompson, 1966).

2.2 Part II

2.2.1 Reagents

Reagents used for the preparation of experimental animals:

- Ketamine and xylazin were purchased from Sigma

2.2.2 Experimental Animals

Experimental animals for FTIR analysis were prepared in Hacettepe University, Medicine Faculty. After the approval of Ethics Committee, male Wistar albino rats were selected for our study with weights ranging between 250-320 g. In order to investigate the effect of radiosurgery on hypoperfusion, the animals were

first operated to form chronic hypoperfusion. After that, stereotactic radiosurgery was applied to the operated animal brains. The operation and the radiosurgery were performed by Prof. Dr. Faruk Zorlu and Assoc. Prof. Kamil Öğe. Rats have been divided into 4 groups:

Group 1: Control (no operation, no stereotactic radiosurgery) (n=5)
Group 2: Radiated (n=5)
Group 3: Operated to form hypoperfusion (n=7)
Group 4: Operated and radiated (n=5)

Group 1 was used as control group without any treatment. In groups 3 and 4, cephalic internal carotid artery to caudal external jugular vein anastomosis was performed as described by Spetzler (Spetzler *et al*., 1978) to by-pass blood through circle of Willis without perfusing main brain vessels. Over eight weeks of waiting period, stealing of blood through the fistula resulted in chronic hypoperfusion of the brains (Bederson *et al*., 1991; Morgan *et al*., 1989a). In group 4, in addition to the surgery, rats were irradiated at the end of 8 weeks. In group 2, rats were only irradiated without preceding surgery. Stereotactically, 2400 cGy (CentiGrays or rad) was applied to right parietal lobe in one fraction with 5 mm collimator. In group 3 and 4, chronic hypoperfusion resulted in hypoxia proved by pathology revealing hippocampal neuronal cell loss and gliosis. The rats were decapitated 72 hours after irradiation. The brains of the rats were removed and stored at –80 ºC for FTIR spectroscopy analysis.

2.2.3 Surgery

In the group 3 and 4, right cephalic internal carotid artery to caudal external jugular vein anastomosis was performed as described by Spetzler (Spetzler *et al*., 1978).

Under the general anesthesia of intraperitoneal ketamin/xylazin (90/10 mg/kg), with the aid of operation microscope and microsurgical techniques and instruments; right common carotid artery, right internal and external carotid arteries, right common jugular vein and right external jugular vein were identified and

dissected. Right external carotid artery was ligated form its origin from common carotid artery. Right common carotid artery was ligated caudally and external jugular vein was ligated cephally. Right common carotid artery superior to ligation, external jugular vein inferior to the ligation were cut using microtechnique. Free ends were end-to-end anastomosed to each with interrupted 10/0 nylon sutures. In each anastomosis, function of fistula was tested with proximal and distal closing tests and confirmed.

Operated rats were kept in normal diurnal rhythm without restriction of any diet or activity for 8 weeks. At the end of the eight week, rats in group 2 and group 4 had been taken under an anesthesis. Rats were stabilized with the help of a mask instead of using stereotactic frame of rats for stabilization. Then, targeting middle line depth of right hemisphere of their brains, rats were radiated using 5 mm collimator and 2400 cGy. For radiation process, 6 MeV X-ray beams have been used. They have been obtained from linear accelerator that was modified for radiosurgery.

Dose selection was made according to the clinical application radiosurgery for benign tumoral lesions and AVMs which is within the tolerance range of normal tissue. Theoretically, since the right brain hemispheres are hypoperfused (Morgan *et al*., 1989b; Nornes and Grip, 1980; Spetzler *et al*., 1978), radisugery was applied to right parietal hemisphere through 5-mm collimator in all subjects with a rate of 350 cGy.

On the 72nd hour post-radiosurgery, euthanasia was applied to all groups at the same time to decrease variability of the results and all rats were decapitated. Brain tissue samples were taken from right frontal lobe of each subject to standardize the results.

2.2.4 FTIR Analysis

The brain samples were homogenized with saline phosphate buffer, pH 7.4, and centrifuged at 125,000 g for 15 minutes. Membrane rich parts (pellet) of these homogenates have been used for FTIR studies. FTIR spectra of samples were recorded at 4000-1000 cm^{-1}. Sample suspensions of 15 µl were placed between water

insoluble CaF_2 windows with 12 μm sample thickness. Infrared spectra were obtained using a BOMEM 157 FTIR spectrometer (The Michelson Series, Bomem, Inc. Quebec, Canada) equipped with a DTGS (deuterated triglycine sulfate) detector. The instrument was under continuous dry air purge to eliminate atmospheric water vapor. Interferograms were averaged for 400 scans at 4 cm^{-1} resolution.

Win Bomem Easy software (Galactic Industries Corporation) was used for the intensity, frequency and bandwidth measurements. Firstly, the spectra of tissues were subtracted from the spectrum of the buffer to remove water absorption bands. In the subtraction process, the water band located around 2125 cm^{-1} was tried to be flattened. The wavenumber values of all function groups were recorded from the subtracted spectra. As an example, the FTIR spectrum of control brain tissue before and after subtraction process is given in figure 16.

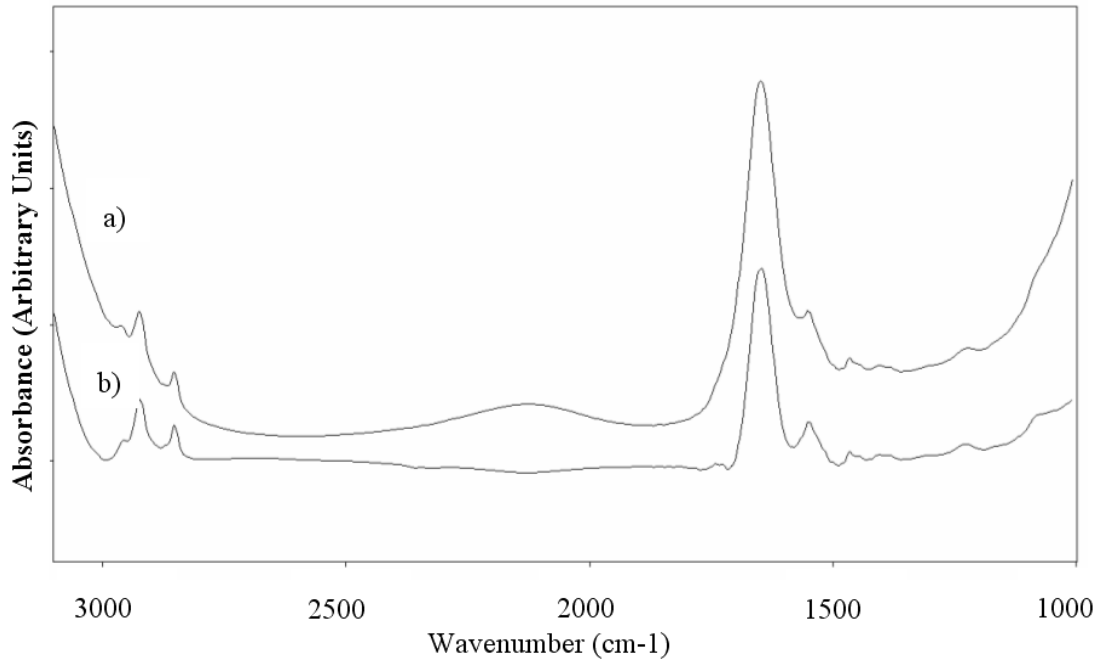

Figure 16. FTIR spectrum of control rat brain homogenate, a) before, and b) after subtraction

The band positions were measured according to the center of weight. The spectra were normalized in specific regions for data analysis by using the same software. After normalization process, different band intensities and their ratios were calculated. The second derivative spectra (Savitsky-Golay as derivative operation, 9

points of smoothing) in the Amide I region (1585 cm^{-1} - 1710 cm^{-1}) was obtained using the same software. After baseline correction, spectral region of interest (1585 cm^{-1}-1710 cm^{-1}) was fitted with Gaussian components by using a computer program called GRAMS/32 (Galactic Industries Corporation, Salem, NH USA). The process was iterated until a satisfactory fit between the computed and experimental band was obtained. The fractional areas of the sub-bands in the Amide I region were calculated from the final fitted band areas. Averages of the spectra belonging to the same experimental groups were calculated by using GRAMS/32 program.

2.3 Statistics

The results were expressed as "mean ± standard deviation". The differences in the means of the treated and control rats were compared by means of Mann-Whitney U test. The p value of less than 0.05 was considered statistically significant ($p<0.05$*, $p<0.01$**, $p<0.00$l ***).

CHAPTER 3

RESULTS

3.1 Part I: Effect of Diabetes Mellitus on Rat Heart and the Effect of Selenium Treatment on Diabetic Rat Heart

This part of the work is precisely addressed to investigate the effect of diabetes mellitus on various regions of the rat heart such as, apex myocardium, left ventricle muscle, right ventricle muscle, and the small vessels on the left ventricle muscle; and the effect of Se treatment on these regions of the diabetic heart at molecular level by FTIR Microspectroscopy.

The changes in the heart structure and dynamics caused by diabetes can be monitored by the nonperturbing technique, namely FTIR spectroscopy. The wavelength of light that is absorbed depends on the nature of the covalent bond (e.g., C=O, N-H), the type of vibration (bending, stretching, etc.), and the environment of the bond. The IR spectrum of a tissue sample can be regarded as a molecular fingerprint of the tissue. If this molecular fingerprint is modified by a disease process, then IR spectroscopy can be used to detect and monitor the disease.

3.1.1 Band Assignment of the Rat Heart Tissue

Using the group frequency approach to spectral analysis the absorptions can be assigned to vibrational modes of chromophores within proteins, lipids, carbohydrates and nucleic acids (Fabian *et al*., 1995). In the present study, the same approach was employed.

Figure 17 displays a second derivative infrared (IR) spectrum of the rat heart (a cryo-section from control vessel). Some important absorption bands of heart tissue IR spectra are labeled in this figure and band assignments are given in table 6.

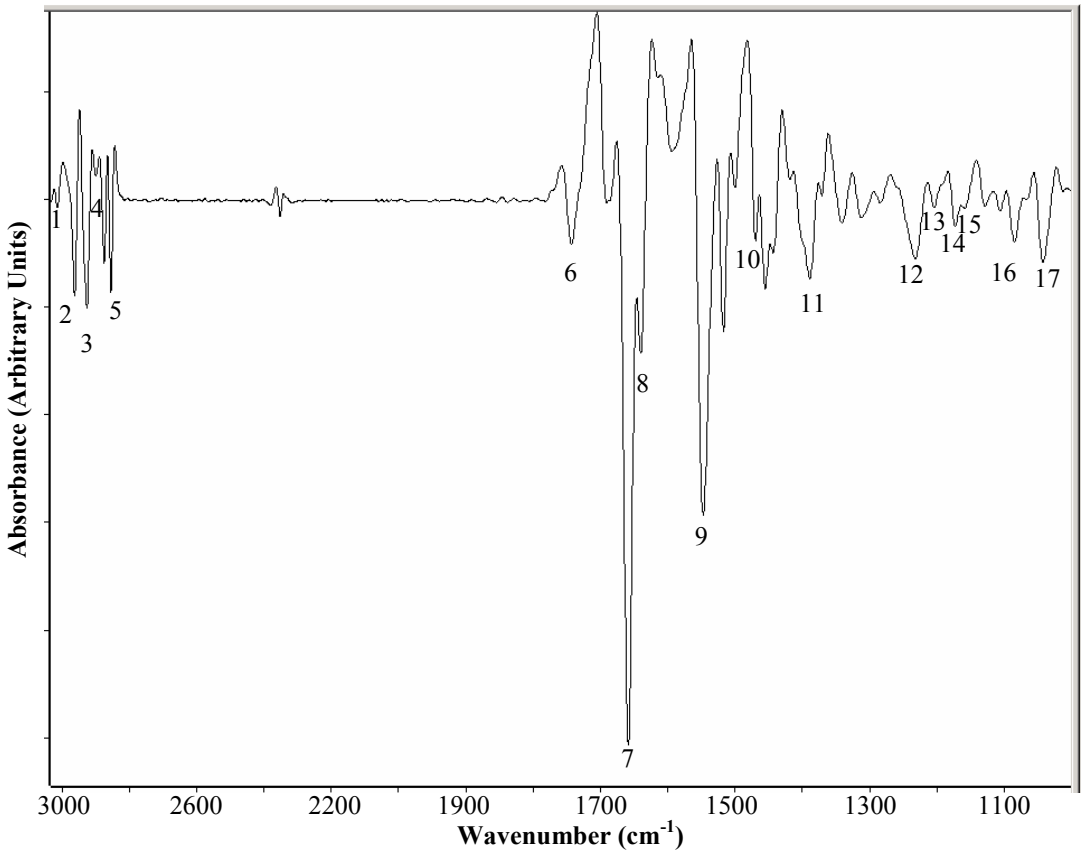

Figure 17. Second derivative infrared spectrum of the rat heart (control vessel).

Table 6. Band assignments of major absorptions in IR spectra of heart tissue in 3300-1000 cm^{-1} region.

Band Numbers	Frequency (cm^{-1})	Assignments
1	3012	Olefinic=CH stretching: unsaturated lipids (Lui *et al*., 1996; Takahashi *et al*., 1991)
2	2956	CH_3 asymmetric stretching: lipids (Kneipp *et al*., 2000)
3	2925	CH_2 antisymmetric stretching: lipids (Liu *et al*., 2002)
4	2873	CH_3 symmetric stretching: mainly proteins (Severcan *et al*., 2000)
5	2854	CH_2 symmetric stretching: lipids (Jackson *et al*., 1997)
6	1733-39	C=O stretching: Ester functional groups in lipids (Kneipp *et al*., 2000)
7	1655	Amid I: (mainly protein C=O stretching), α-helical structure (Liu *et al*., 1996)
8	1638	Amid I: β-sheet (Lui *et al*., 1996)
9	1545	Amid II: (protein N-H bending, C-N stretching), α-helical structure (Lui *et al*., 1996)
10	1468	CH_2 scissoring: lipids (Melin *et al*., 2000; Wong *et al*., 1991)
11	1386	CH_3 bending: lipids (Jackson *et al*., 1998)
12	1228	PO_2^- asymmetric stretching: mainly phospholipids (LeVine and Wetzel, 1993; Wong *et al*., 1991).
13	1201	Collagen (Liu *et al*., 1996)
14	1173	CO-O-C asymmetric stretching: ester bonds in cholesterol esters and phospholipids (Jackson *et al*., 1998)
15	1156	C-O stretching: glycogen (Diem *et al*., 1999; Jackson *et al*., 1998 ;Wong *et al*., 1991)
16	1080-85	PO_2^- symmetric stretching: phospholipids (LeVine and Wetzel, 1993; Manoharan *et al*., 1993) C-O stretching: glycogen, oligosaccharites, glycolipids (Jackson *et al*.,1998; Liu *et al*., 2002; Wong *et al*., 1991)
17	1041	C-O stretching: oligosaccharites, polysaccharites (Lyman and Murray-Wijelath, 1999)

*Peak numbers are the ones illustrated in figure 17.

3.1.2 Effect of Diabetes Mellitus on Different Region of the Rat Heart

3.1.2.1 Apex

Figure 18A shows the H&E staining image of a thin (9 µm) section taken from the rat heart apex at 25 X magnification. In figure 18B, the FTIR microscope mapped region is shown at 40 X and this region on the section is shown in a square. After FTIR microscopy measurements, the data was loaded to cytospec program for data analysis. First steps of data evaluation included a so called "quality test" of the raw spectral data. First derivatives of the all spectra which have passed the quality test were calculated. Then the first derivatives were normalized in the frequency range of 1480 cm^{-1}-950 cm^{-1}. Cluster analysis was performed for the same region and the result of this analysis is shown in figure 18C.

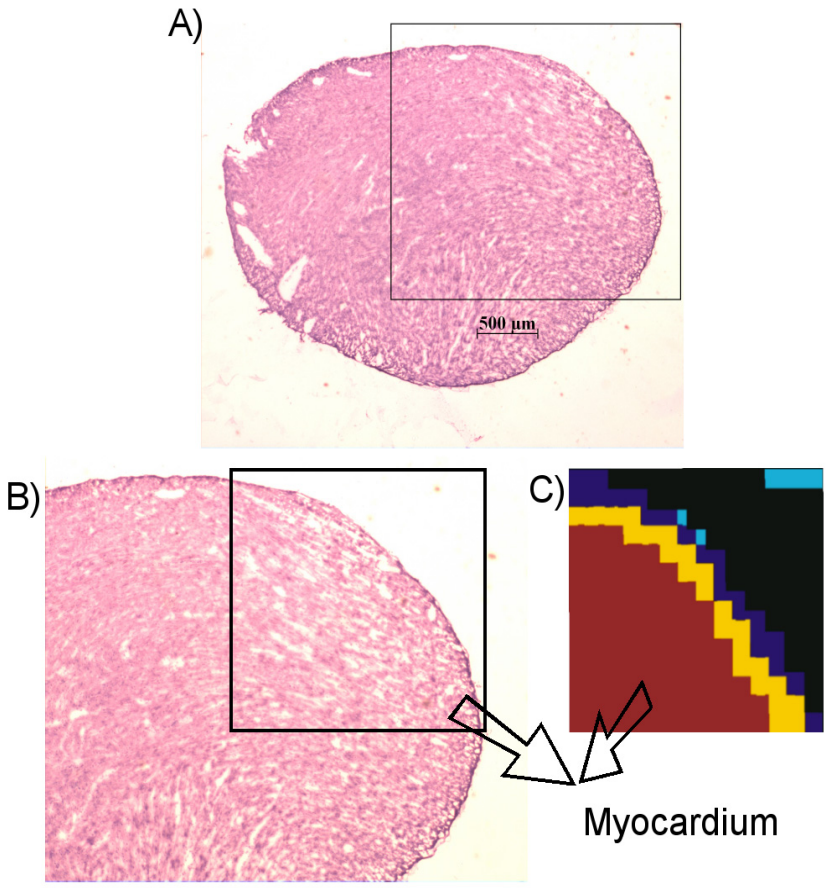

Figure 18. The H&E staining image of a thin (9 µm) section taken from rat heart apex at 25 X (A), the FTIR microscope mapped region is shown at 40 X and this region on the section is shown in a square (B), Cluster analysis results in the frequency range of 1480 cm^{-1} - 950 cm^{-1} (C).

Figure 19 shows the average spectra arising from different clusters (A), the chemical map (B), the image of cluster analysis (C). In figure 19B, the colored chemical map of Amide I band (arising from proteins), which gives absorption in 1620 cm^{-1}-1680 cm^{-1} (Amide I) region, is given. The map was colored according to the Amide I concentrations, where red color corresponds to the highest and blue color corresponds to the lowest concentrations as shown on a color bar in figure 20.

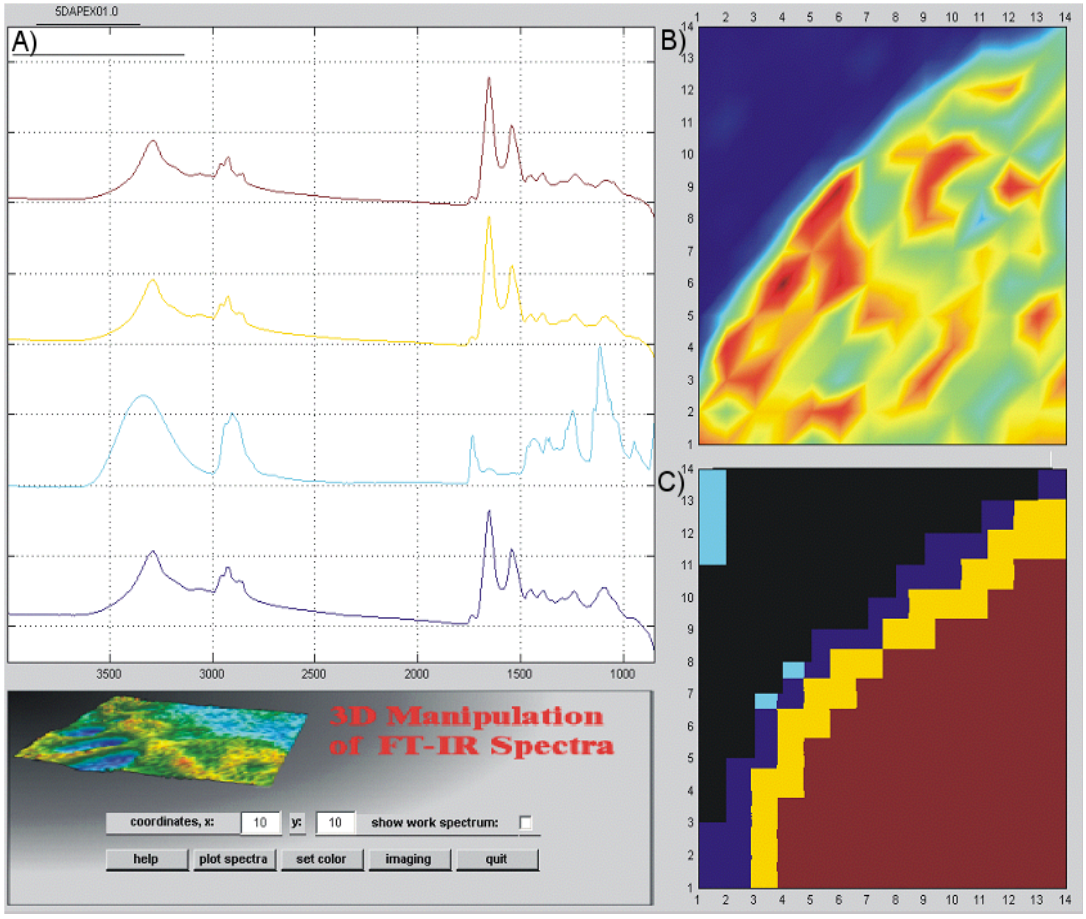

Figure 19. The average spectra arising from different clusters (A), the chemical map (B), the image of cluster analysis (C).

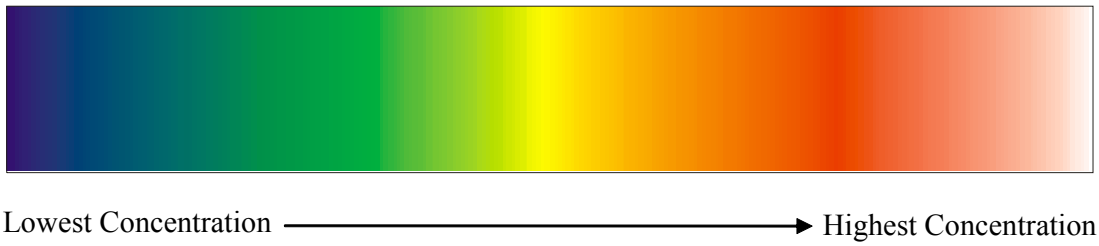

Figure 20. Color bar indicating relative concentration, from lowest to highest

In figure 19C and 19A, it is possible to see the 4 different clusters given with different colors belonging to different tissue components and the original average absorption spectra of these clusters, respectively. The light blue color arises from the tissue freezing medium (optimum cutting tool) (figure 19C) and the spectrum belonging to this cluster is given with the same color. The dark blue color, shown in figure 19A, arises from the epicardium of the apex and the tissue freezing medium. The corresponding original average absorption spectrum is also illustrated with the same color (dark blue). The cluster represented by yellow color belongs to the epicardium of the apex. The cluster shown with dark red color arises from the myocardium of the apex and the same color is used to show the original average absorption spectrum. The aim of this cluster analysis is to obtain the original absorption spectrum coming from the myocardium since we are interested in the changes occurring in myocardium between different treatment groups. The data belonging to this cluster showing the myocardium is used for the comparisons. The cluster analysis was performed for the apex part of all the rat hearts and the original average spectrum arising from myocardium was saved in a format readable by OPUS^{NT} program. Then the data was loaded into this program. The second derivatives of the original average absorption spectra were calculated. For comparisons between different treatment groups, the second derivative spectra were normalized at different spectral regions. Then, the averages of the individuals belonging to the same group were calculated. The same procedure is applied for all the treatment groups and the resultant average spectra of myocardium are compared. The peak positions of the original absorption spectra corresponds to the minimum positions in the second derivative spectra. For this reason, minimum position are used for the comparisons.

3.1.2.1.1 Comparison of the Control and Diabetic Rat Heart Apex Myocardium Spectra in 3030-2800 cm^{-1}

The average spectra belonging to the apex myocardium of control (6 sample), and diabetic (8 samples) groups are given in figure 21 at 3030 cm^{-1}-2800 cm^{-1} region (C-H region). In order to make comparisons between different groups, normalization was done in 3050 cm^{-1}-2800 cm^{-1} region and the resultant spectra were averaged

separately. Table 7 gives the changes in the intensity and intensity ratios of the main bands in this region.

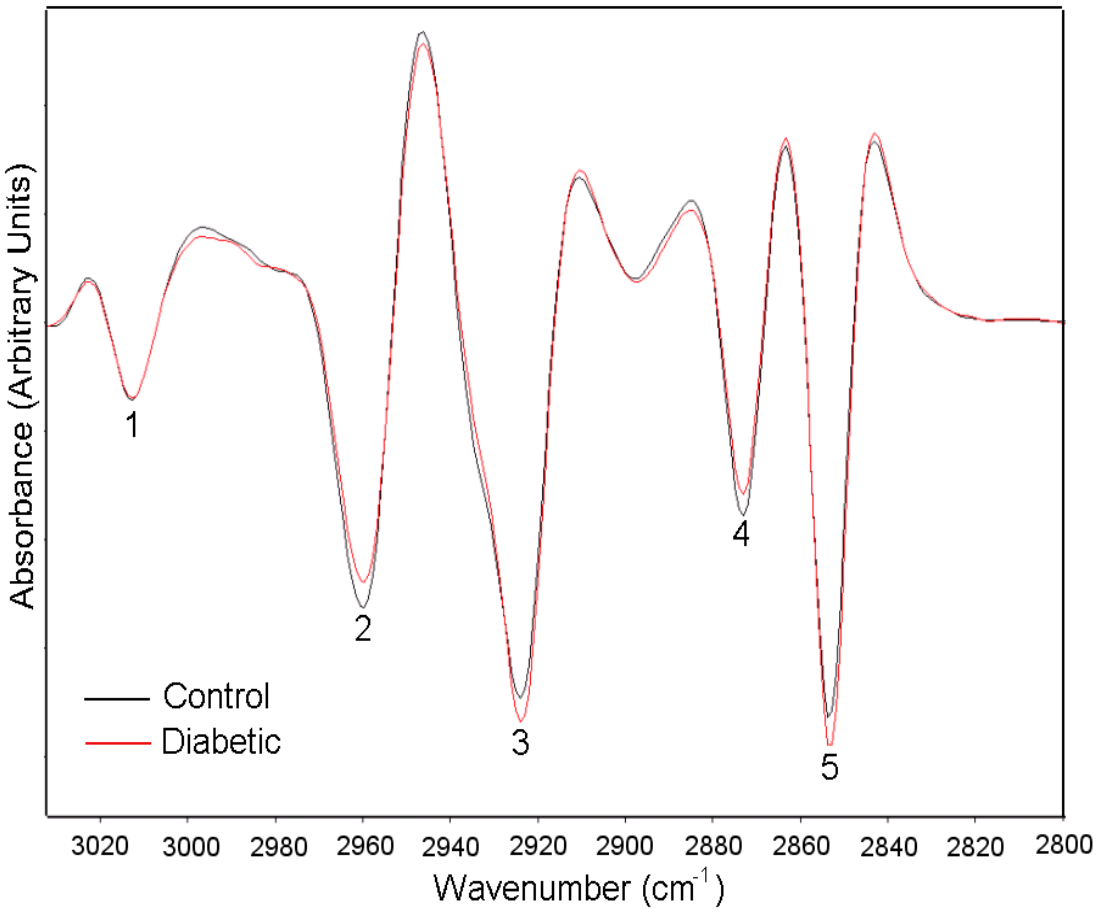

Figure 21. The average spectra belonging to the apex myocardium of control (6 samples), and diabetic (8 samples) groups in 3030 cm^{-1}-2800 cm^{-1} region. Vector normalization was done in 3050 cm^{-1} -2800 cm^{-1} region.

An increase in the intensities of CH_2 asymmetric (at 2923 cm^{-1}) and symmetric stretching modes (at 2853 cm^{-1}) is seen in figure 21 and table 7 in the diabetic group. As it is demonstrated in the figure and the table, there is a decrease in the intensity of the CH_3 symmetric (at 2873 cm^{-1}) stretching bands in the diabetic group. The results of our study clearly show that the intensity ratio of CH_2/CH_3 symmetric stretching vibrations increases in diabetic group.

Table 7. Changes in the intensities and intensity ratios of the main functional groups in 3030 cm^{-1}-2800 cm^{-1} region for control and diabetic rat heart apex myocardium. Values are shown as "mean ± standard deviation"

Functional Groups	**Control**	**Diabetic**	**P values**
CH_3 asymmetric stretching	-0.119±0.005	-0.109±0.007	p<0.017*
CH_2 antisymmetric stretching	-0.168±0.004	-0.180±0.002	p<0,002**
CH_3 symmetric stretching	-0,088±0,006	-0,078±0,005	p<0,003**
CH_2 symmetric stretching	-0.182±0.006	-0.196±0.006	p<0.004**
CH_2 symmetric/ CH_3 symmetric stretching	2.078±0.194	2.528±0.232	p<0.002**

Table 8. Changes in the frequency values of the main functional groups in 3030 cm^{-1}-2800 cm^{-1} region for control and diabetic rat heart apex myocardium. Values are shown as "mean ± standard deviation

Functional Groups	Control	Diabetic	P values
CH_3 asymmetric stretching mode	2957.75±0.20	2957.64±0.53	p<0.699
CH_2 antisymmetric stretching mode	2922.75±0.16	2922.71±0.24	p<0.897
CH_2 symmetric stretching mode	2852.94±0.10	2852.79±0.15	p<0.045*

Changes in the frequency (wavenumber) values of the main functional groups in control and diabetic rat heart apex myocardium are shown in table 8. Figure 21 and table 8 illustrate that there is a significant shift to lower wavenumber values of the CH_2 symmetric stretching vibrations in diabetic rat apex myocardium.

3.1.2.1.2 Comparison of the Control and Diabetic Rat Heart Apex Myocardium Spectra in 1800-1480 cm^{-1} Region

The average spectra belonging to the apex myocardium of control (6 samples) and diabetic (8 samples) groups are given in figure 22 at 1800 cm^{-1}-1480 cm^{-1} region.

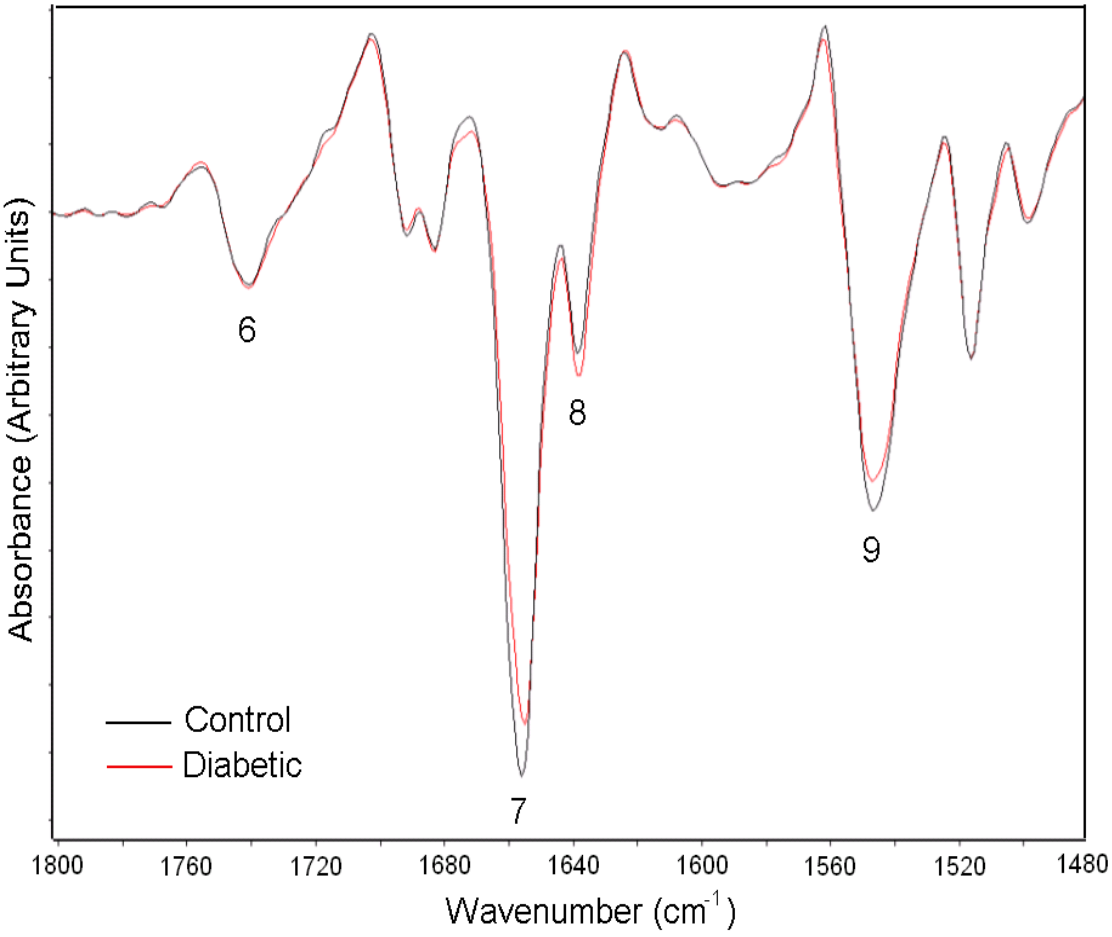

Figure 22. The average spectra belonging to the apex myocardium of control (6 samples), and diabetic (8 samples) groups in 1800 cm^{-1}-1480 cm^{-1} region. Vector normalization was done in 1480 cm^{-1}- 950 cm^{-1} region.

In order to make comparisons between diabetic and control group, normalization was done in 1480 cm^{-1}- 950 cm^{-1} region. The strong Amide I band (1655 cm^{-1}) in the FTIR spectra is widely used for determination of the secondary structure of proteins. Since the peak maximum of the Amide I band occurs at different frequencies for various types of hydrogen-bonded secondary structures, the discrete types of secondary structure in proteins can be identified by the frequencies of their maxima in the FTIR spectra (Takahashi *et al*., 1991). The band at 1655 cm^{-1} is attributable to Amide I of α-helical structures and the band at 1637 cm^{-1} is attributable to Amide I of β- sheet structures. It is possible to see another band in the same figure located around 1548 cm^{-1} which arises from the Amide II of proteins

(Haris and Severcan, 1999). The changes in the intensities of main functional groups in control and diabetic rat heart apex myocardium in this region are given in table 9.

Table 9. Changes in the intensities of the main functional groups in 1800 cm^{-1}-1480 cm^{-1} region for control and diabetic rat heart apex myocardium. Values are shown as "mean ± standard deviation".

Functional Groups	**Control**	**Diabetic**	**P values**
Amid I: α-helical structure	-0.830±0.086	-0.750±0.066	p<0.155
Amid I: β-sheet,	-0.207±0.019	-0.242±0.019	p<0.01**
Amid II: α-helical structure	-0.420±0.021	-0.370±0.024	p<0.007**

Figure 22 and table 9 show that diabetes causes a decrease in the intensities of α-helical structure of Amide I and Amide II, whereas it causes an increase in the intensity of β-sheet structure.

Table 10. Changes in the frequency values of the main functional groups in 1800 cm^{-1}-1480 cm^{-1} region for control and diabetic rat heart apex myocardium. Values are shown as "mean ± standard deviation".

Functional Groups	**Control**	**Diabetic**	**P values**
Amid I: α-helical structure	1655.11±0.48	1654.36±0.36	p<0.007**
Amid I: β-sheet	1637.87±0.20	1637.62±0.23	p<0.04*
Amid II: α-helical structure	1548.00±0.29	1548.36±0.14	p<0.028*

Changes in the frequency values of the main functional groups in control and diabetic rat heart apex myocardium are shown in table 10. As it is seen in figure 22 and table 10, the frequency of the Amide I band shifts to lower frequency values and the frequency of the Amide II band shifts to higher values in the diabetic apex myocardium of rat heart.

3.1.2.1.3 Comparison of the Control and Diabetic Rat Heart Apex Myocardium Spectra in 1480-1000 cm^{-1} Region

The average spectra belonging to the apex myocardium of control (6 samples) and diabetic (8 samples) groups are given in figure 23 at 1480 cm^{-1}-1000 cm^{-1} region.

In order to make comparisons between diabetic and control group, normalization was done in 1480 cm^{-1} - 950 cm^{-1} region. Changes in the intensities of main functional groups in control and diabetic rat heart apex myocardium are shown in table 11. It is clearly seen in figure 23 and table 11 that, the intensity of CH_3 bending band (at 1386 cm^{-1}) decreases in the diabetic group. This result supports the finding which was obtained from the figure 21 (intensities of CH_3 symmetric and asymmetric stretching modes).

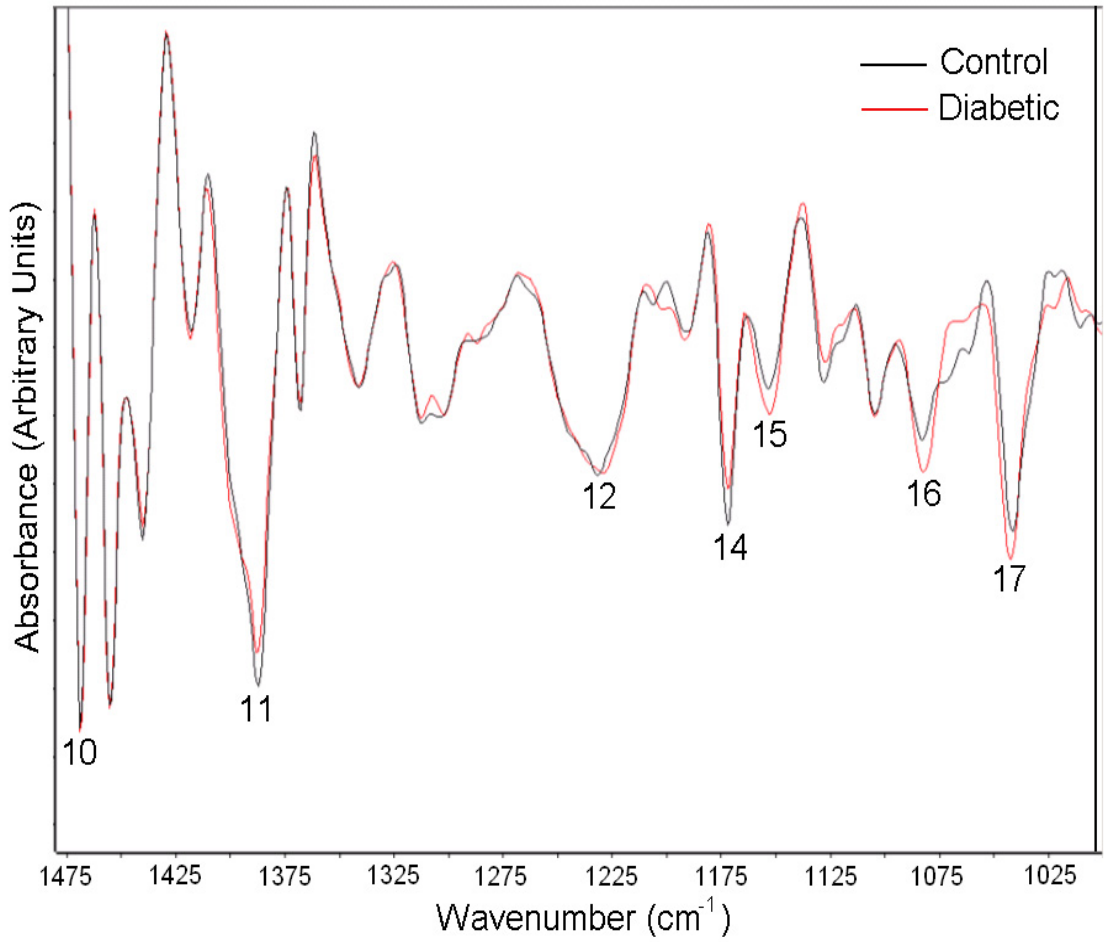

Figure 23. The average spectra belonging to the apex myocardium of control (6 sample), and diabetic (8 samples) groups in 1480 cm^{-1}-1000 cm^{-1} region. Vector normalization was done in 1480 cm^{-1}- 950 cm^{-1} region.

As it is clearly demonstrated in table 11 and figure 23, the ratio of the intensities of the absorptions at 1151 cm^{-1} and 1171 cm^{-1} is reversed in the diabetic group. The band at 1151 cm^{-1} is a C-O stretching band arising due to the presence of glycogen in the system (Diem *et al*., 1999; Jackson *et al*., 1998; Wong *et al*., 1991),

and the band giving an absorption band at 1171 cm-1 is a CO-O-C asymmetric stretching arising from ester bonds in cholesterol esters and phospholipids (Jackson et al., 1998).

Table 11. Changes in the intensities of the main functional groups in 1480 cm^{-1}-l000 cm^{-1} region for control and diabetic rat heart apex myocardium. Values are shown as "mean ± standard deviation".

Functional Groups	Control	Diabetic	P values
CH_3 bending	-0.122±0.006	-0.110±0.008	p<0.024*
CO-O-C asymmetric stretching	-0.065±0.005	-0.051±0.006	p<0.004**
C-O stretching (At 1151 cm^{-1})	-0.014±0.004	-0.022±0.007	p<0.028*
C-O stretching / CO-O-C asymmetric stretching	0.214±0.070	0.444±0.187	p<0.01**
PO_2^- symmetric stretching	-0.033±0.005	-0.046±0.012	p<0.023*
C-O stretching (At 1041 cm^{-1})	-0.067±0.020	-0.079±0.012	p<0.244

The other band in the spectrum of diabetic group in which we see an increase in the intensity value gives an absorption peak at 1083 cm^{-1}. This band can be assigned as PO_2 symmetric stretching band arising from phospholipids (LeVine and Wetzel, 1993; Manoharan *et al*., 1993). This absorption peak can also be due to C-O stretching band which mainly arises from glycogen, oligosaccarites and glycolipids present in the system (Jackson *et al*., 1998; Liu *et al*., 2002; Wong *et al*., 1991). Figure 23 also illustrates the presence of a sharp band at 1041 cm^{-1}, originating from the various C-O stretching vibrations characteristic for polysaccharites (Lyman and Murray-Wijelath, 1999). It is possible to observe a slight increase in the intensity of this band in diabetic group.

3.1.2.2 Left Ventricle Muscle and a Small Vessel on the Left Ventricle Muscle

Figure 24A shows a light microscope image of H&E stained thin slice taken from the left ventricle of rat heart at 25 X magnification. The mapped region of the

left ventricle muscle including the small vessel is shown in a square at 100 X magnification in figure 24B. After mapping measurements, the spectra were loaded into cytospec program. Quality test was performed. First derivatives of the all spectra which have passed the quality test were calculated. Then, the first derivatives were normalized in the frequency range of 1480 cm^{-1} - 950 cm^{-1}. Cluster analysis was performed for the same region and the result of this analysis is shown in figure 24C.

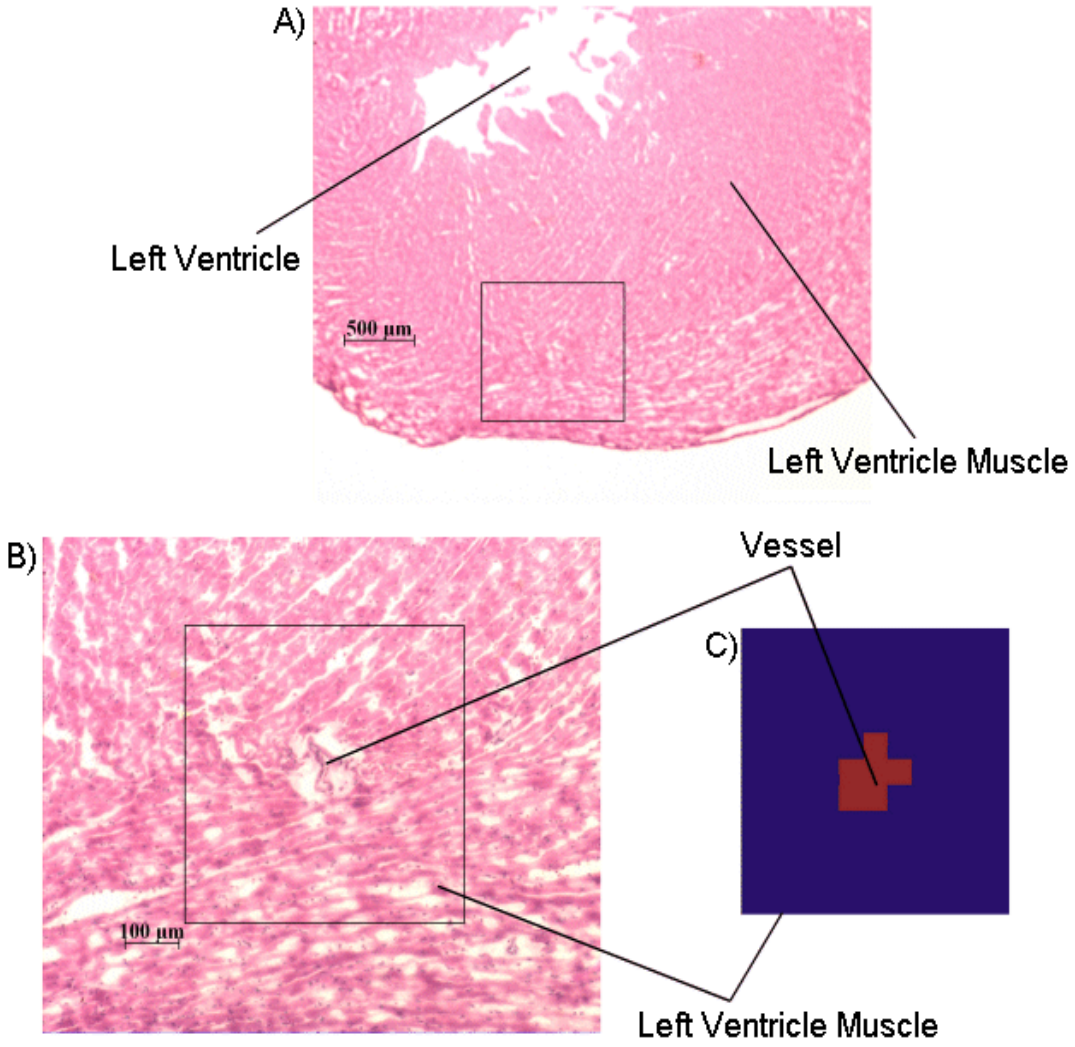

Figure 24 Light microscope image of H&E stained thin slice taken from the left ventricle of rat heart at 25 X magnification (A) the mapped region of the left ventricle muscle including the small vessel shown in a square at 100 X magnification (B) cluster analysis results in 1480 cm^{-1}-950 cm^{-1} region (C).

Figure 25 shows the average spectra arising from different clusters (A), the chemical map (B), the image of cluster analysis (C). In figure 25B, the colored

chemical map of Amide I band (arising from proteins), which gives absorption in 1620 cm^{-1}-1680 cm^{-1} region, is given. The map was colored according to the Amide I concentration, where red color corresponds to the highest and blue color corresponds to the lowest concentrations.

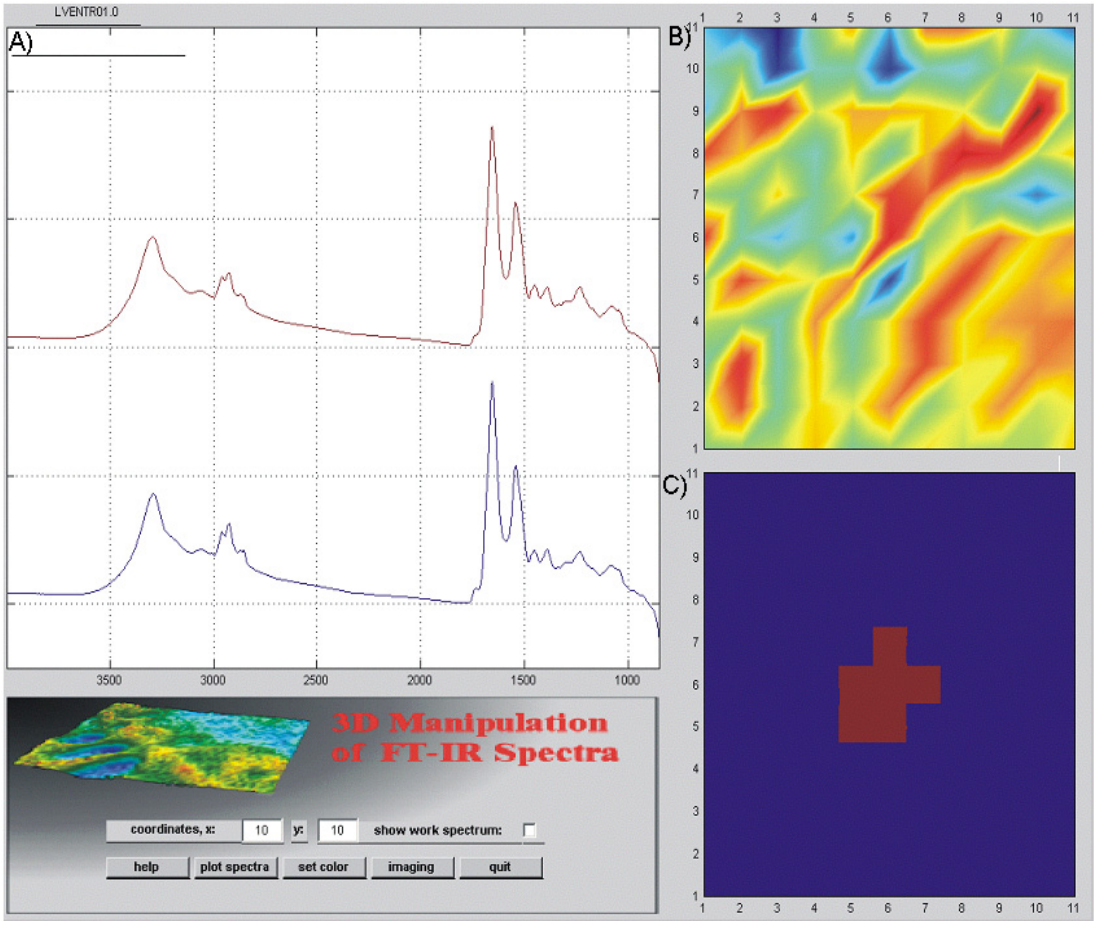

Figure 25. Average spectrum arising from different clusters (A), the chemical map (B), the image of cluster analysis (C).

In figure 25C and 25A, it is possible to see two different clusters given with different colors belonging to different tissue components and the original average absorption spectra of these clusters, respectively. The dark red color arises from the small vessel and the dark blue color arises from the left ventricle muscle. The corresponding original average absorption spectra are shown with the same colors. The aim of this cluster analysis is to distinguish between the signals coming from the vessel and the left ventricle muscle. The cluster analysis was performed for the left ventricle muscle and the vessel of all the rat hearts. The original average spectra

arising from these two different clusters were saved in a format readable by OPUS^{NT} program. Then the data was loaded into this program. The second derivatives of the original average absorption spectra were calculated. For comparisons between different treatment groups, the second derivative spectra were normalized at various spectral regions (3030-2800 cm^{-1} and 1480-950 cm^{-1}). Then the average spectra belonging to members of the same experimental group were averaged. The same procedure was applied for all the treatment groups and the resultant spectra are compared. The peak positions of the original absorption spectra corresponds to the minimum positions in the second derivative spectra. For this reason, minimum positions were used for the comparisons.

3.1.2.2.1 Spectral Changes in the Left Ventricle Muscle

3.1.2.2.1.1 Comparison of the Control and Diabetic Rat Heart Left Ventricle Muscle Spectra in 3030-2800 cm^{-1} Region

The average spectra belonging to the left ventricle muscle of control (8 samples) and diabetic (7 samples) groups are given in figure 26 at 3030 cm^{-1}-2800 cm^{-1} region.

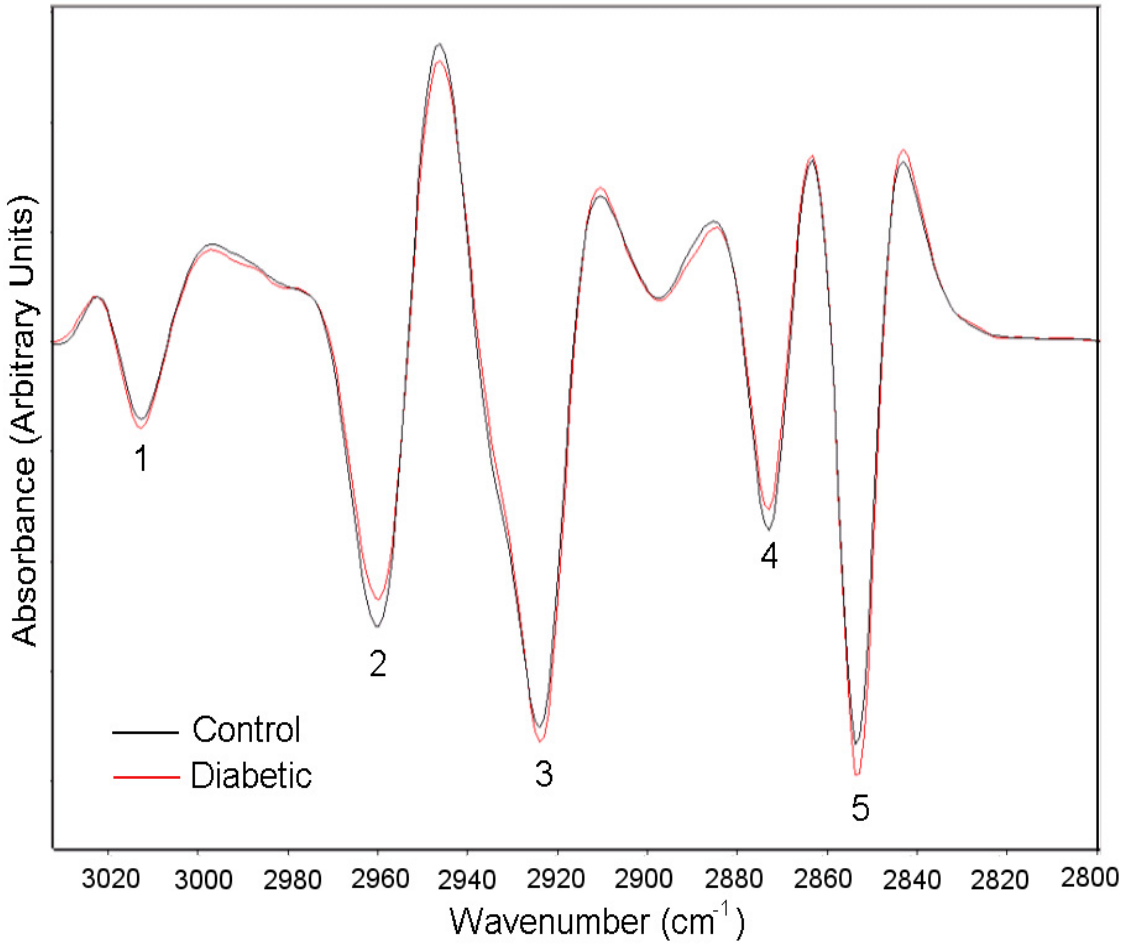

Figure 26. Average spectra belonging to the left ventricle muscle of control (8 samples) and diabetic (7 samples) groups in 3030 cm^{-1} - 2800 cm^{-1} region. Vector normalization was done in 3050 cm^{-1}-2800 cm^{-1} region.

In order to make comparisons between experimental groups, normalization was done in 3050 cm^{-1} - 2800 cm^{-1} region, which mainly gives information about the lipids of the system. The changes in the intensities and intensity ratios of main functional groups in control and diabetic rat heart left ventricle muscle are given in table 12.

As it is seen in figure 26 and table 12, the changes observed in this region are very similar with the changes observed for the apex myocardium, but more significant for the CH_2 symmetric stretching, CH_3 symmetric and asymmetric stretching bands. Furthermore, lipid to protein ratio increases more significantly in the left ventricle muscle of the diabetic group.

Table 12. Changes in the intensities of the main functional groups in 3030 cm^{-1}-2800 cm^{-1} region for control and diabetic rat heart left ventricle muscle. Values are shown as "mean ± standard deviation".

Functional Groups	**Control**	**Diabetic**	**P values**
CH_3 asymmetric stretching	-0.118±0.005	-0.105±0.002	p<0.001***
CH_2 antisymmetric stretching	-0.172±0.003	-0.178±0.003	p<0.002**
CH_3 symmetric stretching	-0.085±0.002	-0.075±0.002	p<0.001***
CH_2 symmetric stretching	-0.184±0.002	-0.198±0.004	p<0.001***
CH_2 symmetric/ CH_3 symmetric stretching	2.168±0.080	2.640±0.126	p<0.001***

Table 13 shows the frequency changes in the left ventricle muscle of the diabetic and control groups.

Table 13. Changes in the frequency values of the main functional groups in 3030 cm^{-1}-2800 cm^{-1} region for control and diabetic rat heart left ventricle muscle. Values are shown as "mean ± standard deviation".

Functional Groups	**Control**	**Diabetic**	**P values**
CH_3 asymmetric stretching	2957.86±0.22	2957.48±0.22	p<0.017*
CH_2 antisymmetric stretching	2922.85±0.07	2922.68±0.13	p<0.011*
CH_2 symmetric stretching	2853.02±0.09	2852.82±0.11	p<0.004**

It is clearly seen from figure 26 and table 13 that, the changes in the frequency values follow the same trend with the apex myocardium but the changes are quite significant for the left ventricle muscle of the diabetic group with respect to control for the main functional groups investigated in this spectral region. An important difference between the diabetic and the control group is seen in the frequency of the CH_3 asymmetric stretching band. A shift in the frequency of this band to lower values is observed in the diabetic group.

3.1.2.2.1.2 Comparison of the Control and Diabetic Rat Heart Left Ventricle Muscle Spectra in 1800 cm^{-1}-1480 cm^{-1} Region

The average spectra belonging to the left ventricle muscle of control (8 samples) and diabetic (7 samples) groups are given in figure 27 at 1800 cm^{-1} -1480

cm^{-1} region. In order to make comparisons between diabetic and control group, normalization was done in 1480 cm^{-1}- 950 cm^{-1} region.

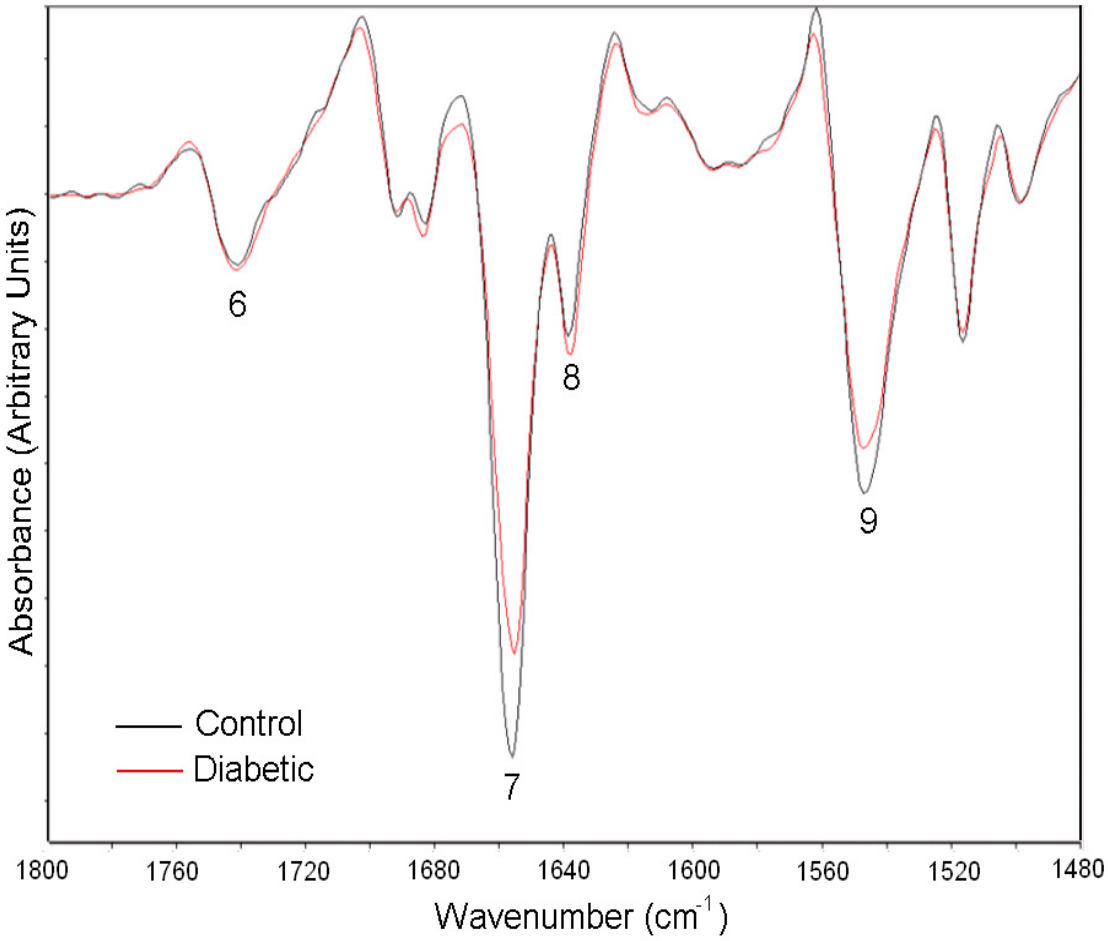

Figure 27. Average spectra belonging to the left ventricle muscle of control (8 samples) and diabetic (7 samples) groups in 1800 cm^{-1}-1480 cm^{-1} region. Vector normalization was done in 1480 cm^{-1}- 950 cm^{-1} region.

The changes in the intensities of main functional groups in control and diabetic rat heart left ventricle muscle are given in table 14.

As it seen in figure 27 and table 14, the changes observed in the intensity of the bands in this region are also very similar with the changes observed for the apex myocardium. The main differences are like the following: Diabetes mellitus causes a significant decrease in the intensity of the Amide I of α-helical structure and the Amide II band; and a more significant increase (with respect to apex myocardium) in

the intensity of the band at 1637 cm^{-1} which is attributable to Amide I of β sheet structure in the diabetic group.

The changes in the frequency of the main bands for the control and the diabetic group of the left ventricle muscle are given in table 15. When figure 27 and table 15 are examined carefully, we see that the changes seen in the frequencies of the Amide I and Amide II bands follow the same trend with the apex myocardium.

Table 14. Changes in the intensities of the main functional groups in 1800 cm^{-1}-1480 cm^{-1} region for control and diabetic rat heart left ventricle muscle. Values are shown as "mean ± standard deviation".

Functional Groups	**Control**	**Diabetic**	**P values**
Amid I: α-helical structure	-0.830±0.065	-0.680±0.100	p<0.008**
Amid I: β-sheet	-0.210±0.011	-0.240±0.010	p<0.002**
Amid II: α-helical structure	-0.420±0.024	-0.358±0.032	p<0.004**

Table 15. Changes in the frequency values of the main functional groups in 1800 crn^{-1}-1480 cm^{-1} region for control and diabetic rat heart left ventricle muscle. Values are shown as "mean ± standard deviation".

Functional Groups	**Control**	**Diabetic**	**P values**
Amid I: α-helical structure	1655.27±0.49	1654.79±1.22	p<0.037*
Amid I: β-sheet	1637.89±0.22	1637.50±0.38	p<0.037*
Amid II: α-helical structure	1547.87±0.32	1548.36±0.47	p<0.037*

3.1.2.2.1.3 Comparison of the Control and Diabetic Rat Heart Left Ventricle Muscle Spectra in 1480-1000 cm^{-1}

The average spectra belonging to the left ventricle muscle of control (8 samples) and diabetic (7 samples) groups are given in figure 28 at 1480 cm^{-1}-1000 cm^{-1} region. In order to make comparisons between diabetic and control group, normalization was done in 1480 cm^{-1}- 950 cm^{-1} region.

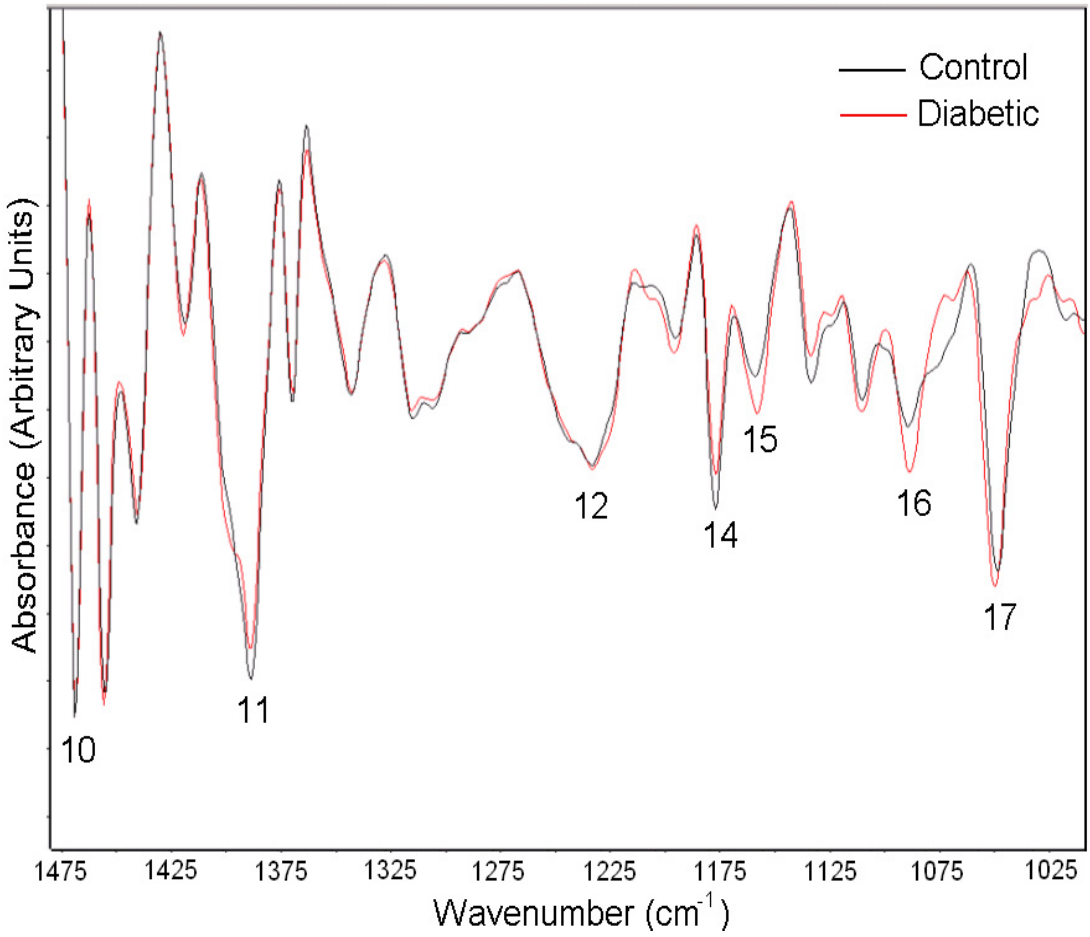

Figure 28. The average spectra belonging to the left ventricle muscle of control (8 samples) and diabetic (7 samples) groups in 1480 cm^{-1}-1000 cm^{-1} region. Vector normalization was done in 1480 cm^{-1}- 950 cm^{-1} region.

Table 16. Changes in the intensities of the main functional groups in 1480 cm^{-1}-1000 cm^{-1} region for control and diabetic rat heart left ventricle muscle. Values are shown as "mean ± standard deviation"

Functional Groups	**Control**	**Diabetic**	**P values**
CH_3 bending	-0.122±0.003	-0.112±0.006	p<0.003**
CO-O-C asymmetric stretching	-0.061±0.003	-0.049±0.008	p<0.013*
C-O stretching (At 1151 cm^{-1})	-0.012±0.002	-0.026±0.004	p<0.001***
C-O stretching / CO-O-C asymmetric stretching	0.197±0.040	0.546±0.162	p<0.001***
PO_2^- symmetric stretching	-0.031±0.003	-0.047±0.012	p<0.003**
C-O stretching (At 1041 cm^{-1})	-0.084±0.005	-0.089±0.014	p<0.324

The main changes in the intensity values of the investigated functional groups are given in table 16. The changes observed in the intensity of the bands in this region are also very similar with the changes observed for the apex myocardium. The main differences are: The increase in the intensity of the glycogen band is more significant, but the decrease in the intensity of the CO-O-C asymmetric stretching band is less significant in the diabetic group of the left ventricle muscle.

3.1.2.2.2 Spectral Changes in the Vessel of the Left Ventricle Muscle

3.1.2.2.2.1 Comparison of the Control and Diabetic Rat Heart Vessel Spectra in 3030-2800 cm^{-1} Region

The average spectra belonging to the vessel on the left ventricle muscle of control (9 samples) and diabetic (8 samples) groups are given in figure 29 at 3030 cm^{-1}-2800 cm^{-1} region. In order to make comparisons between diabetic and control group, normalization was done in 3050 cm^{-1} -2800 cm^{-1} region.

The changes in the intensity of the main functional groups in this region are given in table 17. As it is shown in figure 29 and table 17, the changes observed in the intensity of the band in this region show the same trend with the apex and the left ventrical muscle but the changes are more dramatic with respect to apex in the intensities of the CH_2 symmetric stretching and CH_3 asymmetric stretching bands. As seen in figure 29 and table 17, a significant increase occurs in the intensity of the band at around 3012 cm^{-1} in the diabetic group with respect to control.

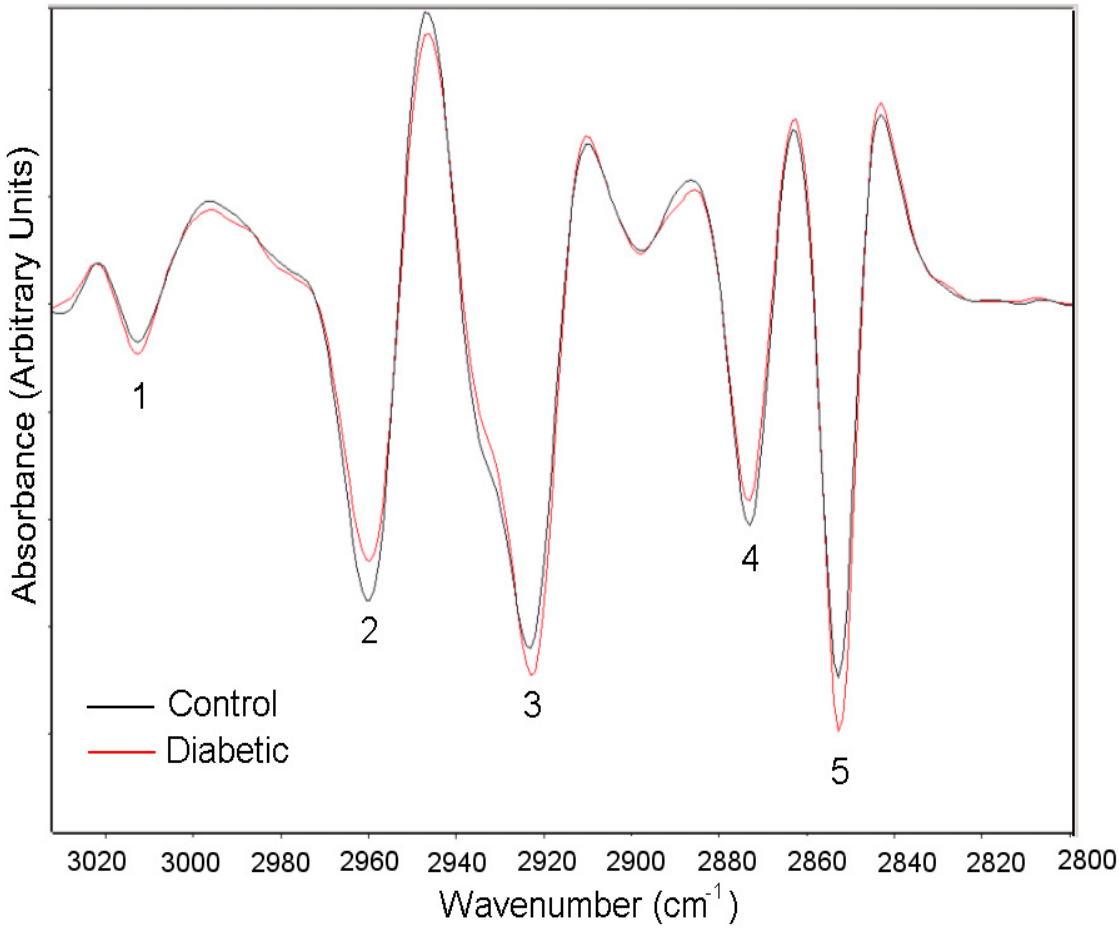

Figure 29. The average spectra belonging to the vessel on the left ventricle muscle of control (9 samples) and diabetic (8 samples) groups in 3030 cm^{-1}-2800 cm^{-1} region. Vector normalization was done in 3050 cm^{-1} -2800 cm^{-1} region.

Table 17. Changes in the intensities and intensity ratios of the main functional groups in 3030 cm^{-1} -2800 cm^{-1} region for control and diabetic rat heart vessel on the left ventricle muscle. Values are shown as "mean ± standard deviation".

Functional Groups	**Control**	**Diabetic**	**P values**
Olefinic =CH stretching	-0.017±0.006	-0.023±0.005	p<0.048*
CH_3 asymmetric stretching	-0.127±0.006	-0.109±0.004	p<0.001***
CH_2 antisymmetric stretching	-0.150±0.007	-0.169±0.006	p<0.004**
CH_3 symmetric stretching	-0.100±0.004	-0.090±0.007	p<0.003**
CH_2 symmetric stretching	-0.170±0.004	-0.200±0.012	p<0.001***
CH_2 symmetric/ CH_3 symmetric stretching	1.709±0.115	2.227±0.290	p<0.001***

Table 18. Changes in frequency values of the main functional groups in 3030 cm^{-1}-2800 cm^{-1} region for control and diabetic rat heart vessel on the left ventricle muscle. Values are shown as "mean ± standard deviation".

Functional Groups	**Control**	**Diabetic**	**P values**
CH_3 asymmetric stretching	2957.95±0.44	2957.69±0.32	p<0.21
CH_2 antisymmetric stretching	2921.90±0.33	2921.44±0.53	p<0.03*
CH_2 symmetric stretching	2852.32±0.21	2852.06±0.28	p<0.05*

Table 18 shows the changes in the frequency values of the control and diabetic vessel on the left ventricle muscle of the rat heart. It is clearly seen from figure 29 and table 18 that, the shift in the frequency of the CH_2 symmetric stretching mode to lower values shows the same trend with the apex myocardium and the left ventricle muscle. The frequency shift of the CH_2 asymmetric stretching band to lower values in the vessel was shown to be as significant as the frequency shift observed for the left ventricle muscle, but much more significant than the change observed for the apex myocardium.

3.1.2.2.2.2 Comparison of the Control and Diabetic Rat Heart Vessel Spectra in 1800-1480 cm^{-1} Region

The average spectra belonging to the vessel on the left ventricle muscle of control (9 samples) and diabetic (8 samples) groups are given in figure 30 at 1800 cm^{-1}-1480 cm^{-1} region. In order to make comparisons between diabetic and control group, normalization was done in 1480 cm^{-1}- 950 cm^{-1} region.

Table 19 displays the changes in the intensity values of the main functional groups investigated in this region for the control and diabetic rat heart vessel on the left ventricle muscle. The changes observed in this region are also very similar with the changes observed for the apex myocardium and the left ventricle muscle, but more significant changes occur in the intensities of the Amide land the Amide II bands of the vessels than the changes observed in the apex and left ventricle muscle of the diabetic group.

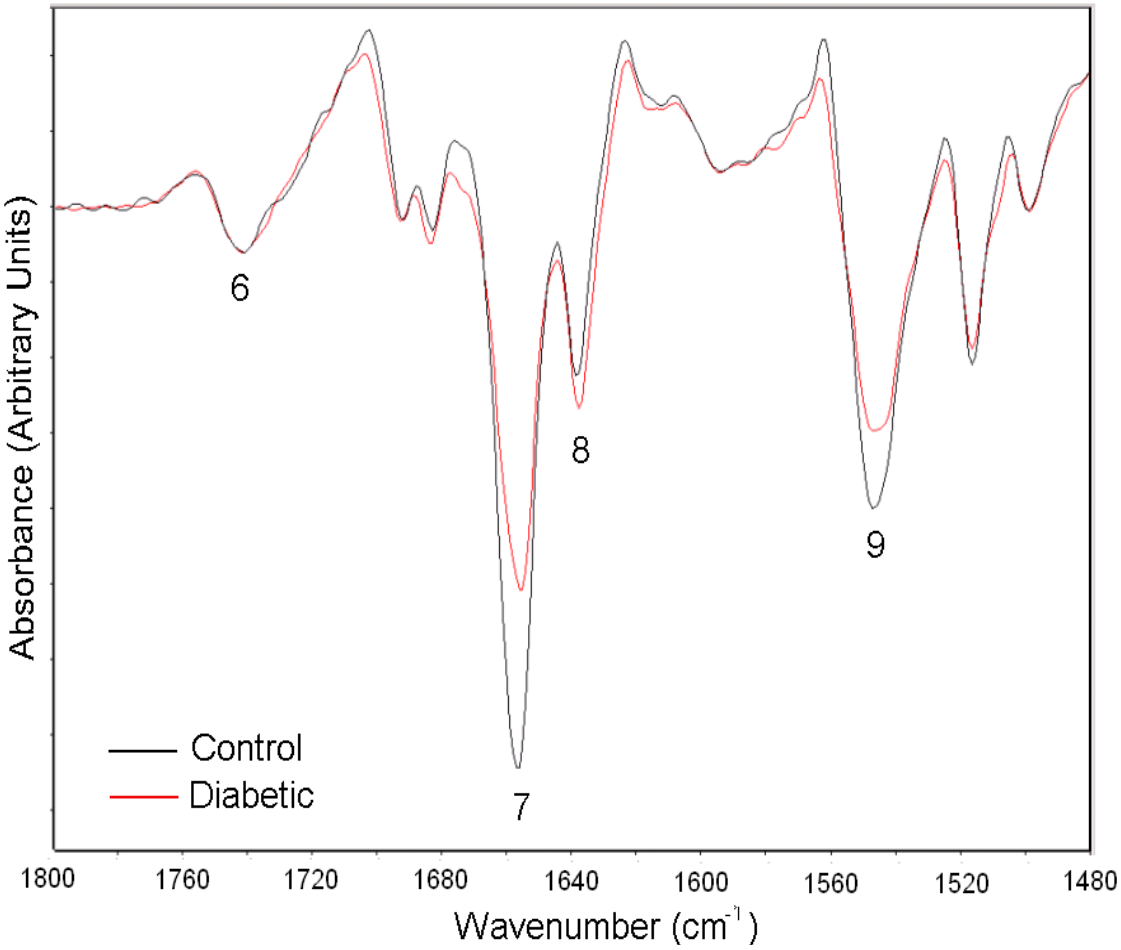

Figure 30. Average spectra belonging to the vessel on the left ventricle muscle of control (9 samples) and diabetic (8 samples) groups in 1800 cm^{-1}-1480 cm^{-1} region. Vector normalization was done in 1480 cm^{-1}- 950 cm^{-1} region.

Table 19. Changes in the intensities of the main functional groups in 1800 cm^{-1}-1480 cm^{-1} region for control and diabetic rat heart vessel on the left ventricle muscle. Values are shown as "mean ± standard deviation".

Functional Groups	**Control**	**Diabetic**	**P values**
Amid I: α-helical structure	-0.730±0.068	-0.510±0.035	p<0.001***
Amid I: β-sheet	-0.220±0.019	-0.260±0.024	p<0.002**
Amid II: α-helical structure	-0.380±0.022	-0.280±0.036	p<0.001***

Table 20 shows the changes in the frequency of the main functional groups investigated in this region for the control and diabetic vessel on the left ventricle muscle of the rat heart. It is clearly seen from the table that the shifts in the frequency

values of the investigated functional group show the same trend with the apex myocardium and the left ventricle muscle of the rat heart in the diabetic group with respect to the control, but the differences between the control and the diabetic groups are not as significant.

Table 20. Changes in the frequency values of the main functional groups in 1800 cm^{-1}-1480 cm^{-1} region for control and diabetic rat heart vessel on the left ventricle muscle. Values are shown as "mean ± standard deviation".

Functional Groups	**Control**	**Diabetic**	**P values**
Amid I: α-helical structure	1655.47±0.71	1654.92±1.47	p<0.06
Amid I: β-sheet	1637.85±0.26	1637.40±0.62	p<0.06
Amid II: α-helical structure	1547.90±0.45	1548.37±0.87	p<0.05*

3.1.2.2.2.3 Comparison of the Control and Diabetic Rat Heart Vessel Spectra in 1480-1000 cm^{-1} Region

The average spectra belonging to the vessel on the left ventricle muscle of control (9 samples) and diabetic (8 samples) groups are given in figure 31 at 1480 cm^{-1}-1000 cm^{-1} region. In order to make comparisons between diabetic and control group, normalization was done in 1480 cm^{-1} - 950 cm^{-1} region.

Table 21 shows the changes in the intensities of the main functional groups in control and diabetic rat heart vessel on the left ventricle muscle.

Figure 31 clearly shows that there is a new band appearing at 1201 cm^{-1} which arises due to the collagen present in the system (Lui *et al*., 1996). There is an apparent increase in the intensity of this collagen band in diabetic groups. So, it might be due to an increase in the content of collagen in diabetic rat vessel in the left ventricle muscle.

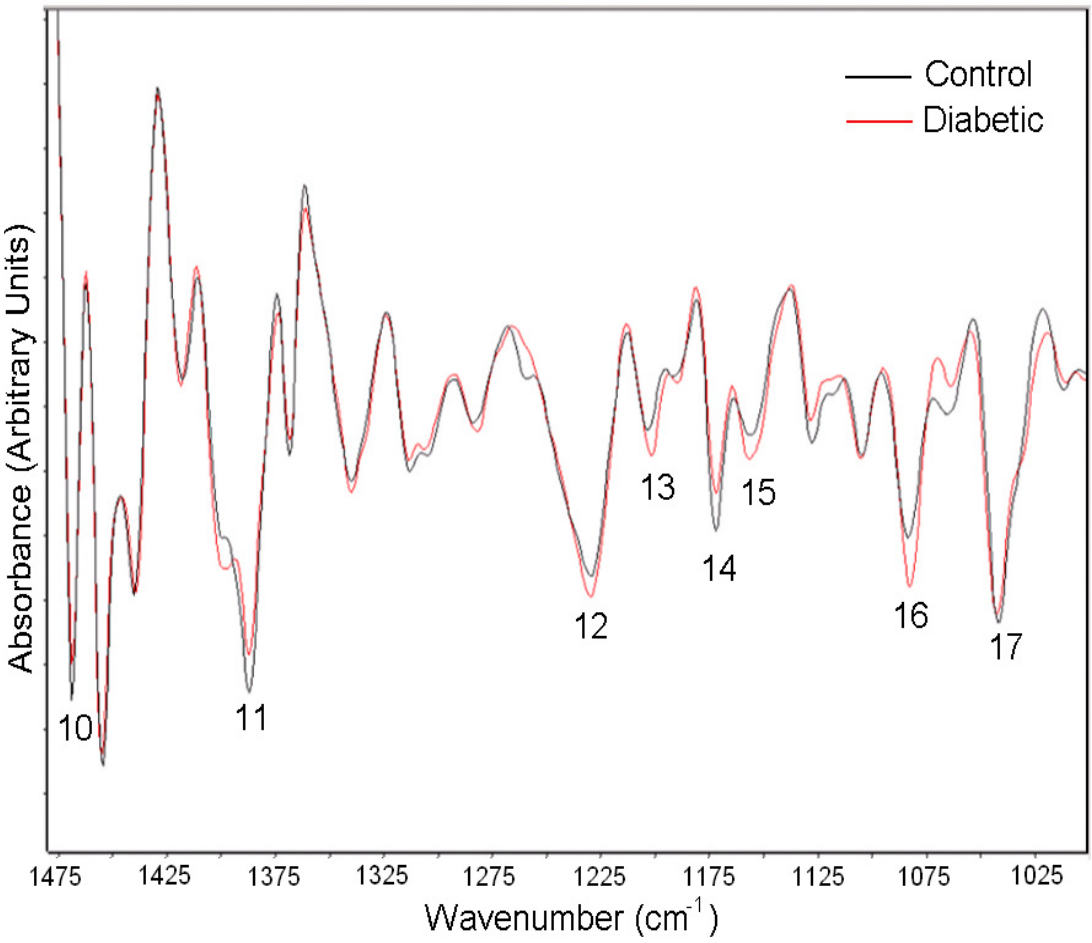

Figure 31. Average spectra belonging to the vessel on the left ventricle muscle of control (9 samples) and diabetic (8 samples) groups in 1480 cm^{-1}-l000 cm^{-1} region. Vector normalization was done in 1480 cm^{-1} 950 cm^{-1} region.

Table 21. Changes in the intensities of the main functional groups in 1480 cm^{-1}-950 cm^{-1} region for control and diabetic rat heart vessel on the left ventricle muscle. Values are shown as "mean ± standard deviation"

Functional Groups	**Control**	**Diabetic**	**P values**
CH_3 bending	-0.109±0.004	-0.096±0.007	p<0.001***
Collagen	-0.009±0.006	-0.021±0.007	p<0.01**
CO-O-C asymmetric stretching	-0.047±0.004	-0.033±0.005	p<0.001***
C-O stretching (At 1151 cm^{-1})	-0.009±0.005	-0.018±0.004	p<0.008**
C-O stretching / CO-O-C asymmetric stretching	0.195±0.127	0.530±0.187	p<0.004**
PO_2^- symmetric stretching	-0.050±0.006	-0.070±0.008	p<0.001***
C-O stretching (At 1041 cm^{-1})	-0.083±0.012	-0.080±0.056	p<0.59

The other changes in the intensity values of the bands in this region are similar to the ones obtained for the apex and the left ventricle muscle with some changes in their significance, like the following: The increase in the intensity of the band at 1081 cm^{-1} is more significant than the changes seen in the apex myocardium and the left ventricle muscle; the increase in the intensity of the band at 1151 cm^{-1} in vessel is less significant than the left ventricle muscle but more significant than the apex myocardium; the decrease in the intensities of the bands at 1171 cm^{-1} and 1386 cm^{-1} is more significant in the vessel than the apex myocardium and the left ventricle muscle (table 21).

3.1.2.3 Right Ventricle Muscle of Rat Heart

Figure 32A shows a light microscope image of H&E stained thin slice taken from the right ventricle of rat heart at 25X magnification. The same image including the mapped region is given in figure 32B at 100X magnification. Cluster analysis was not performed for the right ventricle muscle, because there was no different structure to differentiate in the mapped region.

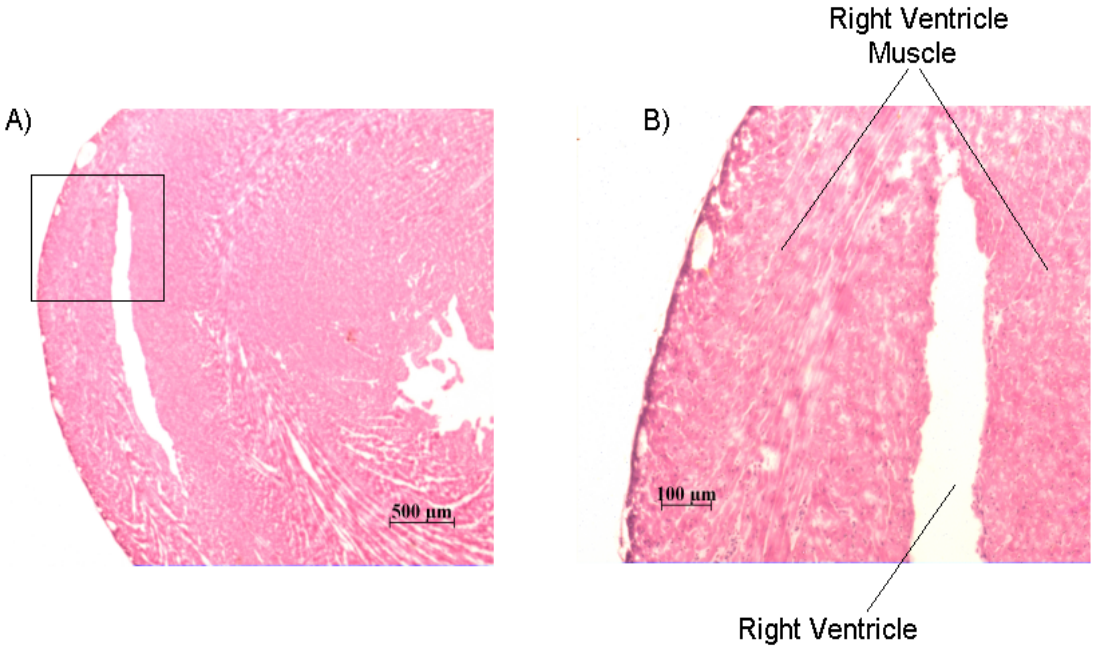

Figure 32. Light microscope image of H&E stained thin slice taken from the right ventricle of rat heart at 25X magnification (A), the same image including the mapped region at 100X magnification (B).

3.1.2.3.1 Comparison of the Control and Diabetic Rat Heart Right Ventricle Muscle Spectra in 3030-2800 cm^{-1} Region

The average spectra belonging to the right ventricle muscle of control (9 samples) and diabetic (9 samples) groups are given in figure 33 at 3030 cm^{-1}-2800 cm^{-1} region. In order to make comparisons between diabetic and control group, normalization was done in 3050 cm^{-1}-2800 cm^{-1} region.

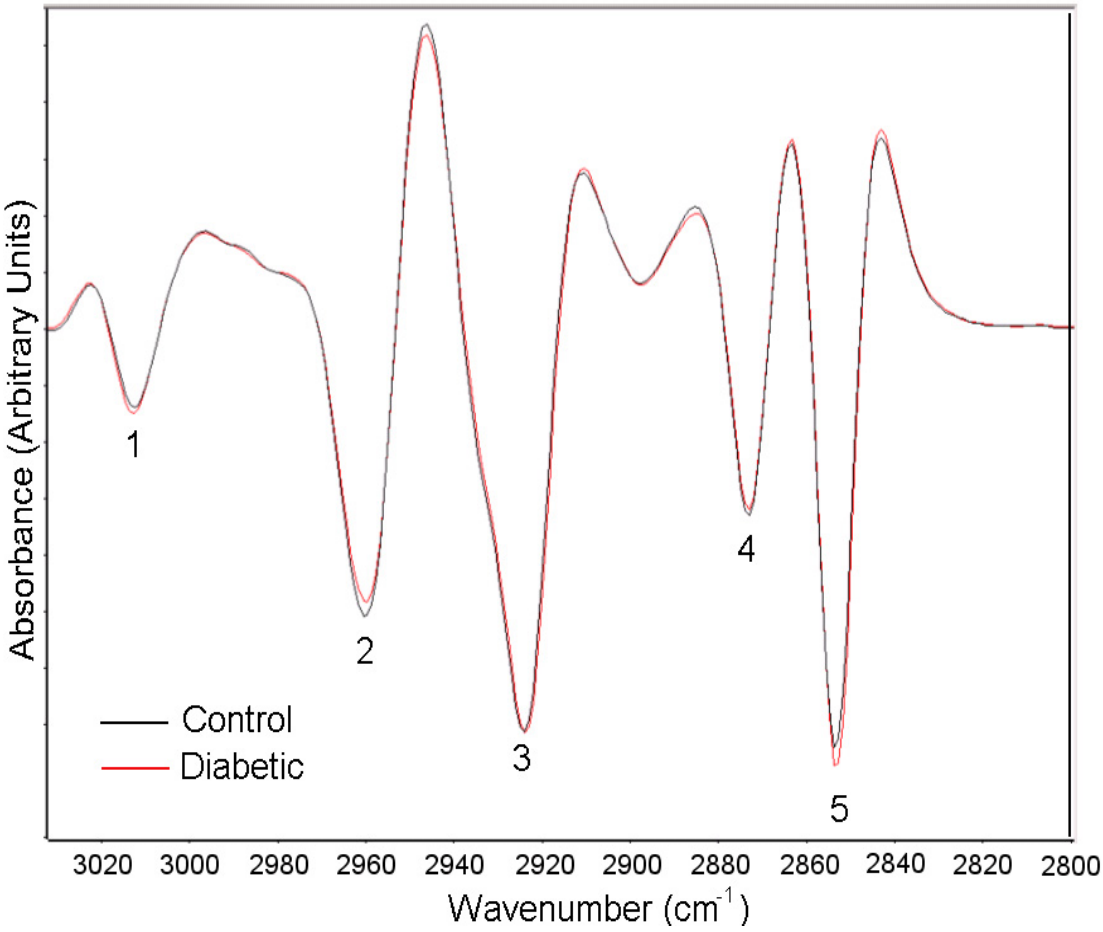

Figure 33. Average spectra belonging to the right ventricle muscle of control (9 samples) and diabetic (9 samples) groups in 3030 cm^{-1}-2800 cm^{-1} region. Vector normalization was done in 3050 cm^{-1}-2800 cm^{-1} region.

Table 22 shows the changes in the intensity values of the functional groups investigated in this region for the right ventricle muscle of the control and the diabetic rat hearts. As it is seen in the table and the figure, the changes observed in the intensities of the bands in this region show the same trend with the apex, the left ventricle muscle and the vessel. However, the changes in the intensities of the CH_3

symmetric and CH_2 asymmetric stretching modes are less significant than the apex myocardium, left ventricle muscle and the vessel; the decrease in the intensity of the CH_3 asymmetric stretching band is less significant than the left ventricle muscle and the vessel, but more significant than the apex. The increase in the intensity of the band at 3012 cm^{-1} is not significant, which was the case for the apex and the left ventricle muscle.

Table 22. Changes in the intensities and intensity ratios of the main functional groups in 3030 cm^{-1}-2800 cm^{-1} region for control and diabetic rat heart right ventricle muscle. Values are shown as "mean ± standard deviation".

Functional Groups	**Control**	**Diabetic**	**P values**
Olefinic =CH stretching	-0.034±0.006	-0.037±0.004	p<0.42
CH_3 asymmetric stretching	-0.116±0.004	-0.108±0.003	p<0.003**
CH_2 antisymmetric stretching	-0.174±0.002	-0.174±0.003	p<0.72
CH_3 symmetric stretching	-0.082±0.002	-0.079±0.002	p<0.088
CH_2 symmetric stretching	-0.185±0.003	-0.190±0.002	p<0.001***
CH_2 symmetric/ CH_3 symmetric stretching	2.260±0.117	2.460±0.113	p<0.005**

Table 23. Changes in frequency values of the main functional groups in 3030 cm^{-1}-2800 cm^{-1} region for control and diabetic rat heart right ventricle muscle. Values are shown as "mean ± standard deviation".

Functional Groups	**Control**	**Diabetic**	**P values**
CH_3 asymmetric stretching	2957.90±0.24	2957.58±0.16	p<0.008**
CH_2 antisymmetric stretching	2922.93±0.10	2922.62±0.19	p<0.001***
CH_2 symmetric stretching	2853.08±0.11	2852.82±0.05	p<0.001***

Table 23 shows the changes in the frequency values of the main functional groups in this region for the right ventricle muscle of the control and diabetic rat heart. When the changes in the frequency values are investigated, it is seen that diabetes causes similar shifts in the frequencies of the functional groups with apex myocardium, left ventricle muscle and the vessel, but the decrease in the frequency of the CH_3 asymmetric stretching mode in the right ventricle muscle (like left

ventricle muscle) is much more significant than the apex and the vessel in the left ventricle muscle.

3.1.2.3.2 Comparison of the Control and Diabetic Rat Heart Right Ventricle Muscle Spectra in 1800-1480 cm^{-1} Region

The average spectra belonging to the right ventricle muscle of control (9 samples) and diabetic (9 samples) groups are given in figure 34 at 1800 cm^{-1}-1480 cm^{-1} region. In order to make comparisons between diabetic and control group, normalization was done in 1480 cm^{-1}- 950 cm^{-1} region.

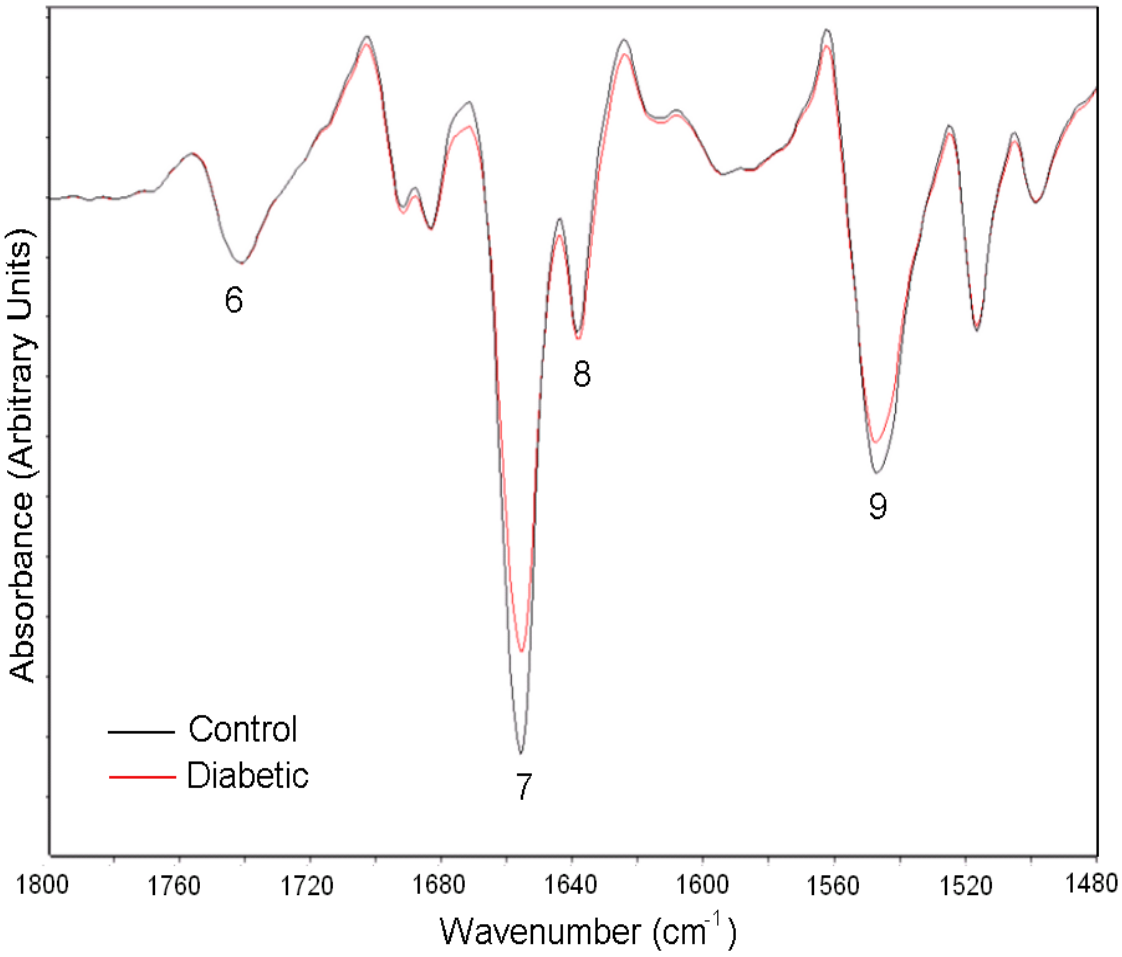

Figure 34. Average spectra belonging to the right ventricle muscle of control (9 samples) and diabetic (9 samples) groups in 1800 cm^{-1}-1480 cm^{-1} region. Vector normalization was done in 1480 cm^{-1}-950 cm^{-1} region.

Table 24 shows the changes in the intensity of the main functional groups investigated in this region for the control and diabetic right ventricle muscle of the heart.

As it is seen from the table and the figure, the changes observed in the intensity of the bands in this region are also very similar with the changes observed fur the apex myocardium, left ventricle muscle and the vessel, but we see less significant decrease in the intensity of the Amide I β sheet and the Amide II band and a more significant decrease in the intensity of the Amide I α-helix band.

Table 24. Changes in the intensities of the main functional groups in 1800 cm^{-1}-1480 cm^{-1} region for control and diabetic rat heart right ventricle muscle. Values are shown as "mean ± standard deviation".

Functional Groups	**Control**	**Diabetic**	**P values**
Amid I: α-helical structure	-0.926±0.089	-0.756±0.069	p<0.001***
Amid I: β-sheet	-0.224±0.017	-0.237±0.010	p<0.102
Amid II: α-helical structure	-0.430±0.035	-0.390±0.027	p<0.01**

Table 25. Changes in the frequency values of the main functional groups in 1800 cm^{-1}-1480 cm^{-1} region for control and diabetic rat heart right ventricle muscle. Values are shown as "mean ± standard deviation".

Functional Groups	**Control**	**Diabetic**	**P values**
Amid I: α-helical structure	1654.83±0.43	1654.78±0.68	p<0.4
Amid I: β-sheet	1637.78±0.16	1637.65±0.29	p<0.21
Amid II: α-helical structure	1548.21±0.24	1548.32±0.35	p<0.17

Table 25 shows the changes in the frequency values of the main functional groups investigated in this region for the control and the diabetic right ventricle muscle of the rat heart. The table clearly shows that the frequency values of the Amide I and Amide II bands do not change significantly in the right ventricle muscle of the diabetic group. Our previous results revealed that (tables 10, 15, 20) diabetes causes a significant shift in the frequency of the Amide I band to lower values, and of

the Amide II band to higher frequency values for the apex myocardium, the left ventricle muscle and the vessel on the left ventricle muscle of the diabetic group.

3.1.2.3.3 Comparison of the Control and Diabetic Rat Heart Right Ventricle Muscle Spectra in 1480-1000 cm^{-1} Region

The average spectra belonging to the right ventricle muscle of control (9 samples) and diabetic (9 samples) groups are given in figure 35 at 1480 cm^{-1}-1000 cm^{-1} region. In order to make comparisons between diabetic and control group, normalization was done in 1480 cm^{-1}-950 cm^{-1} region.

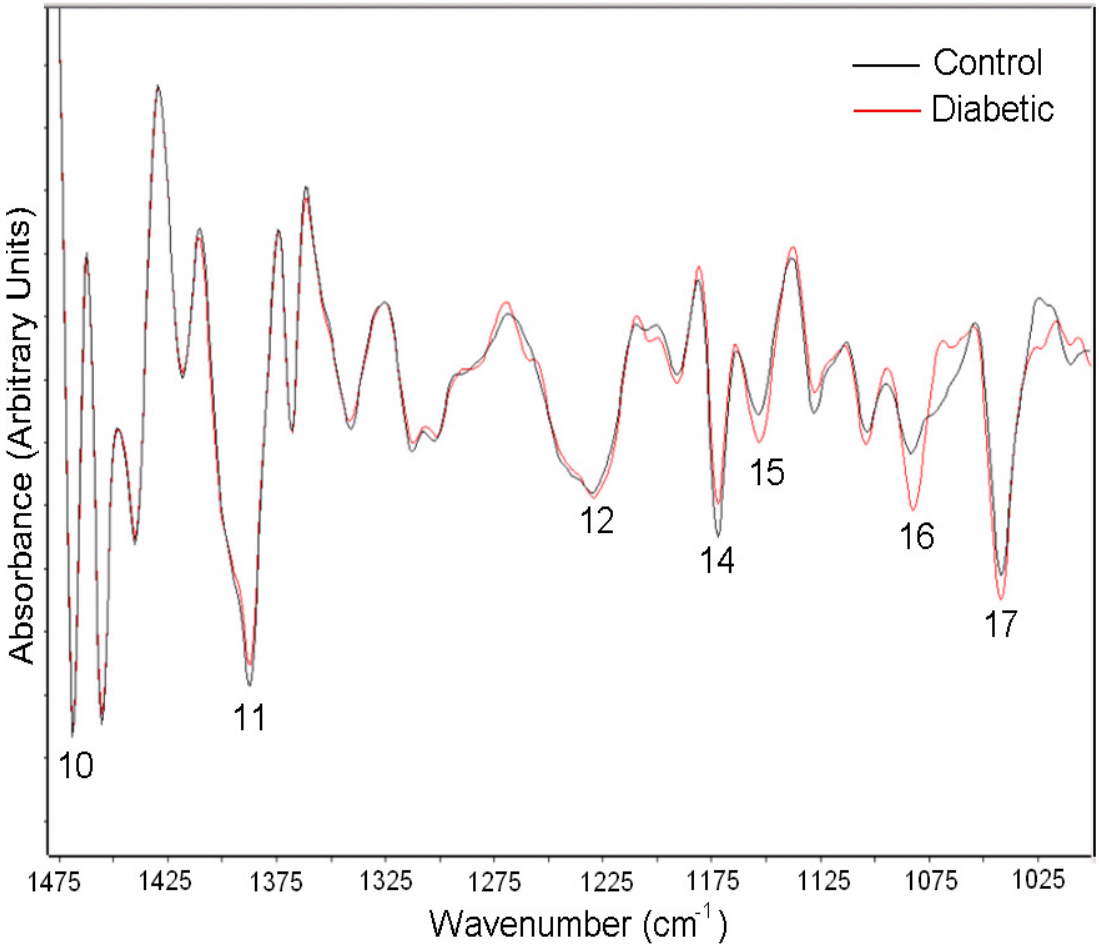

Figure 35. Average spectra belonging to the right ventricle muscle of control (9 samples) and diabetic (9 samples) groups in 1480 cm^{-1}- 1000 cm^{-1} region. Vector normalization was done in 1480 cm^{-1}- 950 cm^{-1} region.

Table 26 shows the changes in the intensity values of the main functional groups investigated in this region for the control and the diabetic rat heart right

ventricle muscle. Figure 35 and table 26 clearly show that the changes in the intensity of the bands in this region which are similar to the ones obtained for the apex myocardium, the left ventricle muscle and the vessel on the left ventricle muscle.

Table 26. Changes in the intensities of the main functional groups in 1480 cm^{-1}-1000 cm^{-1} region for control and diabetic rat heart right ventricle muscle. Values are shown as "mean ± standard deviation".

Functional Groups	**Control**	**Diabetic**	**P values**
CO-O-C asymmetric stretching	-0.119±0.004	-0.111±0.005	p<0.005**
C-O stretching (At 1151 cm^{-1})	-0.062±0.004	-0.049±0.006	p<0.001***
C-O stretching / CO-O-C asymmetric stretching	-0.013±0.004	-0.023±0.006	p<0.004**
PO_2^- symmetric stretching	0.210±0.060	0.490±0.170	p<0.001***
C-O stretching (At 1041 cm^{-1})	-0.029±0.004	-0.052±0.012	p<0.002**
CO-O-C asymmetric stretching	-0.078±-0.015	-0.090±0.009	p<0.05*

3.1.3 Effect of Selenium on Different Regions of the Diabetic Rat Heart

3.1.3.1 Apex

The changes in the intensity and frequency values of the functional groups in the spectra of the apex myocardium of the control, diabetic and selenium treated diabetic rat hearts are given in table 27 and figures 36-38.

It is observed that, the intensity of the Amide I band slightly decreases in the diabetic group, but slightly increases back towards the control value in the Se treated diabetic group. Table 27 clearly shows that diabetes causes a significant decrease in the intensity of the band at 1171 cm^{-1}, and a significant increase in the intensity of the band at 1151 cm^{-1}. However, these changes induced by diabetes in the intensity values are restored in the Se treated diabetic group. This indicates that the differences in the intensity values of these bands between the control and the Se treated diabetic groups are not significant anymore. We see a remarkable increase in the intensity ratios of 1151/1171 cm^{-1} bands, and the band near 1081 cm^{-1} in the diabetic rat heart apex myocardium. The table clearly shows that, when diabetic rats are treated with

Se, the differences in the intensity values between the control and the Se treated diabetic group are no more statistically significant. When the spectral changes between diabetic and Se-treated diabetic groups are investigated, it is seen that the intensity of the band near 1041 cm^{-1} decreases significantly in the Se treated diabetic group with respect to the diabetic rat heart apex.

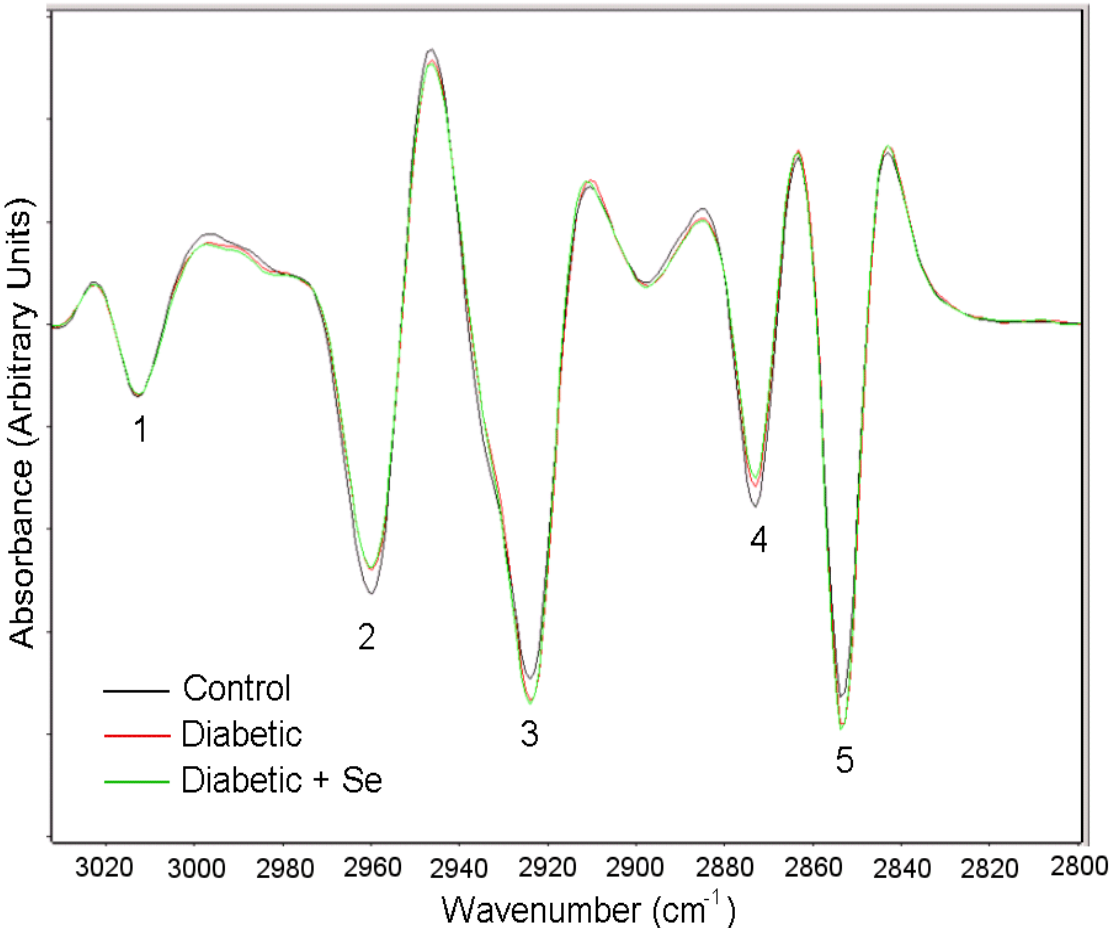

Figure 36. The average spectra belonging to the apex myocardium of control (6 samples), diabetic (8 samples) and Se treated diabetic groups (7 samples) m 3030 cm^{-1}-2800 cm^{-1} region. Vector normalization was done in 3050 cm^{-1}-2800 cm^{-1} region.

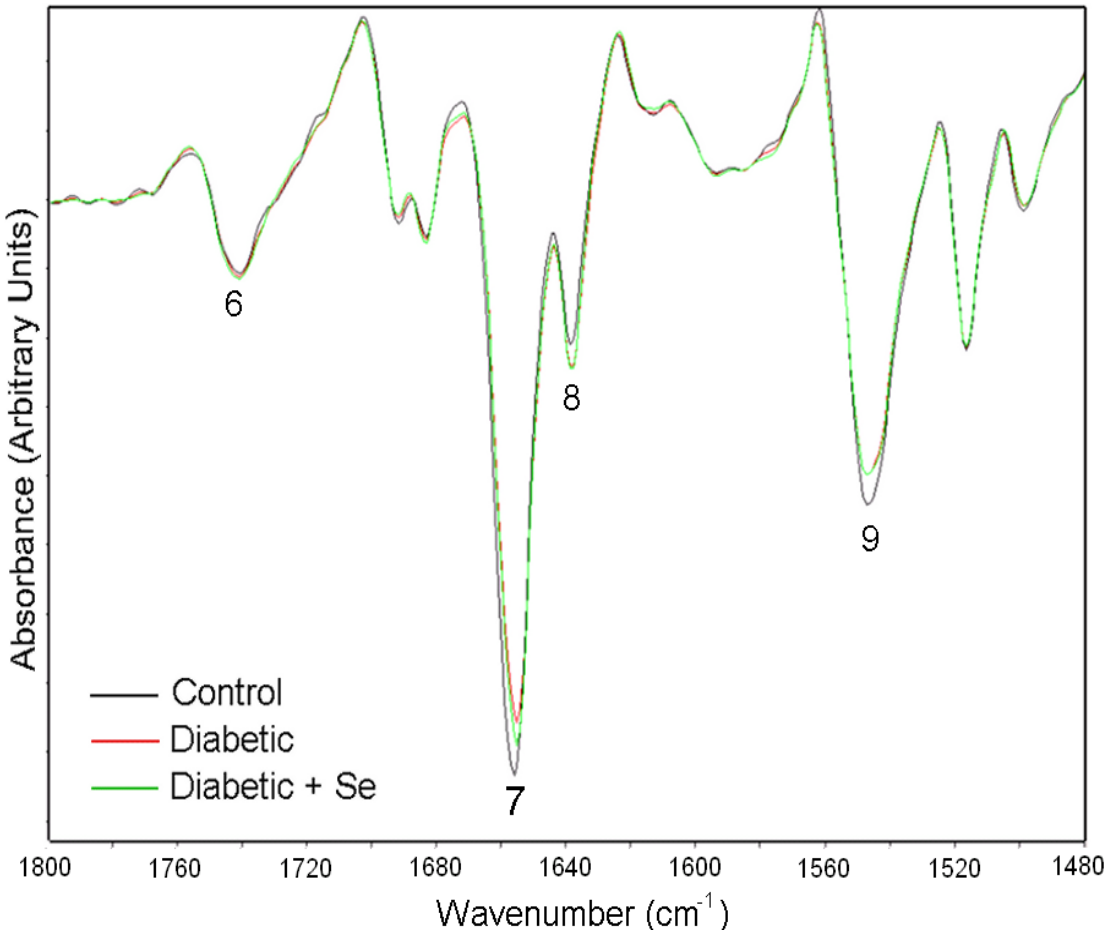

Figure 37. The average spectra belonging to the apex myocardium of control (6 samples), diabetic (8 samples) and Se treated diabetic groups (7 samples) in 1800 cm^{-1}-1480 cm^{-1} region. Vector normalization was done in 1480 cm^{-1}- 950 cm^{-1} region.

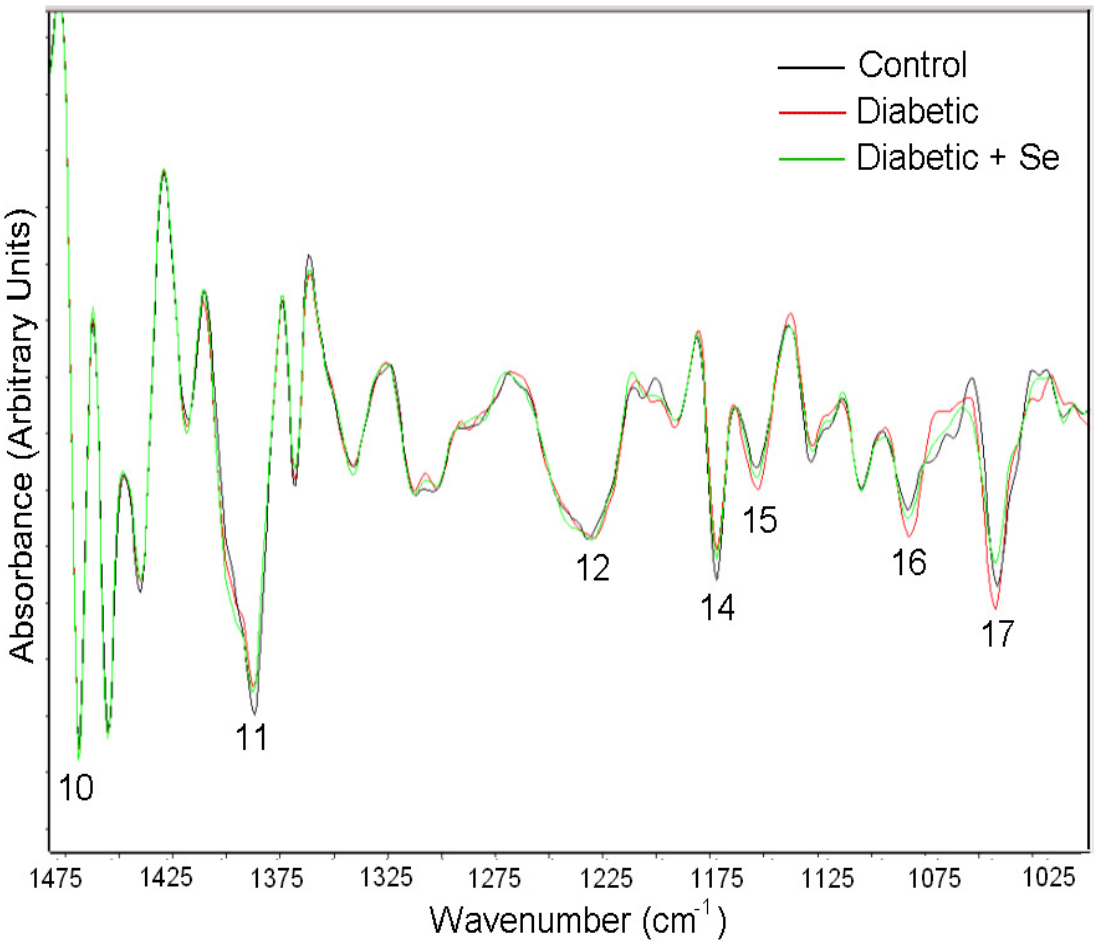

Figure 38. The average spectra belonging to the apex myocardium of control (6 samples), diabetic (8 samples) and Se treated diabetic groups (7 samples) in 1480 cm^{-1}- 1000 cm^{-1} region. Vector normalization was done in 1480 cm^{-1} - 950 cm^{-1} region.

Table 27 shows that the slight decreases in the frequency values of the CH_3 asymmetric and the CH_2 asymmetric stretching modes in the diabetic group increase back to almost their control values in the Se treated diabetic group. In a similar manner but more significant decreases in the frequency values of the CH_2 symmetric stretching and the Amide I bands in the diabetic group are restored in the Se treated diabetic group, by approaching to their control values, so that, the differences in the frequency values of these bands between these two experimental groups are no longer statistically significant. When the spectral changes between diabetic and Se treated diabetic groups are examined, a significant increase in the frequency of the CH_2 symmetric stretching mode is observed in the Se treated diabetic group with respect to the diabetic heart apex.

Table 27. The changes observed in the intensity and frequency values of the functional groups in the spectra of the apex myocardium of the control, diabetic and Se treated diabetic rat hearts. Values are shown as "mean ± standard deviation". First p values are for "control-diabetic" groups, second p values are for "control-diabetic+Se treated" groups and third p values are for "diabetic-diabetic+Se treated groups.

Parameters	Functional groups	Control	Diabetic	Diabetic+Se	P values		
Intensity	Amid I:α-helical structure	-0.830±0.086	-0.750±0.066	-0.800±0.037	p<0.155	p<0.85	p<0.23
	CO-O-C asymmetric stretching	-0.065±0.005	-0.051±0.006	-0.057±0.006	p<0.004**	p<0.067	p<0.064
	C-O stretching (1151 cm^{-1})	-0.014±0.004	-0.022±0.007	-0.018±0.005	p<0.028*	p<0.17	p<0.238
	C-O stretching (1151 cm^{-1}) / CO-O-C asymmetric stretching	0.214±0.070	0.444±0.187	0.319±0.120	p<0.01**	p<0.142	p<0.186
	PO_2^- symmetric stretching	-0.033±0.005	-0.046±0.012	-0.036±0.013	p<0.023*	p<0.58	p<0.258
	C-O stretching (at 1041 cm^{-1})	-0.067±0.020	-0.079±0.012	-0.061±0.008	p<0.24	p<0.27	p<0.02*
Frequency	CH_3 asymmetric stretching	2957.75±0.20	2957.64±0.53	2957.73±0.62	p<0.7	p<0.58	p<0.51
	CH_2 antisymmetric stretching	2922,75±0,16	2922,71±0,24	2922,74±0,29	p<0,89	p<0,72	p<0,884
	CH_2 symmetric stretching	2852.94±0.10	2852.79±0.15	2852.99±0.10	p<0.04*	p<0.465	p<0.02*
	Amid I:α-helical structure	1655.10±0.48	1654.36±0.36	1654.37±0.59	p<0.007**	p<0.06	p<0.8

3.1.3.2 Left Ventricle Muscle

Table 28 and figures 39-41 show the changes in the intensity and frequency values of the functional groups investigated in the left ventricle muscle of the control, diabetic and Se treated diabetic rat hearts.

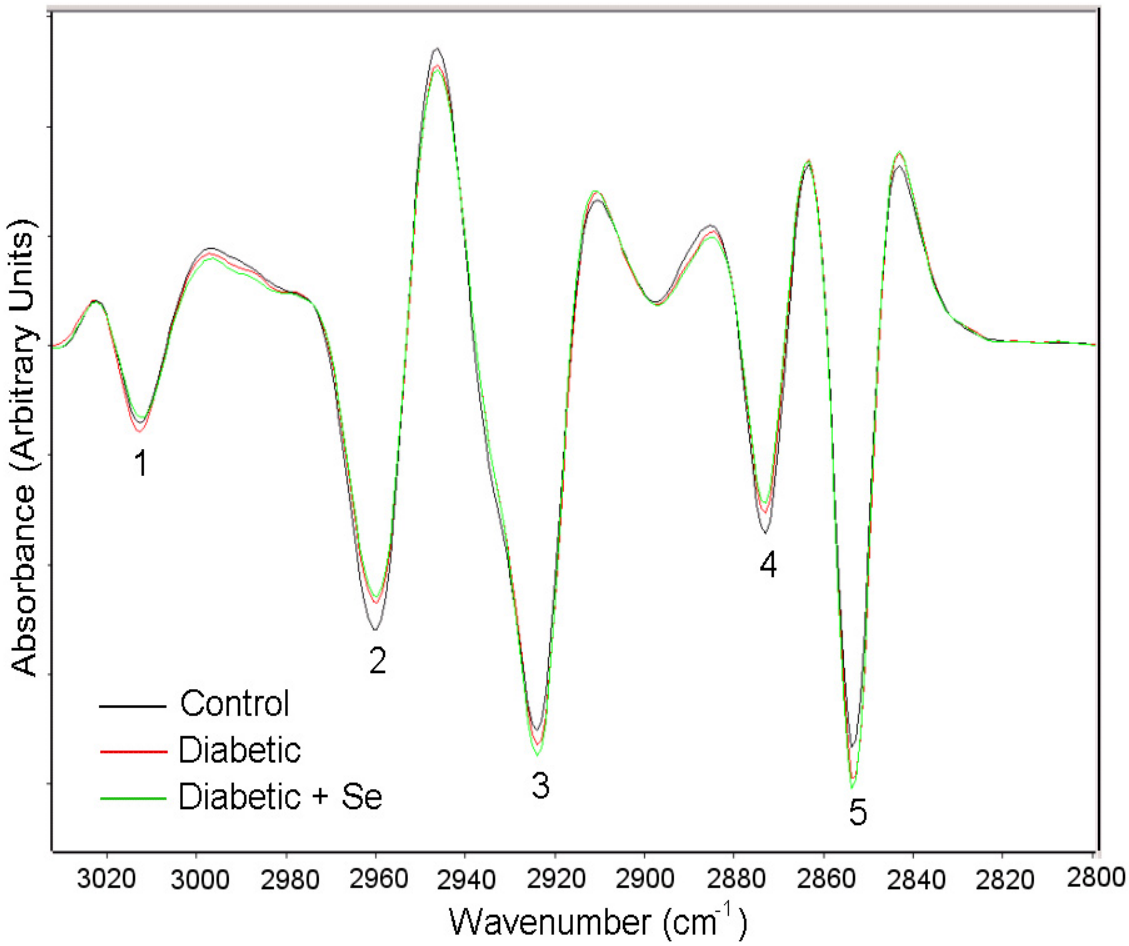

Figure 39. The average spectra belonging to the left ventricle muscle of control (6 samples), diabetic (8 samples) and Se treated diabetic groups (7 samples) in 3030 cm^{-1}-2800 cm^{-1} region. Vector normalization was done in 3050 cm^{-1}-2800 cm^{-1} region.

It is clearly seen in table that the intensity value of the band at 3012 cm^{-1} decreases significantly in the Se treated diabetic group with respect to the diabetic ones. As seen in table 28 that diabetes causes a significant decrease in the intensity of the band at 1171cm^{-1} and a significant increase in the intensity of the band at 1151 cm^{-1}. However, these diabetes mellitus induced changes in the intensity values are restored in the Se treated diabetic group. Because we see that the differences in the intensity values of these bands between the control and the Se treated diabetic groups

are not that significant anymore. In addition, we see a remarkable increase in the intensity ratios of the 1151/1171 cm^{-1} bands, and the band at 1081 cm^{-1} in the diabetic rat heart left ventricle muscle. The table clearly shows that, when diabetic rats are treated with Se, the differences in the intensity values between the control and the Se treated diabetic group are no more statistically significant.

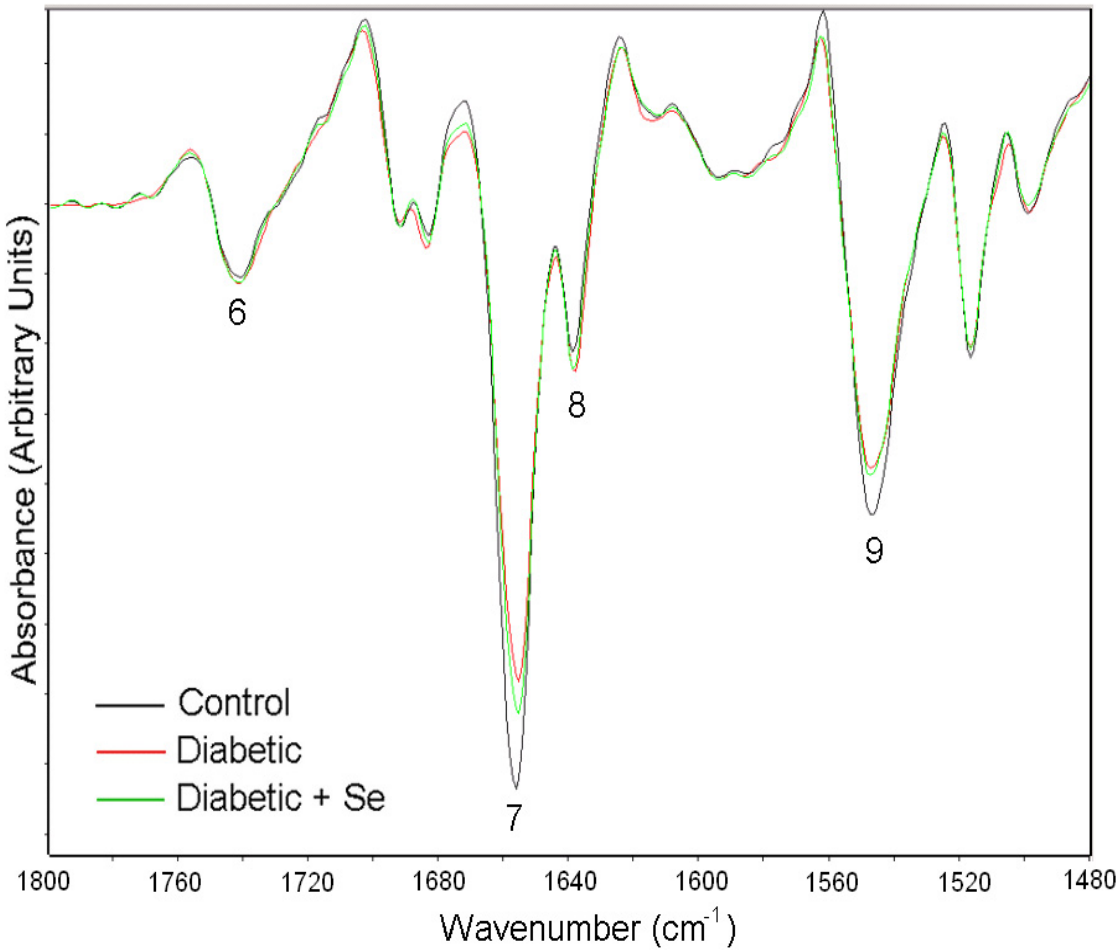

Figure 40. The average spectra belonging to the left ventricle muscle of control (6 samples), diabetic (8 samples) and Se treated diabetic groups (7 samples) in 1800 cm^{-1}-1480 cm^{-1} region. Vector normalization was done in 1480 cm^{-1}- 950 cm^{-1} region.

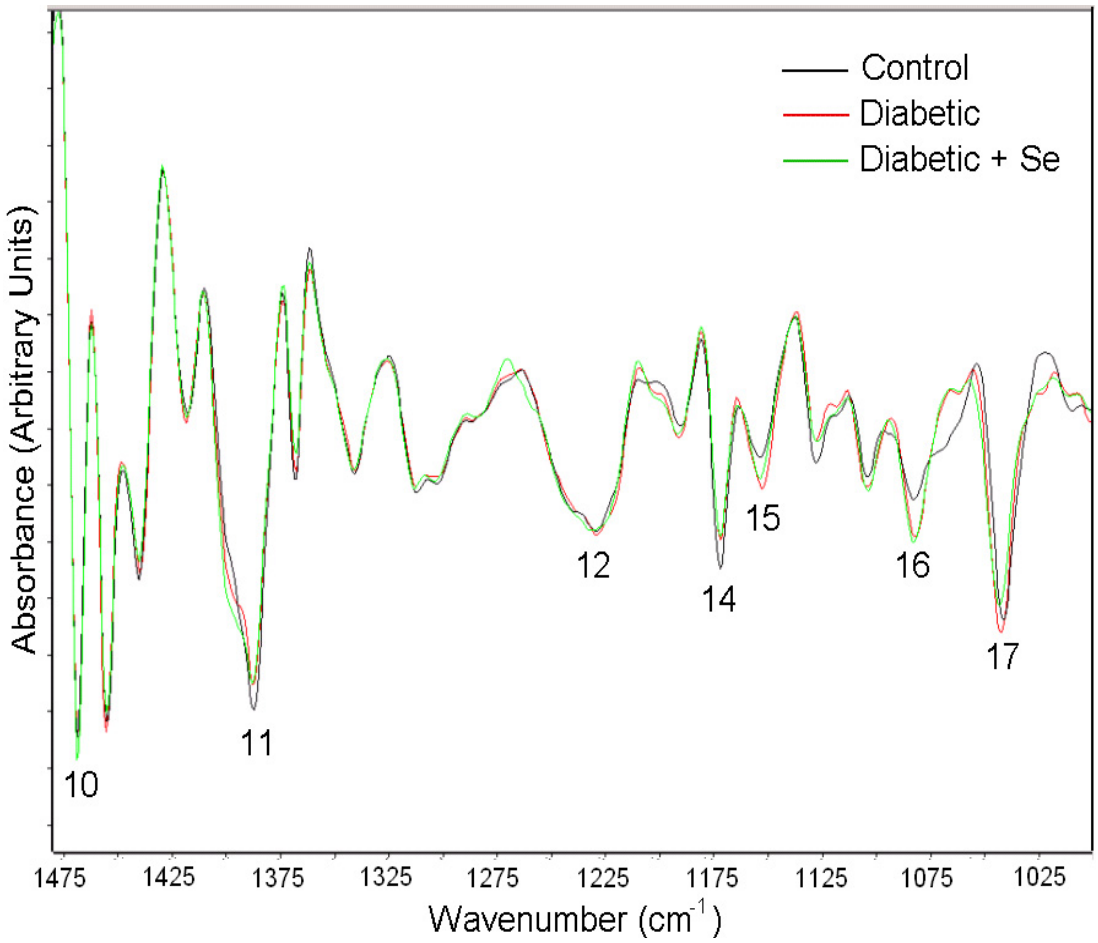

Figure 41. The average spectra belonging to the left ventricle muscle of control (6 samples), diabetic (8 samples) and Se treated diabetic groups (7 samples) in 1480 cm^{-1}-l000 cm^{-1} region. Vector normalization was done in 1480 cm^{-1} - 950 cm^{-1} region.

Table 28 shows significant decreases in the frequency values of the CH_3 asymmetric, the CH_2 asymmetric, the CH_2 symmetric stretching bands and the Amide I band in the diabetic group. It is seen that the frequency values increase back to almost their control values in the Se treated diabetic group, so that the differences in the frequency values of these bands between these two experimental groups are no longer statistically significant for the left ventricle muscle. When the spectral changes between diabetic and Se treated diabetic groups are examined, it is observed that the frequency of the CH_2 symmetric stretching band significantly shifts to higher values in the Se treated diabetic ones with respect to the diabetic group.

Table 28. The changes observed in the intensity and frequency values of the functional groups investigated in the left ventricle muscle of the control, diabetic and Se treated diabetic rat hearts. Values are shown as "mean ± standard deviation". First p values are for "control-diabetic" groups, second p values are for "control-diabetic+Se treated" groups and third p values are for "diabetic-diabetic+Se treated groups.

Parameters	**Functional groups**	**Control**	**Diabetic**	**Diabetic+Se**	**P values**		
Intensity	Olefinic =CH stretching	-0.035±0.004	-0.038±0.004	-0.033±0.002	p<0.069	p<0.118	p<0.029*
	CO-O-C asymmetric stretching	-0.061±0.002	-0.049±0.008	-0.050±0.008	p<0.01**	p<0.046*	p<0.6
	C-O stretching (1151 cm^{-1})	-0.012±0.002	-0.026±0.004	-0.018±0.006	p<0.001***	p<0.18	p<0.1
	C-O stretching (1151 cm^{-1}) / CO-O-C asymmetric stretching	0.197±0.040	0.546±0.162	0.371±0.170	p<0.001***	p<0.241	p<0.167
	PO_2^- symmetric stretching	-0.031±0.003	-0.047±0.012	-0.043±0.014	p<0.003**	p<0.3	p<0.61
Frequency	CH_3 asymmetric stretching	2957.86±0.22	2957.48±0.22	2957.50±0.31	p<0.02*	p<0.06	p<0.94
	CH_2 asymmetric stretching	2922.85±0.07	2922.68±0.13	2922.74±0.13	p<0.01**	p<0.18	p<0.46
	CH_2 symmetric stretching	2853.02±0.09	2852.82±0.11	2853.03±0.08	p<0.004**	p<0.82	p<0.007**
	Amid I: β-sheet	1637.89±0.22	1637.50±0.38	1637.70±0.18	p<0.04*	p<0.07	p<0.16

3.1.3.3 Vessel on the Left Ventricle Muscle

Table 29 and figures 42-44 show the changes in the intensity and frequency values of the functional groups for the vessel on the left ventricle muscle of the control, diabetic and Se treated diabetic rat hearts.

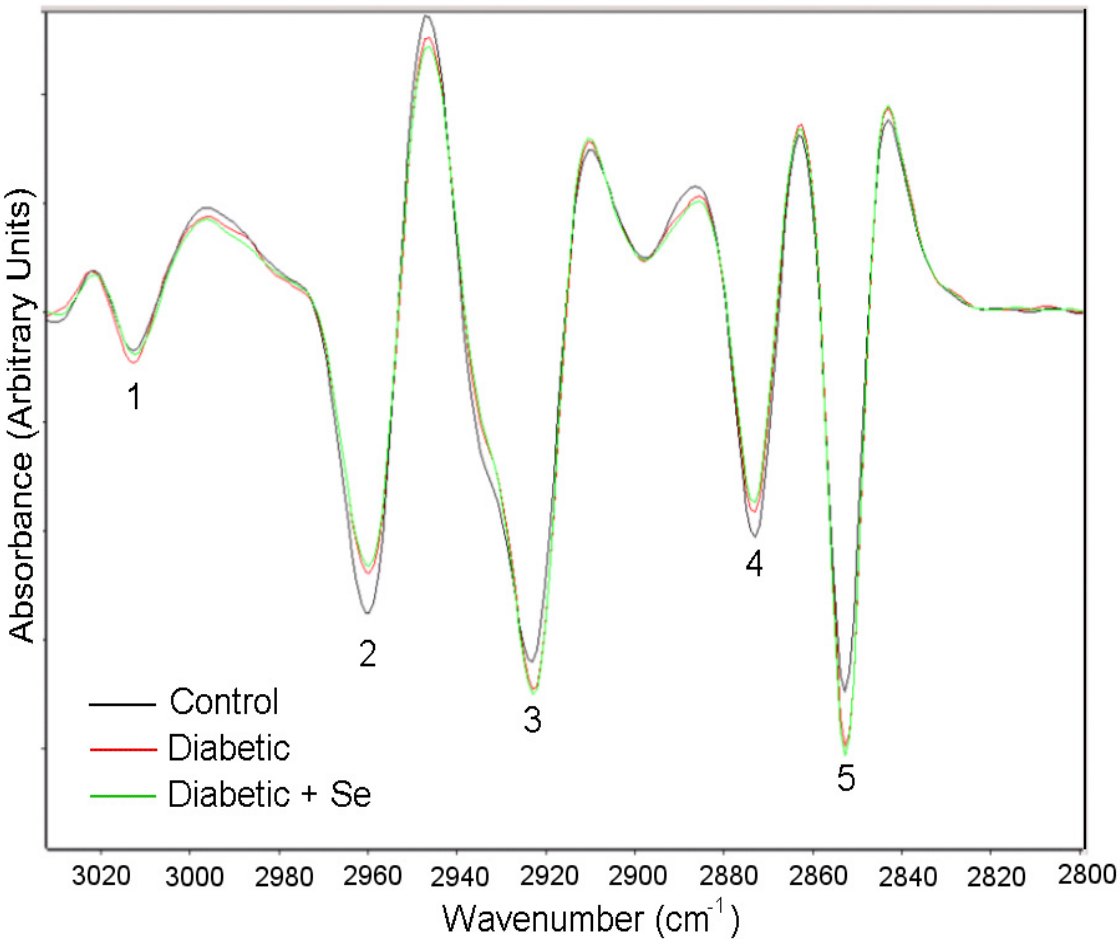

Figure 42. The average spectra belonging to the vessel on the left ventricle muscle of control (6 sample), diabetic (8 samples) and Se treated diabetic groups (7 sample) in 3030 cm^{-1}-2800 cm^{-1} region. Vector normalization was done in 3050 cm^{-1} -2800 cm^{-1} region.

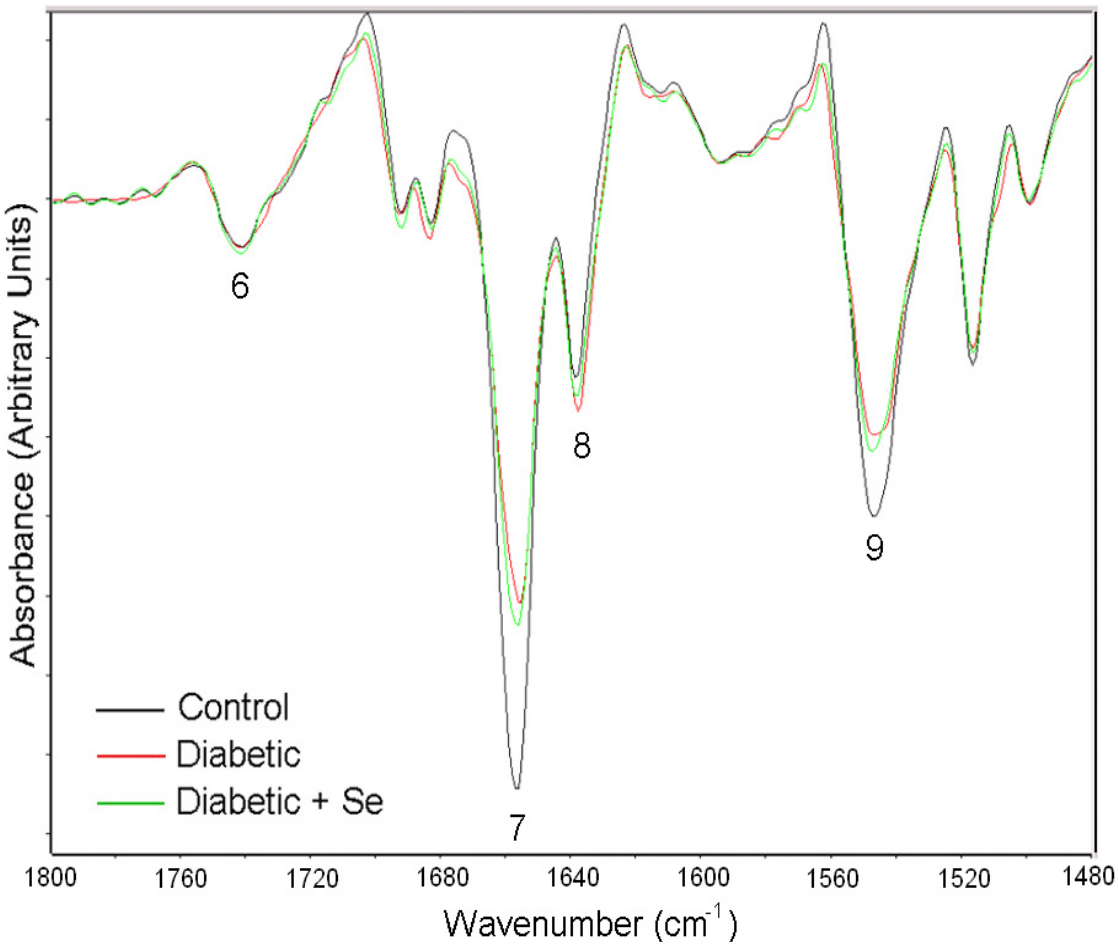

Figure 43. The average spectra belonging to the vessel on the left ventricle muscle of control (6 samples), diabetic (8 samples) and Se treated diabetic groups (7 samples) in 1800 cm^{-1}- l480 cm^{-1} region. Vector normalization was done in 1480 cm^{-1}- 950 cm^{-1} region.

Table 29 clearly shows that diabetes causes a significant increase in the intensity values of the bands at 3012 cm^{-1}, 1637 cm^{-1}, 1151 cm^{-1} and the intensity ratio of 1151/1171 cm^{-1} bands. However, these diabetes mellitus induced changes in the intensity values of these functional groups are restored in the Se treated diabetic group. We see a remarkable decrease in the intensity of the band at 1171 cm^{-1} in the diabetic group. This decrease is less significant in the Se treated diabetic group.

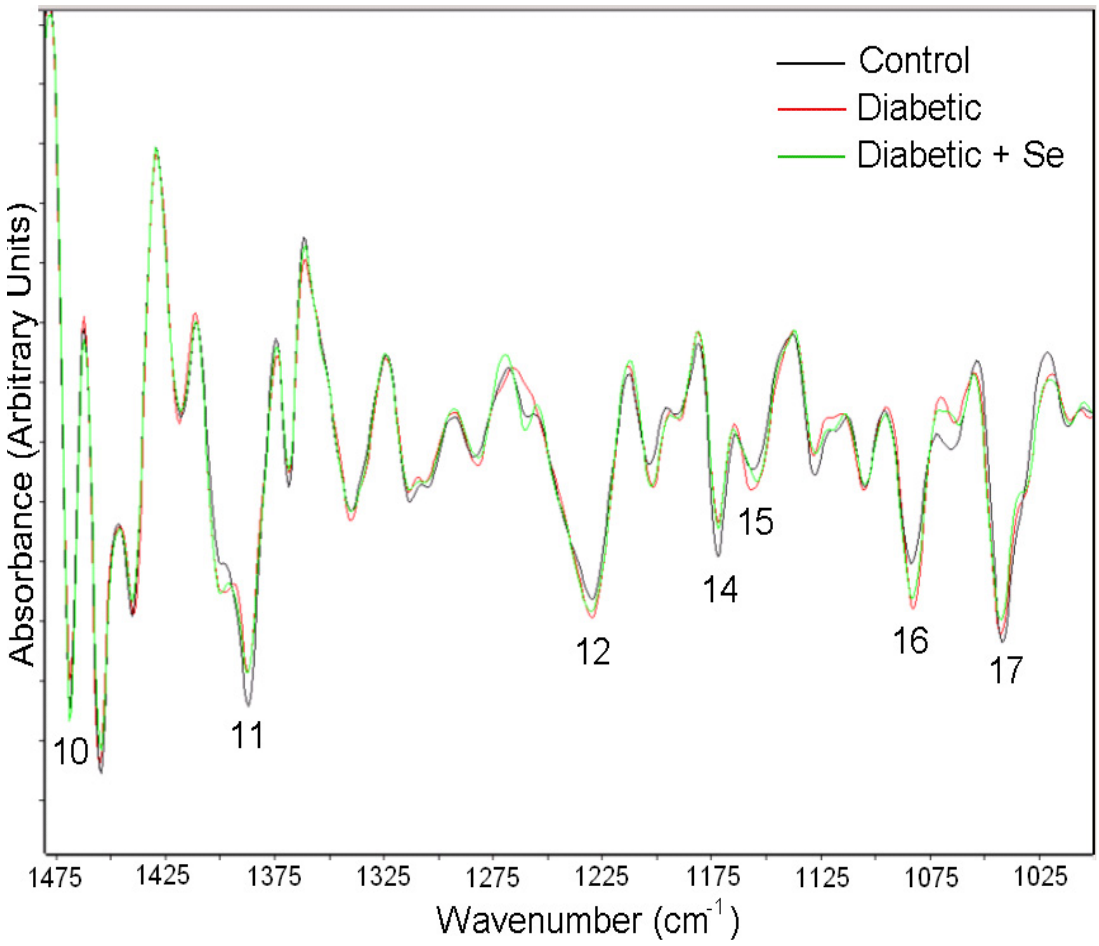

Figure 44. The average spectra belonging to the vessel on the left ventricle muscle of control (6 samples), diabetic (8 samples) and Se treated diabetic groups (7 samples) in 1480 cm^{-1}- 1000 cm^{-1} region. Vector normalization was done in 1480 cm^{-1}- 950 cm^{-1} region.

Table 29 shows significant decreases in the frequency values of the CH_2 asymmetric, the CH_2 symmetric stretching bands and the Amide II bands in the diabetic group. It is clearly seen that the frequency values increase back to almost their control values in the Se treated diabetic group, so that the differences in the frequency values of these bands between these two experimental groups are no longer statistically significant for the vessel on the left ventricle muscle. When the spectral changes between diabetic and Se treated diabetic groups are compared, it is seen that the frequency of the CH_2 symmetric stretching band shifts to higher values in the Se treated diabetic ones with respect to the diabetic group.

Table 29. The changes observed in the intensity and frequency values of the functional groups for the vessel on the left ventricle muscle of the control, diabetic and Se treated diabetic rat hearts. Values are shown as "mean ± standard deviation". First p values are for "control-diabetic" groups, second p values are for "control-diabetic+Se treated" groups and third p values are for "diabetic-diabetic+Se treated groups.

Parameters	**Functional groups**	**Control**	**Diabetic**	**Diabetic+Se**	**P values**		
Intensity	Olefinic =CH stretching	-0.017±0.006	-0.023±0.005	-0.021±0.007	p<0.048*	p<0.2	p<0.88
	Amid I: β-sheet	-0.220±0.019	-0.260±0.024	-0.250±0.015	p<0.002**	p<0.02*	p<0.17
	CO-O-C asymmetric stretching	-0.047±0.004	-0.033±0.005	-0.036±0.005	p<0.001***	p<0.004**	p<0.65
	C-O stretching (1151 cm^{-1})	-0.009±0.005	-0.018±0.004	-0.016±0.007	p<0.008**	p<0.067	p<0.66
	C-O stretching (1151 cm^{-1}) / CO-O-C asymmetric stretching	0.195±0.127	0.530±0.187	0.465±0.267	p<0.004**	p<0.025*	p<0.438
Frequency	CH_2 asymmetric stretching	2921.90±0.33	2921.44±0.53	2921.69±0.53	p<0.034*	p<0.723	p<0.44
	CH_2 symmetric stretching	2852.31±0.21	2852.06±0.28	2852.42±0.26	p<0.054*	p<0.345	p<0.052*
	Amid I: α-helical structure	1655.47±0.71	1654.92±1.47	1655.12±0.78	p<0.067	p<0.376	p<0.24
	Amid I: β-sheet	1637.85±0.26	1637.40±0.62	1637.69±0.33	p<0.067	p<0.637	p<0.2
	Amid II: α-helical structure	1547.90±0.45	1548.37±0.87	1548.24±0.39	p<0.054*	p<0.125	p<0.33

3.1.3.4 Right Ventricle Muscle

Table 30 and figures 45-47 show the changes in the intensity and frequency values of the functional groups for the right ventricle muscle of the control, diabetic and Se treated diabetic rat hearts.

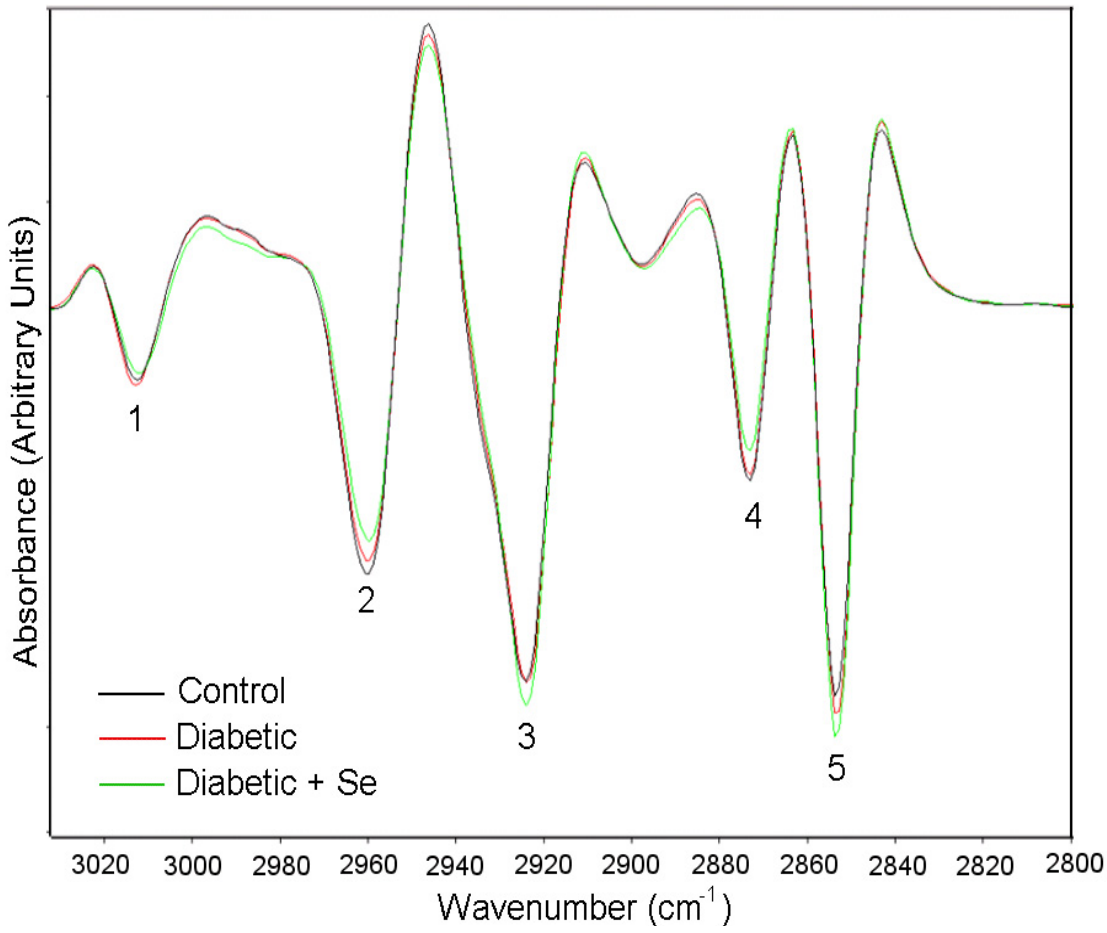

Figure 45. The average spectra belonging to the right ventricle muscle of control (6 samples), diabetic (8 samples) and Se treated diabetic groups (7 samples) in 3030 cm^{-1}- 2800 cm^{-1} region. Vector normalization was done in 3050 cm^{-1}- 2800 cm^{-1} region.

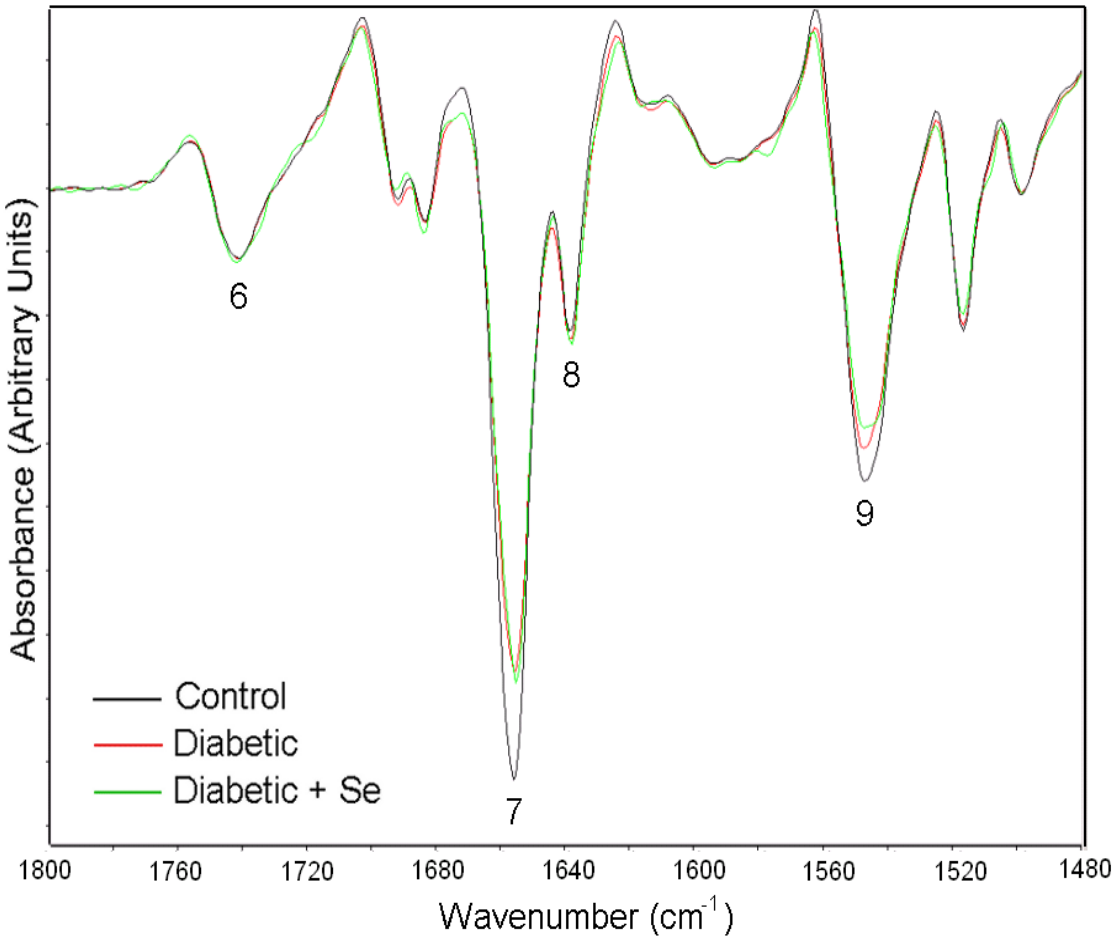

Figure 46. The average spectra belonging to the right ventricle muscle of control (6 samples), diabetic (8 samples) and Se treated diabetic groups (7 samples) in 1800 cm^{-1}- 1480 cm^{-1} region. Vector normalization was done in 1480 cm^{-1}- 950 cm^{-1} region.

Table 30 clearly shows that diabetes causes a significant increase in the intensity values of the bands at 1654 cm^{-1}, 1151 cm^{-1}, the intensity ratio of 1151/1171 cm^{-1} bands and the band at 1040 cm^{-1}. However, these diabetes mellitus induced changes in the intensity values of these functional groups are restored in the Se treated diabetic group. When the spectral changes between diabetic and Se treated diabetic groups are compared, it is observed that the intensity of the band at 1041 cm^{-1} decreases significantly in the Se treated diabetic group with respect to the diabetic ones. In addition to this, a remarkable decrease is observed in the intensity of the band at 1171 cm^{-1} in the diabetic group. This decrease is no longer significant in the Se treated diabetic group.

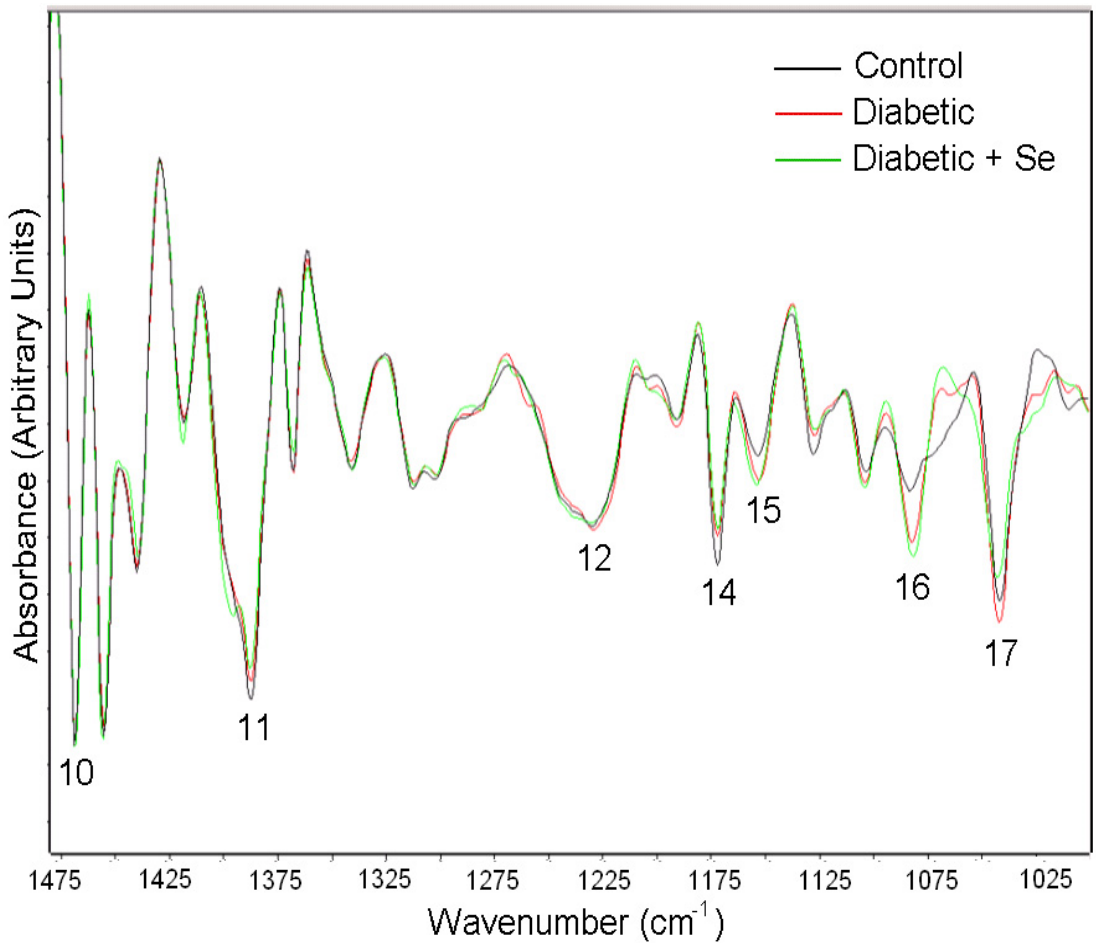

Figure 47. The average spectra belonging to the right ventricle muscle of control (6 samples), diabetic (8 samples) and Se treated diabetic groups (7 samples) in 1480 cm^{-1}-1000 cm^{-1} region. Vector normalization was done in 1480 cm^{-1}- 950 cm^{-1} region.

Table 30 shows significant decreases in the frequency values of the CH_2 asymmetric and symmetric stretching bands in the diabetic group with respect to control group. It is clearly seen that the frequency values increase back to almost their control values in the Se treated diabetic group, so that the differences in the frequency values of these bands between these two experimental groups are no longer statistically significant for the right ventricle muscle. When the spectral changes between diabetic and Se treated diabetic groups are compared, it is seen that the frequencies of the CH_2 antisymmetric and symmetric stretching bands shift to higher values in the Se treated diabetic ones with respect to the diabetic group.

Table 30. The changes observed in the intensity and frequency values of the functional groups for the right ventricle muscle of the control, diabetic and Se treated diabetic rat hearts. Values are shown as "mean ± standard deviation". First p values are for "control-diabetic" groups, second p values are for "control-diabetic+Se treated" groups and third p values are for "diabetic-diabetic+Se treated groups.

Parameters	**Functional groups**	**Control**	**Diabetic**	**Diabetic+Se**	**P values**		
Intensity	Amid I: α-helical structure	-0.926±0.089	-0.756±0.069	-0.792±0.030	p<0.001***	p<0.01**	p<0.179
	CO-O-C asymmetric stretching	-0.062±0.004	-0.049±0.006	-0.050±0.011	p<0.001***	p<0.08	p<0.88
	C-O stretching (1151 cm^{-1})	-0.013±0.004	-0.023±0.006	-0.020±0.010	p<0.004**	p<0.179	p<0.94
	C-O stretching (1151 cm^{-1}) / CO-O-C asymmetric stretching	0.210±0.060	0.490±0.170	0.460±0.280	p<0.001***	p<0.26	p<0.947
	C-O stretching (at 1041 cm^{-1})	-0.078±-0.015	-0.09±0.009	-0.064±0.010	p<0.05*	p<0.06	p<0.004**
Frequency	CH_2 antisymmetric stretching	2922.94±0.10	2922.62±0.19	2922.86±0.15	p<0.001***	p<0.46	p<0.05*
	CH_2 symmetric stretching	2853.08±0.11	2852.82±0.05	2852.99±0.13	p<0.001***	p<0.229	p<0.02*

3.2 Part II: Effect of Stereotactic Radiosurgery on Hypoperfused Rat Brain Tissue Homogenates

In this part of the study, FTIR spectroscopic studies have been carried out on tissue homogenates of rat brain subjected to steal phenomena to identify the biochemical and biophysical changes occurring in brain tissues as a result of hypoperfusion, by comparing the results with those of the control group. Next, the effect of radiation (stereotactic radiosurgery) on control and hypoperfused rat brain homogenates has been investigated by FTIR spectroscopy.

Characteristic frequencies, intensities and bandwidths in an IR spectrum allow the identification of functional groups of molecules and the characterization of conformationally distinct structures in biological molecules, such as proteins, lipids and polysaccharides (Kneipp *et al*., 2000).

An FTIR spectrum of a brain homogenate and the main spectral band assignments are given in figure 48 and table 31, respectively. As seen from the figure and the table, the spectrum is quite complex which contains many bands belonging to several tissue components, such as proteins and lipids.

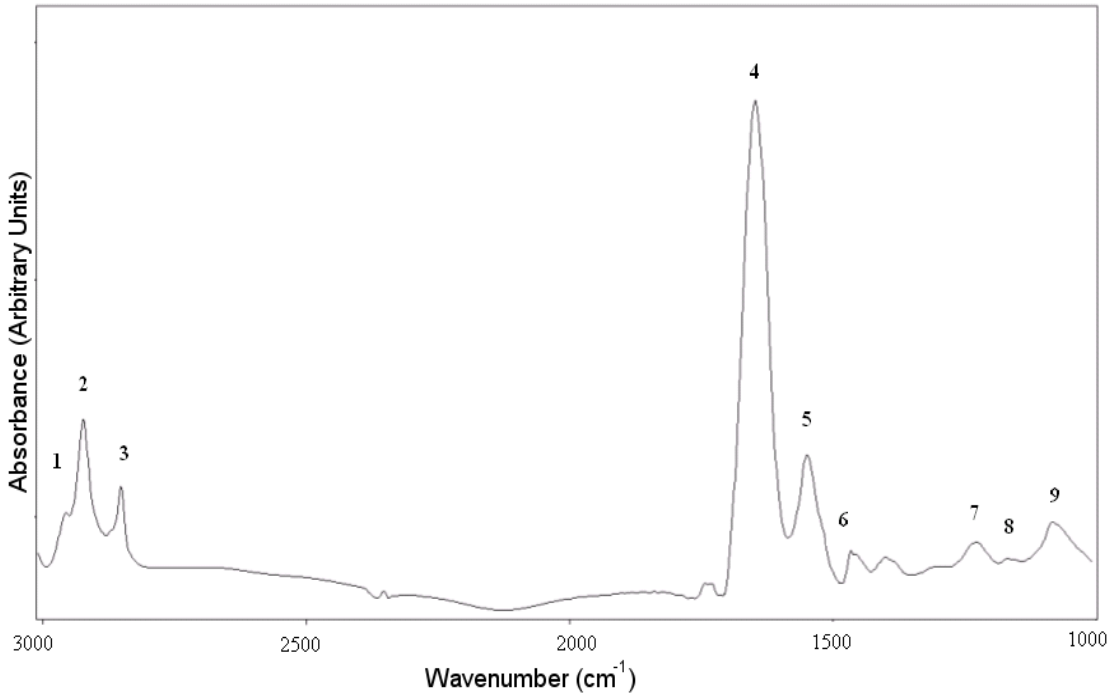

Figure 48. An FTIR spectrum of a brain homogenate and the main spectral band assignments.

Table 31. Major absorptions in IR spectra of brain tissue (Jackson *et al*., 1998; LeVine and Wetzel, 1993; Manoharan *et al*., 1993)

Band Number	**Frequency (cm^{-1})**	**Assignments**
1	2956	CH_3 asymmetric stretching vibrations of fatty acids: mostly of lipids
2	2923	CH_2 asymmetric stretching vibrations of fatty acids: mostly of lipids
3	2852	CH_2 symmetric stretching vibrations of fatty acids: mostly of lipids
4	1648	Amide I (protein C=O stretch), α-helices
5	1549	Amide II (protein N-H bend, C-N stretch), α-helices
6	1466	CH_2 scissoring: lipids
7	1220-1240	PO_2^- asymmetric stretch: mostly of phospholipids and nucleic acids
8	1170	CO-O-C asymmetric stretching vibrations: ester bonds
9	1080	PO_2^- symmetric stretch: mostly of phospholipids

3.2.1 Effect of Chronic Hypoperfusion on Rat Brain Tissue Homogenates

Table 32 shows the main functional groups and the changes in the intensity values in 3000-1480 cm^{-1} region. As seen from the table, there are significant differences in intensity values between hypoperfused brain and control brain samples which will be discussed in detail.

Table 32. Changes in the frequency values of various functional groups in the spectra of control and hypoperfused rat brain tissue homogenates in 3000 cm^{-1}-2800 cm^{-1} region. Values are shown as "mean ±standard deviation".

Functional Groups	**Control**	**Hypoperfused**	**p values**
CH_3 Asymmetric Stretching	0.380±0.006	0.340±0.012	p<0.008**
CH_2 Symmetric Stretching	0.540±0.006	0.580±0.007	p<0.008**
Amide I	3.550±0.108	3.230±0.080	p<0.008**
Amide II	0.884±0.065	0.779±0.093	p<0.01**
AmideI/CH_2 Symmetric Stretching	6.570±0.123	5.567±0.140	p<0.008**

Figure 49 shows the average spectra of control and hypoperfused brain samples in 3000-2800 cm^{-1} region. Spectra were normalized with respect to the CH_2 asymmetric stretching band. As all other forms of optical spectroscopy, the intensity of IR absorptions arising from a particular species is directly proportional to the concentration of that species. Thus, in principle, it is possible to determine the concentration of multiple analytes from a single spectrum, imparting a significant saving of time and labor (Jackson *et al*., 1997). The bands centered at 2956 cm^{-1} and 2923 cm^{-1}, correspond to the stretching mode of asymmetrical CH_3 and CH_2 vibrations, respectively; and the band centered at 2852 cm^{-1} corresponds to CH_2 symmetric stretching vibrations (Melin *et al*., 2000). It is seen from table 32 and figure 49 that there is a decrease in the intensity of the CH_3 asymmetric stretching mode in the hypoperfused brain tissues. An increase in the intensity of CH_2 symmetric stretching mode occurs with the application of operation on the rat brain tissues. The average spectra of control and hypoperfused brain samples in 1285-1000 cm^{-1} region are given in figure 50. Spectra were normalized with respect to the Amide I band. There are slight increases in the intensities of the phosphate asymmetric stretching (from 0.11±0.008 to 0.12±0.008) and symmetric stretching vibrations (from 0.15±0.088 to 0.17±0.09) in the hypoperfused group.

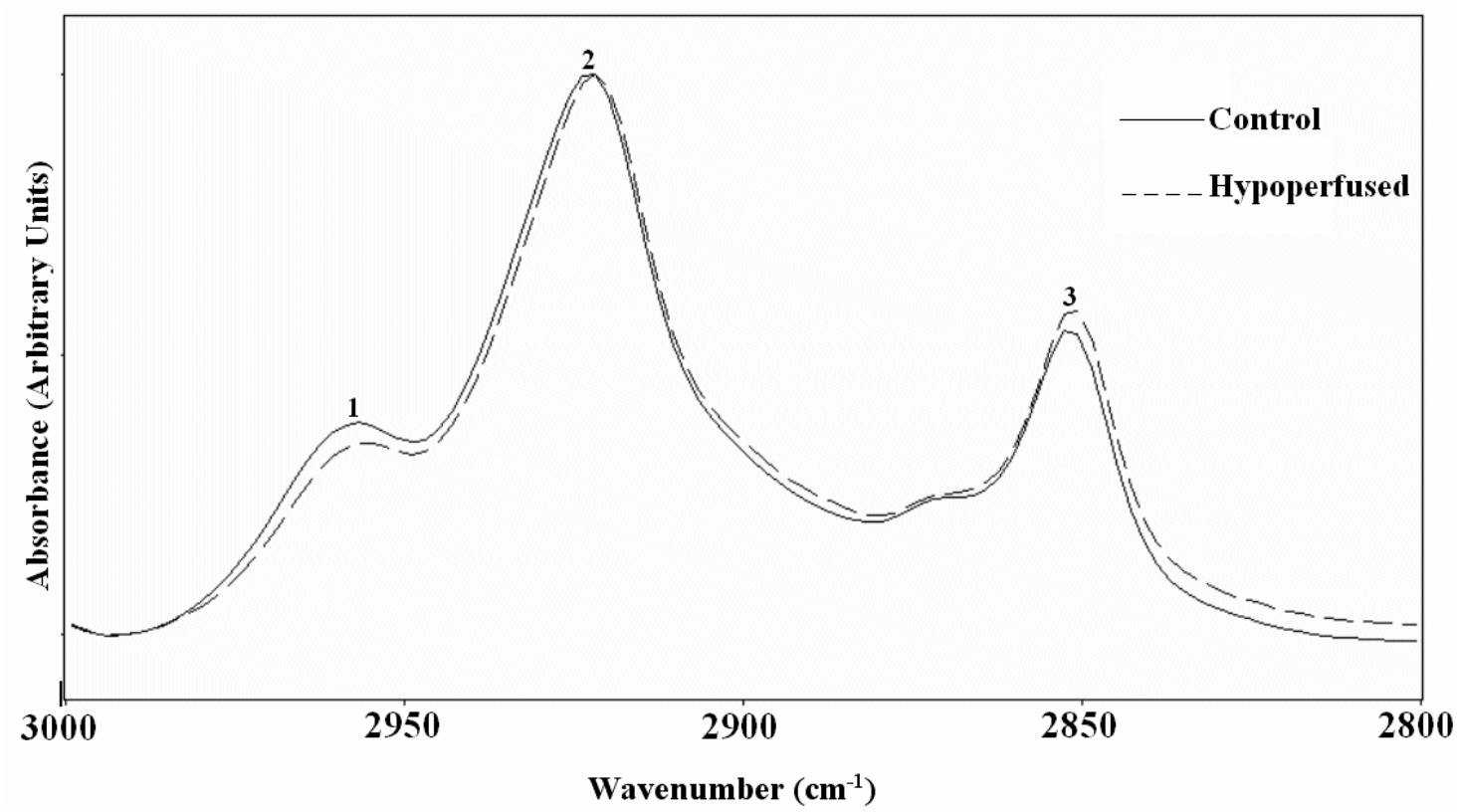

Figure 49. The average spectra of control and hypoperfused brain samples in 3000-2800 cm^{-1} region. Spectra were normalized with respect to the CH_2 asymmetric stretching band.

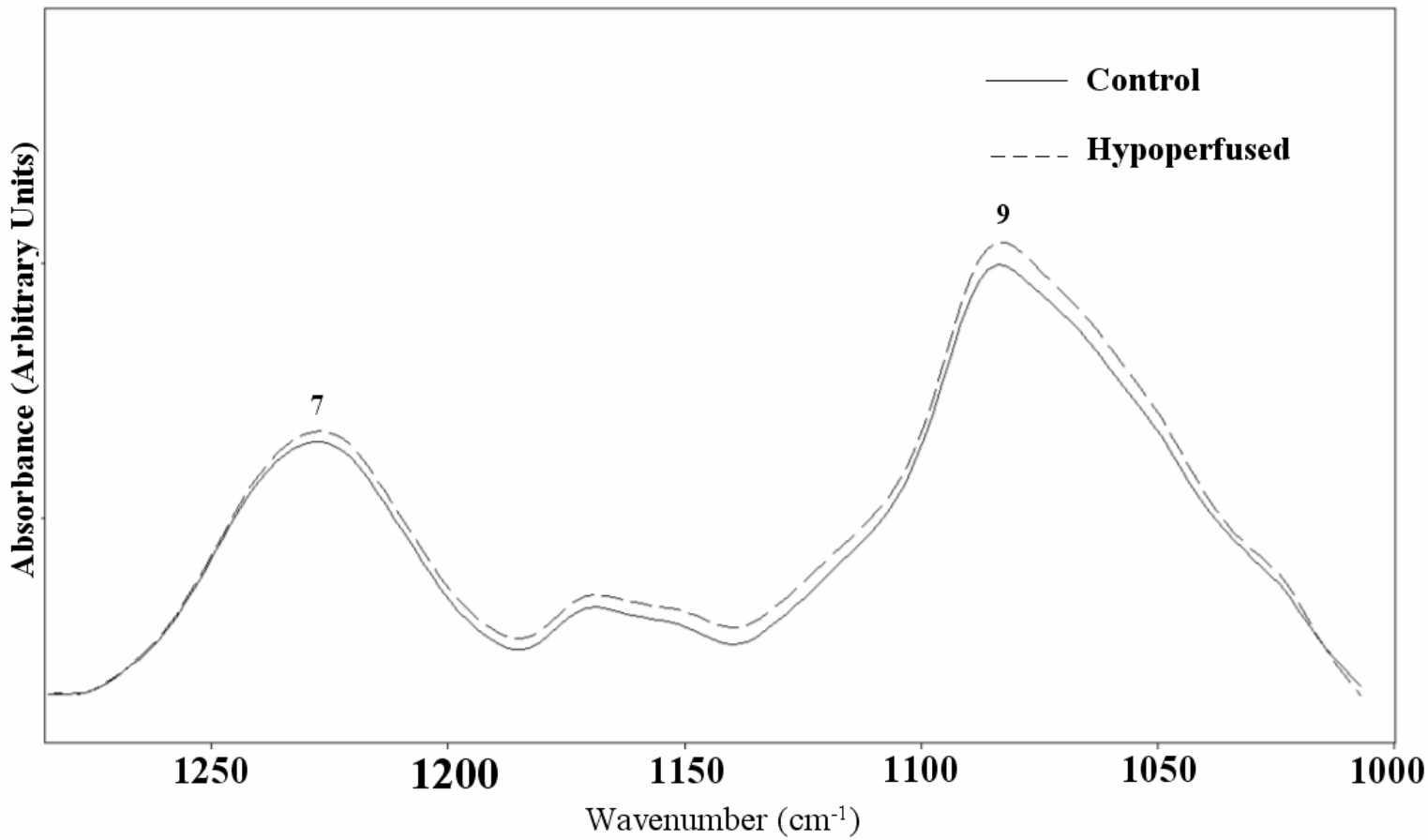

Figure 50. The average spectra of control and hypoperfused brain samples in 1285-1000 cm^{-1} region. Spectra were normalized with respect to the Amide I band

FTIR spectroscopy is one of the major techniques for the determination of protein secondary structures (Arrondo *et al.*, 1993; Haris and Severcan, 1999). Thus FTIR spectroscopy offers unique possibilities for the simultaneous study of proteins together with lipid structures in biological membranes (Szalontai *et al*., 2000). Figure 51 shows the average spectra of control and hypoperfused brain samples in 1720-1480 cm^{-1} region. Spectra were normalized with respect to the CH_2 asymmetric stretching band. The bands at 1647 cm^{-1} and 1549 cm^{-1} are attributable to Amide I and Amide II vibrations of structural proteins, respectively (Haris and Severcan, 1999; Manoharan *et al*., 1993). It is clearly seen in table 32 that, the intensities of Amide I band and Amide II band decrease in the hypoperfused group.

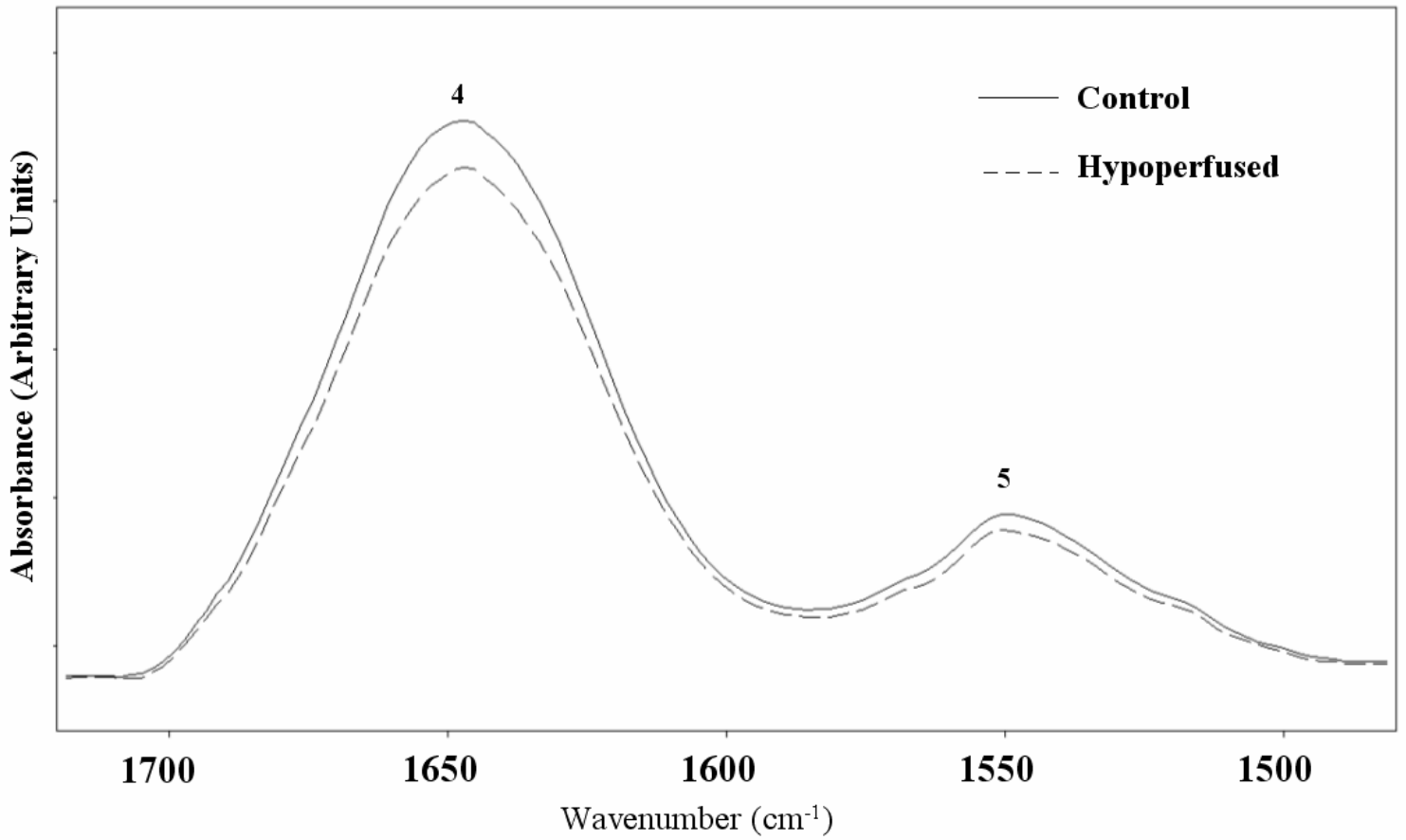

Figure 51. The average spectra of control and hypoperfused brain samples in 1720- 1480 cm^{-1} region. Spectra were normalized with respect to the CH_2 asymmetric stretching band.

From the FTIR spectrum, a precise protein-to-lipid ratio can be derived by calculating the intensity ratio of bands arising from lipids to proteins. As it is seen in table 32, the ratio of the intensity of the Amide I to the intensity of the CH_2 symmetric stretching absorptions decreases in the hypoperfused group.

The changes in the frequency values of control and hypoperfused rat brain tissues in 3000 cm^{-1} -2800 cm^{-1} region are given in table 33. The table shows that there is a significant decrease in the frequency of the CH_2 symmetric and antisymmetric vibrations upon the induction of hypoperfusion in the rat brain.

Table 33: Changes in the frequency values of various functional groups in control and hypoperfused rat brain tissues in 3000 cm^{-1} -2800 cm^{-1} region. Values are shown as "mean ± standard deviation".

Functional Groups	**Control**	**Hypoperfused**	**p values**
CH_3 Asymmetric Stretching	2956.60±0.13	2955.50±0.13	p<0.008**
CH_2 Asymmetric Stretching	2922.90±0.12	2922.20±0.10	p<0.008**
CH_2 Symmetric Stretching	2851.80±0.13	2851.40±0.09	p<0.008**

The change in the deep interior of the bilayer was monitored by the wavenumber of the CH_3 asymmetric stretching mode (figure 49). As it is seen in table 33, there is a decrease in the frequency of the CH_3 asymmetric stretching mode upon application of operation.

The Amide I region, at around 1646 cm^{-1} in our case, is useful for the determination of protein secondary structure (Lyman and Murray-Wijelath, 1999). Further analysis have been carried out for the proteins present in the tissue samples by resolving Amide I band using band fitting methods to have a better understanding of the effect of hypoperfusion on protein structure at molecular level. In Amide I region (1585 cm^{-1} - 1710 cm^{-1}), the underlying bands contributing to the baseline-corrected spectra were determined using a combination of second derivative and curve fit functions. Firstly, by using second derivative arithmetical function, 6 peaks and their relative positions were determined. The second derivative of the original spectra offers a direct way to identify the peak frequencies of the characteristic

components and thus permits much more detailed qualitative study (Susi and Byler, 1983). The frequency values and band assignments of these sub-bands are given in table 34 (Cadrin *et al*., 1991; Kochan *et al*., 1995; Takahashi *et al.*, 1991).

Table 34. Assignments of sub-bands in the 1585 cm^{-1}-1710 cm^{-1} region obtained from the second derivative spectra.

Amide I bands in the second derivative spectra	**Assignments (cm^{-1})**	**Peak Number (Pn)**
β sheet (Antiparallel)	1693	P1
β turn	1680	P2
α helical (unordered)	1660	P3
α helical	1647	P4
Random coil	1637	P5
β sheet	1633	P6

The underlying bands of Amide I as deduced by curve fitting analysis for control and hypoperfused groups are given in figure 52. The fractional areas of each sub-bands and % areas of main protein secondary structures obtained after curve fit analysis are given in tables 35 and 36, respectively for both control and hypoperfused brain samples.

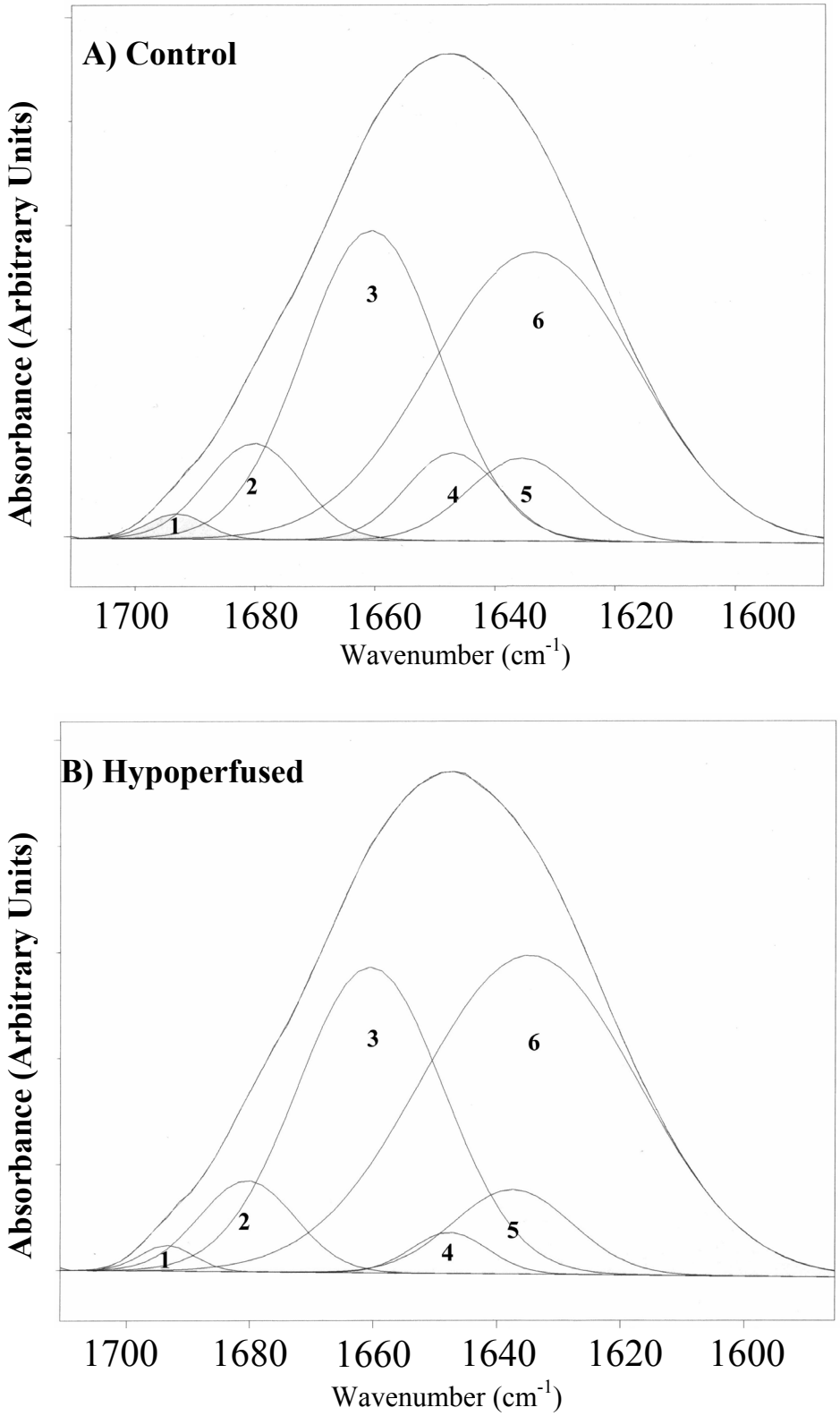

Figure 52. The underlying bands of Amide I in 1585 cm^{-1}- 1710 cm^{-1} region, as deduced by curve fitting analysis for average spectra of the control (A), and the average spectra of the hypoperfused (B) brain samples.

Table 35: The results of curve-fitting analysis expressed as a function of fractional areas of each sub-bands belonging to protein secondary structures for control and hypoperfused rat brain samples. Values are shown as "mean ± standard deviation".

Fractional Areas	**Control**	**Hypoperfused**	**p values**
A(P1)/A(Total)	0.011±0.001	0.010±0.001	<0.12
A(P2)/A(Total)	0.074±0.006	0.060±0.005	<0.01**
A(P3)/A(Total)	0.319±0.026	0.324±0.017	<0.9
A(P4)/A(Total)	0.070±0.008	0.034±0.022	<0.04*
A(P5)/A(Total)	0.070±0.005	0.080±0.002	<0.27
A(P6)/A(Total)	0.450±0.008	0.487±0.013	<0.01**
A(P3+P4)/A(P1+P2+P6)	0.730±0.045	0.642±0.037	<0.03*

Table 36. The results of summary of the curve-fitting analysis expressed as a function of % areas of main protein secondary structures for control and hypoperfused rat brain samples. Values are shown as "mean ±standard deviation".

Structure	**Peak Centers (cm^{-1})**	**Area (%) Control**	**Area (%) Hypoperfused**	**p values**
α helix	1660,1647	39.05±1.73	35.95±1.18	<0.05*
β sheet	1693,1680,1633	53.33±1.02	56.06±1.60	<0.05*
Random coil	1637	7.03±0.92	8.06±0.66	<0.14

Table 35 shows that hypoperfusion does not cause any significant change in the amount of antiparallel β sheet structure but it causes a significant decrease in the content of β turn and a significant increase in the content of β sheet structure. A significant decrease in the amount of ordered α-helical structures is observed in table 35. The amount of random coil structures slightly increases in the hypoperfused group. It can be deduced from these results that hypoperfusion causes a significant decrease in the content of α-helical structure and a significant increase in the content of β sheet structures (table 35 and 36).

3.2.2 Effect of Radiosurgery on Control and Hypoperfused Rat Brain Tissue Homogenates

We have carried out FTIR spectroscopic studies on tissue homogenates from rat brain subjected to "radiation" and "chronic hypoperfusion+radiation" to identify the biochemical and biophysical changes occurring in brain homogenates, by comparing the results with those of the control group.

Table 37 shows the main functional groups and the changes in the intensity values in 3000-1480 cm^{-1} region. Figure 53 shows the average spectra in 3010-2800 cm^{-1} region for control, radiated and hypoperfused+radiated brain samples. Spectra were normalized with respect to the CH_2 asymmetric stretching band. It is seen from the table and the figure that there is s slight increase in the intensity of CH_2 symmetric stretching mode in the radiated group. This increase is significant in the hypoperfused+radiated group. The average spectra of control, radiated and hypoperfused+radiated groups in 1285-1000 cm^{-1} region are given in figure 54. The spectra were normalized with respect to the Amide I band. There is a negligible increase in the intensity of the CH_2 scissoring band in the radiated group. As it is seen in the figure, this increase is quite significant in the hypoperfused+radiated group. There are also significant increases in the intensities of the phosphate asymmetric stretching and symmetric stretching vibrations in the radiated and hypoperfused+radiated groups. The same table also demonstrates significant increases in the content of CO-O-C asymmetric stretching mode in radiated and hypoperfused+radiated groups.

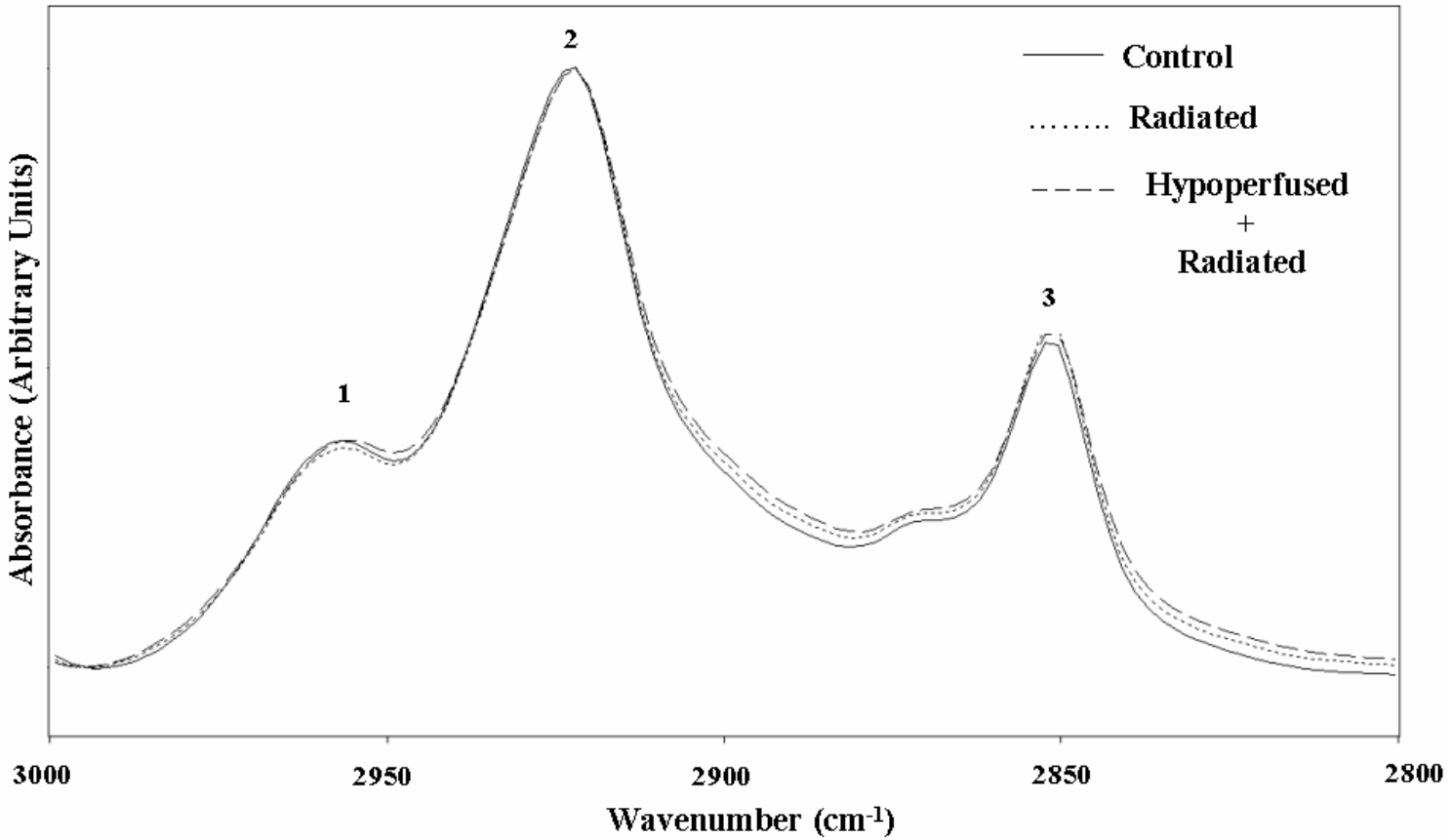

Figure 53. Average spectra of control, radiated and hypeperfused+radiated brain samples in 3010-2800 cm^{-1} region. Spectra were normalized with respect to the CH_2 asymmetric stretching band.

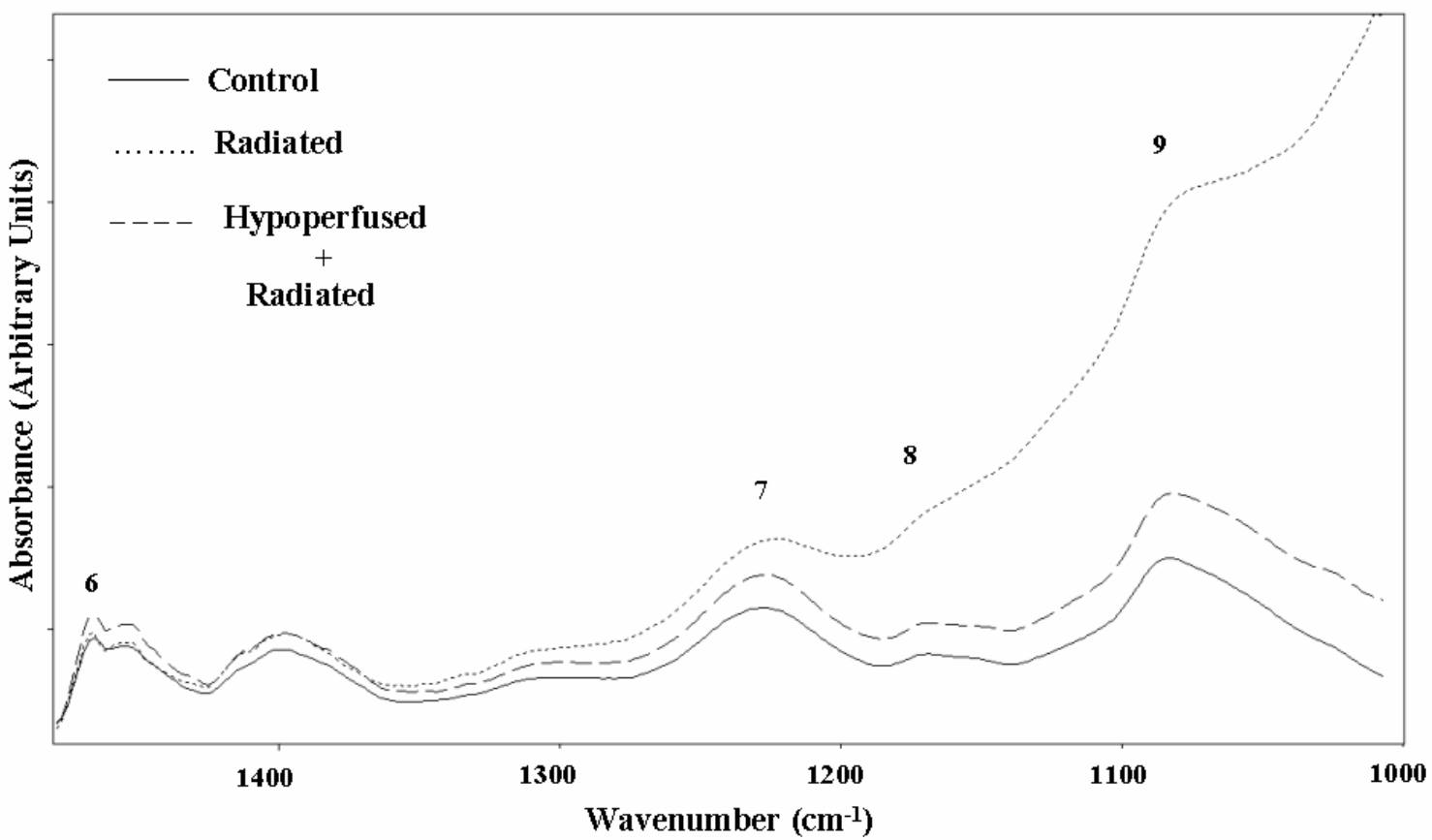

Figure 54. Average spectra of control, radiated and hypeperfused+radiated brain samples in 1285- 1000 cm^{-1} region. Spectra were normalized with respect to the Amide I band.

Table 37. Changes in the intensities and intensity ratios of various functional groups in the spectra of control, radiated and hypoperfused+radiated rat brain tissue homogenates in 3000 cm^{-1}-1480 cm^{-1} region. Values are shown as "mean ± standard deviation". First p values are for "control" and "radiated" groups, second p values are for "control" and "hypoperfused+radiated" groups.

Functional Groups	**Control**	**Radiated**	**Hypoperfused +Radiated**	**p values**	
CH_2 symmetric stretching	0.548±0.006	0.567±0.02	0.558±0.007	<0.46	<0.02*
CH_2 scissoring	0.093±0.009	0.096±0.016	0.112±0.004	<0.9	<0.01**
Amide I	3.550±0.496	3.210±0.660	2.640±0.170	<0.05*	<0.01**
AmideI/CH_2 symmetric stretching	6.478±0.825	5.650±1.100	4.730±0.280	<0.08	<0.01**
PO_2^- asymmetric stretching	0.115±0.010	0.164±0.018	0.137±0.013	<0.014*	<0.01**
CO-O-C asymmetric stretching	0.082±0.006	0.178±0.440	0.104±0.016	<0.01**	<0.01**
PO_2^- symmetric stretch	0.149±0.012	0.390±0.077	0.195±0.027	<0.01**	<0.01**

Figure 55 shows the average spectra for control, radiated, and hypoperfused+radiated groups in 1720-1480 cm^{-1} region. The spectra were normalized with respect to the CH_2 asymmetric stretching band. It is clearly seen in table 37 that, the intensity of Amide I decreases significantly in the radiated group. This decrease is more profound in the hypoperfused+radiated group.

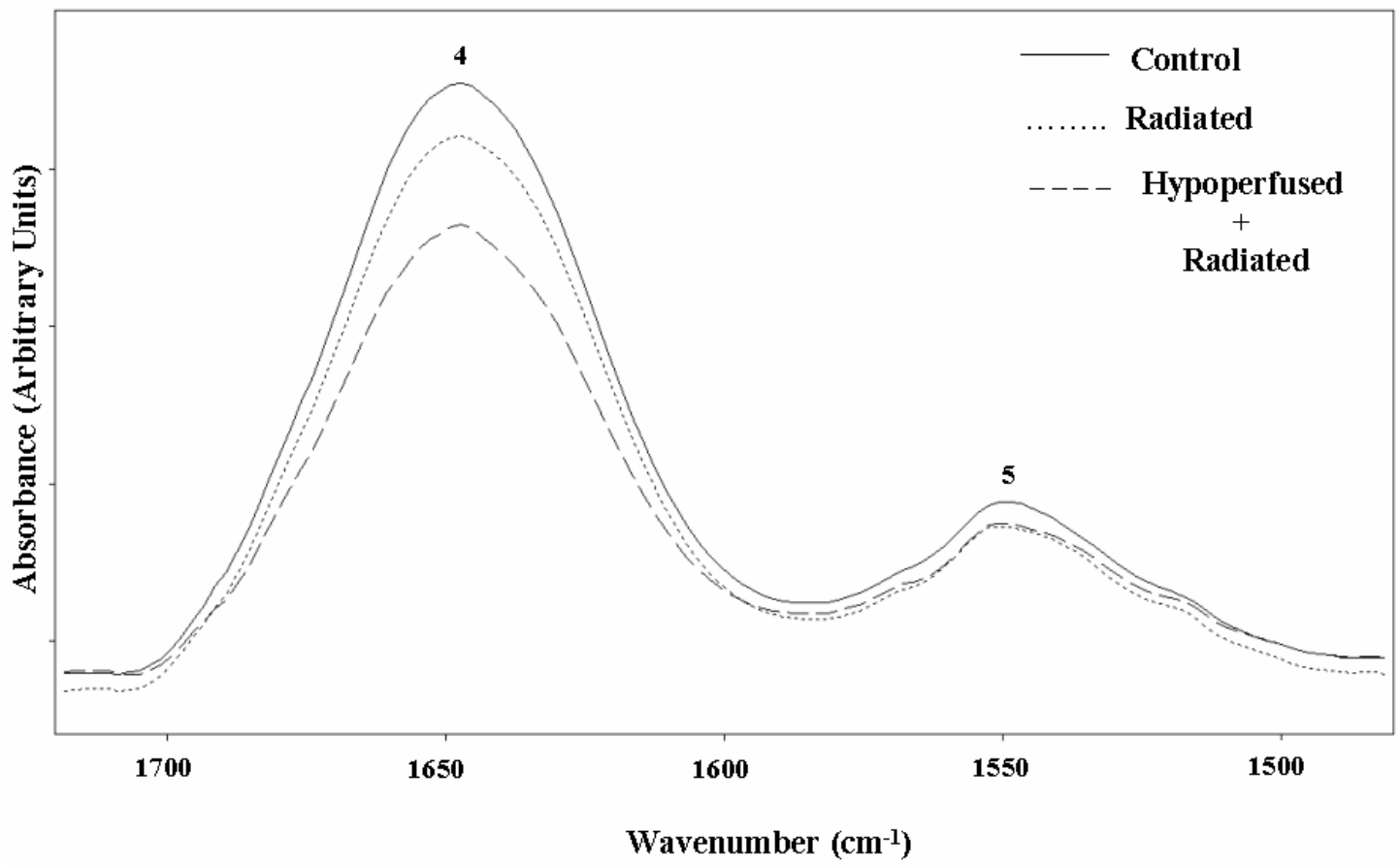

Figure 55. Average spectra of control, radiated and hypeperfused+radiated brain samples in 1720- 1480 cm^{-1} region. Spectra were normalized with respect to the CH_2 asymmetric stretching band.

As it is seen in table 37, the ratio of the intensity of the Amide I to the intensity of the CH_2 symmetric stretching absorptions decreases slightly in the radiated group, but significantly in the radiated+hypoperfused group.

The changes in the frequency values are given in table 38. The table demonstrates that there is no significant change in die frequency of the CH_2 symmetric vibrations upon the application of radiation, but a significant decrease in the frequency of this band occurs in the hypoperfused+radiated group.

The changes in the deep interior of the bilayer is monitored by the wavenumber of the CH_3 asymmetric stretching mode. Table 38 shows that, the frequency of the CH_3 asymmetric stretching mode is not affected by the radiation, but it significantly shifts to lower values in the hypoperfused+radiated group.

As it is seen in figure 55, the whole Amide I band moves to lower frequency values in the radiated group. However, the shift in the frequency of this functional group is not significant in the hypoperfused+radiated group as shown in table 38.

Table 38. Changes in the frequency values of various functional groups in the spectra of control, radiated and hypoperfused+radiated rat brain tissue homogenates. Values are shown as "mean ± standard deviation". First p values are for "control" and "radiated" groups, second p values are for "control" and "hypoperfused+radiated" groups.

Functional Groups	**Control**	**Radiated**	**Hypoperfused +Radiated**	**p values**	
CH_3 asymmetric stretching	2956.20±0.32	2956.30±0.45	2955.60±0.20	<0.32	<0.01**
CH_2 symmetric stretching	2851.67±0.06	2851.70±0.07	2851.50±0.04	<0.1	<0.01**
Amide I	1647.20±0.09	1646.40±0.11	1647.00±0.10	<0.05*	<0.3

Further analysis has been carried out for the proteins present in the tissue samples by resolving Amide I band using band fitting method. As already mentioned, in Amide I region (1585 cm^{-1} - 1710 cm^{-1}), the underlying bands contributing to the baseline-corrected spectra were determined using a combination of second derivative and curve fit functions. The underlying bands of Amide I as

deduced by curve fitting analysis for control, radiated and hypoperfused+radiated groups are given in figure 56. The fractional areas of each sub-band and % areas of main protein secondary structures obtained after curve fit analysis are given in table 39 and 40, respectively for all the experimental groups. As it is seen in the table, the amount of α-helical structure decreases significantly in the radiated group, whereas this effect is negligible in the hypoperfused+radiated group. This table also demonstrates that there is a negligible increase in the amount of β sheet structure in the radiated group and slight increase in the hypoperfused+radiated group. The amount of random coil significantly increase in the radiated group and decreases in the hypoperfused+radiated group.

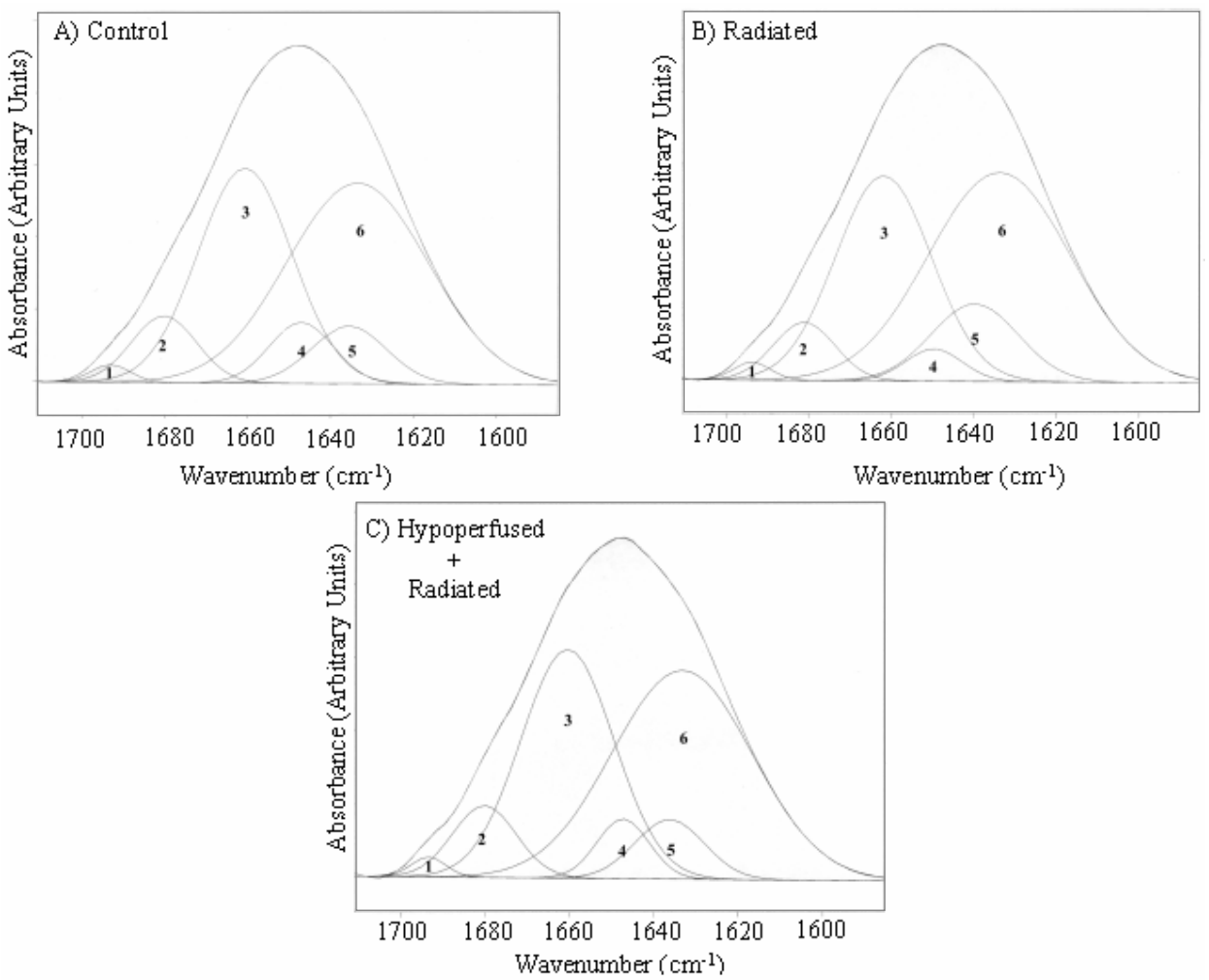

Figure 56. The underlying bands of Amide I in 1585 cm^{-1}- 1710 cm^{-1} region, as deduced by curve fitting analysis for average spectra of the control (A), radiated (B) and hypoperfused+radiated (C) brain samples.

Table 39: The results of curve fitting analysis expressed as a function of the fractional areas of each sub-bands belonging to protein secondary structures for control, radiated and hypoperfused+radiated rat brain homogenates. Values are shown as "mean ± standard deviation". First p values are for "control" and "radiated" groups, second p values are for "control" and "hypoperfused+radiated" groups.

Fractional Areas	**Control**	**Radiated**	**Hypoperfused +Radiated**	**p values**	
A(P1)/A(Total)	0.011±0.001	0.011±0.001	0.010±0.001	<0.3	<0.37
A(P2)/A(Total)	0.074±0.006	0.060±0.006	0.065±0.003	<0.03*	<0.08
A(P3)/A(Total)	0.319±0.026	0.302±0.011	0.340±0.015	<0.22	<0.17
A(P4)/A(Total)	0.070±0.008	0.030±0.010	0.050±0.017	<0.01*	<0.08
A(P5)/A(Total)	0.070±0.005	0.116±0.049	0.050±0.009	<0.14	<0.01**
A(P6)/A(Total)	0.450±0.008	0.467±0.013	0.470±0.020	<0.08	<0.03*
A(P3+P4)/A(P1+P2 +P6)	0.730±0.045	0.620±0.026	0.710±0.061	<0.01**	<0.62

Table 40. The results of summary of the curve fitting analysis expressed as a function of % areas of main protein secondary structures for control, radiated and hypoperfused+radiated rat brain homogenates. Values are shown as "mean ± standard deviation". First p values are for "control" and "radiated" groups, second p values are for "control" and "hypoperfiused+radiated" groups.

Structure	**α helix**		**β sheet**		**Random coil**	
Peak Centers (cm^{-1})	1660,1647		1693,1680,1633		1637	
Area (%) Control	39.05±1.73		53.33±1.02		7.03±0.92	
Area (%) Radiated	33.35±1.90		53.77±1.61		12.87±3.24	
Area(%) Radiated+Hypoperfused	39.22±2.16		55.06±2.05		5.70±0.88	
p values	<0.01**	<0.8	<0.38	<0.08	<0.02*	<0.01**

CHAPTER 4

DISCUSSION

4.1 Part I: Effect of Diabetes Mellitus on Rat Heart and the Effect of Selenium Treatment on Diabetic Rat Heart

In the first part of this study, the effect of diabetes mellitus on different regions of the rat heart, such as apex myocardium, left ventricle muscle, vessel on the left ventricle muscle and right ventricle muscle has been investigated by FTIR microscopy attached to FTIR spectroscopy. IR spectroscopy in combination with microscopy yielded spatially resolved information on unstained thin tissue sections of the heart samples from Wistar rats that allowed the generation of IR maps with high image contrast. Furthermore, the serial tissue sections taken from the investigated regions of the heart were stained with H&E staining for histological studies. Results of this study revealed that diabetes mellitus induces significant and similar changes in the intensity and frequency values of the IR spectra obtained from different regions of the rat heart. In the second part of this study, the effect of Se treatment on the different regions of the diabetic rat heart has been investigated. The findings of the experiments demonstrated that, Se treatment restores the effect of diabetes on different region of the rat heart for some of the functional groups in the investigated spectral regions (tables 27-30).

4.1.1 Effect of Diabetes Mellitus on Different Region of the Rat Heart

4.1.1.1 Apex

The dominant lipid bands in 3030-2800 cm^{-1} region originate from the C-H stretching vibrations of the fatty acyl chains of membrane lipids (Liu *et al*., 2002). As all other forms of optical spectroscopy, the intensity of IR absorptions arising from a particular species is directly proportional to the concentration of that species (Jackson *et al*., 1997). Table 7 and figure 21 show that there is an increase in the intensities of CH_2 asymmetric and symmetric stretching modes in the diabetic group, indicating an increase in phospholipids or fatty acid concentrations (Jackson *et al*., 1997). The same figure and the table also show that there is a decrease in the concentration of the CH_3 symmetric stretching group in the diabetic group. Since CH_2 symmetric stretching arises mainly from lipids and the CH_3 symmetric stretching arises mainly from proteins, the intensity ratio of these absorptions gives information about lipid/protein content of the system (Severcan *et al*., 2003). The results of our study show that the intensity ratio of CH_2/CH_3 symmetric stretching vibrations increases in diabetes which can be due to an increase in the lipid content and/or a decrease in the protein content. The increase in lipid content might be due to the disturbance of lipid metabolism in diabetic myocardium. An increase in lipid content and a strong correlation between elevated levels of lipid and the depression of the heart function was reported in previous studies (Heyliger *et al*., 1986; McNeill, 1996). The heart utilizes fatty acids as a substrate in preference to glucose for the production of energy. The rate of fatty acid uptake and oxidation by heart muscle is controlled by the availability of exogenous fatty acids, the rate of acyl translocation across the mitochondrial membrane and the rate of acetyl-CoA oxidation by the citric acid cycle. Carnitine acyl-CoA transferase appears to have an important function in coupling the fatty acid activation and acyl transfer to the oxidative phosphorylation. Activated fatty acids are also utilized for the synthesis of triglycerides and membrane phospholipids in the myocardium. The inhibition of long chain acyl-carnitine transferase I reduces the oxidation of fatty acids and promotes the synthesis of lipids in the myocardium. It was found in a previous study that, for rats which were diabetic for 16 weeks, the mitochondria was damaged so severely that it no longer

metabolize cardiac lipid properly which results in the breakdown of the mitochondria and accumulation of lipids (Hsiao *et al*., 1987). In our case, the rats were diabetic just for 4 weeks, but we still can see the lipid accumulation in the myocardium which might be an indication for the damage of mitochondria. Accumulation of fatty acids and their metabolites, such as long chain acyl-CoA and long chain acyl-carnitine, has been associated with cardiac dysfunction and cell damage in both ischemic and diabetic hearts. Alterations in the composition of membrane phospholipids are also considered to change the activities of various membrane bound enzymes and subsequently heart function under different pathophysiological conditions (Dhalla *et al*., 1992).

CH_2 stretching vibrations depend on the degree of conformational disorder and hence can be used to monitor the average trans/gauche isomerization in the system (Lopez-Garcia *et al*., 1993; Severcan, 1997). The CH_2 stretching frequencies in phospholipids have been widely used to monitor conformational ordering of the acyl chains in the lipid bilayer (Flach *et al*., 1993). Figure 21 and table 8 illustrate that there is a significant shift to lower wavenumber values of the CH_2 symmetric stretching vibrations in diabetic rat apex myocardium, meaning that diabetes decreases the number of gauche conformers, i.e. ordering of lipid bilayer. This result is in agreement with a previous FTIR study for diabetic platelets (Liu *et al*., 2002). However, they interpreted this frequency decrease as a decrease in the fluidity although changes in frequency values are known to give information about the order of the system, not the dynamics (Boyar and Severcan, 1997; Flach *et al*., 1993; Kneipp *et al*., 2000).

Figure 22 and table 9 show that diabetes causes a slight decrease in the concentration of α-helical structures of Amide I and Amide II, whereas it causes an increase in the concentration of β sheet structure. So we can deduce that diabetes mellitus might be causing some important structural changes in the proteins. The modification of increase in the number of β-sheet at the expense of α-helix possibly might explain the increase in the order of membrane lipids (table 8) which consequently will alter the behavior of membrane phospholipids.

As it is seen in figure 22 and table 10 the frequency of the Amide I band in control group appears around 1655 cm^{-1}, indicating that protein segments with the α-helical conformation are predominant. The frequency of this band shifts to lower values and the frequency of the Amide II band shifts to higher values in the diabetic apex myocardium. These shifts in the frequency values of the Amide I and Amide II bands might be an indicative of either a structural rearrangement of the existing tissue proteins or the expression of a new set of proteins with different structural characteristics (Lui *et al*., 1996). In a previous study, similar but more significant changes in the frequency of these bands were shown to occur in the left ventricle in infarcted heart tissue (Lui *et al*., 1996). The similar frequency decrease in the Amide I band was also reported in the human platelet membranes (Liu *et al*., 2002). In another study it was shown that, in diabetes, proteins exposed to glucose is cleaved, undergoes conformational changes and develops fluorescent adducts (Kugiyama *et al*., 1990). These changes were presumed to result from the covalent attachment of glucose to amino groups. However, the fragmentation and the conformational changes observed have been demonstrated to be dependent upon hydroxyl radicals produced by glucose auto-oxidation, or some closely related processes. Glycated proteins may be rearranged to AGEs which also contribute to the development of diabetic complications (Maxwell and Lip, 1997a). Binding of AGEs to their receptors can lead to modification in cell signaling and further production of free radicals (Penckofer *et al*., 2002).

It is clearly seen in figure 23 and table 11 that, the intensity of CH_3 bending band (at 1386 cm^{-1}) decreases in the diabetic group, which corresponds to a decrease in the content of this functional group. This result supports the finding which was obtained from figure 21 (intensities of CH_3 symmetric and asymmetric stretching modes). The band at 1151 cm^{-1} is a C-O stretching band arising due to the presence of glycogen in the system (Diem *et al*., 1999; Jackson *et al*., 1998; Wong *et al*., 1991), and the band giving an absorption at 1171 cm^{-1} is a CO-O-C asymmetric stretching band arising from ester bonds in cholesterol esters and phospholipids (Jackson *et al*., 1998), as it was previously mentioned. As it is clearly demonstrated in table 11 and figure 23, the ratio of the intensities of the absorptions at 1151 cm^{-1}

and 1171 cm^{-1} is reversed in the diabetic group, meaning that the intensity of the band at 1151 cm^{-1} increased and the intensity of the band at 1171 cm^{-1} decreased in the diabetic group with respect to the control. This type of change in the intensity ratio of these bands was previously observed in the infarcted heart (Lui *et al*., 1996). So it is possible to deduce that, diabetes mellitus causes similar changes with the infarction on heart tissue. The increase in the intensity of the band at 1151 cm^{-1} in the diabetic group might be due to an increase in the content of glycogen in the diabetic rat apex myocardium. It is believed that high levels of plasma free fatty acids increase triglyceride synthesis and accumulation of glycogen in the diabetic heart (Dhalla *et al*., 1992), which might be due to the disturbance of carbohydrate and lipid metabolism in diabetic apex myocardium. The other band in the diabetic group in which we see an increase in the intensity gives an absorption peak at 1083 cm^{-1}. This increase might be due to an increase in the lipid content and/or an increase in the concentration of glycolipids. Figure 23 illustrates the presence of a sharp band at 1041 cm^{-1}, originating from the various C-O stretching vibrations characteristic for oligosaccharites and polysaccharites. It is possible to observe a slight increase in the concentration of this functional group in diabetic group, which implies that diabetes causes oligo- and polysaccharide accumulation in the myocardium of the heart apex.

4.1.1.2 Left Ventricle Muscle and a Small Vessel in the Left Ventricle Muscle

4.1.1.2.1 Spectral Changes in the Left Ventricle Muscle

As it is seen in figure 26 and table 12, the changes observed in the content of the functional groups investigated in 3030-2800 cm^{-1} region were very similar with the changes observed for the apex myocardium, but more significant for the CH_2 symmetric stretching, CH_3 symmetric and asymmetric stretching bands. Furthermore, lipid to protein ratio increases more significantly in the left ventricle muscle of the diabetic group. It is clearly seen from figure 26 and table 13 that, the changes in the frequency values follow the same trend with the apex myocardium in 3030-2800 cm^{-1} region, but the changes are quite significant for the left ventricle muscle of the diabetic group with respect to control for the main functional groups investigated in this spectral region. An important difference between the diabetic and the control group is seen in the frequency of the CH_3 asymmetric stretching band. A shift in the

frequency of this band to lower values is observed in the diabetic group, which corresponds to stiffness of the deep interior of the bilayer (Umemura *et al*., 1980).

As demonstrated in figure 27 and table 14, the changes observed in the content of the functional groups investigated in 1800-1480 cm^{-1} region are also very similar with the changes observed for the apex myocardium. The main differences are like the following: Diabetes mellitus causes a significant decrease in the content of the Amide I of α-helical structure and the amide II band; and a more significant increase (with respect to apex myocardium) in the content of the band at 1637 cm^{-1} which is attributable to Amide I of β sheet structure. When figure 27 and table 15 are examined carefully, we see that the changes seen in the frequency of the Amide I and Amide II bands follow the same trend with the apex myocardium.

The changes observed in the concentration of the functional groups investigated in 1480-1000 cm^{-1} region are also very similar with the changes observed fur the apex myocardium, as seen in figure 28 and table 16. The main differences are: The increase in the concentration of glycogen is more significant, but the decrease in the content of ester bonds is less significant in the diabetic group of the left ventricle muscle.

Generally, it is possible to deduce from the findings that, diabetes induces more significant changes on the left ventricle muscle than the apex myocardium. This might be due to the fact that the left ventricle muscle is a stronger muscle, pumping the blood to all parts of the body via aorta. Since the left ventricle muscle is subject to the primary hemodynamic overload, it is not surprising that the pathologic processes primarily involve the left ventricle muscle than the apex myocardium.

4.1.1.2.2 Spectral Changes in the Vessel of the Left Ventricle Muscle

As it is shown in figure 29 and table 17, the changes observed in the intensity of the bands in 3030-2800 cm^{-1} region show the same trend with the apex myocardium and the left ventricle muscle. The increase in the intensity of the CH_2 symmetric stretching band is more dramatic with respect to apex, indicating a significant increase in the lipid content. These types of lipid abnormalities (such as

hypertriglyceridemia) and fatty acid distribution changes could participate in the development of vascular lesions in diabetes (Dang *et al*., 1988; Fontbonne *et al*., 1989). As seen in the figure and the table, a significant change occurs in the intensity of the band at 3012 cm^{-1} which was assigned as Olefinic=CH band in the average spectrum of the vessel in the diabetic group. The intensity of the Olefinic =CH band can be used as an index of relative concentration of double bonds in the lipid structure of unsaturated lipids (Takahashi *et al*., 1991). Figure 29 and table 17 clearly show that the intensity of the band (Olefinic=CH stretching vibration) at 3012 cm^{-1} increases in the vessels of the diabetic group with respect to the control. So, this result suggests that diabetes mellitus might be causing an increase the concentration of unsaturated fatty acids in vessels of the left ventricle muscle (Kneipp *et al*., 2000). This result is in agreement with a previous study (Liu *et al*., 2002), which has shown that the double bonds (=CH) in diabetic platelets increase which would suggest a higher lipid peroxidation in these platelets since these double bonds mainly originate from lipid peroxidative products, such as malondialdehyde. Consequently, it is possible to deduce that, there is a slight increased peroxidative process in the vessels. On the other hand, our result is in contradiction with a previous study which demonstrated that STZ-induced diabetes decreases the intensity of this functional group (Sills *et al*., 1994). It is clearly seen from figure 29 and table 18 that, the increase in the state of order of acyl chains in the vessel of the diabetic heart similar with the diabetic apex myocardium and the left ventricle muscle.

The changes observed in the intensity of the functional groups in 1800-1480 cm^{-1} region are also very similar with the changes observed for the apex myocardium and the left ventricle muscle as seen in figure 30 and table 19, but more significant changes occur in the content of the Amide I and the Amide II bands of the vessels than the changes observed in the apex and left ventricle muscle of the diabetic group. It is clearly seen from table 20 that the shifts in the frequency values of the investigated functional groups in 1800-1480 cm^{-1} region show the same trend with the apex myocardium and the left ventricle muscle of the rat heart in the diabetic group with respect to control, but the differences between the control and diabetic groups are not as significant.

There is a new band appearing around 1201 cm^{-1} (figure 31) which arises due to the collagen present in the system (Lui *et al*., 1996). There is an apparent increase in the content of this collagen band in diabetic groups as seen in table 21. The other changes in the intensity of the bands in 1480-1000 cm^{-1} region are similar to the ones obtained for the apex and the left ventricle muscle with some changes in their significance, like the following: The increase in the content of glycolipids is more significant in the vessel than apex myocardium and the left ventricle muscle; the increase in the content of the glycogen band in vessel is less significant than the left ventricle muscle but more significant than the apex myocardium; the decrease in the content of the ester bonds and CH_3 bending arising from lipids is more significant in the vessel than the apex myocardium and the left ventricle muscle.

4.1.1.3 Right ventricle muscle

As it seen in table 22 and figure 33, the changes observed in the concentration of the functional groups investigated in 3030-2800 cm^{-1} region show the same trend with the apex, the left ventricle muscle and the vessel but the changes in the content of the CH_3 symmetric and CH_2 asymmetric stretching modes are less significant than the apex myocardium, left ventricle muscle and the vessel. The decrease in the content of the CH_3 asymmetric stretching band is less significant than the left ventricle muscle and the vessel but more significant than the apex. The increase in the content of the unsaturated lipids is not significant, which was the case for the apex and the left ventricle muscle. When the changes in the frequency values are investigated in the same region, it is seen that diabetes causes similar increases in the state of order of the acyl chains with apex myocardium, left ventricle muscle and the vessel, but the increase in the stiffness of the CH_3 asymmetric stretching mode in the right ventricle muscle (like left ventricle muscle) is much more significant than the apex and the vessel in the left ventricle muscle.

As it is clearly illustrated in table 24 and figure 34, the changes observed in the content of the bands in 1800-1480 cm^{-1} region are also very similar with the changes observed for the apex myocardium, left ventricle muscle and the vessel, but we see less significant decrease in the content of the Amide I β sheet and the Amide

II band and a more significant decrease in the amount of the Amide I α-helix band. Table 25 shows that the frequency values of the Amide I and Amide II bands do not change significantly in the right ventricle muscle of the diabetic group. Our previous results revealed that (tables 10, 15, 20) diabetes causes a significant shift in the frequency of the Amide I band to lower values, and Amide II band to higher frequency values for the apex myocardium, the left ventricle muscle and the vessel on the left ventricle muscle of the diabetic group. So it is possible to deduce that diabetes mellitus does not affect the frequency values of the Amide I and Amide II bands in the right ventricle, whereas its effect was quite significant for the rest of the investigated regions of the rat heart.

Figure 35 and table 26 clearly show that the changes in the concentration of the functional groups investigated in 1480-1000 cm^{-1} region are similar to the ones obtained for the apex myocardium, the left ventricle muscle and the vessel on the left ventricle muscle.

By considering the results of all the investigated parts of the heart, an apparent increase in the content of lipids was observed. In previous studies, an increase in triglycerides and cholesterol in rat myocardium was reported after STZ injection after 8 weeks of diabetes (Lui *et al*., 1996). In our study, we see an increase in the lipid content in 4 weeks of diabetes. The findings of our study are important in this aspect since it shows that lipid metabolism is altered at early stages of the diabetes. This increase in the lipid content might lead to cardiomyopathy in diabetes, as suggested by others (Regan *et al*., 1977). The findings regarding all parts of the rat heart investigated in this study reveal that diabetes exerts more significant effects on the vessels than the ventricles and the apex. It is difficult to explain the reason for this difference in the effect of diabetes mellitus on the vessels concerning the molecular basis. But one possible explanation can be that the activity of the antioxidant enzymes in the vessels might be low, which is the case for the aorta (Kakkar *et al*., 1996) compared to other tissues. This suggests that the susceptibility of the vessels to oxidative damage is increased during the development of diabetes

mellitus. This can cause the vascular complications known to occur in diabetes mellitus.

The changes in the bandwidth values of CH_2 stretching bands in 3030-2800 cm^{-1} region, which gives information about the dynamics (fluidity) of the acyl chains, are also investigated. According to the results of the statistical tests, no significant difference was found between the control and the diabetic groups for different regions of the rat heart. Because of this reason, the results of bandwidth values are not given in the tables. In the literature, there are contradictory results regarding the effect of diabetes on dynamics of the membranes. For example, in a previous study it was reported that the membrane fluidity decreases in the diabetic erythrocytes (Candiloros *et al*., 1995). In another study, a slight increase in the fluidity of the acyl chains have been reported for the crude membrane of the diabetic rat heart (Severcan *et al*., 2003).

4.1.2 Effect of Selenium on Different Region of the Diabetic Rat Heart

This part of the study was undertaken to show whether Se, a constituent of glutathione peroxidase and selenoproteins with antioxidant properties, could restore the changes caused by diabetes in different regions of the diabetic rat heart. Only the functional groups which are affected positively by Se treatment are discussed in the following part.

4.1.2.1 Apex

The results given in table 27 and figures 36-38 reveal that diabetes mellitus decreases the content of α-helical structure of the proteins slightly, and the content of ester bonds significantly. Glycogen and glycolipid contents seem to increase in the diabetic rat apex myocardium. Se treatment of diabetic rats restored these parameters to near control values, tended to normalize the content of these molecules. The content of oligo- and polysaccharites decreases significantly in the Se treated diabetic group with respect to the diabetic rat heart apex. Moreover, we see a remarkable increase in the intensity ratios of 1151/1171 cm^{-1} bands in the diabetic rat heart apex myocardium. As previously mentioned, the increase in the ratio of these bands was

shown to occur in the infracted heart. Our results reveal that Se treatment tends to normalize this change in this ratio to control values, suggesting a potent medical effect of Se treatment. The table shows that the slight increase in the stiffness of the deep interior of the bilayer, the significant increase in the order of the acyl chains tended to return to almost their control values in the Se treated diabetic group. A significant decrease in the order of acyl chains is observed in the Se treated diabetic group with respect to the diabetic heart apex. The decrease in the frequency of Amide I bands in the diabetic group seem to approach its control value in the Se treated diabetic group, so that the differences in the frequency value of this band between control and Se treated diabetic are no longer statistically significant. This finding suggests that, diabetes-induced changes in α- helical structure of proteins might be restored with Se treatment.

4.1.2.2 Left Ventricle Muscle

It is clearly seen in table 28 and figures 39-41 that the concentration of unsaturated fatty acids decreases significantly in the Se treated diabetic group with respect to the diabetic ones. The table also shows that diabetes causes a significant decrease in the content of the ester bonds and a significant increase in the content glycogens. These diabetes mellitus induced changes in the contents of these molecules tended to be restored with the Se treatment of the diabetic group. We see a remarkable increase in the intensity ratios of 1151/1171 cm^{-1} bands, and the glycolipids in the diabetic rat heart left ventricle muscle. The table clearly shows that, when diabetic rats are treated with Se, the differences in the intensity values between the control and the Se treated diabetic group become no more statistically significant, revealing the potent treatment effect of Se. The table also shows the significant increase in the stiffness in the deep interior of the bilayer, in the order of the acyl chains and the change in the secondary structure of proteins in the diabetic group. The order of acyl chains significantly decreases in the Se treated diabetic ones with respect to the diabetic group. It is clearly seen from the table that, diabetes-induced alteration in these parameters tend to be restored to near control values in the Se treated diabetic group, so that the differences in these parameters between these

two experimental groups (control and Se treated diabetic groups) are no longer statistically significant for the left ventricle muscle.

4.1.2.3 Vessel

Diabetes mellitus is associated with characteristic vascular complications. Lipid abnormalities, such as hypertriglyceridemia (Fontbonne *et al*., 1989) and fatty acid distribution changes (Dang *et al*., 1988) could participate in the development of vascular lesions in diabetes. However, hyperglycemia alone has been reported to have a casual link with diabetic microangiopathy complications (Pugliese *et al*., 1991). The toxicity of glucose has been confirmed by studies on non-enzymatic glycosylation of proteins, the polyol pathway, and auto-oxidation of sugars and sugar-adduct proteins. These products and unsaturated lipids generate free radicals and may induce an oxidative stress *in vivo* possibly indicating a common pathway linking diverse mechanisms for the pathogenesis of vascular diabetic complications (Baynes, 1991).

Table 29 and figures 42-44 clearly show that diabetes causes a significant increase in the contents of the unsaturated fatty acids, β-sheet of Amide I, glycogen and the intensity ratio of 1151/1171 cm^{-1} bands. However, these diabetes mellitus-induced changes in the intensity values of these functional groups are restored in the Se treated diabetic group. We see a remarkable decrease in the content of the ester bonds in the diabetic group. This decrease is less significant in the Se treated diabetic group as shown in the table.

Table 29 shows significant increase in the order of the acyl chains and in the structure of proteins (Amide II) in the diabetic group. The order of the acyl chains decreases in the Se treated diabetic ones with respect to the diabetic group. It is clearly seen that these diabetes mellitus-induced changes tend to be normalized near to their control values in the Se treated diabetic group, so that the differences in the frequency values of these bands between these two experimental groups are no longer statistically significant for the vessel on the left ventricle muscle.

4.1.2.4 Right Ventricle Muscle

Table 30 and figures 45-47 clearly show that diabetes causes a significant increase in the contents of α-helical structure of the proteins (Amide I), glycogens, the intensity ratio of 1151/1171 cm^{-1} bands and the oligosaccharides. However, these diabetes mellitus-induced changes in the contents of these functional groups are restored in the Se treated diabetic group. We see a remarkable decrease in the content of the ester bonds in the diabetic group. This decrease is not statistically significant anymore in the Se treated diabetic group. It is seen that the content of oligo- and polysaccharides decrease significantly in the Se treated diabetic group with respect to the diabetic ones. The table shows significant increase in the order of the acyl chains in the diabetic group. The order of the acyl chains decreases in the Se treated diabetic ones with respect to the diabetic group. It is clearly seen that these diabetes mellitus-induced changes seem to be restored to near control values in the Se treated diabetic group, so tat the differences in these parameters between these two experimental groups are not anymore statistically significant for the right ventricle muscle.

The findings of our study reveal that Se treatment restores the diabetes-induced increase in the content of glycogen in the rat heart apex myocardium, left ventricle, vessel and the right ventricle muscle. This type of protective effect of Se was shown in a previous study for the glycogen content in rat adipocytes (Ezaki, 1990). In another study, however, using rat soleus muscle, glycogen synthesis was not affected by the treatment with selenate even though glucose uptake was positively affected (Berg *et al*., 1995). These results contrast with those found with insulin, since in muscle and other tissue insulin stimulates glycogen synthesis and storage. Thus, the insulin-like effects of selenate in this regard may differ in different tissues.

By considering the results of all the investigated parts of the heart, it is possible to deduce that, although Se restores the effect of diabetes in many functional groups, some of the alterations caused by diabetes on different regions of the heart are not restored to their control values with Se treatment, meaning that Se treated diabetic rats did not respond to the Se in the doses used in this study for some of the

functional groups investigated in this FTIR study. Maybe a higher dose and a longer-term Se application were necessary to see its full protective effect on diabetes mellitus. In a previous study it was reported that, selenate lowered the serum glucose level in 6 of the 8 treated diabetic rats. 2 treated diabetic rats did not respond to the selenate in the doses used in that study. Further treatment at one higher dose (17 μmole/kg/day) was also not successful. It was shown that STZ induced diabetes produced a variable diabetic response and may account for the lack of response of some rats to selenate at any given dose (McNeill *et al*., 1991). On the other hand, Ghosh *et al*., have reported that sodium selenite reduced hyperglycemia in Swiss albino mice made diabetic with STZ. In this case, the glucose levels were completely normalized. However, treatment of mice with selenite was begun prior to the administration of STZ in that study. Since the mechanism of induction of diabetes by STZ involves destruction of the beta cells that is, at least partially, due to the free radical formation, use of an antioxidant at that time of STZ injection may result in more surviving beta cells and, consequently, a less severe diabetes (Battell *et al*., 1993). Besides, the dose of STZ used to induce diabetes was lower (39 mg/kg) in that study, than the one we used in our study (50 mg/kg). In another study done by Becker *et al*., it was reported that oral selenate improved the glucose homeostasis in diabetic rats (1996). But the severity of diabetes was not as significant as the one we had in our study. A dose of 39 mg/kg was used by Becker *et al*., which is lower that the value we used (50mg/kg) in our study.

4.2 Part II: Effect of Stereotactic Radiosurgery on Hypoperfused Rat Brain Tissue Homogenates

4.2.1 Effect of Chronic Hypoperfusion on Rat Brain Tissue Homogenates

It is seen from table 32 and figure 49 that there is a decrease in the intensity of the CH_3 asymmetric stretching mode in the hypoperfused brain tissues. It means that the number of methyl groups in the acyl chain of lipids in this group decreases (Takahashi *et al*., 1991). An increase in the intensity of CH_2 symmetric stretching mode occurs with the application of operation on the rat brain tissues, indicating an increase in phospholipids or fatty acid concentrations. As seen in figure 50, the slight increases seen in the intensities of the phosphate asymmetric stretching (from 0.11 ±

0.008 to 0.12 ± 0.008) and symmetric stretching vibrations (from 0.15 ± 0.088 to 0.17 ± 0.09) also support the finding that the lipid content increases in the hypoperfused group. (Jackson *et al*., 1998; Man and Setiowaty, 1999; Melin *et al*., 2000). It was shown in a previous study that rapid accumulation of free fatty acids occur during cerebral ischemia and this accumulation was recognized as the first biochemical variable which reflects evolving brain damage with increasing duration of ischemia. This may be the explanation of our results, which reveal that fatty acid content increases in the hypoperfused brain. Another possible reason for the observed increase in the lipid content might be due to the protective mechanism of the brain to maintain membrane content during oxidative stress because of the important physiological functions of lipids in the brain.

It is clearly seen in table 32 that, the intensity of Amide I and Amide II decreases in the hypoperfused group. This decrease in the content of protein can be due to the disruption of protein synthesis which occurs in the case of decreased cerebral blood flow and consequently ATP depletion in hypoperfused brain samples (Fieschi *et al*., 1990; Wang *et al*., 2000). In addition to this, it was reported previously that, amino acid formation is reduced after ischemic insult, which may also explain the observed decrease in the protein content in the hypoperfused brain samples in our case (Sutherland *et al*., 1990).

An important factor affecting the membrane structure and dynamics is the amount of proteins and lipids in membranes. From the FTIR spectrum, a precise protein-to-lipid ratio can be derived by calculating the intensity ratio of bands arising from lipids to proteins. As it is seen in table 32, the ratio of the intensity of the Amide I to the intensity of the CH_2 symmetric stretching absorptions decreases in the hypoperfused group. Generally, this decrease in this ratio suggests a decrease in the protein content of the cells or an increase in the lipid content or both (Jackson *et al*., 1997). In our case, the increase in the lipid content in the hypoperfused groups is supported by the significant increase in the intensity of the CH_2 symmetric stretching, slight increases in the intensities of PO_2^- symmetric and asymmetric stretching vibrations; and the decrease in the protein content is supported by the decrease in the intensities of both

Amide I and Amide II bands. All these results support the finding that lipid to protein ratio increases in the hypoperfused brain samples.

The frequency of the absorptions provides information relating to structure/conformation and intermolecular interactions (Jackson *et al*., 1999; Jackson *et al*., 1997). Table 33 shows that there is a significant decrease in the frequency of the CH_2 symmetric and asymmetric vibrations upon the induction of hypoperfusion in the rat brain. This indicates an increase in the state-of-order in lipids (Kneipp *et al*., 2000).

The changes in the deep interior of the bilayer were monitored by the wavenumber of the CH_3 asymmetric stretching mode. An increase in the frequency of this band reflects increasing librational freedom of the acyl chains in the central area of the bilayer and a decrease in the frequency corresponds to stiffness of the bilayer (Umemura *et al*., 1980). As it is seen in table 33, there is a decrease in the frequency of the CH_3 asymmetric stretching mode, revealing that application of operation decreases the librational freedom of the acyl chains of the phospholipids in the central area of the bilayer of rat brain homogenates.

The Amide I region, at around 1646 cm^{-1} in our case, is useful for the determination of protein secondary structure (Lyman and Murray-Wijelath, 1999). Table 35 shows that hypoperfusion does not cause any change in the amount of antiparallel β sheet structure but it causes a significant decrease in the content of β turn and a significant increase in the content of β sheet structure. A significant decrease in the amount of ordered α-helical structure is observed in table 35. The amount of random coil structures slightly increases in the hypoperfused group. It can be deduced from these results that hypoperfusion causes a significant decrease in the content of α-helical structures and a significant increase in the content of β sheet structures (tables 35 and 36). These findings, together with a slight increase in the content of random coil structures imply that denaturation of proteins might be taking place. Another possibility for the increase in the β sheet structures is that there may be an over expression of β-amyloid precursor protein in the hypoperfused brain which was the case in a previous study on rodent models (Shi *et al*., 2000). By

considering the increase in the β sheet structures and random coils, we can deduce that proteins might be seriously affected in the hypoperfused brains. One possible explanation for this effect can be due to the intracellular acidosis which occurs as a result of the combined extrusion of it ions and lactate accumulation during ischemia/hypoxia (Plaschke *et al*., 2000; Schurr, 2002; Siesjo, 1988). The increase in anaerobic glycolysis, in which glucose is converted to lactate, and the decrease in lactate clearance under hypoperfused conditions leads to the lactate accumulation (Fieschi *et al*., 1990; Ueda *et al*., 2000). Lowering of pH can cause some changes in the protein structure and function which may end up with gross membrane dysfunction (Siesjo, 1988).

4.2.2 Effect of Radiosurgery on Control and Hypoperfused Rat Brain Tissue Homogenates

It is seen from the table 37 and the figure 53 that there is a slight increase in the intensity of CH_2 symmetric stretching mode in the radiated group, indicating either a slight increase in the length of the fatty acids and/or enhanced lipid content (Melin *et al*., 2001). This increase is significant in the hypoperfused+radiated group. These results reveal that radiation is more effective in increasing the length of the fatty acids and/or content of lipids in the hypoperfused brain. The average spectra of control, radiated and hypoperfused+radiated groups in 1285-1000 cm^{-1} region are given in figure 54. The spectra were normalized with respect to the Amide I band. There is a negligible increase in the intensity of the CH_2 scissoring band in the radiated group. CH_2 scissoring vibrations at 1467 cm^{-1} is correlated with the content of fatty acyl chains (Man and Setiowaty, 1999; Melin *et al*., 2000). As it is seen in the figure, this increase is quite significant in the hypoperfused+radiated group, supporting the previous finding that the effect of radiation in increasing the lipid content is more significant in the hypoperfused brain. There are also significant increases in the intensities of the phosphate asymmetric stretching and symmetric stretching vibrations in the radiated and hypoperfused+radiated groups. The same table also demonstrates significant increases in the content of CO-O-C asymmetric stretching mode arising from ester bonds in brain homogenates of radiated and hypoperfused+radiated groups. The absorbances for the CH_2 and P=O stretching

vibrations are expected to decrease when there is lipid peroxidation. The results reveal that there is no decrease in the intensities of these functional groups, suggesting that application of radiosurgery might not be causing lipid peroxidation in our case (LeVine and Wetzel, 1994). A possible explanation for the lack of lipid peroxidation in the radiated samples might be due to the presence of proteins, glycolipids and antioxidants which may protect the fatty acids found within the tissue so that no radiation induced peroxidation occurred in the system as suggested by Edwards *et al*. (1984).

It is clearly seen in table 37 that, the intensity of Amide I, consequently the amount of proteins decreases significantly in the radiated group. The decreases observed after irradiation in the protein content can be correlated with deleterious effects of $OH^{\cdot}$ which lead to protein denaturation and result in increased proteolytic susceptibility, as suggested by Davies (1987). This decrease is more profound in the hypoperfused+radiated group, meaning that the application of radiation is more effective in decreasing the content of proteins on the hypoperfused samples.

As it is seen in table 37, the ratio of the intensity of the Amide I to the intensity of the CH_2 symmetric stretching absorptions decreases slightly in the radiated group, significantly in the radiated+hypoperfused group. Generally, this decrease in the ratio suggests a decrease in the protein content or an increase in the lipid content or both (Jackson *et al*., 1997). In our case, the increase in the lipid content in radiated, and radiated+hypoperfused groups is supported by the increases in the intensities of the CH_2 symmetric stretching, CH_2 scissoring, CO-O-C asymmetric stretching, PO_2^- symmetric and asymmetric stretching vibrations. And the decrease in the content of protein content is supported by the decrease in the intensities of Amide I band in the treatment groups. These finding reveal that, the effect of radiation on decreasing the protein-to-lipid ratio is more dramatic on the hypoperfused brain homogenates, than the control ones.

The frequency of the absorptions provides structural and quantitative information (Jackson *et al*., 1997). Table 38 demonstrates that that there is no significant change in the order of acyl chains upon the application of radiation, but a

significant increase in the state of order occurs in the hypoperfused+radiated group. These results reveal that application of radiation induces more significant effects on the order of the system in the hypoperfused brains than in the control ones. It is difficult to explain this increase in the state of order, but one possible explanation might be the oxidation of proteins which might have influenced the membrane state-of-order via lipid-protein interactions and lead to the increase in the order of the system. In 1992, It was shown by Phelan *et al*. that, the application of radiation with 2.45 GHz pulsed wave to melanin-containing cells and liposomes changed membrane ordering, as measured by electron-paramagnetic-resonance (EPR) spectroscopy. Microwave exposure caused a shift from a fluid-like phase to a more solid or ordered membrane state. Similar results were obtained with liposomes that contained melanin, a redox polymer. Neither amelanotic B16 melanoma cells nor liposomes exhibited the microwave-facilitated increase in membrane ordering (Phelan *et al*., 1992).

The changes in the deep interior of the bilayer were monitored by the wavenumber of the CH_3 asymmetric stretching mode. An increase in frequency of this band reflects increasing librational freedom of the acyl chains in the central area of the bilayer. A decrease in the frequency corresponds to stiffness of the bilayer (Umemura *et al*., 1980). Table 38 shows that, the frequency of the CH_3 asymmetric stretching mode is not affected by the radiation, but it significantly shifts to lower values in the hypoperfused+radiated group, indicating an increase in the stiffness in the deep interior of the bilayer in brain homogenates. These results reveal that application of radiation induces more significant effects on the stiffness of the system in the hypoperfused brains than in the control ones. This effect can be explained starting from the assumption that membrane proteins at least partly compensate for radiation effects leading to a rigidization of membrane lipid regions (Kolling *et al*., 1994).

As it is seen in figure 55, the whole Amide I band, which gives information about the proteins of the system, spectrum moves to lower frequency values in the radiated group. This type of shift was shown to be an indicative of either a structural

rearrangement of the existing tissue proteins or the expression of a new set of proteins with different structural characteristics (Lui *et al*., 1996). Jyothi Lakshmi *et al*. reported previously that the response to the radiation damage to the brain tissue will be immediate activation of protective mechanisms, which includes the expression of proteins (like enzymes) involved in oxidative defense mechanisms (2002). So this might be the possible explanation of our result concerning the frequency shift of Amide I band. However, the shift in the frequency of this functional group is not significant in the hypoperfused+radiated group as shown in table 38. Further analysis has been carried out for the proteins present in the tissue samples by resolving Amide I band using band fitting method. As it is seen in the table 40, the amount of α-helical structure decreases significantly in the radiated group, whereas this effect is negligible in the hypoperfused+radiated group. The table also demonstrates that there is a negligible increase in the amount of β- sheet structure in the radiated group and slight increase in the hypoperfused+radiated group. The amount of random coil significantly increase in the radiated group and decreases in the hypoperfused+radiated group. These findings together with a significant increase in the content of random coil structures imply that denaturation of proteins might be taking place due to the application of radiation on control rat brains. Loss of function of a protein by irradiation may result from a change in a critical side chain or from a break in the hydrogen or disulfide bonds, which maintain the secondary and tertiary structures. Such a break can be lead to a partial unfolding of the tightly-coiled peptide chains which, in turn, can result in a disorganization of the internal structure, a distortion of necessary spatial relationships of side chain groups, or an exposure of amino acid groups resulting in a change in chemical activity. The hydrogen bonds of the secondary and tertiary structure are weak bonds. A number of them will be temporarily broken in the vicinity of ionization because the sudden introduction of a charge disrupts electrical dipoles. One primary ionization, then, can alter the structure of the molecule and lead to extensive change in the overall chemical reactivity (Casarett, 1968).

CHAPTER 5

CONCLUSION

Part I

Cardiovascular disease is the major cause of mortality in diabetic patients regardless of whether they are type I or type II. With the development of effective treatment for the infectious, metabolic and renal complications of diabetes mellitus, cardiovascular disease now looms as the most dreaded complication, striking earlier and with greater severity than in the general population. Thus, the study of heart disease in diabetic patients is of great clinical importance and its prevention, or treatment has become an urgent health care issue in recent years.

Diabetes mellitus is a complex multifactorial condition that undoubtedly leads to myocardial damage. It causes free radical injury, a major oxidative stress element, which proceeds to physiological damage in the body, including the heart and the vessels. Our findings suggest that, by correlating the spectroscopic changes with biochemical and physical profiles in diabetic heart apex myocardium, left ventricle muscle, small vessel on the left ventricle muscle and right ventricle muscle, diabetes mellitus causes some alterations that may contribute to the development of cardiac and cardiovascular disease in diabetes. The main common alterations are: higher lipid peroxidation (mainly for the vessels), increase in lipid content, increase in the order of lipids, altered protein profile, increase in glycogen and glycolipid contents. The findings regarding all parts of the rat heart investigated in this study

reveal that diabetes exerts more significant effects on the vessels than the muscles of the ventricles and the apex, most probably due to the fact that the antioxidant enzymes in the vessels might be low, which is the case for the aorta, compared to other tissues. This suggests that the susceptibility of the vessels to oxidative damage is increased during the development of diabetes mellitus which can cause the vascular complications known to occur in this disease. In previously published articles, the effect of diabetes on animals which were diabetic for long periods of time (mostly from 2 months to 10 years) had been investigated. It is possible to conclude from our study that diabetes induces significant effects, as mentioned above, on different region f the rat heart in a relatively short period of time (5 weeks).

The next section of the study was undertaken to show whether Se, a constituent of glutathione peroxidase and selenoproteins with antioxidant properties, could normalize the changes caused by diabetes on different regions of the diabetic rat heart to control values. The findings of our study revealed that, Se treatment restored some of the changes caused by diabetes, such as the slight decrease the content of α-helical structure of the proteins, the significant decrease in the content of ester bonds, the increase in the content of glycogen and glycolipids, the slight increase in the stiffness of the deep interior of the bilayer, the significant increase in the order of the acyl chains and the change in the secondary structure of proteins in the rat heart apex myocardium; the significant decrease in the content of the ester bonds and the significant increase in the content of glycogens, the increase in the content of glycolipids, the significant increase in the stiffness in the deep interior of the bilayer, in the order of the acyl chains and the change in the secondary structure of proteins in the left ventricle muscle; the significant increase in the contents of the unsaturated fatty acids, β sheet of Amide I and glycogen, the significant increase in the order of the acyl chains and the change in the structure of proteins (Amide II) in the vessel; and the significant increase in the contents of α-helical structure of the proteins (Amide I), glycogens, and the oligosaccharides, the remarkable decrease in the content of the ester bonds, significant increase in the order of the acyl chains in the right ventricle muscle. However, our results also revealed that some of the

alterations caused by diabetes on different regions of the heart were not restored to their control values with Se treatment, meaning that Se treated diabetic rats did not respond to the Se treatment, which was injected everyday to the rats for a period of 5 weeks in this study, for some of the functional groups investigated in this FTIR microscopy study.

In the future, further studies might be performed for longer term Se applications on the diabetic rat heart to see if the Se-induced changes will differ depending on the duration of application. In addition to this, the antioxidant mechanism of Se as a preventive mineral in the development and genesis of cardiovascular diseases through its protective role against LDL oxidation should be considered in future long term studies concominantly with remaining nutrients involved in the oxidative stress as antioxidants, namely vitamin E, C, carotenoids, zinc, cupper, etc. The oxidative stress is a very complex process occurring continuously in the human organism at which many substrates (prooxidant and antioxidant agents) are involved. Therefore future invention trials of supplementation should be focused in the concominant administration and study of all these agents in order to have a better knowledge of their resulting effect in the oxidation process, and consequently in cardiovascular diseases.

As a conclusion, the findings of our study open the possibility that the addition of certain trace elements, like Se, to treatment protocols used for diabetic patients may improve diabetes therapy.

Part II

In the second part of the study, the effects of stereotactic radiosurgery and/or hypoperfusion on rat brain tissue homogenates have been investigated. The results of this study suggest that, hypoperfusion causes significant effects on the structure and content of lipids and proteins in rat brain homogenates. An increase in the content of lipids, a decrease in the content of proteins and an increase in lipid to protein ratio are observed. The state of order of lipids increased in the hypoperfused rat brain samples. FTIR results also revealed that the proteins are affected in terms of content

and secondary structure in favor of β sheets and random coil. These findings clearly demonstrate that FTIR spectroscopy technique can be used to extract valuable information at molecular level about the effect of chronic hypoperfusion on rat brain samples.

Our FTIR results also show that, after a single high dose of X-ray to the healthy rat brain, a number of spectral changes occur revealing slight increase in the lipid synthesis, significant decrease in protein content, slight decrease in protein-to-lipid ratio. The results showed that radiation causes similar but more significant changes on hypoperfused brain samples. In addition to this, the application of radiation increased the order of lipids, increased the stiffness in the deep interior of the bilayer in the hypoperfused brains, but not in the non-hypoperfused ones. These findings suggest that chronically hypoperfused brain might be more vulnerable to the effects of radiation than the control ones, at least for the parameters mentioned above.

The findings of the present study also revealed that the secondary structure of the proteins are altered in the irradiated brain samples in a way that the content of α-helical structures decreases significantly and random coil increases dramatically, which indicates the denaturation of proteins. The effect of radiation on these parameters in the hypoperfused group is not significant, indicating that the secondary structure of proteins is not seriously effected by radiation in the chronically hypoperfused brain.

Our present study adds a valuable contribution to the knowledge on the effect of radiation on the chronically hypoperfused brain.

REFERENCES

Afzal, N., Pierce, G.N., Elimban, V., Beamish, R.E. and Dhalla, N.S. (1989). Influence of verapamil on some subcellular defects in diabetic cardiomyopathy. *Am J Physiol,* **256**, E453-8.

Ahlskog, J.E., Uitti, R.J., Low, P.A., Tyce, G.M., O'Brien, J.F. and Nickander, K.K. (1996). Levodopa and deprenyl treatment effects on peripheral indices of oxidant stress in Parkinson's disease. *Neurology,* **46**, 796-801.

Ahmed, S.S., Jaferi, G.A., Narang, R.M. and Regan, T.J.(1975). Preclinical abnormality of left ventricular function in diabetes mellitus. *Am Heart J,* **89**, 153-8.

Altman, K.I., Gerber, G.B. and Okada, S. (1970). *Radiation biochemistry.* New York,: Academic Press.

Altomare, E., Vendemiale, G., Chicco, D., Procacci, V. and Cirelli, F. (1992). Increased lipid peroxidation in type 2 poorly controlled diabetic patients. *Diabete Metab,* **18**, 264-71.

Altomare, E., Vendemiale, G., Grattagliano, I., Angelini, P., Micelli-Ferrari, T. and Cardia, L. (1995). Human diabetic cataract: role of lipid peroxidation. *Diabete Metab,* **21**, 173-9.

Armstrong, A.M., Chestnutt, J.E., Gormley, MJ. and Young, I.S. (1996). The effect of dietary treatment on lipid peroxidation and antioxidant status in newly diagnosed noninsulin dependent diabetes. *Free Radic Biol Med,* **21**,719-26.

Arrondo, J.L., Muga, A., Castresana, J. and Goni, F.M. (1993). Quantitative studies of the structure of proteins in solution by Fourier-transform infrared spectroscopy. *Prog Biophys Mol Biol,* **59**, 23-56.

Asayama, K., Kooy, N.W. and Burr, I.M. (1986). Effect of vitamin E deficiency and selenium deficiency on insulin secretory reserve and free radical scavenging systems in islets: decrease of islet manganosuperoxide dismutase. *J Lab Clin Med,* **107**, 459-64.

Bakth, S., Arena, J., Lee, W., Torres, R., Haider, B., Patel, B.C., Lyons, M.M. and Regan, T.J. (1986). Arrhythmia susceptibility and myocardial composition in diabetes. Influence of physical conditioning. *J Clin Invest,* **77**, 382-95.

Barbano, R., Hart-Gouleau, S., Pennella-Vaughan, J. and Dworkin, R.H. (2003). Pharmacotherapy of painful diabetic neuropathy. *Curr Pain Headache Rep,* **7**, 169-77.

Battell, M.L., Delgatty, H.L. and McNeill, J.H. (1998). Sodium selenate corrects glucose tolerance and heart function in STZ diabetic rats. *Mol Cell Biochem,* **179**, 27-34.

Baynes, J.W. (1991). Role of oxidative stress in development of complications in diabetes. *Diabetes,* **40**, 405-12.

Baynes, J.W. and Thorpe, SR. (1999). Role of oxidative stress in diabetic complications:a new perspective on an old paradigm. *Diabetes,* **48**, 1-9.

Becker, D.J., Reul, B., Özcelikay, A.T., Buchet, J.P., Henquin, J.C. and Brichard, S.M. (1996). Oral selenate improves glucose homeostasis and partly reverses abnormal expression of liver glycolytic and gluconeogenic enzymes in diabetic rats. *Diabetologia,* **39**, 3-11.

Bederson, J.B., Wiestler, O.D., Brustle, O., Roth, P., Frick, R. and Yaşargil, M.G. (1991). Intracranial venous hypertension and the effects of venous outflow obstruction in a rat model of arteriovenous fistula. *Neurosurgery,* **29**, 341-50.

Bedwal, R.S., Nair, N., Sharma, M.P. and Mathur, R.S. (1993). Selenium--its biological perspectives. *Med Hypotheses,* **41**, 150-9.

Berg, E.A., Wu, J.Y., Campbell, L., Kagey, M. and Stapleton, S.R. (1995). Insulin-like effects of vanadate and selenate on the expression of glucose-6-phosphate dehydrogenase and fatty acid synthase in diabetic rats. *Biochimie,* **77**, 919-24.

Betteridge, D.J. (2000). What is oxidative stress? *Metabolism,* **49**, 3-8.

Bhimji, S., Godin, D.V. and McNeill, J.H. (1986). Myocardial ultrastructural changes in alloxan-induced diabetes in rabbits. *Acta Anat (Basel),* **125**, 195-200.

Biswas, S., Talukder, G. and Sharma, A. (2000). Chromosome damage induced by selenium salts in human peripheral lymphocytes. *Toxicol In Vitro,* **14**, 405-8.

Biswas, S., Talukder, G. and Sharma, A. (1999). Comparison of clastogenic effects of inorganic selenium salts in mice *in vivo* as related to concentrations and duration of exposure. *Biometals,* **12**, 361-8.

Boyar, H. and Severcan, F. (1997). Tamoxifen-model membrane interactions: An FT-IR study. *Journal of Molecular Structure,* **408**, 265-268.

Brownlee, M. *(1995).* Advanced protein glycosylation in diabetes and aging. *Annu Rev Med,* **46**, 223-34.

Brownlee, M., Cerami, A. *and* Vlassara, H. (1988). Advanced glycosylation end products in tissue and the biochemical basis of diabetic complications. *N Engl J Med,* **318**, 1315-21.

Bucala, R. and Cerami, A. (1992). Advanced glycosylation: chemistry, biology, and implications for diabetes and aging. *Adv Pharmacol,* **23**, 1-34.

Bucala., R., Makita, Z., Koschinsky, T., Cerami, A. and Vlassara, H. (1993). Lipid advanced glycosylation: pathway for lipid oxidation *in vivo*. *Proc Natl Acad Sci USA,* **90**, 6434-8.

Burk, R.F. (1986). Selenium and cancer: meaning of serum selenium levels. *J Nutr,* **116**, 1584-6.

Byler, D.M. and Susi, H. (1986). Examination of the secondary structure of proteins by deconvolved FTIR spectra. *Biopolymers,* **25**, 469-87.

Cadrin, M., French, S.W. and Wong, P.T. (1991). Alteration in molecular structure of cytoskeleton proteins in griseofulvin-treated mouse liver: a pressure tuning infrared spectroscopy study. *Exp Mol Pathol,* **55**, 170-9.

Cameron, J.R. and Skofronick, J.G. (1978). Physics of Radiation Therapy. In *Medical Physics.* pp. 448. New York: Wiley.

Campbell, I.D. and Dwek, R.A. (1984). *Biological spectroscopy.* Menlo Park, Calif.: Benjamin/Cummings Pub. Co.

Candiloros, H., Muller, S., Zeghari, N., Donner, M., Drouin, P. and Ziegler, O. (1995). Decreased erythrocyte membrane fluidity in poorly controlled IDDM. Influence of ketone bodies. *Diabetes Care,* **18**, 549-51.

Casarett, A.P., American Institute of Biological Sciences. and U.S. Atomic Energy Commission. (1968). *Radiation biology.* Englewood Cliffs, N.J.,: Prentice-Hall.

Ceriello, A. (1999). Hyperglycaemia: the bridge between non-enzymatic glycation and oxidative stress in the pathogenesis of diabetic complications. *Diabetes Nutr Metab,* **12**, 42-6.

Chance, B., Sies, H. and Boveris, A. (1979). Hydroperoxide metabolism in mammalian organs. *Physiol Rev,* **59**, 527-605.

Cheng, H.M. and Gonzalez, R.G. (1986). The effect of high glucose and oxidative stress on lens metabolism, aldose reductase, and senile cataractogenesis. *Metabolism,* **35**, 10-4.

Ci, Y.X., Gao, T.Y., Feng, J. and Guo, Z.Q. (1999). Fourier transform infrared spectroscopic characterization of human breast tissue: Implications for breast cancer diagnosis. *Applied Spectroscopy,* **53**, 312-315.

Colthup, N.B., Daly, L.H. and Wiberley, S.E. (1975). *Introduction to infrared and Raman spectroscopy.* New York: Academic Press.

Cser, A., Sziklai-Laszlo, I., Menzel, H. and Lombeck, I. (1993). Selenium status and lipoproteins in healthy and diabetic children. *J Trace Elem Electrolytes Health Dis,* **7**, 205-10.

Dai, S. and McNeill, J.H. *(1995).* Ascorbic acid supplementation prevents hyperlipidemia and improves myocardial performance in streptozotocin-diabetic rats. *Diabetes Res Clin Pract,* **27**, 11-8.

Dang, A.Q., Faas, F.H., Lee, J.A. and Carter, W.J. (1988). Altered fatty acid composition in the plasma, platelets, and aorta of the streptozotocin-induced diabetic rat. *Metabolism,* **37**, 1065-72.

Daniels, L.A. (1996). Selenium metabolism and bioavailability. *Biol Trace Elem Res,* **54**, 185-99.

Davies, K.J. (1987). Protein damage and degradation by oxygen radicals. I. general aspects. *J Biol Chem,* **262**, 9895-901.

DCCT_Research_Group (1993). The effect of intensive treatment of diabetes on the development and progression of long-term complications in insulin-dependent diabetes mellitus. The Diabetes Control and Complications Trial Research Group. *N Engl J Med,* **329**, 977-86.

de Wilde, M.C., Farkas, E., Gerrits, M., Kiliaan, A.J. and Luiten, P.G. (2002). The effect of n-3 polyunsaturated fatty acid-rich diets on cognitive and cerebrovascular parameters in chronic cerebral hypoperfusion. *Brain Res,* **947**, 166-73.

Denny, W.A. (2000). The role of hypoxia-activated prodrugs in cancer therapy. *Lancet Oncol,* **1**, 25-9.

Dhalla, N.S., Elimban, V. and Rupp, H. (1992). Paradoxical role of lipid metabolism in heart function and dysfunction. *Mol Cell Biochem,* **116**, 3-9.

Dicko, A., Morissette, M., Ben Ameur, S., Pezolet, M. and Di Paolo, T. (1999). Effect of estradiol and tamoxifen on brain membranes: investigation by infrared and fluorescence spectroscopy. *Brain Res Bull,* **49**, 401-5.

Diem, M., Boydston-White, S. and Chiriboga, L. (1999). Infrared spectroscopy of cells and tissues: Shining light onto a novel subject. *Applied Spectroscopy,* **53**, 148a-161a.

Douillet, C., Bost, M., Accominotti, M., Borson-Chazot, F. and Ciavatti, M. (1998). Effect of selenium and vitamin E supplements on tissue lipids, peroxides, and fatty acid distribution in experimental diabetes. *Lipids,* **33**, 393-9.

Douillet, C., Tabib, A., Bost M., Accominotti, M., Borson-Chazot, F. and Ciavatti, M. (1996). A selenium supplement associated or not with vitamin E delays early renal lesions in experimental diabetes in rats. *Proc Soc Exp Biol Med,* **211**, 323-31.

Dyer, D.G., Dunn, J.A., Thorpe, S.R., Bailie, K.E., Lyons, T.J., McCance, D.R. and Baynes, J.W. (1993). Accumulation of Maillard reaction products in skin collagen in diabetes and aging. *J Clin Invest,* **91**, 2463-9.

Edwards, J.C., Chapman, D. and Cramp, W.A. (1984). The effects of ionizing radiation on the peroxide content of a pure polyunsaturated lipid dispersion and of lipids and membranes derived from Acholeplasma laidlawii. *Int J Radiat Biol Relat Stud Phys Chem Med,* **45**, 33-44.

Ekholm, P., Varo, P., Aspila, P., Koivistoinen, P. and Syrjala-Qvist, L. (1991). Transport of feed selenium to different tissues of bulls. *Br J Nutr,* **66**, 49-55.

Ezaki, O. (1990). The insulin-like effects of selenate in rat adipocytes. *J Biol Chem,* **265**, 1124-8.

Fabian, H., Jackson, M., Murphy, L., Watson, P.H., Fichtner, I. and Mantsch, H.H. *(1995).* A Comparative Infrared Spectroscopic Study of Human Breast-Tumors and Breast-Tumor Cell Xenografts. *Biospectroscopy,* **1**, 37-45.

Factor, S.M., Bhan, R., Minase, T., Wolinsky, H. and Sonnenblick, E.H. (1981). Hypertensive-diabetic cardiomyopathy in the rat: an experimental model of human disease. *Am J Pathol,* **102**, 219-28.

Factor, S.M., Borczuk, A., Charron, M.J., Fein, F.S., van Hoeven, K.H. and Sonnenblick, E.H. (1996). Myocardial alterations in diabetes and hypertension. *Diabetes Res Clin Pract,* **31 Suppl**, S133-42.

Factor, S.M., Minase, T. and Sonnenblick, E.H. (1980a). Clinical and morphological features of human hypertensive-diabetic cardiomyopathy. *Am Heart J*, **99**, 446-58.

Factor, S.M., Okun, E.M. and Minase, T. (1980b). Capillary microaneurysms in the human diabetic heart. *N Engl J Med,* **302**, 384-8.

Favier, A.E. (1993). Nutritional and clinical factors affecting the bioavailability of trace elements in humans. In *Bioavailability '93: nutritional, chemical, and food processing implications of nutrient availability: Ettlingen, May 9-12:proceedings. Berichte der Bundesforschungsanstalt feur Ernèahrung, BFE-R— 93-01.* ed Schlemmer, U. pp. 202-211. Karlsruhe: Bundesforschungsanstalt fèur Ernèahrung.

Fein, F.S., Cho, S., Zola, B.E., Miller, B. and Factor, S.M. (1989). Cardiac pathology in the hypertensive diabetic rat. Biventricular damage with right ventricular predominance. *Am J Pathol,* **134**, 1159-66.

Fein, F.S., Kornstein, LB., Strobeck, J.E., Capasso, J.M. and Sonnenblick, E.H. (1980). Altered myocardial mechanics in diabetic rats. *Circ Res,* **47**, 922-33.

Fein, F.S. and Sonnenblick, E.H. *(1985).* Diabetic cardiomyopathy. *Prog Cardiovasc Dis,* **27**, 255-70.

Ferrari, R., Ceconi, C., Curello, S., Cargnoni, A., Alfieri, O., Pardini, A., Marzollo, P. and Visioli, O. (1991). Oxygen free radicals and myocardial damage: protective role of thiol containing agents. *Am J Med,* **91**, 95S-105S.

Fieschi, C., Di Piero, V., Lenzi, G.L., Pantano, P., Giubilei, F., Buttinelli, C. and Carolei, A. (1990). Pathophysiology of ischemic brain disease. *Stroke,* **21**, IV9-11.

Flach, C.R., Brauner, J.W. and Mendelsohn, R. (1993). Calcium ion interactions with insoluble phospholipid monolayer films at the A/W interface. External reflection-absorption IR studies. *Biophys J,* **65**, 1994-2001.

Flickinger, J.C., Pollock, B.E., Kondziolka, D. and Lunsford, L.D. (1996). A dose-response analysis of arteriovenous malformation obliteration after radiosurgery. *Int J Radiat Oncol Biol Phys,* **36**, 873-9.

Fontbonne, A., Eschwege, E., Cambien, F., Richard, J.L., Ducimetiere, P., Thibult, N., Warnet, J.M., Claude, J.R. and Rosselin, G.E. (1989). Hypertriglyceridaemia as a risk factor of coronary heart disease mortality in subjects with impaired glucose tolerance or diabetes. Results from the 11-year follow-up of the Paris Prospective Study. *Diabetologia,* **32**, 300-4.

Freifelder, D. (1982). *Physical biochemistry: applications to biochemistry and molecular biology.* San Francisco: W.H. Freeman.

Frol'kis, R.A., Voronkov, G.S., Dubur, G., Tsiomik, V.A. and Gomon, I.V. (1983). [Creatine phosphokinase activity in myocardial sarcoplasmic reticulum membranes in experimental coronary insufficiency]. *Biull Eksp Biol Med,* **95**, 53-5.

Fyles, A.W., Milosevic, M., Wong, R., Kavanagh, M.C., Pintilie, M., Sun, A., Chapman, W., Levin, W., Manchul, L., Keane, T.J. and Hill, R.P. (1998). Oxygenation predicts radiation response and survival in patients with cervix cancer. *Radiother Oncol,* **48**, 149-56.

Ganther, H.E. and Kraus, R.J. (1989). Chemical stability of selenious acid in total parenteral nutrition solutions containing ascorbic acid. *JPEN J Parenter Enteral Nutr,* **13**, 185-8.

Gebre-Medhin, M., Ewald, U., Plantin, L.O. and Tuvemo, T. (1984). Elevated serum selenium in diabetic children. *Acta Paediatr Scand,* **73**, 109-14.

Gentner, J.M., Wentrup-Byme, E., Walker, P.J. and Walsh, M.D. (1998). Comparison of fresh and post-mortem human arterial tissue: an analysis using FT-IR microspectroscopy and chemometrics. *Cell Mol Biol (Noisy-le-grand),* **44**, 251-9.

George, W.O., McIntyre, P.S., Mowthorpe, D.J. and ACOL (Project) (1987). *Infrared spectroscopy.* Chichester West Sussex ; New York: Published on behalf of ACOL London by Wiley.

Ghosh, R., Mukherjee, B. and Chatterjee, M. (1994). A novel effect of selenium on streptozotocin-induced diabetic mice. *Diabetes Res,* **25**, 165-71.

Giacomelli, F. and Wiener, J. (1979). Primary myocardial diseasein the diabetic mouse. An ultrastructural study. *Lab Invest,* **40**, 460-73.

Gillery, P., Monboisse, J.C., Maquart, F.X. and Borel, J.P. (1988). Glycation of proteins as a source of superoxide. *Diabete Metab,* **14**, 25-30.

Giugliano, D., Ceriello, A. and Paolisso, G. (1995). Diabetes mellitus, hypertension, and cardiovascular disease: which role for oxidative stress? *Metabolism,* **44**, 363-8.

Glatz, J.F., van Breda, E., Keizer, H.A., de Jong, Y.F., Lakey, JR., Rajotte, R.V., Thompson, A., van der Vusse, G.J. and Lopaschuk, G.D. (1994). Rat heart fatty acid-binding protein content is increased in experimental diabetes. *Biochem Biophys Res Commun,* **199**, 639-46.

Gotzsche, O. (1983a). The adrenergic beta-receptor adenylate cyclase system in heart and lymphocytes from streptozotocin-diabetic rats. *In vivo* and *in vitro* evidence for a desensitized myocardial beta-receptor. *Diabetes,* **32**, 1110-6.

Gotzsche, O. (1983b). Decreased myocardial calcium uptake after isoproterenol in streptozotocin-induced diabetic rats. Studies in the in vitro perfused heart. *Lab Invest,* **48**, 156-61.

Greger, J.L. (1992). Using animals to assess bioavailability of minerals: implications for human nutrition. *J Nutr,* **122**, 2047-52.

Gressier, B., Cabanis, A., Lebegue, S., Brunet, C., Dine, T., Luyckx, M., Cazin, M. and Cazin, J.C. (1993). Comparison of in vitro effects of two thiol-containing drugs on human neutrophils hydrogen peroxide production. *Methods Find Exp Clin Pharmacol,* **15**, 101-5.

Griffiths, P.R. and De Haseth, J.A. (1986). *Fourier transform infrared spectrometry.* New York: Wiley.

Grossman, E. and Messerli, F.H. (1996). Diabetic and hypertensive heart disease. *Ann Intern Med,* **125**, 3 04-10.

Hadjipanayis, C.G., Levy, E.I., Niranjan, A., Firlik, A.D., Kondziolka, D., Flickinger, J.C. and Lunsford, L.D. (2001). Stereotactic radiosurgery for motor cortex region arteriovenous malformations. *Neurosurgery,* **48**, 70-6; discussion 76-7.

Haider, B., Yeh, C.K., Thomas, G., Oldewurtel, H.A., Lyons, M.M. *and* Regan, T.J. (1981). Influence of diabetes on the myocardium and coronary arteries of rhesus monkey fed an atherogenic diet. *Circ Res,* **49**, 1278-88.

Halliwell, B. (1994). Free radicals, antioxidants, and human disease: curiosity, cause, or consequence? *Lancet,* **344**, 721-4.

Halushka, P.V., Lurie, D. *and* Colwell, J.A. (1977). Increased synthesis of prostaglandinE-like material by platelets from patients with diabetes mellitus. *N Engl J Med,* **297**, 1306-10.

Hamby, R.I., Zoneraich, S. *and* Sherman, L. (1974). Diabetic cardiomyopathy. *Jama,* **229**, 1749-54.

Haris, P.I. and Severcan, F. (1999). FTIR spectroscopic characterization of protein structure in aqueous and non-aqueous media. *Journal of Molecular Catalysis B-Enzymatic,* **7**, 207-221.

Hassan, S., Hakkarainen, R.V., Lindberg, P.O. *and* Sankari, S. (1990). Utilization of dietaiy sodium selenite, barley, oats and meat meal selenium by the chick. *Zentralbl Veterinarmed A,* **37**, 270-7.

Head, K.A. (2001). Natural therapies for ocular disorders, part two: cataracts and *glaucoma. Altern Med Rev,* **6**, 141-66.

Herrman, C.E., Sanders, R.A., Klaunig, J.E., Schwarz, L.R. *and* Watkins, J.B., 3rd (1999). Decreased apoptosis as a mechanism for hepatomegaly in streptozotocin-induced diabetic rats. *Toxicol Sci,* **50**, 146-51.

Hershey, J.W., Oostdyk, T.S. and Keliher, P.N. (1988). Determination of arsenic and selenium in environmental and agricultural samples by hydride generation atomic absorption spectrometry. *J Assoc Off AnaI Chem,* **71**, 1090-3.

Heyliger, C.E., Rodrigues, B. and McNeill, J.H. (1986). Effect of choline and methionine treatment on cardiac dysfunction of diabetic rats. *Diabetes,* **35**, 1152-7.

Hofmeister, C., Stapf, C., Hartmann, A., Sciacca., R.R., Mansmann, U., terBrugge, K., Lasjaunias, P., Mohr, J.P., Mast, H. and Meisel, J. (2000). Demographic, morphological, and clinical characteristics of 1289 patients with brain arteriovenous malformation. Stroke, **31**, 1307-10.

Holecek, V., Racek, J. and Jerabek, Z. *(1995).* [Administration of multivitamin combinations and trace elements in diabetes]. *Cas Lek Cesk,* **134**, 80-3.

Horackova, M. and Murphy, M.G. (1988). Effects of chronic diabetes mellitus on the electrical and contractile activities, *45Ca2+* transport, fatty acid profiles and ultrastructure of isolated rat ventricular myocytes. *Pflugers Arch,* **411**, 564-72.

Hossmann, K.A. (1999). The hypoxic brain. Insights from ischemia research. *Adv Exp Med Biol,* **474,** 155-69.

Hsiao, Y.C., Suzuki, K., Abe, H. and Toyota, T. (1987). Ufltrastructural alterations in cardiac muscle of diabetic BB Wistar rats. *Virchows Arch A Pathol Anat Histopathol,* **411**, 45-52.

Ingebretsen, W.R., Jr., Peralta, C., Monsher, M., Wagner, L.K. and Ingebretsen, C.G. (1981). Diabetes alters the myocardial cAMP-protein kinase cascade system. *Am J Physiol,* **240**, H375-82.

Inoguchi, T., Battan, R., Handler, E., Sportsman, J.R., Heath, W. and King, G.L. (1992). Preferential elevation of protein kinase C isoform beta II and diacylglycerol levels in the aorta and heart of diabetic rats: differential reversibility to glycemic control by islet cell transplantation. *Proc Natl Acad Sci USA,* **89**, 11059-63.

Iyoda, M., Kuroki, A., Kato, K., Kato, N., Hirano, T. and Sugisaki, T. (2003). A case of acute renal failure due to rhabdomyolysis, associated with non-autoimmune fulminant type lB diabetes mellitus. *Clin Nephrol,* **59**, 301-4.

Jackson, C.V., McGrath, G.M., Tahiliani, A.G., Vadlamudi, R.V. and McNeill, J.H. (1985). A functional and ultrastructural analysis of experimental diabetic rat myocardium. Manifestation of a cardiomyopathy. *Diabetes,* **34**, 876-83.

Jackson, M., Mansfield, J.R., Dolenko, B., Somorjai, R.L., Mantsch, H.H. and Watson, P.H. (1999). Classification of breast tumors by grade and steroid receptor status using pattern recognition analysis of infrared spectra. *Cancer Detect Prev,* **23**, 245-53.

Jackson, M., Ramjiawan, B., Hewko, M. and Mantsch, H.H. (1998). Infrared microscopic functional group mapping and spectral clustering analysis of hypercholesterolemic rabbit liver. *Cell Mol Biol (Noisy-ie-grand),* **44**, 89-98.

Jackson, M., Sowa, M.G. and Mantsch, H.H. (1997). Infrared spectroscopy: a new frontier in medicine. *Biophys Chem,* **68**, 109-25.

Jaffe, W. (1992). [Selenium, an essential and toxic element. Latin American data]. *Arch Latinoam Nutr,* **42**, 90-3.

Johnson, P.E. (1989). What can in vitro methods tell us about mineral availability? *Biol Trace Elem Res,* **19**, 3-10.

Junod, A., Lambert, A.E., Stauffacher, W. and Renold, A.E. (1969). Diabetogenic action of streptozotocin: relationship of dose to metabolic response. *J C/in Invest,* **48**, 2129-39.

Jyothi Lakshmi, R., Kartha, V.B., Murali Krishna, C., JG, R.S., Ullas, G. and Uma Devi, P. (2002). Tissue Raman spectroscopy for the study of radiation damage: brain irradiation of mice. *Radial Res,* **157**, 175-82.

Kainulainen, H., Breiner, M., Schurmann, A., Marttinen, A., Virjo, A. and Joost, H.G. (1994). *In vivo* glucose uptake and glucose transporter proteins GLUT1 and GLUT4 in heart and various types of skeletal muscle from streptozotocin-diabetic rats. *Biochim Biophys Acta,* **1225**, 275 -82.

Kakkar, R., Mantha, S.V., Kalra, J. and Prasad, K. (1996). Time course study of oxidative stress in aorta and heart of diabetic rat. *Clin Sci (Lond),* **91**, 441-8.

Kamimura, S., Gaal, K., Britton, R.S., Bacon, B.R., Triadafilopoulos, G. and Tsukamoto, H. (1992). Increased 4-hydroxynonenal levels in experimental alcoholic liver disease: association of lipid peroxidation with liver fibrogenesis. *Hepatology,* **16**, 448-53.

Kannel, W.B., Hjortland, M. and Castelli, W.P. (1974). Role of diabetes in congestive heart failure: the Framingham study. *Am J Cardiol,* **34,** 29-34.

Kannel, W.B. and McGee, D.L. (1979). Diabetes and cardiovascular disease. The Framingham study. *Jama,* **241**, 2035-8.

Karpen, C.W., Pritchard, K.A., Jr., Merola, A.J. and Panganamala, R.V. (1982). Alterations of the prostacyclin-thromboxane ratio in streptozotocin induced diabetic rats. *Prostaglandins Leukot Med,* **8**, 93-103.

Kawaguchi, C., Takizawa, S., Niwa, K., Iwamoto, T., Kuwahira, I., Kato, H. and Shinohara, Y. (2002). Regional vulnerability to chronic hypoxia and chronic hypoperfusion in the rat brain. *Pathophysiology,* **8**, 249-253.

Kneipp, J., Lasch, P., Baldauf, F., Beekes, M. and Naumann, D. (2000). Detection of pathological molecular alterations in scrapie-infected hamster brain by Fourier transform infrared (FT-IR) spectroscopy. *Biochim Biophys Acta,* **1501,** 189-99.

Kochan, Z., Karbowska, J., Bukato, G., Zydowo, M.M., Bertoli, E., Tanfani, F. and Swierczynski, J. (1995). A comparison of the secondary structure of human brain mitochondrial and cytosolic 'malic' enzyme investigated by Fourier-transform infrared spectroscopy. *Biochem J,* **309 (Pt 2)**, 607-11.

Kolling, A., Maldonado, C., Ojeda, F. and Diehl, H.A. (1994). Membrane fluidity of microsomal and thymocyte membranes after X-ray and UV irradiation. *Radiat Environ Biophys,* **33**, 303-13.

Koltai, M.Z., Balogh, I., Wagner, M. and Pogatsa, G. (1984). Diabetic myocardial alterations in ultrastructure and function. Exp *Pathol,* **25**, 215-21.

Kowluru, R.A., Engerman, R.L. and Kern, T.S. (1999). Abnormalities of retinal metabolism in diabetes or experimental galactosemia.. VI. Comparison of retinal and cerebral cortex metabolism, and effects of antioxidant therapy. *Free Radic Biol Med,* **26**, 371-8.

Kowluru, R.A., Engerman, R.L. and Kern, T.S. (2000). Diabetes-induced metabolic abnormalities in myocardium: effect of antioxidant therapy. *Free Radic Res,* **32**, 67-74.

Kugiyama, K., Kems, S.A., Morrisett, J.D., Roberts, R. and Henry, P.D. (1990). Impairment of endothelium-dependent arterial relaxation by lysolecithin in modified low-density lipoproteins. *Nature,* **344**, 160-2.

Kurita, H., Kawamoto, S., Sasaki, I., Shin, M., Tago, M., Terahara,, A., Ueki, K. and Kirino, T. (2000). Results of radiosurgery for brain stem arteriovenous malformations. *J Neurol Neurosurg Psychiatry,* **68**, 563-70.

Lane, H.W., Strength, R., Johnson, J. and White, M. (1991). Effect of chemical form of selenium on tissue glutathione peroxidase activity in developing rats. *J Nutr,* **121**, 80-6.

Lawton, M.T., Hamilton, M.G. and Spetzler, R.F. (1995). Multimodality treatment of deep arteriovenous malformations: thalamus, basal ganglia, and brain stem. *Neurosurgery,* **37**, 29-35; discussion 35-6.

Lee, S.L., Ostadalova, I., Kolar, F. and Dhalla, N.S. (1992). Alterations in Ca(2+)-channels during the development of diabetic cardiomyopathy. *MoI Cell Biochem,* **109**, 173-9.

Lee, T.S., MacGregor, L.C., Fluharty, S.J and King, G.L. (1989). Differential regulation of protein kinase C and (Na,K)-adenosine triphosphatase activities by elevated glucose levels in retinal capillary endothelial cells. *J Clin Invest,* **83**, 90-4.

Levander, O.A. (1983). Considerations in the design of selenium bioavailability studies. *Fed Proc,* **42**, 1721-5.

Levander, O.A. and Burk, R.F. (1994). Selenium. In *Modern nutrition in health and disease.* ed Shike, M. pp. 242-251. Philadelphia: Lea and Febiger.

LeVine, S.M., Radel, J.D., Sweat, J.A. and Wetzel, D.L. (1999). Microchemical analysis of retina layers in pigmented and albino rats by Fourier transform infrared microspectroscopy. *Biochim Biophys Acta,* **1473**, 409-17.

LeVine, S.M. and Wetzel, D.L. (1994). In situ chemical analyses from frozen tissue sections by Fourier transform infrared microspectroscopy. Examination of white matter exposed to extravasated blood in the rat brain. *Am J Pathol,* **145**, 1041-7.

Levine, S.M. and Wetzel, D.L.B. (1993). Analysis of Brain-Tissue by FT-IR Microspectroscopy. *Applied Spectroscopy Reviews,* **28**, 385-412.

Litwin, S.E., Raya, T.E., Anderson, P.G., Daugherty, S. and Goldman, S. (1990). Abnormal cardiac function in the streptozotocin-diabetic rat. Changes in active and passive properties of the left ventricle. *J Clin Invest,* **86**, 481-8.

Liu, K.Z., Bose, R. and Mantsch, H.H. (2002). Infrared spectroscopic study of diabetic platelets. *Vibrational Spectroscopy,* **28**, 131-136.

Liu, K.Z., Dixon, I.M. and Mantsch, H.H. (1999). Distribution of collagen deposition in cardiomyopathic hamster hearts determined by infrared microscopy. *Cardiovasc Pathol,* **8**, 41-7.

Loeffler, D.A., Connor, J.R., Juneau, P.L., Snyder, B.S., Kanaley, L., DeMaggio, A.J., Nguyen, H., Brickman, C.M. and LeWitt, P.A. (1995). Transferrin and iron in normal, Alzheimer's disease, and Parkinson's disease brain regions. *J Neurochem,* **65**, 710-24.

Lopaschuk, G.D., Saddik, M., Barr, R., Huang, L., Barker, C.C. and Muzyka, R.A. (1992). Effects of high levels of fatty acids on functional recovery of ischemic hearts from diabetic rats. *Am J Physiol,* **263**, E1046-53.

Lopaschuk, G.D., Tahiliani, A.G., Vadlamudi, R.V., Katz, S. and McNeill, J.H. (1983). Cardiac sarcoplasmic reticulum function in insulin- or carnitine-trealed diabetic rats. *Am J Physiol,* **245**, H969-76.

Lopez-Garcia, F., Micol, V., Villalain, J. and Gomez-Fernandez, J.C. (1993). Infrared spectroscopic study of the interaction of diacylglycerol with phosphatidylserine in the presence of calcium. *Biochim Biophys Acta,* **1169**, 264-72.

Lui, K., Jackson, M., Sowa, M.G., Ju, H., Dixon, I.M. and Mantsch, H.H. (1996). Modification of the extracellular matrix following myocardial infarction monitored by FTIR spectroscopy. *Biochim Biophys Acta,* **1315**, 73-7.

Lunsford, L.D., Kondziolka, D., Flickinger, J.C., Bissonette, D.J., Jungreis, C.A., Maitz, A.H., Horton, J.A. and Coffey, R.J. (1991). Stereotactic radiosurgery for arteriovenous malformations of the brain. *J Neurosurg,* **75**, 512-24.

Lyman, D.J. and Murray-Wijelath, J. (1999). Vascular graft healing: I. FTIR analysis of an implant model for studying the healing of a vascular graft. *J Biomed Mater Res,* **48**, 172-86.

Lyons, T.J., Li, W., Wells-Knecht, M.C. and Jokl, R (1994). Toxicity of mildly modified low-density lipoproteins to cultured retinal capillary endothelial cells and pericytes. *Diabetes,* **43**, 1090-5.

Maccarrone, M., Bladergroen, M.R., Rosato, N. and Finazzi Agro, A.F. (1995). Role of lipid peroxidation in electroporation-induced cell permeability. *Biochem Biophys Res Commun,* **209**, 417-25.

Malhotra, A., Penpargkul, S., Fein, F.S., Sonnenblick, E.H. and Scheuer, J. (1981). The effect of streptozotocin-induced diabetes in rats on cardiac contractile proteins. *Circ Res,* **49**, 1243 -50.

Man, Y.B.C. and Setiowaty, G. (1999). Application of Fourier transform infrared spectroscopy to determine free fatty acid contents in palm olein. *Food Chemistry,* **66**,109-114.

Manoharan, R., Baraga, J.J., Rava, R.P., Dasari, R.R., Fitzmaurice, M. and Feld, M.S. (1993). Biochemical analysis and mapping of atherosclerotic human artery using FT-IR microspectroscopy. *Atherosclerosis,* **103**, 181-93.

Mantsch, H.H., Casal, H.L. and Jones, R.N. (1986). Resolution enhancement of infrared spectra of biological systems. In *Spectroscopy of Biological Systems.* ed Hester, R.E. pp. 1-46. Chichester England; New York: Wiley.

Marion, J.B. and Thornton, S.T. (1988). Classical dynamics of particles and systems. pp. 430-431. San Diego: Harcourt Brace Jovanovich.

Maxwell, S.R. and Lip, G.Y. (1997a). Free radicals and antioxidants in cardiovascular disease. *Br J Clin Pharmacol,* **44**, 307-17.

Maxwell, S.R., Thomason, H., Sandler, D., Leguen, C., Baxter, M.A., Thorpe, G.H., Jones, A.F. and Barnett, A.H. (1997b). Antioxidant status in patients with uncomplicated insulin-dependent and non-insulin-dependent diabetes mellitus. *Eur J Clin Invest,* **27**, 484-90.

McNeill, J.H. (1996). Role of elevated lipids in diabetic cardiomyopathy. *Diabetes Res Clin Pract,* **31 Suppl**, S67-71.

McNeill, J.H., Delgatty, H.L. and Battell, M.L. (1991). Insulinlike effects of sodium selenate in streptozocin-induced diabetic rats. *Diabetes,* **40,** 1675-8.

Melin, A.M., Perromat, A. and Deleris, G. (2000). Pharmacologic application of fourier transform IR spectroscopy: *in vivo* toxicity of carbon tetrachloride on rat liver. *Biopolymers,* **57**, 160-8.

Melin, A.M., Perromat, A. and Deleris, G. (2001). Sensitivity of Deinococcus radiodurans to gamma-irradiation: a novel approach by Fourier transform infrared spectroscopy. *Arch Biochem Biophys,* **394**, 265-74.

Mishra, O.P. and Delivoria-Papadopoulos, M. (1999). Cellular mechanisms of hypoxic injury in the developing brain. *Brain Res Bull,* **48**, 233-8.

Morgan, M.K., Anderson, R.E. and Sundt, T.M., Jr. (1989a). The effects of hyperventilation on cerebral blood flow in the rat with an open and closed carotid-jugular fistula. *Neurosurgery,* **25**, 606-11; discussion 611-2.

Morgan, M.K., Anderson, R.E. and Sundt, T.M., Jr. (1989b). A model of the pathophysiology of cerebral arteriovenous malformations by a carotid-jugular fistula in the rat. *Brain Res,* **496**, 241-50.

Morris, T.E. and Sulakhe, P.V. (1997). Sarcoplasmic reticulum Ca(2+)-pump dysfunction in rat cardiomyocytes briefly exposed to hydroxyl radicals. *Free Radic Biol Med,* **22**, 37-47.

Mossine, V.V., Linetsky, M., Glinsky, G.V., Ortwerth, B.J. and Feather, M.S. (1999). Superoxide free radical generation by Amadori compounds: the role of acyclic forms and metal ions. *Chem Res Toxicol,* **12**, 230-6.

Mozumder, A. (1999). *Fundamentals of radiation chemistry.* San Diego: Academic Press.

Mullarkey, C.J., Edelstein, D. and Brownlee, M. (1990). Free radical generation by early glycation products: a mechanism for accelerated atherogenesis in diabetes. *Biochem Biophys Res Commun,* **173**, 932-9.

Nathan, D.M. (1998). Some answers, more controversy, from UKPDS. United Kingdom Prospective Diabetes Study. *Lancet,* **352**, 832-3.

Naumann, D. (2000). Infrared spectroscopy in microbiology. In *Encyclopedia of analytical chemistry: applications, theory, and instrumentation.* ed Meyers, R.A. pp. 102-31. Chichester; New York: Wiley.

Navarro-Alarcon, M., de la Serrana, H.L., Perez-Valero, V. and Lopez-Martinez, C. (1998). Serum selenium levels as indicators of body status in cancer patients and their relationship with other nutritional and biochemical markers. *Sci Total Environ,* **212**, 195-202.

Navarro-Alarcon, M., Lopez, G.d.l.S.H., Perez-Valero, V. and Lopez-Martinez, C. (1999). Serum and urine selenium concentrations as indicators of body status in patients with diabetes mellitus. *Sci Total Environ,* **228**, 79-85.

Navarro-Alarcon, M. and Lopez-Martinez, M.C. (2000). Essentiality of selenium in the human body: relationship with different diseases. *Sci Total Environ,* **249**, 347-71.

Naziroğlu, M. and Çay, M. (2001). Protective role of intraperitoneally administered vitamin E and selenium on the antioxidative defense mechanisms in rats with diabetes induced by streptozotocin. *BioI Trace Elem Res,* **79**, 149-59.

Naziroğlu, M., Dilsiz, N. and Çay, M. (1999). Protective role of intraperitoneally administered vitamins C and E and selenium on the levels of lipid peroxidation in the lens of rats made diabetic with streptozotocin. *Biol Trace Elem Res,* **70**, 223 -32.

Ng, Y.C., Tolerico, P.H. and Book, C.B. (1993). Alterations in levels of Na(±)-K(+)-ATPase isoforms in heart, skeletal muscle, and kidney of diabetic rats. *Am J Physiol,* **265**, E243-51.

Nishikawa, T., Edelstein, D., Du, X.L., Yamagishi, S., Matsumura, T., Kaneda, *Y.,* Yorek, M.A., Beebe, D., Oates, P.J., Hammes, H.P., Giardino, I. and Brownlee, M. (2000). Normalizing mitochondrial superoxide production blocks three pathways of hyperglycaemic damage. *Nature,* **404**, 787-90.

Nornes, H. and Grip, A. (1980). Hemodynamic aspects of cerebral arteriovenous malformations. *J Neurosurg,* **53**, 456-64.

Nourooz-Zadeh, J., Rahimi, A., Tajaddini-Sarmadi, J., Tritschler, H., Rosen, P., Halliwell, B. and Betteridge, D.J. (1997). Relationships between plasma measures of oxidative stress and metabolic control in NIDDM. *Diabetologia,* **40**, 647-53.

Nyyssonen, K., Porkkala, E., Salonen, R., Korpela, H. and Salonen, J.T. (1994). Increase in oxidation resistance of atherogenic serum lipoproteins following antioxidant supplementation: a randomized double-blind placebo-controlled clinical trial. *Eur J Clin Nutr,* **48**, 633-42.

Okayama, H., Hamada, M. and Hiwada, K. (1994). Contractile dysfunction in the diabetic-rat heart is an intrinsic abnormality of the cardiac myocyte. *Clin Sci (Lond),* **86**, 257-62.

Ortwerth, B.J., James, H., Simpson, G. and Linetsky, M. (1998). The generation of superoxide anions in glycation reactions with sugars, osones, and 3 -deoxyosones. *Biochem Biophys Res Commun,* **245**, 161-5.

Osterode, W., Holler, C. and Ulberth, F. (1996). Nutritional antioxidants, red cell membrane fluidity and blood viscosity in type 1 (insulin dependent) diabetes mellitus. *Diabet Med,* **13**, 1044-50.

Öztürk, ***Y.,*** Altan, V.M. and Yıldızoğlu-Arı, N. (1996). Effects of experimental diabetes and insulin on smooth muscle functions. *Pharmacol Rev,* **48**, 69-112.

Pandya, D.P. (2001). Oxidant injury in coronary heart disease (Part-I). *Compr Ther,* **27**, 284-92.

Panzram, G. (1987). Mortality and survival in type 2 (non-insulin-dependent) diabetes mellitus. *Diabetologia,* **30**, 123-31.

Paolisso, G., Esposito, R., D'Alessio, M.A. and Barbieri, M. (1999). Primary and secondary prevention of atherosclerosis: is there a role for antioxidanis? *Diabetes Metab,* **25**, 298-306.

Parinandi, N.L., Thompson, E.W. and Schmid, H.H. (1990). Diabetic heart and kidney exhibit increased resistance to lipid peroxidation. *Biochim Biophys Acta,* **1047**, 63-9.

Pellettieri, L. and Blomquist, E. (1999). Differences in radiosensitivity between brain, small and large arteriovenous malformations. A tentative explanation of the incongruent results of radiotherapy. *Med Hypotheses,* **52**, 551 -6.

Penckofer, S., Schwertz, D. and Florczak, K. (2002). Oxidative stress and cardiovascular disease in type 2 diabetes: the role of antioxidants and pro-oxidants. *J Cardiovasc Nurs,* **16**, 68-85.

Pennathur, S., Wagner, J.D., Leeuwenburgh, C., Litwak, K.N. and Heinecke, J.W. (2001). A hydroxyl radical-like species oxidizes cynomolgus monkey artery wall proteins in early diabetic vascular disease. *J Clin Invest,* **107**, 853-60.

Penpargkul, S., Fein, F., Sonnenblick, E.H. and Scheuer, J. (1981). Depressed cardiac sarcoplasmic reticular function from diabetic rats. *J Mol Cell Cardiol,* **13**, 303-9.

Phelan, A.M., Lange, D.G., Kues, H.A. and Lutty, G.A. (1992). Modification of membrane fluidity in melanin-containing cells by low-level microwave radiation.*Bioelectromagnetics,* **13,** 131-46.

Plaschke, K., Weigand, M.A., Michel, A., Martin, E. and Bardenheuer, H.J. (2000). Permanent cerebral hypoperfusion: 'preconditioning-like' effects on rat energy metabolism towards acute systemic hypotension. *Brain Res***, 858**, 363-70.

Prasad, S., Kamath, **G.G.,** Jones, K., Clearkin, L.G. and Phillips, R.P. (2001). Prevalence of blindness and visual impairment in a population of people with diabetes. *Eye,* **15**, 640-3.

Pugliese, G., Tilton, R.G. and Williamson, J.R. (1991). Glucose-induced metabolic imbalances in the pathogenesis of diabetic vascular disease. *Diabetes Metab Rev,* **7**, 35-59.

Regan, T.J., Lyons, M.M., Ahmed, S.S., Levinson, G.E., Oldewurtel, H.A., Ahmad, M.R. and Haider, B. (1977). Evidence for cardiomyopathy in familial diabetes mellitus. *J Clin Invest,* **60**, 884-99.

Regan, T.J., Wu, C.F., Yeh, C.K., Oldewurtel, H.A. and Haider, B. (1981). Myocardial composition and function in diabetes. The effects of chronic insulin use. *Circ Res,* **49**, 1268-77.

Reinila, A. and Akerblom, H.K. (1984). Ultrastructure of heart muscle in short-term diabetic rats: influence of insulin treatment. *Diabetologia,* **27**, 397-402.

Robberecht, H. and Deelstra, H. (1994). Factors influencing blood selenium concentration values: a literature review. *J Trace Elem Electrolytes Health Dis,* **8**, 129-43.

Rosen, P., Ballhausen, T., Bloch, W. and Addicks, K. (1995). Endothelial relaxation is disturbed by oxidative stress in the diabetic rat heart: influence of tocopherol as antioxidant. *Diabetologia,* **38**, 1157-68.

Rosen, P., Du, X. and Tschope, D. (1998). Role of oxygen derived radicals for vascular dysfunction in the diabetic heart: prevention by alpha-tocopherol? *Mol Cell Biochem,* **188**, 103-11.

Rubin, P., Constine, L. and Nelson, D.F. (1992). Late effects of cancer treatment In *Principles and practice of radiation oncology.* ed Brady, L.W. pp. 138-42. Philadelphia: J.B. Lippincott.

Rubler, S., Sajadi, R.M,, Araoye, M.A. and Holford, F.D. (1978). Noninvasive estimation of myocardial performance in patients with diabetes. Effect of alcohol administration. *Diabetes,* **27**, 127-34.

Saito, K., Nishi, S., Kashima, T. and Tanaka, H. (1984). Histologic and ultrastructural studies on the myocardium in spontaneously diabetic KK mice: a new animal model of cardiomyopathy. *Am J Cardiol,* **53**, 320-3.

Sakurai, T. and Tsuchiya, S. (1988). Superoxide production from nonenzymatically glycated protein. *FEBS Lett,* **236**, 406-10.

Sano, T., Umeda, F., Hashimoto, T., Nawata, H. and Utsumi, H. (1998). Oxidative stress measurement by *in vivo* election spin resonance spectroscopy in rats with streptozotocin-induced diabetes. *Diabetologia,* **41**, 1355-60.

Santini, S.A., Cotroneo, P., Marra, G., Manto, A., Giardina, B., Mordente, A., Greco, A.V., Martorana, GE., Magnani, P. and Ghirlanda, G. (1996). NA^+/K^+ ATPase impairment and experimental glycation: the role of glucose autoxidation. *Free Radic Res,* **24**, 381-9.

Sasaki, T., Kurita, H., Saito, I., Kawamoto, S., Nemoto, S., Terahara, A., Kirino, T. and Takakura, K. (1998). Arteriovenous malformations in the basal ganglia and thalamus: management and results in 101 cases. *J Neurosurg,* **88**, 285-92.

Schaffer, S.W. (1991). Cardiomyopathy associated with noninsulin-dependent diabetes.*Mol Cell Biochem,* **107**, 1-20.

Schurr, A. (2002). Energy metabolism, stress hormones and neural recovery from cerebral ischemia/hypoxia. *Neurochem Int,* **41**, 1-8.

Sell, D.R., Lapolla, A., Odetti, P., Fogarty, J. and Monnier, V.M. (1992). Pentosidine formation in skin correlates with severity of complications in individuals with long-standing IDDM. *Diabetes,* **41**, 1286-92.

Sell, D.R. and Monnier, V.M. (1989). Structure elucidation of a senescence cross-link from human extracellular matrix. Implication of pentoses in the aging process. *J Biol Chem,* **264**, 21597-602.

Severcan, F. (1997). Vitamin E decreases the order of the phospholipid model membranes in the gel phase: an FTIR study. *Biosci Rep,* **17**, 231-5.

Severcan, F., Kaptan, N. and Turan, B. (2003). Fourier transform inftared spectroscopic studies of diabetic rat heart crude membranes. *Spectroscopy-an International Journal,* **17**, 569-577.

Severcan, F., Toyran, N., Kaptan, N. and Turan, B. (2000). Fourier transform infrared study of the effect of diabetes on rat liver and heart tissues in the C-H region. *Talanta,* **53**, 55-59.

Shapiro, L.M. (1982). Echocardiographic features of impaired ventricular function in diabetes mellitus. *Br Heart J,* **47**, 439-44.

Shapiro, L.M., Howat, A.P. and Calter, M.M. (1981). Left ventricular function in diabetes mellitus. I: Methodology, and prevalence and spectrum of abnormalities. *Br Heart J,* **45**, 122-8.

Shen, L., Van Dael, P. and Deelstra, H. (1993). Evaluation of an in vitro method for the estimation of the selenium availability from cow's milk. *Z Lebensm Unters Forsch,* **197**, 342-5.

Shertzer, H.G., Lastbom, L., Sainsbury, M. and Moldeus, P. (1992). Menadione-mediated membrane fluidity alterations and oxidative damage in rat hepatocytes. *Biochem Pharmacol,* **43**, 2135-41.

Shi, J., Yang, S.H., Stubley, L., Day, A.L. and Simpkins, J.W. (2000). Hypoperfusion induces overexpression of beta-amyloid precursor protein mRNA in a focal ischemic rodent model. *Brain Res,* **853**, 1-4.

Shiba, T., Inoguchi, T., Sportsman, J.R., Heath, W.F., Bursell, S. and King, G.L. (1993). Correlation of diacylglycerol level and protein kinase C activity in rat retina to retinal circulation. *Am J Physiol,* **265**, E783 -93.

Shimoni, Y., Firek, L., Severson, D. and Giles, W. (1994). Short-term diabetes alters K+ currents in rat ventricular myocytes. *Circ Res,* **74**, 620-8.

Siesjo, B.K. (1988). Mechanisms of ischemic brain damage. *Crit Care Med,* **16**, 954-63.

Sills, R.H., Moore, D.J. and Mendelsohn, R. (1994). Erythrocyte peroxidation: quantitation by Fourier transform infrared spectroscopy. *Anal Biochem,* **218**, 118-23.

Silver, M.D., Huckell, V.F. and Lorber, M. (1977). Basement membranes of small cardiac vessels in patients with diabetes and myxoedema: preliminary observations. *Pathology,* **9**, 213-20.

Sohar, E., Ravid, M., Ben-Shaul, Y., Reshef, T. and Gafni, J. (1970). Diabetic fibrillosis. A report of three cases. *Am J Med,* **49**, 64-9.

Solberg, T.D., Selch, M.T., Smathers, J.B. and DeSalles, A.A. (1998). Fractionated stereotactic radiotherapy: rationale and methods. *Med Dosim,* **23**, 209-19.

Spetzler, R.F., Wilson, C.B., Weinstein, P., Mehdorn, M., Townsend, J. and Telles, D. (1978). Normal perfusion pressure breakthrough theory. *Clin Neurosurg,* **25**, 651-72.

Stadtman, E.R. and Oliver, C.N. (1991). Metal-catalyzed oxidation of proteins. Physiological consequences. *J Biol Chem,* **266**, 2005-8.

Stapleton, S.R. (2000). Selenium: an insulin-mimetic. *Cell Mol Life Sci,* **57**, 1874-9.

Stauble, B., Boscoboinik, D., Tasinato, A. and Azzi, A. (1994). Modulation of activator protein-1 (AP-1) transcription factor and protein kinase C by hydrogen peroxide and D-alpha-tocopherol in vascular smooth muscle cells. *Eur J Biochem,* **226**, 393-402.

Steiner, L., Lindquist, C., Adler, J.R., Tomer, J.C., Alves, W. and Steiner, M. (1992). Clinical outcome of radiosurgery for cerebral arteriovenous malformations. *J Neurosurg,* **77***,* 1-8.

Stuart, B. and Ando, D.J. (1996). *Modern infrared spectroscopy*. New York: Published on behalf of ACOL (University of Greenwich) by Wiley.

Surewicz, W.K., Mantsch, H.H. and Chapman, D. (1993). Determination of protein secondary structure by Fourier transform infrared spectroscopy: a critical assessment. *Biochemistry,* **32**, 389-94.

Susi, H. and Byler, D.M. (1983). Protein structure by Fourier transform infrared spectroscopy: second derivative spectra. *Biochem Biophys Res Commun,* **115**, 391-7.

Sutherland, G., Peeling, J., Lesiuk, H. and Saunders, J. (1990). Experimental cerebral ischemia studied using nuclear magnetic resonance imaging and spectroscopy. *Can Assoc Radiol J,* **41**, 24-31.

Sykes, C.A., Wright, A.D., Malins, J.M. and Pentecost, B.L. (1977). Changes in systolic time intervals during treatment of diabetes mellitus. *Br Heart J*, **39**, 255-9.

Szalontai, B., Nishiyama, *Y.,* Gombos, Z. and Murata, N. (2000). Membrane dynamics as seen by fourier transform infrared spectroscopy in a cyanobacterium, Synechocystis PCC 6803. The effects of lipid unsaturation and the protein-to-lipid ratio. *Biochim Biophys Acta,* **1509**, 409-19.

Taegtmeyer, H. and Passmore, J.M. *(1985).* Defective energy metabolism of the heart in diabetes. *Lancet,* **1**, 139-41.

Takagi, Y., Hattori, I., Nozaki, K., Ishikawa, M. and Hashimoto, N. (2000). DNA fragmentation in central nervous system vascular malformations. *Acta Neurochir (Wien),* **142**, 987-94.

Takahashi, H., French, S.W. and Wong, P.T. (1991). Alterations in hepatic lipids and proteins by chronic ethanol intake: a high-pressure Fourier transform infrared spectroscopic study on alcoholic liver disease in the rat. *Alcohol Clin Exp Res,* **15**, 219-23.

Tarjâan, I. and Berkes, L. (1987). *An introduction to biophysics with medical orientation.* Budapest: Akadâemiai Kiadâo : Distributor Kultura.

Tatum, L., Shankar, P., Boylan, L.M. and Spallholz, J.E. (2000). Effect of dietary copper on selenium toxicity in Fischer 344 rats. *Biol Trace Elem Res,* **77**, 241-9.

Thompson, E.W. (1988). Structural manifestations of diabetic cardiomyopathy in the rat and its reversal by insulin treatment *Am J Anat,* **182**, 270-82.

Thompson, S.W. (1966). *Selected histochemical and histopathological methods.* Springfield, :Ill.,: C.C. Thomas.

Thomson, C.D., Robinson, M.F., Campbell, D.R. and Rea, H.M. (1982). Effect of prolonged supplementation with daily supplements of selenomethionine and sodium selenite on glutathione peroxidase activity in blood of New Zealand residents. *Am J Clin Nutr,* **36**, 24-31.

Tomlinson, K.C., Gardiner, S.M., Hebden, R.A. and Bennett, T. (1992). Functional consequences of streptozotocin-induced diabetes mellitus, with particular reference to the cardiovascular system. *Pharmacol Rev,* **44**, 103-50.

Trautner, C., Haastert, B., Richter, B., Berger, M. and Giani, G. (2003). Incidence of blindness in southern Germany due to glaucoma and degenerative conditions. *Invest Ophthalmol Vis Sci,* **44**, 1031-4.

Trivin, F., Chevenne, D. and Hautecouverture, M. (1999). [Maillard reaction products and chronic diabetic complications]. *Ann Biol Clin (Paris),* **57**, 445-54.

Turan, B., Bayarı, S., Balcik, C., Severcan, F. and Akkaş, N. (2000). A biomechanical and spectroscopic study of bone from rats with selenium deficiency and toxicity. *Biometals,* **13**, 113-21.

Twardowska-Saucha, K., Grzeszczak, W., Lacka, B., Froehlich, J. and Krywult, D. (1994). [Lipid peroxidation, antioxidant enzyme activity and trace element concentration in II and III trimester of pregnancy in pregnant women with diabetes]. *Pol Arch Med Wewn,* **92**, 313-21.

Ueda, M., Muramatsu, H., Kamiya, T., Muramatsu, A., Mori, T., Terashi, A. and Katayama, Y. (2000). Pyruvate dehydrogenase activity and energy metabolite levels following bilateral common carotid artery occlusion in rat brain. *Life Sci,* **67**, 821-6.

UKPDS_Group (1998). Intensive blood-glucose control with sulphonylureas or insulin compared with conventional treatment and risk of complications in patients with type 2 diabetes (UKPDS 33). UK Prospective Diabetes Study (UKPDS) Group. *Lancet,* **352**, 837-53.

Umemura, J., Cameron, D.G. and Mantsch, H.H. (1980). A Fourier transform infrared spectroscopic study of the molecular interaction of cholesterol with 1,2-dipalmitoyl-sn-glycero-3-phosphocholine. *Biochim Biophys Acta,* **602**, 32-44.

Valentovic, M.A. and Lubawy, W.C. (1983). Impact of insulin or tolbutamide treatment on 14C-arachidonic acid conversion to prostacyclin and/or thromboxane in lungs, aortas, and platelets of streptozotocin-induced diabetic rats. *Diabetes,* **32**, 846-51.

Van Dael, P., Davidsson, L., Munoz-Box, R., Fay, L.B. and Barclay, D. (2001). Selenium absorption and retention from a selenite- or selenate-fortified milk-based formula in men measured by a stable-isotope technique. *Br J Nutr,* **85**, 157-63.

van Hoeven, K.H. and Factor, S.M. (1990). A comparison of the pathological spectrum of hypertensive, diabetic, and hypertensive-diabetic heart disease. *Circulation,* **82**, 848-55.

Vendemiale, G., Grattagliano, I. and Altomare, E. (1999). An update on the role of free radicals and antioxidant defense in human disease. Int J *Clin Lab Res*, **29**, 49-55.

Wang, L.M., Han, Y.F. and Tang, X.C. (2000). Huperzine A improves cognitive deficits caused by chronic cerebral hypoperfusion in rats. *Eur J Pharmacol,* **398**, 65-72.

Wang, W.C., Makela, A.L., Nanto, V. and Makela, P. (1995). Serum selenium levels in diabetic children. A follow up study during selenium-enriched agricultural fertilization in Finland. *Biol Trace Elem Res,* **47**, 355-64.

Wautier, J.L., Wautier, M.P., Schmidt A.M., Anderson, G.M., Hori, O., Zoukourian, C., Capron, L., Chappey, O., Yan, S.D., Brett, J. and *et al*. (1994). Advanced glycation end products (AGEs) on the surface of diabetic erythrocytes bind to the vessel wall via a specific receptor inducing oxidant stress in the vasculature: a link between surface-associated AGEs and diabetic complications. *Proc Natl Acad Sci USA,* **91**, 7742-6.

Wells-Knecht, K.J., Zyzak, D.V., Litchfield, J.E., Thorpe, S.R. and Baynes, J.W. (1995 a). Mechanism of autoxidative glycosylation: identification of glyoxal and arabinose as intermediates in the autoxidative modification of proteins by glucose. *Biochemistry,* **34**, 3702-9.

Wells-Knecht, M.C., Lyons, T.J., McCance, D.R., Thorpe, S.R. and Baynes, J.W. (1997). Age-dependent increase in ortho-tyrosine and methionine sulfoxide in human skin collagen is not accelerated in diabetes. Evidence against a generalized increase in oxidative stress in diabetes. *J Clin Invest,* **100**, 839-46.

Wells-Knecht, M.C., Thorpe, S.R. and Baynes, J.W. (1995b). Pathways of formation of glycoxidation products during glycation of collagen. *Biochemistry,* **34**, 15134-41.

West, I.C. (2000). Radicals and oxidative stress in diabetes. *Diabet Med,* **17**, 171-80.

Wigg, D.R. (1999). Is there a role for fractionated radiotherapy in the treatment of arteriovenous malformations? *Acta Oncol,* **38**, 979-86.

Wohaieb, S.A. and Godin, D.V. (1987). Alterations in free radical tissue-defense mechanisms in streptozocin-induced diabetes in rat. Effects of insulin treatment. *Diabetes,* **36**, 1014-8.

Wolff, S.P. and Dean, R.T. (1987). Glucose autoxidation and protein modification. The potential role of 'autoxidative glycosylation' in diabetes. *Biochem J,* **245**, 243-50.

Wolff, S.P., Jiang, Z.Y. and Hunt, J.V. (1991). Protein glycation and oxidative stress in diabetes mellitus and ageing. *Free Radic Biol Med,* **10**, 339-52.

Wong, P.T., Cadrin, M. and French, S.W. (1991). Distinctive infrared spectral features in liver tumor tissues of mice: evidence of structural modifications at the molecular level. *Exp Mol Pathol,* **55**, 269-84.

Wouters, B.G., Weppler, S.A., Koritzinsky, M., Landuyt, W., Nuyts, S., Theys, J., Chiu, R.K. and Lambin, P. (2002). Hypoxia as a target for combined modality treatments. *Eur J Cancer,* **38**, 240-57.

Wu, J.R. and Lentz, B.R. (1991). Fourier transform infrared spectroscopic study of Ca2+ and membrane-induced secondary structural changes in bovine prothrombin and prothrombin fragment 1. *Biophys J,* **60**, 70-80.**,**

Yamamoto, Y., Coffey, R.J., Nichols, D.A. and Shaw, E.G. (1995). Interim report on the radiosurgical treatment of cerebral arteriovenous malformations. The influence of size, dose, time, and technical factors on obliteration rate. *J Neurosurg,* **83**, 832-7.

Yano, K., Ohoshima, S., Shimizu, Y., Moriguchi, T. and Katayama, H. (1996). Evaluation of glycogen level in human lung carcinoma tissues by an infrared spectroscopic method. *Cancer Lett,* **110**, 29-34.

Young,I.S., Tate, S., Lightbody, J.H., McMaster, D. and Trimble, E.R. (1995). The effects of desferrioxamine and ascorbate on oxidative stress in the streptozotocin diabetic rat. *Free Radic Biol Med,* **18**, 833-40.

Yu, Z., Tibbits, G.F. and McNeill, J.H. (1994). Cellular functions of diabetic cardiomyocytes: contractility, rapid-cooling contracture, and ryanodine binding. *Am J Physiol,* **266***,* H2082-9.

Zarain-Herzberg, A., Yano, K., Elimban, V. and Dhalla, N.S. (1994). Cardiac sarcoplasmic reticulum Ca(2+)-ATPase expression in streptozotocin-induced diabetic rat heart. *Biochem Biophys Res Commun,* **203**, 113-20.

Zarling, E.J., Mobarhan, S., Bowen, P. and Kamath, S. (1993). Pulmonary pentane excretion increases with age in healthy subjects. *Mech Ageing Dev,* **67**, 141-7.

Zhong, G.G., Jiang, Y., Li, Z.B., Zhang, B.G., Zhang, W.J. and Yue, G. (1990). Protective action of selenium and manganese on xanthine and xanthine oxidase induced oxidative damage to cultured heart cells. Chin Med J (Engl), 103, 735-42.

CURRICULUM VITAE

Name:	Neslihan Toyran Al-Otaibi
Date of Birth:	28.06.1974
Nationality:	Turkish
Tel:	+90 (312) 210 5157, Fax: +90 (312) 210 1289
E-mail:	toyran@metu.edu.tr
Address:	Middle East Technical University, Department of Biology, 06531, Ankara, TURKEY.

Education

- Faculty of Science, Department of Biology, Middle East Technical University, Ankara, Turkey. **1999-2003**, Ph.D., Cumulative: 3.92 out of 4.

  Thesis Title: Molecular Approach with Fourier Transform Infrared Spectroscopy to different pathological systems (diabetes mellitus and arteriovenous malformation) with various treatments.

- Faculty of Science, Department of Biology, Middle East Technical University, Ankara, Turkey. **1997-1999**, M.S. Degree, Cumulative: 3.64 out of 4.

  Thesis Title: The Effect of Divalent Ions on Antioxidant-Phospholipid Model Membrane Interactions.

- Faculty of Education, Department of Biology, Middle East Technical University, Ankara, Turkey. **1993-1997**, B.S. Degree, (Honor Student).

- Faculty of Science, Department of Biology, Middle East Technical University, Ankara, Turkey. **1993-1997**, B.S. Degree, (Double Major, Honor Student)

Publications

Journal Paper

Toyran, N. and Severcan F., "Competitive Effect of Vitamin D_2 and Ca^{2+} on Phospholipid Model Membranes: An FTIR. Study", *Chemistry and Physics of Lipids*, **123** (2): 165-176 (2003).

Toyran, N. and Severcan F., "Infrared spectroscopic studies on the dipalmitoyl phosphatidylcholine bilayer interactions with calcium phosphate: Effect of vitamin D_2", *Spectroscopy*, **16**: 399-408 (2002).

Kazanci, N., **Toyran, N**., Haris, P.I. and Severcan, F., "Vitamin D_2 at high and low concentrations exert opposing effects on molecular order and dynamics of dipalmitoyl phosphatidylcholine membranes", *Spectroscopy*, **15**: 47-55 (2001).

Toyran, N. and Severcan, F., "The Effect of Magnesium Ions on Vitamin D_2-Phospholipid Model Membrane Interactions in the Presence of Different Buffer Media", *Talanta*, **53**: 23-27 (2000).

Severcan, F., **Toyran, N**., Kaptan, N. and Turan, B., Fourier Transform "Infrared Study of the Effect of Diabetes on Rat Heart and Liver Tissues", *Talanta*, **53**: 55-59 (2000).

Abstracts in Referred Journals

Kazanci, N., **Toyran, N**., Eker, F. and Severcan, F. "Estimation of the Location of Vitamin D_2 in Lipid Bilayers by Fourier Transform Infrared Spectroscopy". *Chemistry and Physics of Lipids*, **110**, 200-201. 40^{th} International Conference on the Biochemistry of Lipids (ICBL), September 1999, Dijon, France.

Toyran, N., Ayaz, M., Turan, B. and Severcan, F. "Comparison of Streptozotocin-Induced Diabetic and Control Rat Liver Tissue by Fourier Transform Infrared Spectroscopy". *Physiological Research*, **48**, S131. Federation of European Physiological Society Meeting (FEPS), June 29-July 4 1999, Praque, Czeck Republic.

Toyran N., Eker, F. and Severcan F. "The Effect of Ca^{++} Ions on Vitamin D_2-Phospholipid Model Membrane Interactions". *Chemistry and Physics of Lipids,* **94 (2)**, 163. 39^{th} International Conference on the Biochemistry of Lipids (ICBL), August 1998, Davos, Switzerland.

Abstracts in Congress Proceedings

Toyran, N., Dönmez, G., Öğe, K., Zorlu, F. and Severcan, F. "The investigation of the effect of hypoperfusion and radiosurgery on rat brain tissues by FTIR spectroscopy" XIIIth National Biophysics Congress, 5-7 September 2001, "Eskişehir, Turkey. (Turkish Poster presentation).

Kaptan, N., **Toyran, N**., Turan B. and Severcan, F. "The Investigation of the effect of diabetes on soft tissues by FTIR spectroscopy". XIIth National Biophysics Congress, 7-9 September 2000, "Istanbul, Turkey. (Turkish Oral presentation).

Severcan, F., Boyar, H., **Toyran, N**., Turan, B. and Zorlu, F. "The investigation of the Effect of Disease and Radiation on Bone and Soft Tissues of Rat by Fourier Transform Infrared Spectroscopy". VIIth. National Medical Physics Congress, 11-13 November 1999, Izmir (Poster presentation).

Toyran, N., Severcan, F. "Investigation of Divalent ion-Vitamin D2-DPPC interactions by Fourier Transform Infrared Spectroscopy". XIth National Biophysics Congress, 31 October-2 November 1999, Antalya, Turkey. (Turkish Oral presentation).

Toyran, N., Severcan, F. "The Effect of Magnesium Ions on Vitamin D_2-Phospholipid Model Membrane Interactions in the Presence of Different Buffer Media". Colloquium Spectroscopicum Internationale XXXI, 5-10 September 1999, Ankara, Turkey. (Poster presentation).

Kaptan, N., **Toyran, N**., Severcan, F. and Turan, B. "Fourier Transform Infrared Study of the Effect of Diabetes on Rat Heart and Liver Tissues". Colloquium Spectroscopicum Internationale XXXI, 5-10 September 1999, Ankara, Turkey (Poster Presentation).

Toyran, N., Severcan, F. "Spectroscopic Studies of the Effect of Divalent ions on Vitamin D_2-Phospholipid Model Membrane systems". NATO Summer School, 16-28 August 1999, Spetses, Greece. (Poster Presentation).

Toyran, N., Severcan, F. "The Effect of Calcium Ions on Antioxidant-Phospholipid Model Membrane Interactions in the Presence of Different Buffer Media". Xth National Biophysics Conference, 10-12 September 1998, Istanbul, Turkey. (Turkish Oral presentation).